Tailor-made nanocrystals for the treatment of oxidative stress-related diseases

PhD-Thesis

zur

Erlangung des Doktorgrades

der Naturwissenschaften

(Dr. rer. nat.)

dem

Fachbereich Pharmazie

der Philipps-Universität Marburg

vorgelegt von

Pascal L. Stahr

aus Berlin

Marburg (Lahn), 2021

Erstgutachter: Prof. Dr. Cornelia M. Keck

Zweitgutachter: Prof. Dr. Udo Bakowsky

Eingereicht am: 19.05.2021

Tag der mündlichen Prüfung: 07.07.2021

Hochschulkennziffer: 1180

Die vorliegende Arbeit entstand auf Anregung und unter Leitung von

Prof. Dr. Cornelia M. Keck

Im Fachbereich Pharmazie am Institut für Pharmazeutische Technologie und Biopharmazie

der Philipps-Universität Marburg

ERKLÄRUNG

Ich versichere, dass ich meine dem Fachbereich Pharmazie Marburg Promotionsprüfung eingereichte Dissertation mit dem Titel

„Tailor-made nanocrystals for the treatment of oxidative stress-related diseases“

selbständig ohne unerlaubte Hilfe angefertigt und mich dabei keiner anderen als der von mir ausdrücklich bezeichneten Quellen bedient habe. Alle vollständig oder sinngemäß übernommenen Zitate sind als solche gekennzeichnet.

Die Dissertation wurde in der jetzigen oder einer ähnlichen Form noch bei keiner anderen Hochschule eingereicht und hat noch keinen sonstigen Prüfungszwecken gedient.

Marburg, den 19.05.2021

……

Pascal L. Stahr

Meiner Familie in Liebe und Dankbarkeit

„Success is the ability to go from failure to failure,
without losing your enthusiasm."

(Erfolg ist die Fähigkeit, von einem Misserfolg zum anderen zu gehen,
ohne seine Begeisterung zu verlieren.)

Winston Churchill

Table of content

1 Introduction

1.1 Oxidative stress

What do Alzheimer's disease, chronic obstructive pulmonary disease (COPD), and asthma have in common? Despite the systematic and intensive research, they can currently not be cured but only treated and are also associated with an inflammatory reaction caused by oxidative stress [1,2].

Oxidative stress is defined as the excess level of reactive oxygen species (ROS) compared to the level of neutralizing antioxidants. Depending on the reactive radical derivate, the term reactive nitrogen species (RNS) is used and both are likely summarized under the term RONS, respectively [3]. A cumulative effect of elevated RONS can increase oxidative stress at the systemic level and manifests thus itself as a variety of health problems, such as the diseases mentioned above [4]. Such an increased level of RONS, in turn, damages the structure of biomolecules and alters their functions, leading to cellular dysfunction, inflammation and even cell death. Hence, they play a major role in aging and age-related diseases [3,4]. RONS are formed by losing or accepting a single electron during various, regular daily metabolic processes in all aerobic cells and by environmental pollution, i.e. they are generated endogenously and exogenously [5,6].

1.1.1 Physiological production and scavenging of ROS

Endogenously generated RONS include especially enzymes of the mitochondrial respiratory chain, nicotinamide adenine dinucleotide phosphate (NADPH) oxidase, xanthine oxidase, and uncoupled endothelial nitric oxide synthase (eNOS) [5]. Further sources are myeloperoxidase (MPO), lipoxygenase, cyclooxygenase, cytochrome P450, and angiotensin II [7]. While cellular respiration, NADPH oxidase is the predominant source of the radical superoxide anion ($\cdot O_2^-$) formed by the one-electron reduction of molecular oxygen (**Figure 1**). A small part can affect vascular cells directly, whereas most of the $\cdot O_2^-$ is converted into hydrogen peroxide (H_2O_2) by the superoxide dismutase (SOD) [8]. H_2O_2 is not a free radical, because of the lack of unpaired electrons, but it can produce the highly reactive ROS hydroxyl ion (OH^-) via the Haber-Weiss and Fenton reaction (**Figure 1**). Hydroxyl radicals possess extreme reactivity, especially with phospholipids in cell membranes and proteins. When exposed to chloride and MPO in neutrophils, H_2O_2 can be converted into hypochlorous acid (HOCl), that in turn can damage cellular proteins [9]. Moreover, the free radical nitric oxide ($\cdot NO$) is produced from L-arginine by three main isoforms of nitric oxide synthase (NOS): (1) the epithelial NOS, which is associated with vasodilation and vascular regulation, (2) the neuronal NOS for intracellular signals, and (3) the inducible NOS, activated in response to various endotoxin or cytokine signals. Additionally, $\cdot O_2^-$ can react with $\cdot NO$ and produce a further relatively reactive molecule, peroxynitrite ($ONOO^-$) [10].

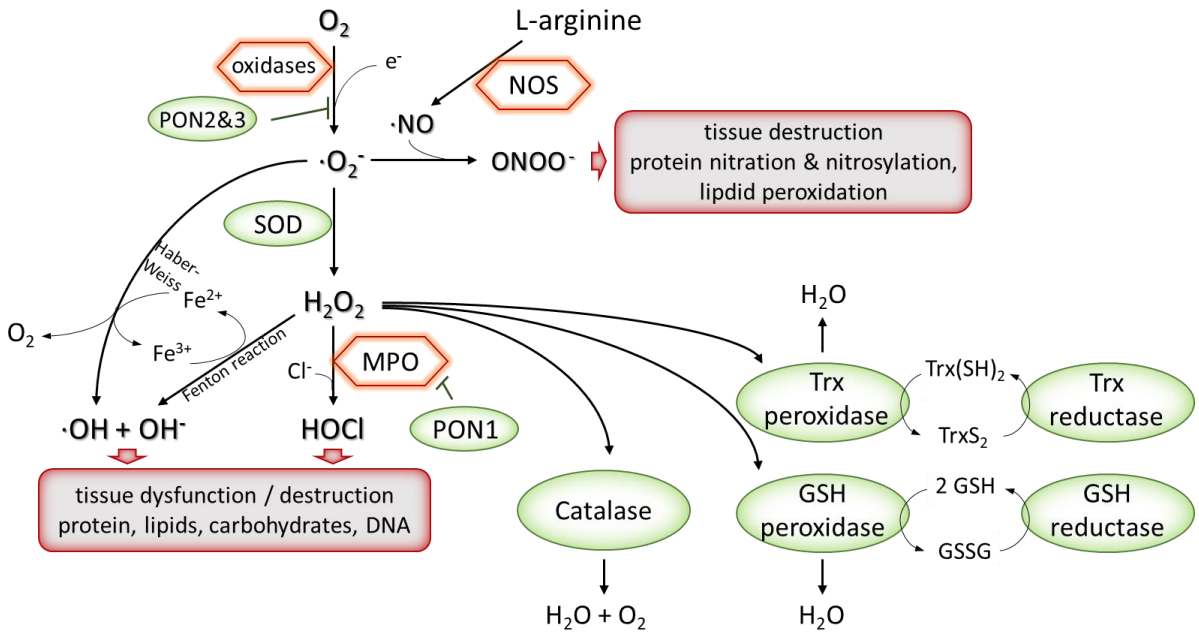

Figure 1: *Schematic overview of the relationships between the most common RONS formed and erased in aerobic cell processes. Different enzymatic oxidases, e.g. NADPH and xanthine oxidases, and uncoupled endothelial nitric oxide synthase (that produces $\cdot O_2^-$ instead of NO), convert molecular oxygen to the superoxide anion ($\cdot O_2^-$). H_2O_2 generated by superoxide dismutase (SOD) can be converted into other radical species or neutralized to water by catalase, glutathione (GSH), and thioredoxin (Trx) peroxidases.*

As high as the amount of pro-oxidative systems seemed to be, on the other side, cellular mechanisms also possess a variety of antioxidants to actively protect against injury by the ROS production. The primary antioxidant enzymes include SOD (responsible for the conversion from $\cdot O_2^-$ into H_2O_2), catalase, Thioredoxin (Trx), and glutathione (GSH) peroxidase [11,12]. The GSH peroxidase eliminates also peroxides and hydroxyl ions by oxidation of the reduced GSH to glutathione disulfide (GSSG), which will be then re-reduced to GSH by glutathione reductase. PON1, a member of the paraoxonase family (PON), is mainly found in high-density and low-density lipoproteins in the plasma where it protects those from peroxidation and degrades cholesteryl esters and lipoproteins [13]. Furthermore, PON1 inhibits MPO and thus the formation of HOCl [14]. PON2 and PON3 interact with coenzyme Q10 and then reduce the $\cdot O_2^-$ production, yielded by the mitochondrial respiratory chain [15,16]. Other antioxidant enzymes are heme oxygenase, glutathione S-transferase and glutathione 6-phosphate dehydrogenase. Thus, generation and degradation of ROS are usually balanced in cells and organisms.

Inflammation is the response to cellular injury caused by physical and chemical stress, infectious agents, toxins and more. An acute inflammatory reaction is essential for the immune response that could lead to a repair of the injury, while in contrast chronic inflammation can cause tissue destruction and is involved in the pathogenesis of autoimmune, neurodegenerative, and respiratory diseases. Hence, the inflammatory response is part of the innate immune response [17]. Upon injury, macrophages are mainly activated, which are a source of mediators such as histamine. These and other

cells release pro-inflammatory cytokines such as tumor necrosis factor (TNF-α), interleukin-1 and -6 (IL-1, IL-6) which trigger the inflammatory cascade by addressing end-organ receptors. These pro-inflammatory cytokines can induce the adhesion of leukocytes to endothelial cells, the release of proteases and arachidonic acid metabolites, and the activation of the coagulation cascade [18–20].

Besides the enzymatic-based redox systems, there are small molecules that interact with RONS and are classified as antioxidants. These include the bilirubin, vitamin E (α-tocopherol), pro-vitamin A (β-carotene), albumin and uric acid, as the main compounds present in blood [21–23]. Exogenous antioxidants involve the vitamins A, C (ascorbic acid) and E as well as selenium, zinc, and phenol and stilbene derivates, such as resveratrol, phenolic acids, curcumin, and flavonoids. Due to the reduction of oxidative stress, they are also associated to reduce the inflammatory response, descript in the pathogenesis of oxidative stress-related diseases [24]. In other words, an imbalanced ratio of oxidants leads to pathological cell dysfunction and may cause inflammatory and degenerative diseases.

1.1.2 ROS-related neuronal cell death pathophysiology

Regardless of the cause, an increased level of ROS in neurons leads to cell death and is a characteristic marker in the pathology of neurodegenerative diseases, such as Alzheimer's (AD) [25] and Parkinson's disease [26,27] as well as after acute brain injury due to cerebral ischemia [28], hemorrhagic insults [29], or brain trauma [30]. Oxidative stress and calcium homeostasis have been reported as major triggers for death signaling in neurons, with mitochondria identified as the principal cell organelle for this programmed cell death pathway.

At this point, it is necessary to specify that cell death is distinguished in apoptosis and necrosis. Apoptosis occurs as a programmed cell death process, which is itself actively induced and is thus part of the metabolism without damaging neighboring tissue. It can be triggered by internal cell processes or externally, e.g. by immune cells [31]. In contrast, irreversible and rapid necrosis is initiated by harsh mechanical, chemical or temperature stimuli. The resulting plasma membrane rupture, cell leakage and dilatation of cellular organelles result in inflammation in the surrounding environment [32]. Necrosis induced by elevated ROS level in neuronal cells is defined as oxytosis, and in non-neuronal cells as ferroptosis. As both seemed to share a similar pathway, the oxytosis is explained in the following [33].

In the progression of oxytosis due to the increased ROS level in the neuronal cytosol, mitochondria are impaired by the trans-activation of the pro-apoptotic BH3 interacting-domain death agonist (BID), a member of the BCL-2 family [34]. After translocation on the mitochondrial outer membrane, BID induces fission of the mitochondrial network, mitochondrial ROS production, as well as the loss of the mitochondrial membrane potential and ATP production due to electron leakage from the electron transport chain (**Figure 2**). Consequently, the ROS level within the mitochondria increases that in turn induces the release of the apoptosis inducing factor (AIF), which was located on their inner membrane.

Then, this flavoprotein migrates to the cell nucleus, where it signals the cell to condense its chromosomes and to fragment its DNA molecules to induce programmed cell death [35].

However, BID is also involved in the apoptosis pathway, where it is activated by caspase-8 and then links to the mitochondria. The cascade of caspases can be triggered extrinsically when death receptors on the plasma membrane are linked to, e.g. with TNF-α (**Figure 2**). Intrinsic apoptosis induced cascade of caspases can be initiated by increased ROS and calcium concentration, by endoplasmic reticulum stress and radiation (**Figure 2**). Hence, it can be summarized that neuronal cell death with accumulated ROS is linked to BID activation, which makes it an interesting target for treating neurodegenerative diseases [36,37].

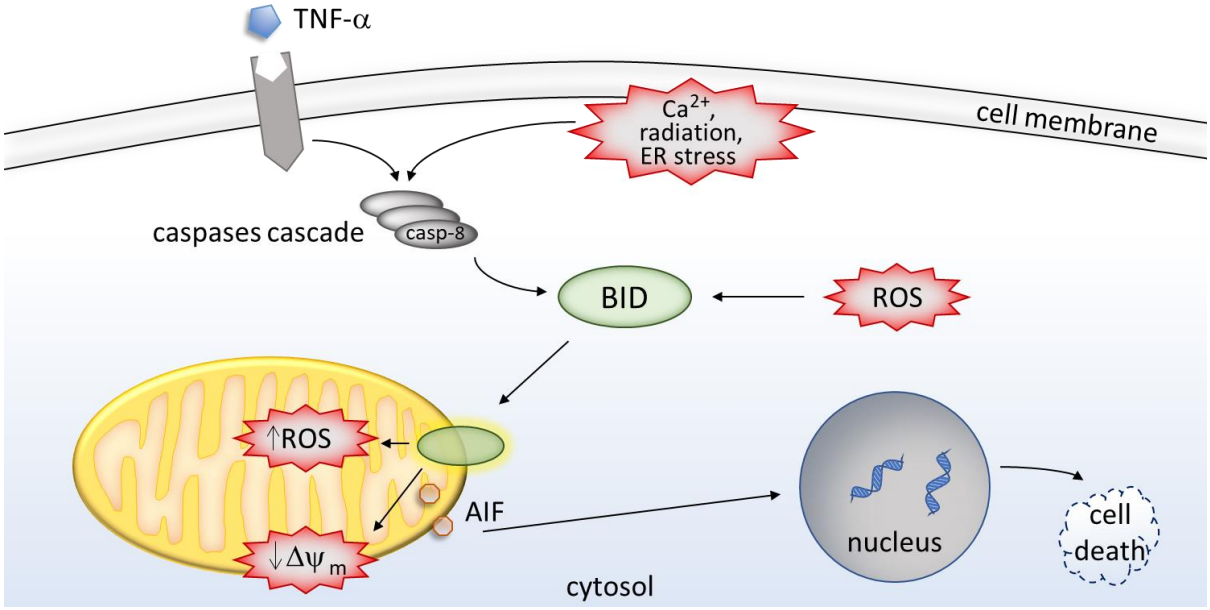

Figure 2: *Simplified illustration of programmed cell death by induction of the BID cascade. This can be triggered extrinsically, e.g. by TNF-α, intrinsically by higher Ca^{2+} concentration, radiation and endoplasmic reticulum (ER) stress, or elevated intracellular ROS level.*

1.1.3 ROS in Alzheimer's disease

Neurons are susceptible to oxidative stress due to their high oxygen uptake, lipid content and reduced antioxidant enzymes compared to non-neuronal cells [38]. Again, ROS are highly reactive substances that can react with all macromolecules such as the DNA. Patients with AD possess an elevated level of neuronal oxidative stress and thus damages in the cellstructures can be expected. Also, the degree of damaged DNA and oxidized DNA bases, pyrimidine and purine, is 2 times higher in leukocytes of patients with mild cognitive impairment and early state of AD, compared to those without these diseases [39,40]. In 2006, more than 26 million patients worldwide were suffering from AD, a number that is expected to four-fold by 2050 with increasing age of the population [41]. Amyloid plaques and neurofibrillary tangles are regarded as the histologic feature of AD and thus the origin of oxidative

stress. Amyloid plaques are aggregates of the amyloid beta peptide (Aβ), formed by the Amyloid-Precursor Protein (APP). An over-expression of APP results in aggregation Aβ and then in the formation of amyloid plaques. Neurofibrillary tangles are aggregates of Tau protein being hyperphosphorylated by kinases, which lead to a breakdown of microtubules [42]. All in all, the process of Alzheimer's disease is driven by excessive damage in the genome [43].

The ROS production is then induced by an elevated metal ion concentration such as zinc, iron and copper that have been found in Amyloid plaques and neurofibrillary tangles deposits [44]. This allows a conversion of H_2O_2 into hydroxyl radicals by the Fenton reaction to take place more frequently. Furthermore, Aβ itself produces ROS in the presence of metal ions like Fe^{2+} and Cu^{2+} [45,46]. The presence of metal ions in neurofibrillary tangles stimulates iron-induced lipid peroxidation of polyunsaturated fatty acids that exist in higher amounts in neuronal cells and are part of their membrane as phospholipids. As result, aldehydes such as acrolein and 4-hydroxy-2-nonenal are formed, whose accumulation is involved in tau phosphorylation, injury of primary hippocampus neurons, impairment of histone binding to DNA and increased likelihood of DNA oxidation [47].

Finally, besides disrupting cellular functions, the increased production of ROS also activates the BID cascade, leading to the degeneration of synapses and the death of neurons (**Figure 2**).

1.1.4 Pulmonary oxidative stress

The aforementioned diseases described the pathology as intrinsic overproduction of ROS. In contrast, chronic obstructive pulmonary disease (COPD) is a classic example of the exogenous environmental generation of oxidative stress as almost all COPD patients smoke cigarettes or are exposed to dust e.g. occupational in mining. Smoking exposes the lungs to more than 4,700 harmful chemical substances and high concentrations of oxidants with about 10^{14} molecules and 3,000 ppm NO per puff [48]. The oxidants consist of a variety of ROS ranging from short-living $\cdot O_2^-$ and NO to long-living organic radicals such as tar-semiquinones [49,50]. Other exogenous sources that could affect the lungs include oxidant gases, such as ozone, nitrogen dioxide, and sulfur dioxide, as well as airborne particulate matter < 10 µm from diesel car exhaust fumes that can generate ROS *in-situ* [51].

Although the pathogenesis and origin of asthma as another lung disease is different, it is also associated with an inflammatory response caused by oxidative stress [52]. In both diseases inflammatory and immune cells, i.e. macrophages, neutrophils and eosinophils, are considered the main cause of induction and progression of lung inflammation [53,54]. Lung macrophages are also involved in the control and limitation of inflammatory events in the lung [55]. This vast number of different and even contradictory tasks is mediated by distinct polarized "activation" states of the macrophages. Signals from the surrounding tissue determine the polarization state of the macrophages and prepare them for their different roles. The altered polarization interferes with the phagocytosis and efferocytosis of macrophages in asthma and COPD. This leads to impaired responses

to exogenous irritants, resulting in excessive inflammation of the respiratory tract and oxidative stress [56–58]. At the same time, high oxidative stress stimulates an increase in NADPH oxidases, mitochondrial dysfunction and reduced Nrf2-activity, which affects immune responses and further enhances respiratory inflammation and oxidative stress [59].

So, it is not surprising that alveolar macrophages and neutrophils derived from asthmatic patients produce more ROS compared to a healthy control group [60,61]. Likewise, alveolar macrophages from smokers' lungs exhibited higher ROS amounts [62]. Moreover, the intracellular iron content of alveolar macrophages from smokers and from persons developing chronic bronchitis is higher compared to non-smokers, which increases the formation of ROS in the epithelial lining fluid [63,64]. RNS exposed by smoking triggers nitration and oxidation of plasma proteins and thus the levels of nitrated proteins (fibrinogen, transferrin, plasminogen and ceruloplasmin) were higher for smokers than for non-smokers [65]. Finally, the development of obstructive diseases can climax in the acute worsening of these diseases, known as exacerbations. It is characterized by an increased airway inflammation, a decline in lung function and increased mortality [66].

1.1.5 Antioxidant paradox

Considering the importance of oxidative stress in the development of diseases, it might be easy to conclude that antioxidants can be used to counteract them. However, supplementation with antioxidants has been reported to offer little to no therapeutic effects. In this way, it was revealed that antioxidant supplements do not offer beneficial effects (vitamin C and selenium) or that they even potentially increase the mortality (vitamin E and β-carotene) [67–69].

An explanation could be the limited accessibility of the given natural antioxidants to the specific target where ROS is produced, i.e. within cellular organelles such as mitochondria. Even if they would reach them in an appropriate concentration, H_2O_2 and HOCl are not decomposed by antioxidant vitamins [70]. Additionally, many studies on antioxidants have been conducted in large groups of human subjects with no attention paid to their basic nutritional status or even their "oxidative damage status".

Another popular theory concerns the pro-oxidant effects of antioxidants. In this way, for example, the anticancer actions of vitamin C were explained, used as a reversal of concepts by proponents of mega-supplementation [71]. This assumption is strengthened by observations in cell culture media, where ascorbate could produce H_2O_2 [72]. An additional *in-vivo* study demonstrated that the oxidation activity level measured in the blood of the vitamin E receiving group was 27% higher. Consequently, serval antioxidative vitamins possess pro-oxidative effects in higher doses causing increased mortality [73]. One possible explanation is the circumstance that antioxidants may be easily oxidized to their inactive and potentially pro-oxidant form. Overall, due to the complexity in the signaling cascade of ROS, chronic antioxidant exposure could lead to compensatory up-regulation of ROS-producing systems.

In the search for alternative antioxidants, the two main criteria for combating oxidative stress are therefore the two properties of not forming pro-oxidative forms and being effective against ROS. Besides this, the suitable candidate should not only work theoretically but should also be able to be uptaken by the body, i.e. have sufficient bioavailability. The question of how the alternative antioxidant is distributed in the body and excreted must also be clarified. As with all drugs, the new candidate or its metabolites must not cause serious side effects such as causing cancer, altering genes or harming the fetus.

1.2 APIs for the treatment of oxidative stress-related diseases

Based on the impact of oxidative stress outlined above, several approaches can be pursued. These are aimed at the exogenous supply of compounds that either inhibit the cascade of cell death or scavenge ROS before the cascade is even induced. The latter must not reveal any pro-oxidative properties, even in higher concentrations.

1.2.1 BI-6C9

Today's drug discovery for potential new compounds is proceeding by modern scientific advances in synthetic, analytical and purification chemistry, as well as the development of specialized tools such as high-throughput screening, combinatorial chemistry, computer-based 3D models of drug targeting and proteomics [74]. Such an approach was adopted to search for a compound affecting the BID pathway. At first, it was proven that *in-vitro* BID-knockout neurons significantly survive glutamate-induced oxidative stress, where the cysteine-glutamate antiporter is blocked, and the glutathione level decreases due to the lack of cysteine intake [75,76]. Research consequently focused on finding a chemical structure that enables the specific inhibition of BID for protecting against oxidative stress-related diseases. For this purpose, the structural analysis of the peptide identified the presence of a hydrophobic crevice on its surface, in which a target structure might achieve the inhibition of BID [77]. Next, by using a combined spectroscopically fragment-based design the interaction of smaller and well-known substructures within the crevice was characterized and the final target structure could be predicted [78]. After synthesis and investigations in a cell culture model, its specific and high affinity was finally demonstrated [79]. The developed structure is called BI-6C9 (**Figure 3**) and is one of the best-studied oxytosis inhibitors for preventing mitochondrial cell death [78,79]. So far, these findings remain limited to the cellular level, as the *in-vivo* application was not possible due to very poor solubility in water. Up to now, the drug is applied in cell culture studies by dissolving it in solvents, which may become hazardous when injected.

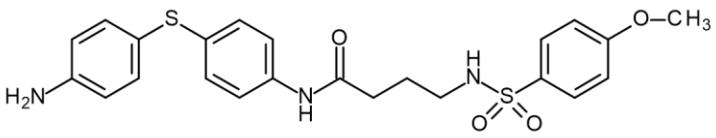

Figure 3: *Chemical structure of the BID inhibitor BI-6C9.*

1.2.2 Flavonoids

At the same time, the search for sustainable and natural products is experiencing a renaissance. Many antioxidants from food and medicinal plants are now at the center of science [80]. Such sources include fruits/ vegetables, cereals, mushrooms, beverages, flowers, spices, and medical herbs where the antioxidants are classified mainly in polyphenols (phenolic acids, flavonoids, anthocyanins, lignans and stilbenes), carotenoids (xanthophylls and carotenes), and vitamins (vitamin E and C). Among these, the literature mainly describes flavonoids, curcumin, and carotenoids, that have a broad spectrum of biological effects, such as anti-inflammatory, -bacterial, -viral, -aging and -cancer [81–84]. For instance, flavonoids provide cellular protection through the inhibition of enzymes involved in cell proliferation and modulate the expression of proteins associated with apoptosis [85]. Moreover, a few epidemiological studies have reported a possible protective role against coronary heart disease upon consumption of flavonoids [86].

Chemically, the flavonoids are derived from flavan (Figure 4, central structure in blue). However, flavonoids are present universally in plants as secondary metabolites and derived from the precursor chalcone by ring closure to form the chromone unit. By hydroxylation at C3 and dehydration at C3-C4, different superior parent structures (groups) can be classified, e.g. flavone, flavanone, flavanol, flavanonol. It is also possible that the phenyl group is located at C3 (isoflavones) or C4 (neoflavones). Structures with a covalent bond between two flavonoids are called biflavonoids. Starting from the parent structure, metabolites constitute the addition of hydroxyl, methyl, methoxy, and other groups resulting in functional compounds like hesperetin and rutin (**Figure 4**). Furthermore, flavonoids are found with sugar molecules attached (glycoside) or in a non-glycosylated form (aglycone). Due to the high number of chemical combinations, it is not surprising that more than 8,000 different flavonoids have been discovered yet.

What they all have in common is their antioxidant activity. The antioxidant activity is the result of inhibiting enzymatic free radical production, scavenging ROS or upregulating antioxidant defense. So, they fulfill the criteria of the alternative antioxidant defined above. The antioxidant properties of flavonoids are mainly associated with the ability to scavenge radicals and chelate metal ions, with both effects increasing with the number of hydroxyl groups [87]. With the transfer of a hydrogen atom and an electron from the hydroxylated phenyl group to hydroxyl, peroxyl and peroxynitrite radicals, a

relatively stable flavonoid radical is formed. It is therefore not surprising that flavonoids perform very well in various *in-vitro* assays to provide antioxidant activity and that O-methylation or glycosidation decreases their radical scavenging activity [88,89]. On the other hand, glycosidic flavonoids sometimes possess higher bioavailability than their aglycones [90,91].

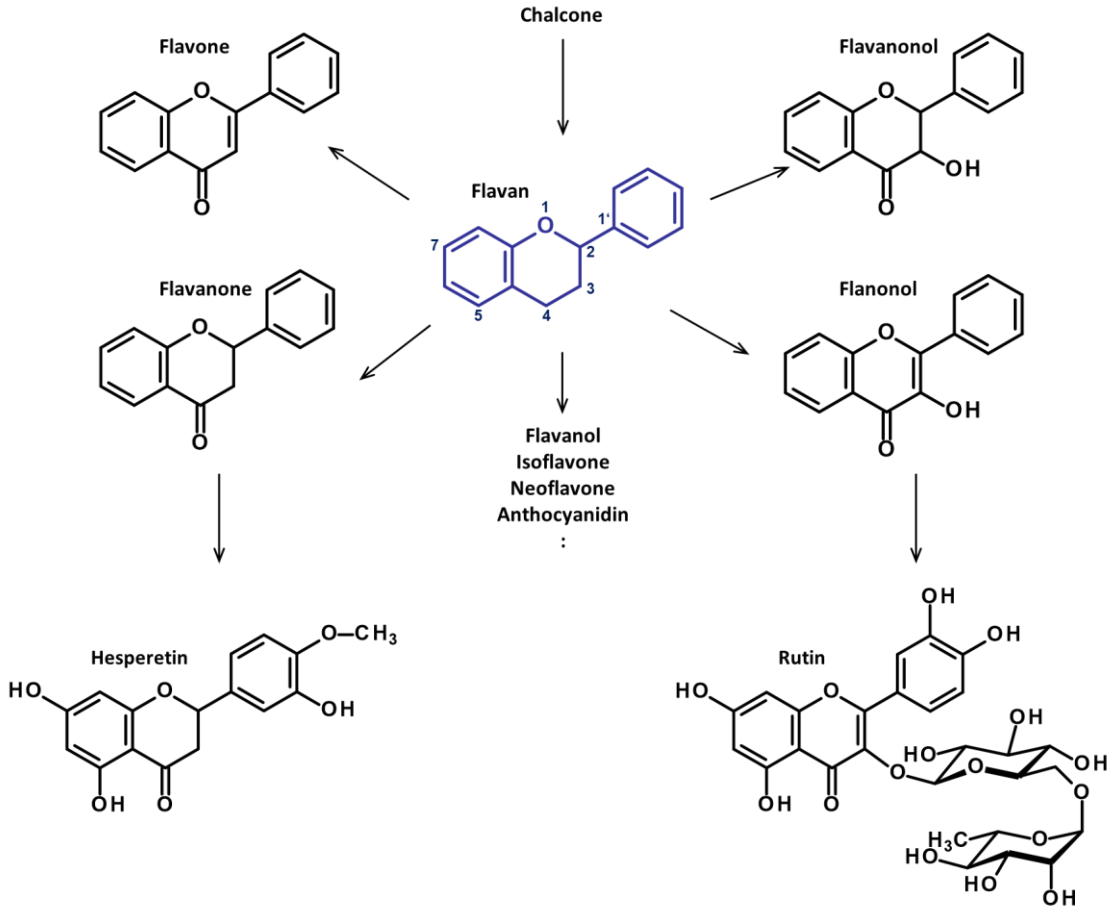

Figure 4: *Flavonoids belong to a group of polyphenols, named after the principal structure flavan (IUPAC: 3,4-dihydro-2-phenyl-2H-1-benzopyran). Depending on the position of the phenyl group, the presence of a C3-C4 double bond and/or a hydroxyl group, flavonoids are classified in various groups. Attachment of functional groups and glycosides creates pharmacologically actives such as Hesperetin and Rutin.*

Moreover, their antioxidant effect is also enhanced due to the inhibition of the xanthine oxidase [92], and the stimulation of the glutathione-S-transferase [93]. Moreover, an anti-inflammatory effect is realized by inhibition of the enzymes cyclooxygenase and 5-lipoxygenase [94], by modulation of the pro-inflammatory genes (lipoxygenase, cyclooxygenase and NOS), but also by acting on the NF-κB signaling and mitogen-activated protein kinase [95] and activation of the Nrf2/Keap1 pathway [96]. NF-κB itself is responsible for the release of pro-inflammatory cytokines, chemokines, acute-phase proteins and growth factors and its inhibition is, therefore, a useful strategy in the treatment of inflammatory disorders.

1.2.2.1 Rutin

Rutin belongs to the most extensively studied flavonoids, exhibiting numerous additional pharmacological activities, like cytoprotective, vasoprotective, anticarcinogenic, neuroprotective and cardioprotective ones [84]. Its name springs from the plant Ruta Graveolens and it is also called rutoside, vitamin P, sophorin, and quercetin-3-O rutinoside, which illustrate the bond between its aglycone quercetin and disaccharide rutinoside. However, its strong anti-inflammatory and -oxidative effects were used to investigate possible treatment in lung diseases.

In a recent study by L.L. Liu et al., mice were treated with cigarette smoke (passive smoking), which worsened the inflammatory reactions used for an asthma model [97]. Rutin was administrated orally with 37.5 or 75 mg/kg daily resulting in strong anti-inflammatory effects in both exposed and non-exposed animals by marked down-regulation of NF-κB, TNF-α and cytokines. Likewise, elevated iNOS gene expression was demonstrated to be significantly down-regulated, and consequently rutin improved lung function and inhibited airway hyperresponsiveness [97]. A similar set-up was performed by C. H. Jung et al. with guinea pigs treated with aerosolized ovalbumin and compared with quercetin, dexamethasone, and salbutamol [98]. Rutin and quercetin significantly reduced the specific airway resistance during the immediate- and late-phase response (10 min and 24 h after exposure) compared to the control group. Also, both were more effective in the immediate-phase response and in the late-phase response compared with dexamethasone and salbutamol, respectively. Results correlated with reduced releases of eosinophils, neutrophils and lymphocytes, as well as with the lower production of phospholipase A2 and eosinophil peroxidase detected in bronchoalveolar lavage fluid [98]. In another study, mice were exposed to benzopyrene, which can lead to structural and physiological changes in the lungs, up to the possible development of various chronic lung diseases such as emphysema, lung fibrosis, COPD and lung cancer [99]. Feeding with rutin restored the elevated activities of xanthine oxidase and SOD, elevated values of H_2O_2 and depleted activity of catalase to normal levels. A high dose of rutin only, i.e. without the addition of stress or inflammation inducing benzopyrene, did not affect these markers [99].

On the other hand, the glycosylation is associated with weaker antioxidant activity. It was recently shown that quercetin derivates possessed lower antioxidant effects compared to its aglycone. Reasons might be the blockage of the hydroxyl group responsible for scavenging radicals and chelating metals as well as the more difficult access through the cell membrane due to the larger and more hydrophilic structure [87,100].

1.2.2.2 Hesperetin

The aglycon hesperetin (**Figure 4**) mainly found in citrus fruits is known for its anti-oxidative, -allergic, and -inflammatory properties [101,102]. Due to these properties, hesperetin was used in different studies focusing on a dermal application for the treatment of aging and inflammatory skin diseases [103–106]. In addition, hesperetin was found to reduce the hepatic content of triacylglycerol [107].

However, the scientific focus is currently on the investigation of hesperetin for the treatment of neuronal diseases. Again, oxidative stress and neuroinflammation induce neurodegenerative diseases. Since hesperetin, as a potent ROS scavenger and lipophilic aglycone, is capable to penetrate membranes and even through the blood-brain-barrier, its use is predestinated [108]. For example, in a comprehensive study hesperetin was more effective than its glycoside hesperidin in H_2O_2 and glutamate treated cortical neuronal cells [109]. H_2O_2 induced neuronal cell toxicity is associated with loss in mitochondrial membrane potential, reduced activities of antioxidant enzymes like glutathione peroxidase or catalase and apoptosis by the caspase cascade. These effects were inhibited when adding hesperetin [110]. In another *in-vitro* study, where hippocampal HT22 and microglia BV2 cells were oxidatively stressed by lipopolysaccharide (LPS), hesperetin significantly reduced inflammation according to markers such as NF-κB [111]. These studies, however, addressed hesperetin's prevention of neuroinflammation only by inducing ROS in neurons briefly but did not consider the pathophysiology or native source of ROS in neurodegenerative diseases.

In a recent study, Aβ 1-42 peptide was added to HT22 hippocampal cells and its decrease in cell viability could be prevented by adding hesperetin [112]. Depending on the hesperetin concentration, the degree of cell survival correlated with the ability to reduce the intracellular amount of lipid peroxidation and ROS. In the same study, Aβ 1-42 peptide was injected intracerebroventricularly into mice leading to reduced expression of Nrf2 and Heme oxygenase-1 that could be up-regulated by hesperetin. Thus, the amounts of ROS and lipid peroxidation were also reduced when treating with hesperetin. Also, the release of inflammatory markers such as TNF-α, IL-1 and NF-κB were significantly lower, compared to the non-hesperetin Aβ-injected group or at least on the same level as the control group [112]. To sum up, hesperetin seemed to efficiently reverse the pathology of Alzheimer's disease and could be hence a new drug candidate for the treatment of this neurodegenerative disorder.

Based on the current knowledge it can be concluded that the highlighted APIs (BI-6C9, hesperetin and rutin) are very promising in terms of their antioxidant capacity. However, they possess the disadvantage of being poorly water-soluble and thus are poorly absorbed by the body, i.e. they possess a low bioavailability. Without sufficient absorption, no pharmacological effect can be achieved. Hence, the drawback of poor aqueous solubility must be overcome for the successful treatment of oxidative stress-related diseases. Strategies and requirements for this are presented in the following.

1.3 Formulation principles to overcome poor solubility

Not only the drugs presented, but also an estimated 70 % or more of the newly developed drugs are poorly soluble in water [113,114]. An active pharmaceutical ingredient (API) must be present in dissolved form to be absorbed by the body and to exert its pharmacological effect. On the other side, successful uptake depends additionally on the specific permeability. Concerning the Biopharmaceutical Classification System (BCS), poorly soluble drugs with a high and low permeability can be categorized in class II and IV, respectively [115]. Furthermore, poorly soluble compounds can exhibit such a slow dissolution rate that not enough drug molecules are dissolved. For this reason, J.M. Butler and J.B. Dressman created the Developability Classification System (DCS) in 2010, where they distinguish between dissolution rate-limited compounds (II a) and solubility-limited compounds (II b) [116]. When administered orally, very slightly water-soluble or practically water-insoluble APIs have limited and variable or erratic absorption in the gastrointestinal tract. Similarly, low solubility in other types of application leads to treatment failure. Therefore, the knowledge about API-specific bioavailable limiting factors represents the major feature to successfully deliver the right dose into the body.

Based on this, a variety of different formulation strategies to overcome solubility issues, have been developed over the last decades, which can be distinguished into two main categories:

1) increasing the apparent equilibrium drug solubility and dissolution rate, and
2) increasing the dissolution rate and facilitating the formation of meta-stable supersaturated drug solutions,

where sophisticated formulations combine both strategies.

Chemical modifications, in terms of attachment of hydrophilic functional groups or development of pro-drugs, will not be discussed further because they may affect efficacy and permeability and are not a method of formulation development, i.e. the use of specific additives or physical procedures.

One of the classic and popular methods is salt formation if an API is ionizable. The advantages are obvious with the simplicity, cost efficiency and no need for chemical modifications, which is the reason for its widespread use. To reach a complete proton transfer, a difference of > 2 units between pK_a values of drug and counterion is necessary [117]. The resulting increase in solubility can exceed 3 orders of magnitude [118], where the success depends on crystal lattice and hydration free energy, and cannot be predicted. Processability and stability also play a crucial role in the selection of the right counterion or even the use of the non-ionized form.

However, this approach has its limitations in the case of extremely poorly soluble APIs, where salt formation does not sufficiently increase the degree of solubility. This circumstance can be handled by the combination of the salt with another method, like amorphous systems and precipitation inhibitors,

or by the development of ionic liquids. Ionic liquids are low melting point (T_m < 100 °C) salts composed of bulky counterions, e.g. cholinium and docusate. The characteristically low melting point results from the structural heterogeneity of a sterically hindered asymmetric ion, which hampers strong ionic interactions and disables ordered packing within the crystal lattice [119]. They can be used for oral administration or combined with lipid-based formulations when a hydrophobic counterion was selected.

In case that no salts can be formed due to the absence of ionizable groups or the pK_a value falls in an unsuitable range, co-crystals can be performed. The difference between co-crystal and salt is that there is no proton transfer, even when formulated with an acid or base. According to the FDA, co-crystals are defined as solids that are crystalline materials composed of two or more molecules in the same crystal lattice and thus exclude single-drug polymorphic modifications, an amorphous state and solvate/ hydrate forms (**Figure 5 A-D**) [120]. Intermolecular interaction changes the crystal lattice energy within the solid state which correlates directly with the solubility. Enhanced solubility and dissolution rates could lead to a supersaturated solution, which in turn facilitates precipitation. However, a sharp distinction between salt formation and co-crystallization (**Figure 5 E** and **F**) is not always possible. For example, it was shown that escitalopram oxalate, expected as 1:1 salt, is characterized by salt and co-crystal in the same lattice, i.e. one molecule of oxalic acid is co-crystallized with the ionic bonding from two molecules of escitalopram cation and one molecule of oxalate di-anion (**Figure 5 G**) [121].

Salt formation and co-crystallization are characterized by stoichiometric ordered coupling, whereas other approaches are characterized by disordered or lack of crystal lattice structures. This can be achieved by embedding them in a matrix. Such matrices are, for example, cyclodextrin and lipid-based formulations. Cyclodextrins are cyclically linked α-1,4 glucopyranose oligomers with typically 6, 7 or 8 units, referred to as α-, β- or γ-cyclodextrin. Based on their conformation, the typical toroid structure results, which is hydrophobic on the inside due to the carbon-scaffold and hydrophilic on the outside due to the hydroxyl groups. This hollow geometry allows the hosting of hydrophobic molecules (**Figure 5 I**) [122]. Lipid-based formulations dissolve the API in the preparation, which consist of triglycerides, water-soluble and -insoluble surfactants as well as hydrophilic co-solvents such as polyethylene glycol (PEG). Depending on the proportion of individual components, a high solvent capacity or stability of that solvency within the intestinal fluid is created [123,124]. Another method of embedding an API in a matrix to enhance its solution involves micelles developed by surfactants like phospholipids, alkylsulfates and polysorbates (**Figure 5 J**). They share an amphiphilic structure that spontaneously forms micelles when exceeding a critical concentration, the so-called critical micelle concentration (CMC). Structures with varying polarity are developed that facilities the incorporation of the poorly

soluble drug (**Figure 5 J**). Thus, the CMC directly correlates with the stability of the micelles. Depending on the type of surfactant used, different kinds of interactions occur that increase the solubility of the API by serval orders of magnitude [125,126]. Maintaining the stability of the drug-loaded micelles can be challenging. Ionic surfactants tend to become unstable mixed micelles when exposed to bile salt containing media, which causes the embedded API to be excluded and, in the worst case, to precipitate. However, this is unlikely to occur with non-ionic surfactants like polysorbate [127].

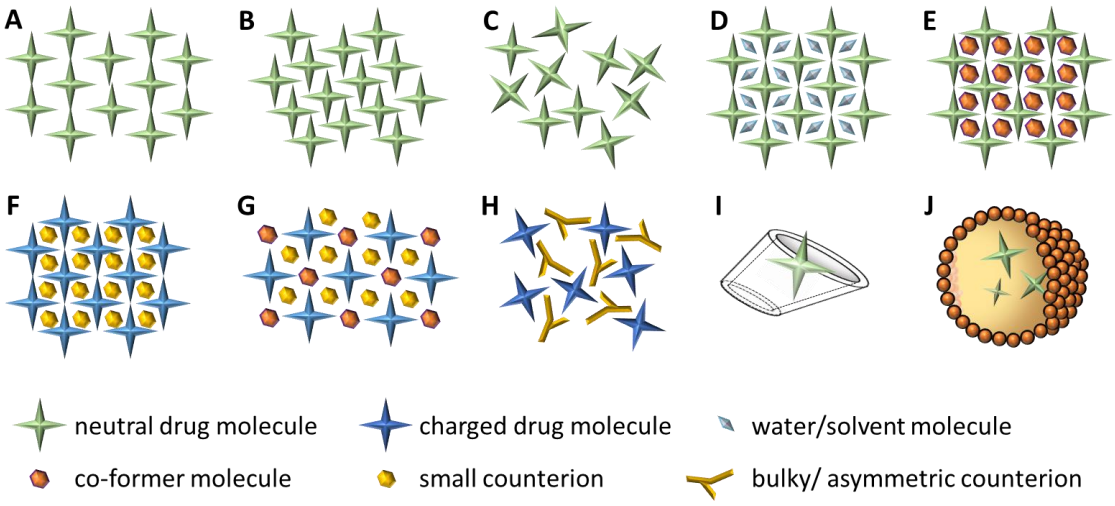

Figure 5: *Schematic illustration of different states and form options for an API: A and B are polymorphs orientating in the crystal lattice, C is the amorphous state, D a hydrate/ solvate, E a co-crystal, F a classic salt, G an ionic co-crystal (classic salt and co-former in the same crystal lattice). Similar to the A and B the formulations D to G are also capable to form polymorphs. Formulation H is an ionic liquid, the method I represents a cyclodextrin-API complex and J a drug-loaded surfactant micelle.*

Apart from the advantages associated with the development of methods to increase solubility, there is also a risk: As a result of supersaturation, precipitation is facilitated and can thus occur if the precipitation rate is higher than the absorption rate. This can be avoided by using a sustained drug release formulation or precipitation inhibitors such as polymers, cyclodextrins and low molecular weight surfactants (both also used as solubilization enhancer). Their mechanisms of inhibition are explained by modifying the nucleation and/ or crystal growth due to absorption or complexation [128,129].

In the following, the attention will be focused on and mesoporous silica particles, since they offer many further advantages. For example, these approaches are also suitable for APIs whose physico-chemical properties have so far made it almost impossible to bring them into a bioavailable formulation. Especially with nanocrystals, environmentally harmful solvents and other excipients can be largely dispensed with. For this reason, both methods are investigated in the present thesis for the antioxidants introduced prior.

1.4 Mesoporous silica

Much more modern approaches for increased drug solubility and dissolution rate involve amorphous solid dispersions or nanoparticular systems. Instead of a fixed crystal lattice structure, APIs in an amorphous state are characterized by a disordered three-dimensional configuration of the molecules. This can be achieved by a mechanical energy input, solvents or by melt methods. The main problem of amorphous dispersions, however, concerns their thermodynamic instability, namely reverting preferably to its stable crystalline form. Thus, long-term stabilization is the subject of current research. This is commonly achieved by using polymers, mesoporous silica and the preparation of co-amorphous formulations with a second drug or low molecular weight excipient.

Mesoporous silica materials are characterized by a huge porous surface area, that is easy to functionalize, an uniform pore size and biocompatibility. The principle of drug amorphization can be explained by their ability to confine drug molecules within their pore structure ranging in the nanoscale. Crystallization is then completely suppressed below a certain pore diameter because the surface energy contributions overcompensate the energetic advantage associated with the release of internal energy during crystallization [130]. Furthermore, drug nucleation needs to occur in each pore which tremendously slows down crystallization time [131,132]. In a recent study, stability regarding amorphous state was realized over seven months of storage when using pore sizes as small as possible and a filling level of 25% [133]. By varying parameters such as pore size, surface area and hydrophilicity, mesoporous silica formulations can be tailored to the drug's needs. Normally, the pore sizes range between 2 and 5 nm, whereas silica with a pore size up to 30 nm were synthesized allowing to host also larger molecules, e.g. proteins or nucleic acids [134,135]. Consequently, a variety of chemically different poorly soluble compounds can be applied in this way.

It was proven in *in-vitro* dissolution studies that the dissolution rate was enhanced [133]. On the other hand, studies demonstrated that API release could be incomplete due to reversible adsorption and interaction between drug molecules and silica surface [136,137]. Nevertheless, *in-vivo* studies on dogs and rabbits confirmed the enhanced bioavailability of mesoporous silica formulated itraconazole compared to its crystalline state [138].

Conclusively, silica mesoporous materials are a sophisticated approach for increasing the solubility and dissolution rate *in-vitro* and *in-vivo* for almost all kinds of drugs. In general, it must be considered that the stability regarding an amorphous state can be challenging. Hence, if the amorphous state can not be maintained, other approaches are needed to overcome poor water solubility.

1.5 Nanocrystals

Such another modern and sophisticated method is the development of nanoparticles or nanocarriers. This study focused on the production, characterization and optimization of drug nanocrystals (NC). For this reason, they will be described in the following in more detail. Drug NC are the pure active ingredient that has been ground down to the submicron range, i.e. to sizes between 100-1,000 nm. They are only layered by a stabilizing agent and thus there is no need for adding complex and expensive polymers, lipids or other excipients. So, the API is not embedded in a matrix/ carrier and thus the associated instabilities in an aqueous medium do not occur, e.g. drug leakage out of the matrix/ carrier and non-enzymatic polymer hydrolysis [139]. Furthermore, NC have the big advantage of enhancing even the solubility of so-called "brickdust" drug candidates, which are neither soluble in water, nor in oils [140]. The question is, how NC can achieve this and how they can be produced.

1.5.1 Properties of nanocrystals

1.5.1.1 Saturation solubility

Normally, the solubility of an active pharmaceutical ingredient, sized in the micrometer scale and larger, is a function of the solvent and temperature. In contrast, the saturation solubility is enhanced for submicron sized particles. Derived from the Kelvin equation, which describes the relationship between the curvature of a liquid drop and its increasing vapor pressure, the Ostwald–Freundlich equation was established:

$$ln\frac{S}{S_0} = \frac{2\gamma \cdot V_m}{r \cdot R \cdot T} = \frac{2\gamma \cdot M}{r \cdot \rho \cdot R \cdot T}$$

where S is the solubility of the nanosized drug and S_0 the solubility of an infinitely large drug particle, γ is the surface free energy, V_m the molar volume, r the particle radius, R the gas constant, T the temperature, M and ρ are the molecular weight and density of the drug, respectively. An increase in the surface free energy and the reduction of the particle radius result in higher solubility. In addition, the enhanced solubility is obtained by increased curvature of the NC resulting in increased dissolution pressure and drug solubility [141].

1.5.1.2 Dissolution rate

Furthermore, the particle size reduction results in an enormous increase in the total surface area. This fact is commonly used to explain the increased dissolution rate, according to the Noyes-Whitney equation:

$$\frac{dc}{dt} = \frac{A \cdot D \cdot (c_s - c_t)}{V \cdot h}$$

The dissolution rate of drug particles *dc/dt* depends on the surface area *A*, its diffusion coefficient *D*, the volume *V*, the diffusion layer thickness *h,* the concentration gradient of saturation solubility c_s, and drug concentration at the time c_t. Due to the higher saturation solubility (c_s) the dissolution rate is also increased [142]. There is also an inverse dependence on the thickness of the diffusion layer *h*, which is decreased for NC according to the Prandtl equation:

$$h = k \cdot \frac{\sqrt[2]{L}}{\sqrt[3]{V}}$$

where *k* is a constant, *L* the length of surface in flow direction, and *V* the relative velocity of flowing liquid against a flat surface [143]. Consequently, in addition to the surface effect, the simultaneous increase of the saturation solubility and the decrease of the diffusion distance increase the concentration gradient $(c_s\text{-}c_t)/h$, and this in turn facilitates the dissolution rate according to the Noyes-Whitney equation. Finally, both improvements result in elevated bioavailability when compared to larger sized materials. Based on these equations and the observation of van Eerdenbrugh et al. only an increase in solubility of 15% would be reached [144]. Hence, more factors may affect the solubility including changes in the crystal lattice due to different breaking sites caused by different forces. Also conceivable is the increase in surface wettability due to the use of surfactants as stabilizer.

1.5.1.3 Adhesiveness

Nanocrystals possess a third special feature, namely increased adhesiveness [145]. Their enlarged surface enables more interaction forces between the NC and the surface. Additionally, many small particles can cover a surface much more densely than larger particles leading to higher numbers of contact points and thus to a larger contact surface area. These circumstances allow NC to adhere longer onto the gastrointestinal mucosa after oral ingestion and thus to a forced uptake at this place. Consequently, higher bioavailability is observed. Besides the oral application, the adhesiveness is also beneficially applied to the skin and lung.

1.5.1.4 Stability

Nanocrystals are produced in a liquid medium and for this reason, a solid in liquid dispersion is created, i.e. a nanosuspension. Due to the large surface area and adhesiveness, nanosuspensions are thermodynamically unstable. Physically, the high interfacial free energy is described by the Gibb's equation:

$$\Delta G = \gamma_{SL} \cdot \Delta A - T \cdot \Delta S$$

Where ΔG is the surface free energy, γ_{SL} the interfacial tension between the solid and liquid interface, ΔA the change in surface area, *T* the absolute temperature, and ΔS the change in entropy of the system. To reduce the surface energy of the system, nanoparticles (of all kinds) tend to either dissolve

incipient crystalline nuclei or agglomerate small particles. To prevent this, stabilizers need to be added to the system, which can be illustrated by the DLVO theory, named after Boris Derjaguin, Len Landau, Evert Verwey, and Theodoor Overbeek [146]. The total potential energy V_T is used to describe how particles behave at a certain distance from each other. It is a function of the attractive Van-der-Waals forces and the electrostatic repulsion due to the so-called double layer of counterions (**Figure 6 A**). When two particles are approaching, they will agglomerate, defined as loosely bound particles due to weaker attractive forces and found in the secondary minimum. However, closing in and overcoming the energy barrier, they reach the primary minimum and thus aggregate, meaning that the particles fuse with permanent bonds between them.

The mechanisms of stabilizers can be classified as electrostatic repulsion and steric shielding where both are conducted by the addition of ionic and non-ionic surfactants or polymers to the dispersant, respectively. In electrostatic stabilization, ionic charges are adsorbed on the particle surface, leading to mutual repulsion forces between the particles and thus increasing the energy barrier (**Figure 6 B**) [147,148]. In contrast, steric stabilization is mainly obtained by amphiphilic non-ionic stabilizers and can be explained by the solvation effect as follows: the non-ionic macromolecules arrange at the solid-liquid interface, where they are adsorbed onto the particle surface by an anchor group, while the well soluble tail segment enters the medium. These stabilizer tails can penetrate each other whenever two particles are approaching (**Figure 6 C**). However, if the medium is a good solvent for the stabilizer molecules, the adsorbed segments cannot interpenetrate because the resulting de-solvation is thermodynamically unfavorable [149]. Similar to the micelles, steric stabilization is relatively unaffected by the presence of electrolytes in the media, compared to stabilization by electrostatic repulsion. Hence, by considering the changes in pH along the gastrointestinal tract, steric stabilization offers advantages over electrostatic repulsion. Also, steric shielding is effective for both, aqueous and non-aqueous dispersion media.

Electrosteric stabilization means the combination of both and is achieved using a non-ionic polymer together with an ionic surfactant or by applying a surfactant containing a polymeric chain and a charged group in one molecule (**Figure 6 D**) [150,151].

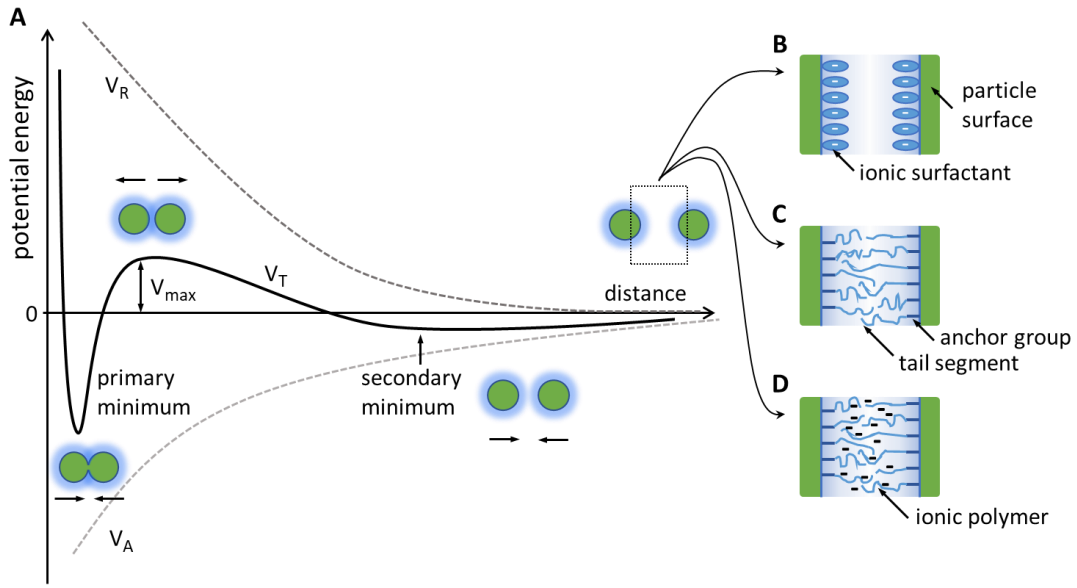

Figure 6: *A - Illustration of the DLVO theory. The total potential curve (V_T) is a function of the attractive curve (V_A) by Van-der-Waals force and repulsion curve (V_R) by electronic layer. Both opposing forces alternately prevail depending on the distance between two particles. Those can agglomerate in the second minimum or aggregate in the first minimum if they overcome the energy barrier of maximum potential (V_{max}). Stabilization can be achieved by B - increasing the electrostatic repulsion by adding ionic surfactants, C - increasing the free energy and steric shielding through dehydration in overlapping zones, and D - by a combination of these.*

1.5.2 Production methods of nanocrystals

1.5.2.1 Bottom-up methods

Classically, the bottom-up method is realized by a solvent-antisolvent method, where the API is dissolved organic solvent and then added to an anti-solvent, e.g. water. For the formation of a stable nanosuspension with the smallest particle size, a high nucleation rate, and a low growth rate are required. Both process rates are dependent on temperature, expressed by the Arrhenius function, and supersaturation state. The optimal temperature for nucleation has to be lower than the growth temperature, allowing selective optimization for nucleation. From this, the Nanomorph® technology was developed, which is able to generate NC in an amorphous state [152]. It, therefore, increases the solubility but could suffer from re-crystallization and particle growth. Another disadvantage is the use and disposal of organic solvent, increasing the costs, and requiring complex analytics and processes.

High nucleation processes concerning bottom-up methods are also achieved by solvent evaporation technologies, like freeze-, spray- and electro-spray-drying or cryogenic solvent evaporation [153]. Advantages of the bottom-up methods include its relative simplicity, low-cost equipment and the possibility for industrial scale-up. By contrast, this method needs to handle issues, such as uncontrolled particle growth and incomplete crystallization.

1.5.2.2 Top-down methods

Due to the application challenges of the bottom-up method, the more promising top-down methods are used widely for pharmaceutical purposes. The most important technologies, also used in this thesis, are high pressure homogenization (HPH) and bead milling (BM).

The main principle of HPH is the breakage of coarse material and larger crystals by cavitation forces. These are generated when the coarse suspension passes a piston-gap homogenizer with a high velocity (e.g. 500 m/s), as developed by R. H. Müller and co-workers [154]. The piston-gap size ranges about 10-25 µm in dependence on the pressure applied and the viscosity of the sample. The cavitation development can be explained as follows: According to Bernoulli's law, the flow volume of a liquid substance within a closed system is constant per cross-section. As the diameter decreases at the transition from the flow tube to the homogenization gap, the dynamic pressure increases and the static pressure decreases. As the vapor pressure equals the static pressure of the environment, the liquid begins to boil and forms gas bubbles. Upon passing through the gap, the diameter increases again, leading to an increase in static pressure and the implosion of the gas bubbles, the so-called cavitation. Besides the cavitation forces, shear forces during the gap passage occur but play only a minor role in the process of crystal breakage. Whenever the forces hit the particles, they are broken at their weak points, the imperfections. Therefore, the success of nanonization depends on the drug's hardness and structure as well as on the power density and the temperature of the suspension [155]. The power density is specified as the energy introduced per homogenization volume and time period. Based on this, the energy and the time can be increased with the pressure and repeating numerous homogenization cycles, respectively. It should be noted that there is no linear relationship between the particle size reduction and the number of HPH cycles or the pressures applied, which strongly limits the success in nanonization even at very high pressures such as 4,000 bar [156]. For this reason, HPH is usually performed at 1,500 bar and 20 cycles [104,105,157].

Based on the proportion of nano-formulations on the market, the wet BM process is dominating as BM is simple, inexpensive, and easily scalable [158]. The coarse suspension is ground in a chamber in which spherical beads and balls rotate at a speed of typically 250-400 rpm [159,160]. Different impact and shear forces between the drug particles among themselves and with the beads cause a reduction of the particle size. In order to reduce contamination in the final product due to possible abrasion of the milling beads and also to exclude interactions with the API, yttria-stabilized zirconia beads should be used [161]. The effectiveness of nanonization by BM is related directly to the bead size and can additionally be modified by milling time, the ratio of API to beads, API concentration, and milling temperature. Another vital factor is the rotational speed applied: If the rotational speed is too low, the beads do not rotate and grind enough, whereas if the speed is too high, the uniformly rotating beads can remain on the top surface of the medium without milling taking place.

1.5.2.3 Combined technologies

The use of top-down technologies requires micronized powder as the starting material, and the step-by-step application of numerous cycles with a possible cooling phase in between may lead to long process times. After that, the resulting particle size could also not be sufficiently small. To overcome these drawbacks and especially, to produce even smaller NC, several combination processes have been developed.

First, Baxter Inc. introduced the Nanoedge® technology, a combination of microprecipitation (solvent-antisolvent) and subsequent HPH in two separate steps [162]. Further improvement offers the H69® technology, which uses HPH at the time of precipitation formation [163]. For this purpose, the dissolved active ingredient of the drug is placed in the homogenization gap, while the antisolvent is added shortly before the gap is reached. H42 and H96 technology use spray-drying and freeze-drying, respectively, before further processing by HPH [164,165]. Advantages lie in the prior removal of solvents, and these dried particles are more brittle and therefore more fragile in a subsequent top-down step. Especially, spray-drying with polymers can lead to amorphous forms which may later cause difficulties of the stability by re-crystallization during storage. NanoCrySP technology can be seen as an improved concept because it forces crystallization but prevents further particle growth for example by adding mannitol and surfactants [166]. A smart combination method is the ARTcrystal® technology, which is based on an HPH step after a short-term rotor-stator use which manages without the need of solvents nor an energy-consuming pre-milling step [167].

These different production techniques were developed to improve a formulation or bring a suitable formulation to the market. Today, some products containing NC are available for different applications, which are presented below.

1.5.3 Applications of nanocrystals

Peroral administration of medication is the most popular and convenient administration route for nanocrystalline-based products, formulated as tablets/ capsules and suspension. The first pharmaceutical product on the market consisting of immunosuppressive drug sirolimus NC (rapamycin) was Rapamune® (Wyeth). It was produced by BM and is available as suspension and tablet. Other NC formulations produced by BM for oral administration include: Theodur® (Mitsubishi Tanabe Pharma), Tricor® (Abbott), Zanaflex® (Acorda), Cesamet® (Lilly) and more. Additionally, there is one NC product on the market produced by HPH, namely Triglide® (SkyePharma) containing fenofibrate [158]. Using NC for parenteral administration might have great potential for selective and controlled drug delivery to target cells and organs and the advantages of high drug loading and sterilization [168]. To avoid capillary blockage and embolism, all particles of the formulation must have and maintain a size < 5 µm, when applied intravenously. Promising NC formulations developed for an i.v.-application

include APIs such as oridonin [169], melarsoprol [170], and nevirapine [171]. Up to now the nanocrystalline product InvegaSustenna® (Johnson & Johnson) as an extended-release formulation is the only one on the market but for an i.m. application [158].

Furthermore, NC are particularly suitable for a dermal application, since their high adhesiveness combined with a high dissolution rate and solubility ensures optimal skin penetration. Antioxidants such as rutin and hesperetin were formulated in the cosmetic products Juvedical® (Juvena AG) and Platinum Rare collection (La Prairie®). Independent research groups confirmed the benefit of NC in a dermal formulation in terms of improved skin penetration. For example, tretinoin, for the treatment of acne vulgaris, demonstrated higher accumulation in the skin (dermal delivery) without diffusing through the skin into the systemic circulation (transdermal delivery) [172].

The same beneficial properties of NC can be extended to pulmonary drug delivery. Pulmonary drug absorption and bioavailability depend on the amount of the drug that is deposited and dissolved in the lung fluids. Upon deposition of the particle on the lung surface, mucociliary clearance and drug absorption act competitively. Therefore, the rapid absorption and dissolution rate directly reflects the enhancement in bioavailability, as demonstrated for the budesonide nanosuspension Nanagel® [173]. To reach the lungs, the particles must have a size of 1-5 µm. This is achieved by using a nebulizer to atomize the nanosuspension, where each droplet contains the NC. In the case of solidified NC, agglomerations and larger carrier particles might play a crucial role in successful inhalation. Detailed technological formulation principles for the pulmonary application are the subject of this thesis.

To sum up, NC can be produced and formulated to serval conditions and wishes, and they might thus represent a universal feature to enhance the bioavailability of poorly soluble drugs. The challenge is to find the right parameter like stabilizer and production conditions to produce a stable and tailor-made nanosuspension.

2 Aims of the thesis

Many newly developed APIs are poorly soluble in water. This, however, is associated with a low bioavailability and with the difficulty to reach the necessary pharmacological concentration in the blood. For this reason, technological investigations are urgently needed to handle this drawback of poor solubility. Ideally, the technological approach should be independent of the physico-chemical properties of the APIs to obtain a universal formulation principle. Such an approach is the development of drug NC. Different production methods and production conditions lead to different particle size populations. The impact of different particle sizes on the solubility and dissolution velocity but also their pharmacological effect, is not yet clear.

Therefore, the aim of this thesis was the development, characterization, and testing of tailor-made NC. The three different antioxidants BI-6C9, hesperetin and rutin, were chosen because of their great potential in treating oxidative stress-related diseases, i.e. for the treatment of AD and COPD. The different diseases require different administration routes, where specific formulation requirements, such as the particle size and excipient compatibility, need to be considered.

This thesis was subdivided into three independent parts, where the aims are described as following.

It was first aimed to develop a formulation to increase the solubility of the synthetic compound BI-6C9 for the treatment of AD. For this, tailor-made NC should be produced and optimized regarding stability using surfactants that can be applied intracortical or intraventricular. In this context, a rapid method should be investigated to find the suitable stabilizer for the API, even before the production of the NC to reduce time and costs in the future. Also, the API should be formulated in an amorphous state by using mesoporous silica particles. These two technological approaches should be compared with each other in terms of physical stability and pharmacological effect in a cell culture model.

The second aim was to produce tailor-made hesperetin NC for the treatment of AD. The differently sized particle populations should be produced by different production methods and conditions, then characterized regarding kinetic solubility, dissolution velocity and crystallinity, and finally tested in a cell culture model for the early and progressed AD. By testing different particle sizes, a size-dose-correlation should be investigated.

Finally, a dry powder for inhalation should be developed containing rutin NC for the treatment of COPD and asthma. Different stabilizers suitable for pulmonary application should be investigated for their ability to physically stabilize rutin NC for one year or more. The aim was also to develop a technological method that ensures microbiological, chemical, and physical stability without the need for additional additives such as preservatives. The idea behind this, was that a long-term stable nanosuspension would also be best for its scalability to larger process volume and subsequent formulation steps.

Thereafter, the process transfer from a small to a larger batch volume should also be investigated in terms of particle size and stability. After the most suitable NC formulation was identified, different methods for drying the nanosuspension should be applied to produce an inhalable powder. This powder should be characterized and optimized in terms of the particle size of the NC in this formulation, the antioxidant capacity and the aerodynamic property. The perfect dry powder formulation should exhibit similar properties to the nanosuspension such as an increased dissolution velocity, increased solubility and ideally a better pharmacological effect when compared to the bulk material. Hence, it was aimed to create a tailor-made dry NC formulation for the treatment of oxidative stress-related diseases in the lung.

3 Materials and Methods

3.1 Materials

3.1.1 Active pharmaceutical ingredients

In this thesis three antioxidative active pharmaceutical ingredients: BI-6C9, hesperetin and rutin were formulated (**Figure 3** and **4**).

The compound BI-6C9 was kindly synthesized by the working group of Prof. Dr. Martin Schlitzer (Department of Pharmaceutical Chemistry, Marburg, Germany), by a modified scale-up [79]. In addition, BI-6C9 was purchased as standard from Sigma-Aldrich Chemie GmbH (Germany).

The flavanone aglycone hesperetin, (S)-2,3-dihydro-5,7-dihydroxy-2-(3-hydroxy-4-methoxyphenyl)-4*H*-1-benzopyran-4-one, was purchased from Exquim S.A. (Spain), and an analytical reference was obtained from (Sigma-Aldrich Chemie GmbH, Germany).

The flavonol glycoside Rutin, 2-(3,4-dihydroxyphenyl)-3,5,7-trihydroxy-4*H*-1-benzopyran-4-one-3-O-glucorhamnosid, was purchased from Denk Ingredients GmbH (Germany). The calibration curve was created by using the analytical standard of rutin from TCI chemicals (Japan).

3.1.2 Stabilizers

Stabilizing the amorphous state was realized by using AEROPERL® 300 (in the following abbreviated as aeroperls), obtained as a gift from Evonik Industries AG (Essen, Germany). For the stabilization of NC surfactants and polymers were used as listed in **Table 1**.

Table 1: *Overview of all nanocrystal's stabilizer used.*

stabilizer	Abbreviation, other names	Type	Company (Germany)
Bovine serum albumin	BSA	polypeptide	Thermo Fisher Scientific Inc.
Lecithin E80	E80, egg lecithin	mixture of phospholipids	Lipoid GmbH
Lecithin S75	S75, soy lecithin	mixture of phospholipids	Lipoid GmbH
Plantacare® 2000 UP	PLC	alkyl (8 – 16) glucoside, non-ionic	BASF SE
Poloxamer® 188	PLX, Kolliphor P188	triblock copolymers (A-B-A), non-ionic	BASF SE
Polyvinyl alcohol 4-88	PVA, Poval 4-88, Mowiol 4-88	water soluble synthetic polymer, increasing viscosity	Kuraray Europe GmbH
Sodium dodecyl sulfate	SDS	anionic	Carl Roth GmbH & Co. KG
Span® 20		Sorbitan monolaurate, non-ionic	Croda GmbH
Tween® 80	Tw80, Polysorbat 80	Polyoxyethylene (20) sorbitan monooleate, non-ionic	VWR International GmbH

3.1.3 List of other chemicals and materials

Purified water was obtained from a PURELAB® flex 4 equipped with a point-of-use biofilter (ELGA LabWater, UK) and used for all experiments. The preservative Euxyl® 9010 consists of 90% (w/w) 2-phenoxyethanol and 10% (w/w) of 1,2-propanediol as ready-to-use mixture from Schülke & Mayr GmbH (Germany). All solvents were of analytical grade and used as received. Further chemical compounds used for analysis, *in-vitro* assays and cell studies, are listed in **Table 2**.

Aeroperl® 300 was a gift from Evonik (Germany). Other materials included plastic ware intended for single-use such as pipette tips (10, 200, 1,000 µL) utilized with the corresponding single- and multi-channel pipettes ranging from 1-20, 20-200 and 100-1,000 µM (Brandt, Germany). Petri dishes for cell culture, safe-lock microcentrifuge tubes, 20 and 50 mL screw capped tubes were purchased from Sarstedt (Germany) and 0.2 µm pore size syringe PP-membrane filters from VWR (Germany). Nunclon Delta, flat bottom 96-well microplates were used from Thermo Fisher Scientific (Germany). The size 3 hard capsule shells were a gift from ACG (India) and are made of hydroxypropyl methyl cellulose.

Table 2: *List of the chemicals used.*

compound	origin
Ascorbic acid	Sigma-Aldrich Chemie GmbH, Germany
Brij® 35	Thermo Fisher Scientific, Germany
Cysteine	VWR, Germany
DCFDA	Abcam, Cambridge, UK
DMEM	Capricorn Scientific, Germany
DPPH	Sigma-Aldrich Chemie GmbH, Germany
fetal calf serum	Thermo Fisher Scientific, Germany
Isomalt	BENEO GmbH, Germany
Lactose	FlowLac 100 and InhaLac 500 from Meggle, Germany
Lipopolysaccharide	Sigma-Aldrich Chemie GmbH, Germany
Magnesium stearate	Carl Roth, Germany
Mannitol	Carl Roth, Germany
Methylenblau	Carl Roth, Germany
MTT	Sigma-Aldrich Chemie GmbH, Germany
Müller-Hinton agar	Sigma-Aldrich Chemie GmbH, Germany
NaOH	Carl Roth, Germany
Potassium dihydrogen phosphate	Merck KGaA, Germany
RPMI 1640	Capricorn Scientific, Germany
Sodium chloride	Carl Roth GmbH Germany
Sodium hydrogen phosphate	Merck KGaA, Germany
Soy saccharide	Emcosoy® from JRS Pharma, Germany
tert-Butyl hydroperoxide	Thermo Fisher Scientific, Germany
Triton X-100®	Sigma-Aldrich Chemie GmbH, Germany

3.2 Methods

3.2.1 Production of drug loaded mesoporous silica particles

For embedding BI-6C9 into mesoporous silica particles, aeroperls were used. These are highly pure and amorphous colloidal silicon dioxide granules with a particle size in the range of about 20-60 µm, a pore volume of about 1.7 mL/g, and a specific surface (by BET) of about 300 m^2/g. Loading of BI-6C9 into aeroperls was performed according to Hespeler et al. [133] with modifications: 40 mg of the aeroperls were added to 20 mg of BI-6C9 being completely dissolved in ethyl acetate. Then, ethyl acetate was removed by using a rotary evaporator (Hei-VAP Core, Heidolph, Germany) at 300 mbar for 4 h at 45 °C followed by a second drying step at 80 mbar for 10 min. After the removal of the solvent, the dried aeroperls were analyzed by microscopy.

3.2.2 Production of nanocrystals

Three approaches, bead milling, high pressure homogenization and ARTcrystal®-technology, for the production of NC were performed in different ways to obtain tailored particle sizes and quantities.

3.2.2.1 Bead milling

Bead milling (BM) is a suitable method to produce NC in a small scale batch size of a few milliliters, that allows pre-investigations of the expensive and quantity limited API, and also gives a hint for appropriate formulations without a large amount of waste [174]. For this reason, BM was applied to BI-6C9. The BM approach has also the advantage of yielding to smaller particle sizes compared to HPH [175], which is why it was used for tailor-made hesperetin NC.

3.2.2.1.1 BI-6C9

NC from the API BI-6C9 were produced by a small scale wet BM process, modified after Romero et al. [174]. For this, a 4.5 mL amber glass vial was filled with 10.6 g yttria-stabilized zirconia milling beads (diameter 1 mm, Retsch, Germany), 4 stirring bars (10 x 6 mm) and 2 mL aqueous suspension containing BI-6C9 and surfactant (each 0.5%, w/w). Pre-micronized BI-6C9 was obtained by crushing with a mortar and pestle. SDS and Tween 80 were used as stabilizers. Finally, the filled vials were stirred on a magnetic stirrer (RCT standard, IKA, Germany) at 1,500 rpm in ice water (0 °C) for 24 h and 90 h, respectively. The production processes were carried out in triplicate.

3.2.2.1.2 Hesperetin

Hesperetin NC were produced by BM for two different applications: once as part of a tailor-made study for the treatment of Alzheimer's disease in cell culture study and once to produce a nanosuspension for pulmonary use against COPD and asthma. The different administration routes require varying sizes and stabilizers.

Hesperetin NC against AD were produced by BM according to Romero et al. [174] with a couple of alterations: the vial was filled with 11.0 g of g yttria-stabilized zirconia milling beads (diameter 1 mm), 1.75 mL of the aqueous dispersion that contained hesperetin and Plantacare® 2000 (PLC) as stabilizer in a concentration of 5% and 1% (w/w), respectively. The preparation was stirred on a magnetic stirrer at 1,200 rpm for 8 h, with the vial placed in ice water (0 °C) throughout the procedure.

3.2.2.2 High pressure homogenization

HPH was used to produce rutin and hesperetin NC by using a Micron LAB 40 (GEA, Germany). It possesses a batch size of 40 mL allowing the production of adequate quantities for further investigations such as monitoring of long-term stability or subsequent formulation steps. That was exploited for the development of rutin NC for the pulmonary application. This production method represents a discontinuous process, whereby the suspension undergoes a defined number of cycles at a specified pressure [155]. Hence, by varying the number and pressure of the HPH cycles, tailor-made hesperetin NC were produced for the treatment of AD.

3.2.2.2.1 Rutin

All formulations were composed of 5% coarse rutin (w/w) and 1% surfactant or 1% surfactant mixture (w/w) in purified water up to 50.0 g. Surfactant mixtures were formulated in equal parts (50/50), except for the lecithin-Tween-mixtures, which have been composed in a 33.3 : 66.7 ratio (lecithin : Tween 80). After the coarse bulk suspension was prepared, they were pre-milled by HPH with increasing pressure each 3 cycles of 250, 500, 750 and 1,000 bar. Subsequently, the main HPH was performed at 1,500 bar for 20 cycles. Between all HPH cycles, the suspensions were manually and strictly cooled under 10 °C in ice water bath. The effectiveness of the milling was verified by monitoring the particle size reduction after the last pre-milling step and after 1, 5, 10 and 15 HPH cycles. Nanosuspensions obtained were filled in falcon tubes, stored in the fridge, and characterized regarding size after 1, 7, 14, 28, 60, 90, 180 and 365 days of storage.

3.2.2.2.2 Hesperetin

Tailor-made hesperetin NC were produced similarly to the rutin NC according to the concentrations of API and stabilizer as well as the cooling condition. The differences are the number of cycles and pressure which are summarized in **Table 3**. All hesperetin suspensions used for the investigation of Alzheimer's diseases were stabilized by PLC.

Table 3: *Summary of the production conditions to create the tailor-made hesperetin NC. Formulation A-H was produced by using HPH, whereas for formulation I the BM was applied. The formulations B-H result cumulatively from the previous formulation.*

formulation	prerequisite	pressure [bar]	number of cycles
A	bulk suspension	200	5
B	formulation A	300	5
C	formulation B	500	5
D	formulation C	500	5
E	formulation D	500	5
F	formulation E	700	3
G	formulation F	900	5
H	formulation G	1,500	20
I	bulk suspension	produced by BM technique	

3.2.2.3 ARTcrystal®-technology

For producing higher quantities of rutin NC the ARTcrystal®-technology according to Scholz and Keck was applied, where coarse rutin was dispersed in an aqueous surfactant solution to a final concentration of 5% rutin and 1% surfactant (w/w) [167]. At first, the suspension was pre-milled by a MICCRA D-27 (Miccra, Germany) at 24,000 rpm for 5 min and subsequently homogenized by an EmusiFlex C50 (Avestin, Germany) at 20 cycles. By using the EmusiFlex C50, it is possible to produce NC in a continuous process without changing vessels or suspensions. However, the temperature of suspensions increases during the process, which could lead to larger particles due to Ostwald ripening. Furthermore, it cannot be guaranteed that each particle passes through the homogenization gap the same number of times. Therefore, the process was carried out semi-continuously, i.e. the entire suspension has been transferred from one vessel via HPH into another allowing counting of cycles. During and between the cycles, the suspension was strictly cooled to below 10 °C using an ice water bath (0 °C).

3.2.3 Characterization of nanocrystals

Regardless of the production condition or API used, all NC were thoroughly characterized for size, shape, stability, and zeta potential.

3.2.3.1 Dynamic light scattering

Dynamic light scattering also known as photon correlation spectroscopy (PCS) is a common technique for size measurements of nanomaterials in a range between 0.3 up to 5,000 nm depending on the particle density. The measurement is based on the fluctuations of non-invasive back-scattered laser light (back-scatter angle of 173°) due to the particle diffusion in dispersion media caused by Brownian motion. This leads to time-dependent fluctuations in the intensity of the scattered light, with smaller

particles having a higher scattering velocity than larger ones [176]. Particle size and diffusion coefficient are related to the Stokes-Einstein-equation which is used to calculate the intensity weighted hydrodynamic mean diameter (also called average particle size) and the polydispersity index (PdI). The PdI is a dimensionless value between 0.0 and 1.0, and an assumption for the distribution width of the population. A PdI of 0.0 indicates a monodisperse population, below 0.1 a narrow size distribution, and above 0.5 broad particle size distribution [177]. For the measurements, the nanosuspensions must be diluted until a weakly tyndallizing dispersion has been obtained so that the light beam is not scattered or absorbed by too many particles before its detection. Otherwise, it would result in more fluctuating light intensities and would imply smaller particles. If the dispersion is too diluted, no clear signal would be obtained.

All samples were diluted in distilled water and then characterized using the Zetasizer NanoZS (Malvern-Panalytical, Germany) in ten sub-runs at 22 °C to calculate the means and standard deviations (SD).

3.2.3.2 Laser diffraction

Since larger particles or agglomerates can easily be overlooked with the PCS or are outside its detection range, laser diffraction (LD) provides an ideal complement to the particle size characterization [178,179]. In laser diffraction measurement, a laser beam passes through a disperse particle sample and measures the resulting angle-dependent scattered light intensity. From this, particle size distribution is calculated as volume weighted diameter by Mie theory in a range between 10 nm and 3.5 mm [179]. The results are expressed as d(v)0.50, 0.90, 0.95, and 0.99 as a measure of the distribution and indicator for the presence of larger particles and agglomerates, respectively. The d(v)0.5 value indicates that 50% of all particles are as large or smaller than the measured size. Conversely, the d(v)0.99 value gives a hint of a small fraction of larger particles and agglomerations.

In this thesis, LD measurements were performed using a Mastersizer 3000 (Malvern-Panalytics, Germany) equipped with a Hydro MV unit being filled with purified water. The optical parameters for rutin and hesperetin were 1.57 and 1.59, respectively for the refractive index and 0.01 (both) for the imaginary refractive index [105]. The measurements were carried out in five sub-runs with a measuring time of 10 s each with red light (632,8 nm) and then blue light (470 nm).

3.2.3.3 Light microscopy

The previously described measurement techniques for size characterization (LD and PCS) provide only a simplified representation of the particles, i.e. particle sizes are calculated as perfect spheres, where aggregations and agglomerations cannot be distinguished from microparticles.

For a deeper understanding of shape and tendency for agglomeration, microscopy was applied by using an Olympus BX53 light microscope (Olympus Cooperation, Japan), which is equipped with an Olympus SC50 CMOS color camera (Olympus soft imaging solutions GmbH, Germany).

3.2.3.4 Zeta potential

The physical long-term stability of the nano-formulations produced was estimated by zeta potential (ZP) measurements. Applying an electric field causes the particles to move to the opposite pole of their natural charge. The measuring principle of laser Doppler anemometry is used to determine the velocity of particles where the higher charged particles exhibit a higher velocity [180]. Hence, zeta potentials were calculated from the electrophoretic mobility of the particles by the Helmholtz-Smoluchowski equation at 22°C using the Zetasizer NanoZS (Malvern-Panalytics, Germany).

The ZP measurements were performed by diluting the samples in water which was adjusted to a conductivity of 50 µS/cm with sodium chloride. Further information about the stabilizing ability of the surfactant can be obtained by analyzing the ZP in the original medium, i.e. in 1% respective surfactant solution.

3.2.3.5 Determination of crystalline state

The crystalline state of the NC and the raw material was determined by X-ray diffraction. The X-rays are diffracted at the electron shell of the irradiated atoms. The thus diffracted waves - emitted by the individual atoms - interfere with each other, with constructive or destructive interference depending on the distance between the atoms. Since crystals consist of three-dimensional and periodically arranged atoms, constructive interference occurs only for very specific angles, which are described by the Bragg's law:

$$n\lambda = 2d \cdot \sin(\theta)$$

where λ is the wavelength of the beam, n is any integer, d is the spacing between diffracting planes and θ is the incident angle. Thus, constructive interference can only arise when its path-length difference $2d \cdot \sin(\theta)$ is equal to an integer multiple of the wavelength λ (**Figure 7**). In such a case, the incident beam is deflected by an angle 2θ, creating a reflection spot in the diffraction pattern.

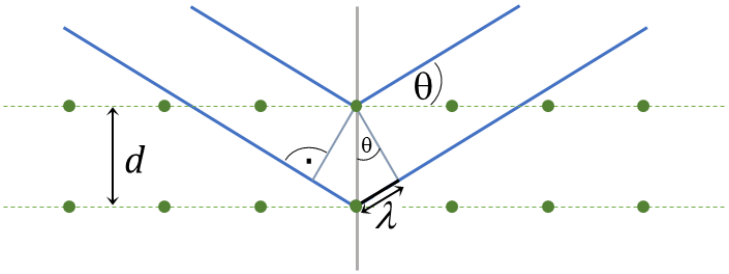

Figure 7: *Schematic image of a section of a crystal lattice on which X-rays interact. At the correct angle θ and wavelength λ, the incoming beam is scattered in the same direction at all atoms on lattice planes that behave like semi-transparent mirrors.*

A X'Pert Pro MPD powder X-ray diffractometer with a PIXcel detector (Panalytical, The Netherlands) and a Coα radiation source (λ = 1.54187 Å) was used to characterize the crystallinity. Samples were measured to CoKα radiation (40 kV, 35 mA) at a scanning rate of 2.4°/min between 10° and 70° 2θ with a step size of 0.039° 2θ. To enhance the viscosity of the liquid suspensions, locust beam gum (3% (w/w)) was added to the aqueous suspensions prior to the measurements. This was done to avoid the need for drying of the samples before analysis, which in turn could induce crystallization or crystal growth and thus lead to changes in the crystalline structure of the original suspensions.

3.2.4 Determination of microbiological stability

3.2.4.1 Preservation

Directly after production of the rutin nanosuspensions stabilized by PLX and PLC, they were equally separated each into two fractions where one of them was preserved by adding Euxyl PE9010 to a final concentration of 1.0% (w/w) while the other fraction remained non-preserved. Euxyl PE9010 is a liquid preservative, suitable for leave-on and rinse-off, stable against temperature (< 120 °C), pH (< 12) and hydrolysis. It consists of 90% phenoxyethanol and the addition of 10% ethylhexylglycerin impacts the interfacial affects the interfacial tension at the cell membrane of microorganisms, allowing to improve the preservative activity of phenoxyethanol.

3.2.4.2 Determination of the microbiological contamination in the nanosuspensions

To assess the biological stability of differently stored rutin NC (preserved and non-preserved), the agar plate test based on Ph. Eur. 8, method 2.6.12, was used. For this, the Müller-Hinton agar was dispersed in water, autoclaved using a Truttnauer 3850 ELC (Truttnauer GmbH, Linden, Deutschland) and directly filled into sterile petri dishes (60 mm in diameter) freshly at the day of seeding. Immediately after the agar has cooled down to a solid gel, 10 µL of the (non-diluted) nanosuspension or 10 µL of a 1:100 dilution in water were distributed evenly over the entire surface using a cell spreader. The ager plates (layered with non-diluted and diluted nanosuspension) were then incubated for 24 h at 36 °C and 90% humidity to induce the growth of bacteria. Another layered (non-diluted) agar plate was stored for 7 days at 25° C in a climate chamber to detect a possible contamination of fungi. After the incubation times, the visible bacterial colonies were counted, and the presence of fungal growth was noted. In this study, if a dense colonization of bacteria onto the agar surface was detected, the number of colony forming units (CFU) was set to 10,000 CFU/µL.

3.2.5 Determination of antioxidant capacity

The antioxidant capacity (AOC) was determined by a radical scavenging *in-vitro* assay, where the stable free radical 2,2-diphenyl-1-picrylhydrazyl (DPPH or ·DPPH) changes its dark-violet color to yellow through a reduction reaction (**Figure 8**), e.g. when reacting with an antioxidant. The reduction of DPPH

correlates with the decrease in absorbance that was measured spectroscopically at 517 nm. As a measure for the AOC, the percentage inhibition activity was calculated as:

$$\text{inhibition } [\%] = \left(1 - \frac{\mathrm{A_{sample}}}{\mathrm{A_0}}\right) \cdot 100,$$

where A_{sample} is the absorbance with sample and A_0 is the absorbance of the DPPH-solution without any further excipients. The calculated inhibition was graphically plotted over the concentration and the resulting curve was used to determine the IC_{50}. Thus, the IC_{50} value – the concentration at which 50% of the given DPPH-radicals were metabolized – was used to compare the formulations among each other. An incubation time of 30 minutes in the dark is advised according to the standard protocol [181]. Additional investigations were performed after an incubation time of 5, 10, 20 and 45 min in the dark for further insight into the reaction velocity.

For rutin nanosuspensions, 100 µL of sample diluted in methanol (0.3 – 20 mg/L) were added to 100 µL of a 0.1 mg/mL methanolic solution of DPPH. Ascorbic acid as a strong antioxidant and the lyo-protectants mannitol and cysteine were used as controls.

For hesperetin, the same procedure was performed with the difference of using ethanol instead of methanol for diluting the hesperetin nanosuspension (0.01 – 1.5 mg/L) and solving DPPH.

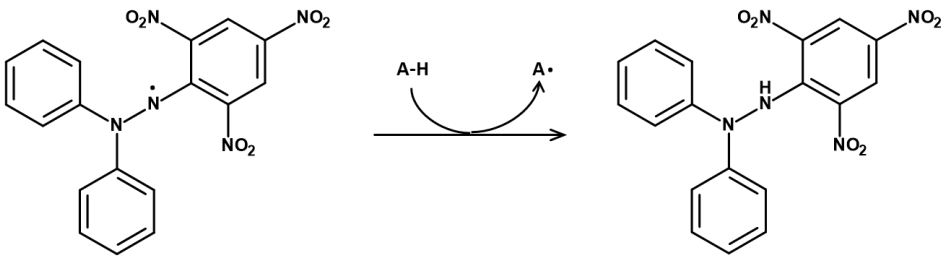

Figure 8: *Reaction of the ·DPPH radical with an antioxidant (AH) to its reduced form ($DPPH_2$).*

3.2.6 Drying of the nanosuspensions

Rutin nanosuspensions were dried in two different ways to increase physical, biological and chemical stability and to obtain a more versatile form. A dry powder can easily re-dispersed but can also be formulated into a solid dosage form or - as aimed in this thesis - into a powder for inhalation.

3.2.6.1 Spray-drying

Widely used in the pharma and food industry, the spray-drying process is a fast and gentle method for drying solutions and dispersions. This method was used in this thesis to dry the nanosuspensions while producing inhalable particles at the same time. The mechanism consists of atomizing the solution, transporting the generated fine droplets with a pre-heated air stream, and drying them meanwhile.

On the way, the water evaporates very quickly because the droplets with their small size offer a large surface area. Due to a cyclonic separator mechanism, the dried particles are separated from the air stream and retained in the collection vessel. By modifying various parameters such as the in-let temperature, airflow volume and humidity, and the feed rate and viscosity, the final product can be tailored regarding the yield, residual moisture, particle size and distribution. However, depending on the in-let air volume, small and light particles might be entrained with the airflow in the cyclone [182].

In the present work, three different rutin nanosuspensions stabilized with Poloxamer® 188 (PLX) only or with mixtures of BSA and Tween 80 or BSA and PLX, each obtained by the continuous scale-up batch, were spray-dried using a B-190 mini spray-dryer (Büchi, Switzerland). Mannitol or lactose was added as a carrier to avoid the formation of pure NC, which could agglomerate or be discharged with the airflow. The settings and concentrations are summarized in **Table 4**.

Moreover, the nozzle was blown free every minute by an extra pressure to reduce clogging. The resulting dried powders were analyzed under the microscope and re-dispersed with water to verify particle stability during the process, i.e. re-dispersed suspensions were characterized by PCS and LD regarding particle size and distribution.

Table 4: *Summary of the spray-drying trials with the differently stabilized rutin nanosuspensions. Various concentrations of mannitol (M) or lactose (L) served as carrier and were dissolved in the suspension before atomization. The gas spray flow was set to 600 l/h in all experiments, whereby parameters such as airflow and inlet and outlet temperatures were varied.*

N°	stabilizer	quantity [g] of			in-let [°C]	out-let [°C]	airflow [L/min]
		additive	water	NS			
SD1	BSA + Tween 80	2.5 (M)	27.5	20.0	63	48	160
SD2		1.5 (M)	18.5	30.0	63	49	160
SD3		1.5 (L)	18.5	30.0	63	50	160
SD4		1.5 (L)	18.5	30.0	107	77	160
SD5	BSA + PLX	4.0 (M)	-	50.0	89	63	110
SD6		4.0 (M)	-	50.0	151	101	102
SD7		6.0 (M)	-	50.0	120	90	120
SD8	PLX	4.0 (M)	-	50.0	63	52	160
SD9		4.0 (M)	-	50.0	90	66	110
SD10		4.0 (M)	-	50.0	150	101	100
SD11		4.0 (M)	-	50.0	148	100	110
SD12		4.0 (M)	-	50.0	148	100	120

3.2.6.2 Freeze-drying

Lyophilization, also known as freeze-drying, is based on the sublimation of water from a frozen state directly into the vapor phase by lowering the pressure to a few millibars. This means that there is no melting under any circumstances and consequently all dissolved molecules retain their confirmation and place in the initially frozen solution. After the removal of all water, a (fragile) porous structure is obtained, which is hygroscopic due to its extremely high surface and can be thus re-dispersed quickly. Produced by the scale-up batch, the rutin nanosuspensions stabilized with PLX, PLX/BSA mixture and Tween 80, respectively, were freeze-dried using the ALPHA 1-4 LSC (Martin Christ Gefriertrocknungs-anlagen GmbH, Osterode am Harz, Germany). For this purpose, 3 g nanosuspension were transferred to 8 mL glass-vials in which mannitol and cysteine as cryo-protectants were added to a final concentration of 0, 80, 120 and 150 mg/$g_{suspension}$ (corresponding 0, 160, 240 and 300% relative to rutin). Additionally, lactose, soy saccharides, and isomaltose were added in each case to a rutin nanosuspension stabilized with PLX to a final concentration of 80 mg/$g_{suspension}$ (corresponding 160% to rutin). Care was taken to freeze the samples quickly to avoid agglomerations. The main drying step was performed at 0.1 mbar for 24 h while secondary drying was not necessary.

The vials with the freeze-dried samples, lyophilizates, were sealed under atmospheric pressure and stored at room temperature in the dark until further investigations. The lyophilizates obtained were characterized regarding particle size and distribution of the incorporated NC by re-dispersing in water and measuring subsequently via PCS, LD and light microscopy. Light microscopy was additionally used to investigate the lyophilizate's macro-structure, i.e. the extent to which the NC are aligned in the matrix. Freeze-dried rutin NC stabilized with PLX were also characterized after six months and one year of storage at room temperature to ensure that neither particle growth and recrystallization nor collapse have occurred.

3.2.7 Release studies

3.2.7.1 Preparation of phosphate buffer solution (pH 6.8)

For the dissolution studies, a phosphate buffer was freshly prepared as follows: 69.36 g potassium dihydrogen phosphate (KH_2PO_4) and 87.05 g sodium hydrogen phosphate ($Na_2HPO_4 \cdot 2\,H_2O$) were completely dissolved in 5 l water and then adjusted with sodium hydroxide if necessary to a pH value of 6.8.

3.2.7.2 Solubility determination

The aqueous solubility of coarse bulk material (rutin or hesperetin) was analyzed using a stirrer (RCT basic, IKA, Germany) for 24h at 37 °C. For this, excess rutin and one stirring bar were added to a flask, which was tightly closed after filling with water or phosphate buffer, respectively [183]. Thereafter,

samples were filled in 1.5 mL safe-lock tubes and centrifuged for 30 min at 14,000 rpm, where the resulting supernatant was quantified directly by UV-spectroscopy (rutin) or HPLC (hesperetin).

3.2.7.3 Dissolution behavior

All dissolution studies were performed using a USP II paddle apparatus (Pharmatest, PTWS 120D, Germany) at 37 ± 0.5 °C and a rotating speed of 100 rpm in accordance with the FDA dissolution method for suspensions [184,185].

Tailor-made hesperetin NC were added to the vessels filled with 900 mL of purified water and the dissolution studies were performed in non-sink conditions, i.e. in saturated medium. The amount of added hesperetin was 24.57 mg for each formulation resulting in a final concentration of 27.3 mg/L. For this, the accurate total amount of hesperetin in each suspension was quantified and then calculated individually for each formulation, because the different production methods led to slightly different content in final formulations. Reasons for this are for example the adsorption of some hesperetin to the beads in the BM process or sedimentation of larger non-homogenized particles to the bottom of the product container during the discontinuous HPH process used in this study. The exactly required volume of each hesperetin formulation was therefore calculated after the hesperetin content was analyzed by HPLC analysis for each formulation individually. After predetermined time intervals, samples of 1 mL were drawn, and the equal volume was re-filled with fresh medium. To ensure the complete retention of the non-dissolved particles within the collected samples, all samples were filtered directly through 0.22 µm filters, and centrifuged for 30 min at 14,000 rpm, immediately after drawing the samples. The amount of dissolved hesperetin was determined by HPLC analysis. Experiments were performed in triplicate and the results are presented as mean ± SD.

Tailor-made rutin NC were added to the vessels filled with 400 mL purified water and phosphate buffer (pH 6.8), respectively. The dissolution studies were performed in sink conditions, i.e. with a rutin concentration of 10% from its determined kinetic solubility. For this, the accurate total amount of rutin in the lyophilizates, suspensions and coarse material was analyzed by UV spectroscopy and calculated. The calculation is based on the results of the solubility study (c.f. section 3.2.7.2), and the individual amount needed for each formulation was added to the vessels allowing for compliance with the sink conditions. Samples of 2 mL were withdrawn after 5, 10, 20, 30, 45 and 60 min, filtered through a 0.22 µm pore-size filter, centrifuged immediately in a safe-lock microcentrifuge tube at 14,000 rpm for 30 min and their supernatants were quantified. Preheated medium was added to the vessel directly after sampling to re-fill them to 400 mL. Dissolution tests were carried out in triplicate and the results are presented as mean ± SD.

3.2.8 Determination of the aerodynamic properties

3.2.8.1 NGI

Apart from the patients' physiology, such as humidity and respiratory flow, the physical properties of the particles, such as density and shape, play a major role in their separation from the gas phase [186]. Hence, the determination of aerodynamic properties deals with the ability of the generated particles to be inhaled. For this, a Next Generation pharmaceutical Impactor (NGI), an advanced high-performance cascade impactor with seven stages, has become the standard used in the Ph. Eur. and USP guidelines. In general, the functional principle of cascade impactors consists of separating the particles from a moving gas stream due to their mass-inertia. This occurs when a particle moving in a gas stream cannot follow a change in direction of this gas stream and thus encounters where it is deposited, also called impaction. Coating with an adhesive layer ensures that deposited particles are kept on the stages. In the NGI, the airflow is directed horizontally and zigzaggingly over the successive stages 1 to 7 (one hole with a diameter of 14.3 mm to 630 holes with a diameter of 0.206 mm each) and a “micro-orifice-collector (MOC)” as final retention mechanisms (**Figure 9**). Depending on the flow rate of the carrier gas used, particle sizes ranging from 0.24 µm to 11.7 µm can be collected.

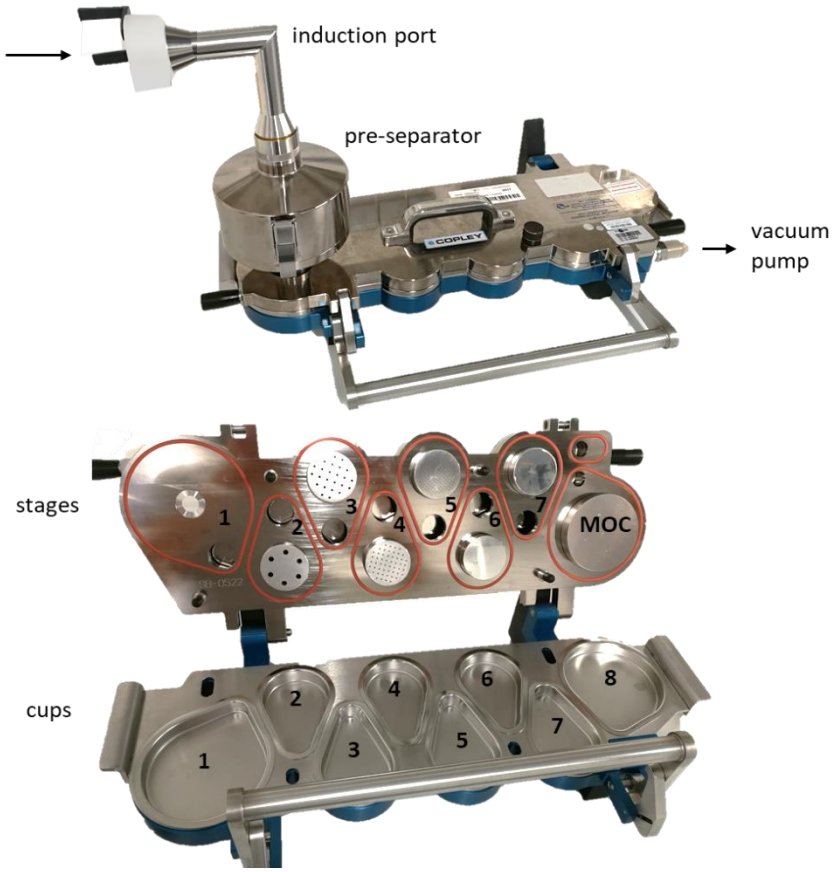

Figure 9: *Design of the complete NGI ready for use (upper), and the opened impactor body with its seven stages and MOC (lower).*

In this work, the aerodynamic particle size distribution was determined by using the NGI from Copley Scientific AG (UK) (**Figure 9**), according to the Ph. Eur. 8, method 2.9.18. The pre-separator was filled with 15 mL purified water, while 1.0 mL coating agent was filled in the first cup, 0.25 mL in the second to seventh cup and 0.5 mL in the last cup. The coating agent consists of 4 parts 15% aqueous Brij L23 solution (w/w) and 6 parts glycerin. Prior to each NGI run, an airflow rate of 60 L/min was verified for the test period of 4 s, resulting in a total air volume of 4 L. Spray-dried rutin NC powder was used directly without any further processing, filled in capsules size 3 and applied by using the HandiHaler®. Freeze-dried formulations needed to undergo an additional crushing procedure before filling in capsules, followed by the application using the HandiHaler® and Breezhaler®, respectively.

3.2.8.2 Calculation of the fine particle fraction and mean mass aerodynamic diameter

The NGI can be operated with different airflow rates from 30 to 100 L/min, resulting in different effective cut-off diameters (ECD), which are calculated with the following equation:

$$ECD = (60/Q)^X$$

where *Q* is the volumetric airflow and *x* represents a specific correction factor for each stage, calculated on an airflow of 60 L/min which is typically applied and thus also in this thesis [187,188]. Particle cut-off diameters from 8.06 - 0.34 µm are resulting when applying an airflow of 60 L/min (**Table 5**).

***Table 5**: Assembly of the NGI body with the nozzle design according to the number of holes and their diameters, as well as the x values and resulting cut-off diameters of the aerosol particles at an airflow rate of 60 l/min.*

stage	nozzle		cut-off diameter [µm] at 60 l/min	x
	number of holes	diameter [mm]		
1	1	14.3	8.06	0.54
2	6	4.88	4.46	0.52
3	24	2.185	2.82	0.50
4	52	1.207	1.66	0.47
5	152	0.608	0.94	0.53
6	396	0.323	0.55	0.60
7	630	0.206	0.34	0.67
MOC	4032	0.070		

The amount of rutin deposited on the pre-separator and each cup was quantified. The cumulative quantity can be plotted against the cut-off diameter to calculate the mass median aerodynamic diameter (MMAD). It describes the diameter at which 50% of the particles of an aerosol are larger and 50% smaller in relation to their mass. Also, the fine particle fraction (FPF), defined as the percentage

of an aerosol with particles below 5 µm, can be calculated by this plot. All calculations are related to the metered dose.

3.2.9 Cell culture studies

Cell culture studies were performed to assess the antioxidant capacity and toxic concentration of the rutin formulatons in a complex metabolic environment. Moreover, an improved cellular uptake and thus higher bioavailability should be demonstrated when NC are compared to the bulk material.

3.2.9.1 Cell growth conditions

The human lung adenocarcinoma cell line (A549) purchased from American Type Culture Collection (ATCC, Manassas, USA) and the human lung adenocarcinoma epithelial cell line (H441) were grown in Dulbecco's modified Eagle's medium (DMEM) and RPMI 1640, respectively. Both media were enriched with 10% fetal calf serum (Sigma-Aldrich Chemie GmbH, Germany). The cells were cultured in a monolayer at 37 °C and 5% CO_2 under humid conditions upon reaching 80% confluency. For investigation purposes, A549 and H441 cells were seeded in a 96-well plate with a density of 1.0×10^5 and 1.2×10^5 cells/ well, respectively, and subsequently incubated overnight. All investigations described in the following sections were carried out with pre-heated solutions/ medium and incubation conditions at 37 °C and 5% CO_2.

3.2.9.2 Cell viability assay

This modified 3-(4,5-dimethylthiazol-2-yl)-2,5-diphenyltetrazolium bromide (MTT) assay was used to investigate the dose-depending cytotoxicity of rutin as well as its protective effects against oxidative stress-induced cell death. After the incubation time, the cell medium was removed, the cells were washed with buffer and then the cells were incubated with 200 µL at a concentration of 2 mg/mL in cell culture medium for 1 h. Meanwhile, MTT is reduced inside intact cells by usual mitochondrial-associated respiratory processes. The medium was removed and cellularly formed purple formazan, which precipitates in cells, was dissolved in DMSO for at least 30 min by shaking. Absorbance was then measured at 570 nm versus 630 nm using the microplate plate reader (FLUOstar Optima, BMG Labtech, Germany) [112]. The viability of untreated cells was considered as 100% and the viability of Triton-X 100® treated cells as a negative control was assessed to 0%.

3.2.9.3 Condition of the stress generators

To determine the best condition for generating oxidative stress-related cell death, which rutin must reduce, the compounds *tert*-butyl hydroperoxide (TBH) and lipopolysaccharide (LPS) were used. In the following, they are called “stress generators”. After overnight growth of the cells in 96 well plates, medium was removed from the cells, then 200 µL of TBH diluted in DMEM was incubated for 4, 6 and 8 h in a final concentration of 100 and 200 µm, respectively. The same procedure was performed with LPS dissolved in DMEM up to a final concentration of 1 µg/mL and incubation times of 4, 6, 8 and 12 h.

Applying a simple medium change and 1% Triton-X 100 in PBS buffer served as positive and negative control, respectively. Afterward, a cell viability test was performed by an MTT assay.

The same procedure was repeated with H441 cells with the difference of using only TBH as stress generator in the final concentration of 100, 150 and 200 µm diluted in RPMI 1640 and of incubating for 2, 4 and 6 h. Also, the same positive and negative controls as well as a subsequent MTT cell viability test was included.

3.2.9.4 Protective effects against stress generators

A549 cells were seeded at a density of 1 x 10^5 cells/well in 96-well plates, incubated overnight and then treated with rutin. For this, freeze-dried formulations with cysteine and mannitol were dispersed in medium and added to the cells in a concentration of 50, 10 and 300 µM in relation to the pure rutin amount. Additionally, the following controls were used: 100 µM ascorbic acid as water soluble antioxidant, mannitol and cysteine in the highest correlating concentration as possible influence through the carrier, pure DMEM as positive control and 1% Triton-X 100 as negative control. This procedure was repeated three times, whereby after an incubation time of 4 h, the cells were either directly subjected to a cell viability test (MTT) or stressed with TBH and LPS, respectively. In the case of inducing stress, the cells were first washed with PBS buffer and then treated with TBH at a concentration of 200 µM and LPS in a concentration of 1 µg/mL each for 4 h. Subsequently, the cell viability was investigated by an MTT assay.

3.2.9.5 DCFDA assay for cellular ROS amount

A549 cells and H441 cells were cultivated and seeded to the same conditions as aforementioned but incubated overnight in black 96-well plates. Then, used medium was removed from cells and fresh medium was added that contained rutin formulations or controls to be tested. Freeze-dried NC (with cysteine or mannitol as carrier and lyoprotectant) were dispersed, while the controls were dissolved in the corresponding medium. These controls included: a mixture of PLX with mannitol or cysteine in the highest correlating concentration as possible influence through the carrier (vehicle), 100 µM ascorbic acid as water soluble antioxidant and as positive control, and finally a blank (control) where the cells were treated with the same media and procedure but without additional antioxidants. After an incubation time of 2, 4, 8, 16 and 24 h the test medium was discarded, and the cells washed with PBS buffer. The cell-permeable non-fluorescent 2',7'-dichlorofluorescein diacetate (DCFDA) was added onto the cells at a concentration of 25 µM for 45 min. By intracellular esterases, the acetate groups are cleaved off, whereby the more hydrophilic dye is retained effectively inside the cells, and through ROS this dye is oxidized into the strongly fluorescent 2',7'-dichlorofluorescein (DCF) (**Figure 10**). Therefore, after the incubation time, the extracellular DCFDA was removed and the cells were incubated with a colorless nutrient buffer supplemented with TBH [189].

Moreover, ROS scavenging efficacy was also investigated when TBH and rutin were applied onto cells at the same time. For this, DCFDA solution was added to cells, grown overnight in a black 96-well plate, in a concentration of 50 µM and incubated for 30 min. After removing and washing, 100 µL of rutin formulations and controls were added and immediately topped with the TBH solution.

Fluorescence was recorded directly and each 30 min up to 2h incubation time using a FLUOstar Optima plate reader (BMG Labtech, Germany). The excitation and emission filter were set λ_{ex}=480 nm and λ_{em}=520 nm, respectively. The increase in intracellular ROS amount correlates with the fluorescence and thus its increase was determined per well as following:

$$\text{increase in ROS} = \frac{Ft_i - Ft_0}{Ft_0}$$

, where *F* means the detected fluorescence after the incubation time (t_i) and at the beginning (t_0). This method of analysis allows determining just the net change in fluorescence over time from the cells in the same well. It also directly controls the variability of each well, cancels out background fluorescence and makes the need for a "no cell" control unnecessary [189]. Data obtained were normalized to the non-stressed control, which was set to 100%.

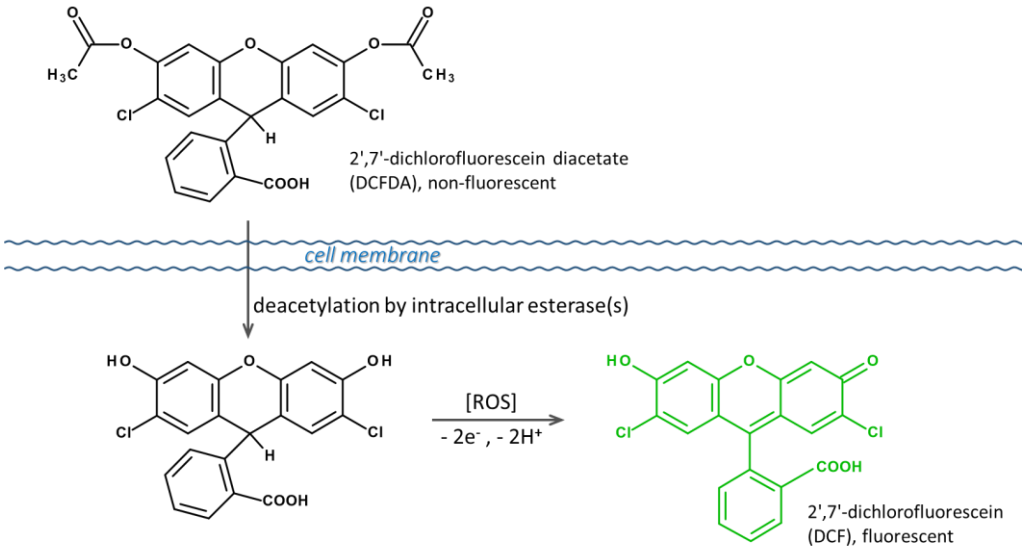

Figure 10: *Schematic image of the pathway and reaction of DCFDA via passive cell uptake, deacetylation and oxidation to the fluorescent DCF to be detected.*

3.2.10 Content analysis

3.2.10.1 Hesperetin

The concentration of hesperetin for its dissolution profiles was analyzed by high-performance liquid chromatography (HPLC), using an Agilent 1260 Infinity II LC system (Agilent Technology Inc., Böblingen, Germany), equipped with a pump: G7111A 1260 Quat Pump VL; sampler: G7129A 1260, column: Agilent Poroshell 120 EC-C18, 4.6×50 nm, 2.7 µm and UV detector: diode array detector (G7117C 1260

DAD HS, wavelength 288 nm). Analysis was performed under isocratic elution using a mixture consisting of methanol : water : acetic acid = 50 : 48 : 2 (V/V/V) as mobile phase with a flow rate of 0.450 mL/min and a temperature of 45 °C. The injection volume was 5 µL and the retention time was about 2.8 min. Calibration curves were obtained prior to each day of analysis and linearity was confirmed from 0.98 to 125 µg/mL (R^2=0.9999). Only hesperetin concentrations within this range were used for calculation of the results and all measurements were performed in triplicate [175].

3.2.10.2 Rutin

The quantification of the rutin samples was developed in this study. For this, all samples containing rutin were dissolved and diluted with 25 mM NaOH solution and subsequently quantified spectroscopically (Multiskan GO, Thermo scientific, Germany) at 266 nm. At this wavelength, the maximum absorption was detected and was also robust for the addition of stabilizers and excipients like mannitol. For the calibration curve stock solution of rutin standard dissolved in 25 mM NaOH was diluted in the range 5 – 30 µg/mL, where the linearity was ensured with R^2= 0.999. Calibration and solubility investigation were performed fast to ensure that no chemical degradation might occur. Likewise, the excipients such as mannitol, cysteine or the NGI coating agent were also included in the same ratio used to adjust the calibration. Samples were measured in triplicate using a 96-well plate.

3.2.11 Statistical analysis

All data are presented as mean ± SD. Statistical analysis of treatment groups was performed using a one-way ANOVA followed by Scheffe's post-hoc test to correct for multiple comparison. The standard statistical software R was used for calculations.

4 Results and Discussion

4.1 BI-6C9 nanocrystals and aeroperls for the treatment of neurodegenerative diseases

Mitochondrial impairment or dysfunction has been identified in diverse neuropathological diseases such as Parkinson's and Alzheimer's disease or ischemic stroke. One prominent pathway of mitochondrial damage was justified by the transactivation of BID in the mitochondria. Consequently, its inactivation successfully rescued cells *in-vitro*. A promising candidate for this inactivation is the BID inhibitor BI-6C9. Up to now, it cannot be successfully applied *in-vivo* because of its very poor solubility. Nevertheless, to give the candidate a high profile as it deserved, a sophisticated formulation should be developed that increases the solubility and thus its bioavailability. Two approaches were investigated to achieve this purpose, namely the production of loaded aeroperls and NC.

4.1.1 Production and characterization of BI-6C9 aeroperls

The first approach for increasing the solubility was the transformation of BI-6C9 into an amorphous state by the formulation of loaded aeroperls, a species of mesoporous silica particles. The embedding success of BI-6C9 has been verified microscopically (**Figure 11**), meaning that no particles or precipitations outside the aeroperls were detected. Under the microscope, pure aeroperls without API appeared as round bright spheres. In contrast, the loaded silica appeared dark because they are completely filled by BI-6C9 molecules. Interestingly, not all aeroperls are equally filled, but they seem to be either completely full or empty. To better recognize the presence or absence of BI-6C9 within the aeroperls, they were characterized using polarized light. However, the more API is embedded, the brighter the silica shines. In this way, it could be confirmed that about half of the aeroperls remained empty. Reasons for this may be the strongly hydrophobic properties of the BI-6C9 leading to a strong tendency to form ordered structures and larger units to keep little contact with water. Similar to the nature of BI-6C9 in water, the building of a lesser amount of highly concentrated aeroperls seemed to be thermodynamically the most stable state. The main challenge for the formulation development of this compound is its propensity to clump in water. Even a fine powder forms directly one sticky lump in the water making further processing impossible (**Figure 12 A**). Again, it was aimed to prevent such clumping by incorporation into aeroperls which also would benefit the development of an applicable formulation for future *in-vivo* studies. The fact that no externally isolated crystals or aggregates of aeroperls were observed, gives the first hint of success.

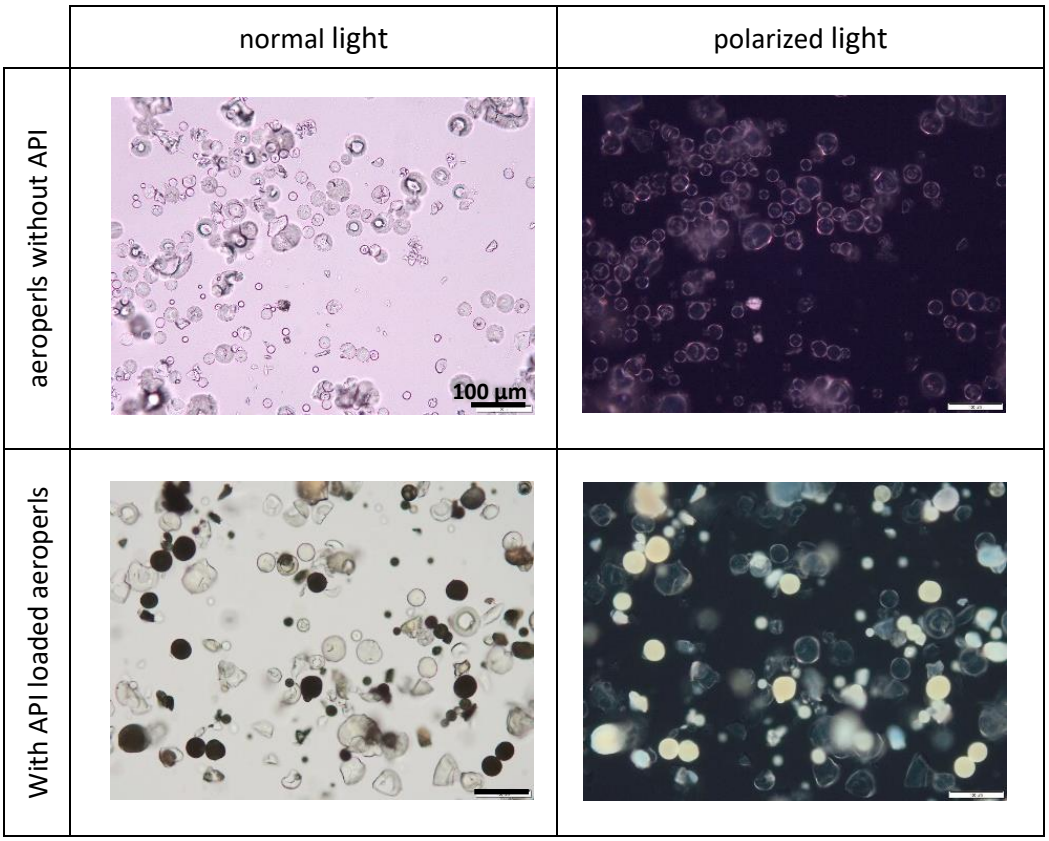

***Figure 11**: Microscopic images of empty aeroperls (upper line) and loaded aeroperls with BI-6C9 (lower line) under normal light (left) and polarized light (right); 200-fold magnification.*

4.1.2 Production and characterization of BI-6C9 nanocrystals

4.1.2.1 Stabilizer screening

Another approach for increasing the saturation solubility is the production of NC composed of pure nanosized API, only stabilized by surfactants. As already mentioned, BI-6C9 forms a sticky, compact lump when surrounded by water (**Figure 12 A**) indicating that the preparation of NC urgently requires stabilizing adjuvants. Up to now, the key challenge of the physical NC stabilization is still accomplished by an empirical trial-and-error approach. This procedure ensures absolute certainty but is very time and material-consuming. Thus, a pre-selection of commonly used stabilizers was performed that might minimize the number of errors. For this purpose, the interaction between the surfactant solution and BI-6C9 crystals was observed microscopically and compared to water. The idea was inspired by the fact that stabilizers are promising if they result in a low contact angle between medium and particle surface, and if they create well-dispersed API without microscopically visible agglomerations before the nanonization [190].

It was expected that a steric shielding of the particles would be achieved by a long-chain non-ionic surfactant. Neither the non-ionic hydrophilic surfactant Tween 80 nor the hydrophobic Span 20 (probably also due to its poor water solubility) prevented the clumping. The small non-ionic surfactant

Plantacare® 2000 (alkyl-polyglucoside) discolored the liquid phase red and induced agglomeration. A solution enriched with sodium dodecyl sulfate (SDS) as an electrostatic stabilizer showed adequate wetting of the particles and thus prevention of the clumping so that SDS was used for further studies (**Figure 12 B**). Despite the poor performance in the screening approach, Tween 80 was also used comparatively for the formulation study, as it is approved for parenteral administration.

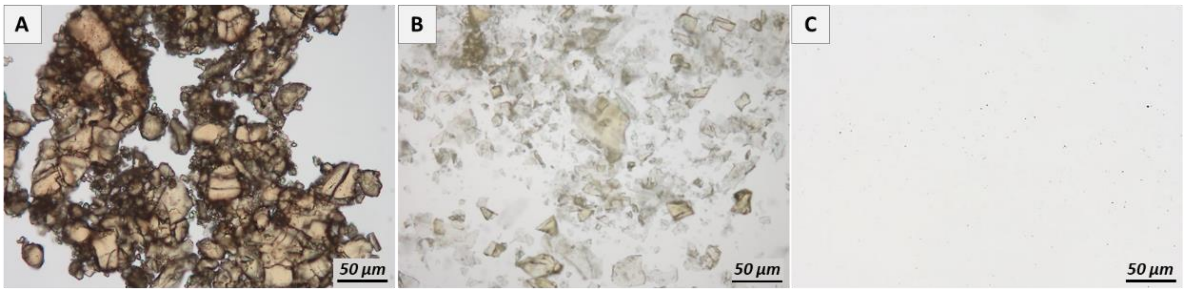

Figure 12: *Microscopic images of BI-6C9 forming a lump in water (A), which was prevented by adding SDS solution (B) and transformed into a nanosuspension (C), each 400-fold magnification.*

4.1.2.2 Small scale bead milling

Because BI-6C9 is expensive, it was kindly synthesized and provided by the working group of Prof. Dr. M. Schlitzer. Moreover, to save the limited quantity of the API, the small scale BM process was performed. It was found that a milling time of at least 24 hours was required to minimize the SDS-stabilized particles sufficiently (**Figure 12 C** and **13**), i.e. to obtain a hydrodynamic diameter below 1,000 nm.

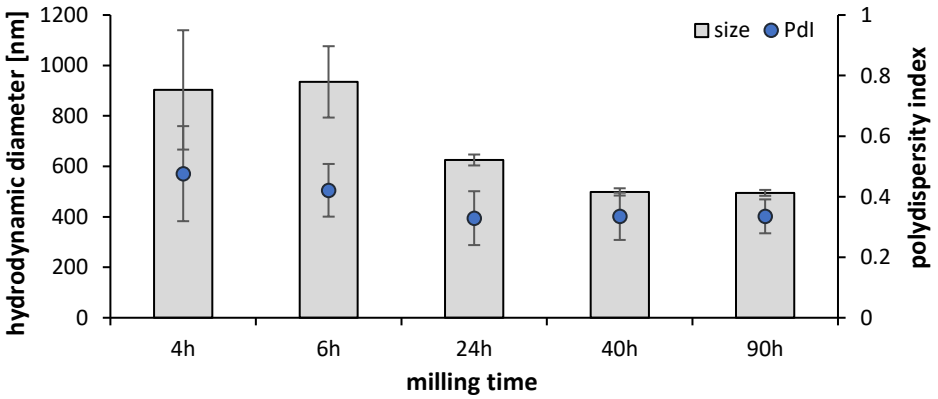

Figure 13: *The hydrodynamic diameter and polydispersity measured by PCS and in dependence of milling time for SDS-stabilized BI-6C9 NC.*

Running a longer milling time of 90 h led to barely better results (500 vs. 600 nm) but could chemically stress the unstable compound. It should be noted that this method-stabilizer combination with BI-6C9 seemed to reach its limits at this point and further comminution would not be possible. Since PCS is

unable to detect particles being larger than 6 µm, microscopy was used as an additional technique (**Figure 14**). By doing so, particles and agglomerations with sizes up to 50 µm were detected. These larger particles could, however, not be nanosized completely through longer milling time since they were found in all formulations regardless of the processing time. The presence of these large particles could also be confirmed by the polydispersity index (PdI), which can be considered as a measure of the broadness of the particle size distribution. The higher the PdI value, the broader the particle size distribution [177]. In this study, the PdI value decreased up to a processing time of 24 h and then increased minimally with longer processing times. This also indicates that the prolonged processing time of 90 h was also insufficient to nanosize all particle agglomerates.

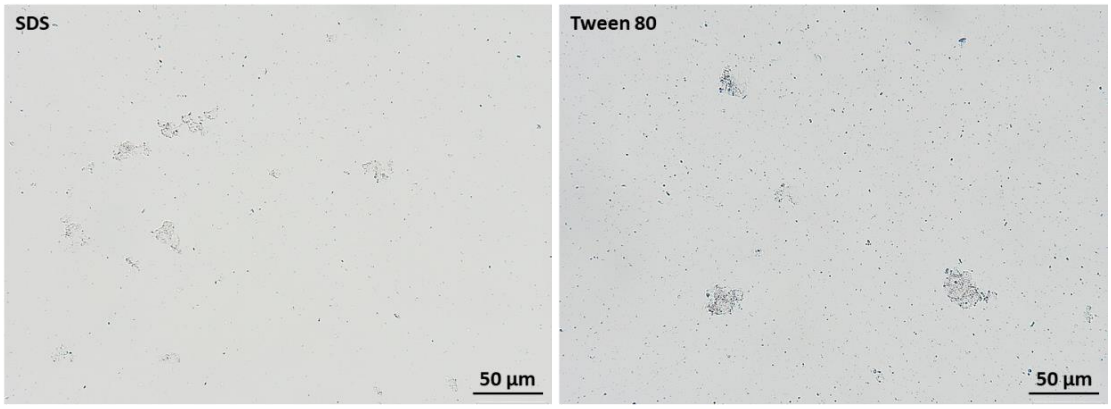

Figure 14: *Microscopic images of the nanosuspension stabilized with SDS (left) and Tween 80 (right) in 400-fold magnification. Some larger particles exist in both formulations but were not detected by PCS.*

To sum up, it was possible to formulate a nanosuspension of BI-6C9 for further investigations on a cell culture model. Nevertheless, this study was aimed to formulate BI-6C9 ideally for an intracortical or intracerebral application. Besides the presence of large particles in the SDS-stabilized formulation, SDS itself also has an unfavorable effect when applied in the brain. However, the SDS-stabilized formulation can be used for an oral applical. To achieve the goal of the development of an i.v.-applicable NC formulation, Tween 80 – the only stabilizer possessing the GRAS status for these administration routes – was used as stabilizer at the same BM process and concentration. As confirmed in the microscopic pre-selection study, BI-6C9 NC stabilized with Tween 80 could not be processed in the same way as the SDS-stabilized one because performing the milling time of 24 h did not result in any measurable size reduction due to the detection limit of the PCS. In contrast, after a milling time of ≥ 90 h, measurable BI-6C9 NC stabilized with Tween 80 were obtained being comparable in particle size to the SDS-stabilized formulation (**Figure 14** and **15**). Contrary to expectations, electrostatic repulsion by SDS seemed to stabilize more effectively than a steric shielding by Tween 80, although BI-6C9 is highly hydrophobic.

Besides the production conditions, further optimization regarding particle size can be achieved by adjusting the ratio of API and stabilizer [190], by increasing the drug concentration [191] and by keeping the viscosity low [192]. In this study, the viscosity was not increased to keep the impact force as high as possible. Thus, further improvement in size could be reached by adjusting the concentration of stabilizer and API, respectively.

4.1.2.3 Physical stability

After NC of BI-6C9 have been successfully produced, the next step was to investigate its physical stability. For this, the BI-6C9 NC were characterized by PCS and microscopy at the day of production as well as after 1, 4 and 7 days of storage in 1.5 mL safe-lock microcentrifuge tubes which were placed in the fridge, i.e. at a storage temperature of 5 ± 3 °C. Since the substance exhibited a high tendency to aggregate, it was expected that the physical stability would be low and thus the NC might merge to macro structures after a short time. In addition, uncontrolled crystal growth, known as Ostwald ripening, might occur. This is particularly the case when the size differences and/ or the solubility are high [193].

In this study, at a storage time of seven days at 5 ± 3 °C, the SDS-stabilized nanosuspension showed a slight increase in the average particle size and PdI (**Figure 15**). Fluctuations in the average size observed in the Tween 80-stabilized formulation could give a hint of Ostwald ripening and could be explained as follows: smallest particles possess the highest kinetic solubility and dissolve hence preferentially. This leads to saturation solubility being exceeded in the proximity of larger particles with lower saturation solubility. Consequently, the supersaturation re-crystallizes on these larger particles, which were discovered by microscopy (**Figure 14**). It follows, that the average size within the detection range shifts due to the disappearance of small particles. Thereafter, residual small particles dissolve, which results in a reduction of the measured particle size value and an increase in the PdI value. In other words, the higher PdI value of the Tween 80-stabilized formulation indicates a broad particle size distribution and thus an increased Ostwald ripening, i.e. lower physical stability. However, the slight increase in particle size is not significant and hence both formulations can be considered stable for at least one week. Interestingly, the expected rapid fusion of the particles to the lump did not appear in the time interval, indicating an adequate steric or electrostatic shielding.

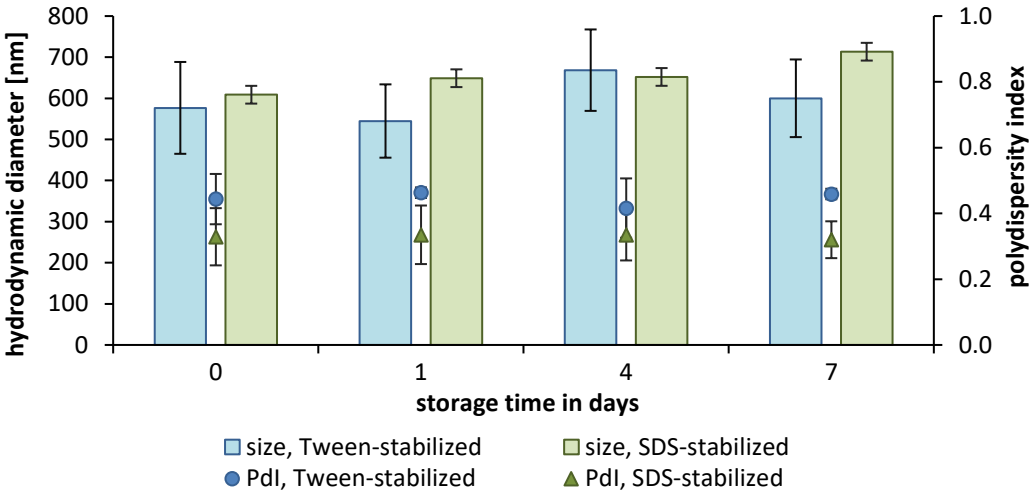

Figure 15: *Particle sizes and dispersity over a storage period of one week and depending on stabilizer used. No statically significant differences between the formulations and over the storage time ($p \leq 0.05$, ANOVA).*

The physical stability of the nanosuspensions was also estimated by zeta potential measurements. Interestingly, a zeta potential of -20 mV was obtained for all formulations measured in water adjusted to a conductivity of 50 µS/cm (**Figure 16**). If surfactants adhere loosely onto the surface, they can be easily washed off, and then the potential of the resulting nanoparticles with lower amounts of surfactants was measured. Washing off of the surfactants seemed to happen in both formulations because the ZP reached the same value after dilution but the respective ZP differed when measured in the original medium.

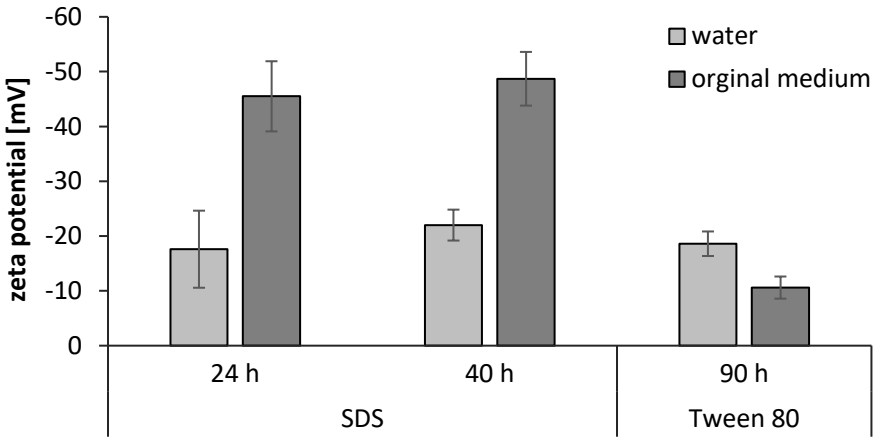

Figure 16: *Zeta potential of differently stabilized BI-6C9 NC measured in water (conductivity of 50 µS/cm) and original medium (corresponding surfactant solution) depending on the milling time.*

In the case that surfactants are loosely absorbed on the surface, they are likely to desorb leading to a higher number of surfactants in the water phase and a lower amount on the particle surface. This in turn could weaken the shielding efficacy and hence facilitate agglomerations. In this study, the

hydrophobic surface of the BI-6C9 NC seemed to hamper the absorption of surfactants. Nevertheless, to still reach a sufficient shielding efficacy, the surfactant concentration was adjusted to an API to surfactant ratio of 1:1 (w/w). Additionally, it was shown that the increasing milling time did not alter the surface charge and therefore no changes in shape and hydrophobicity were achieved (**Figure 16**). On the one hand, this suggested that the particles were completely broken in the early process time, as far as the general conditions allowed. Such limitations comprise, for example, the energy introduced and the crystal lattice energy. On the other hand, a long process time was essential to prevent the agglomeration process in such a way that surfactants had enough time and opportunity to adhere to the particle surface. During the milling process, particles and agglomerates are repeatedly broken up or separated and can immediately re-fuse with other particles due to their high surface energy. Concurrently, the particles can also interact with a surfactant instead, which creates a shielding effect and delays further agglomeration. In other words, the longer the processing time, the higher the chance of contact between surfactant and particle surface. Another critical factor for the successful attachment of surfactant molecules to the particle surface involves the physical properties of the surfactant in solution. These are the faster diffusion rate of smaller molecules - an advantage for the small and agile SDS molecule - and how fast the micelles convert into monomers. Hence, SDS could be absorbed faster onto the particle surface, which explains the difference in processing time with Tween 80 (24 h versus 90 h).

Zeta potentials measured in the original medium, i.e. the surfactant solution, differed greatly from those measured in water (**Figure 16**). Based on previous results, this was expected. Nanosuspensions stabilized by ionic surfactants possess high zeta potentials due to their ionic charge which yields predominantly electrostatic shielding against agglomeration. Therefore, by adding a surfactant solution to these nanosuspensions no wash off could occur and the zeta potential of -45 mV was measured. In contrast, nanosuspensions stabilized by non-ionic surfactants possessed a low zeta potential of -10 mV because their long polymer chains shift the shear plane (**Figure 17**). It is postulated that polymer surfactants could not be washed off from surfaces due to their size and multiple contact points. In this study, the opposite was observed. The decreasing zeta potential indicated that the surfactant layer became smaller due to washing off by adding water. However, this implied rather insufficient long-term stability of Tween 80-stabilized BI-6C9 NC.

At this point, this observation could additionally explain the very low water solubility because not even amphiphilic surfactants with a lipophilic moiety could be retained on the highly hydrophobic surface. The hydrophilic water molecule would then be displaced even stronger and promote fusion with other BI-6C9 fragments.

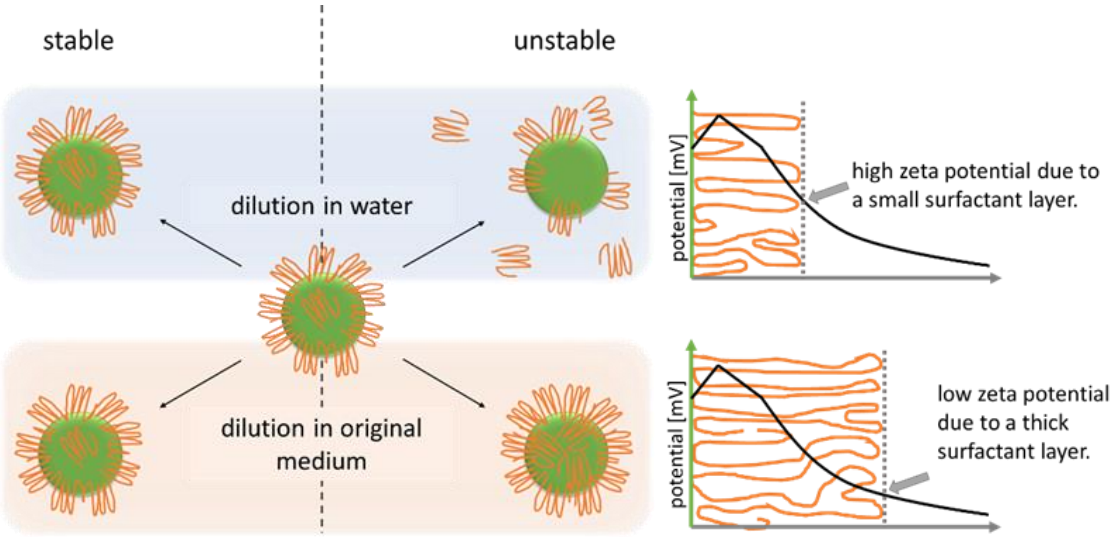

Figure 17: *Schematic representation of non-ionic surfactants on the particle surface and the related zeta potential, which depends on the layer thickness. A very thick surfactant layer shifts the shear plane and therefore the measurable potential to zero, while the zeta potential of a washed off, thin layer remains close to the particle's charge.*

For the sophisticated formulation development, not only the storage stability should be considered, but also the physical stability during application, e.g. in the cell culture model. Therefore, the stability of the nanosuspensions was also investigated in the cell culture medium throughout the incubation time. It was believed that in addition to the surfactant wash off, proteins and electrolytes could negatively affect the physical stability. No significant change in particle size was observed in both formulations whereas the ZP values approached those of the cell culture medium (**Figure 18**). The cell culture medium is free of particles but contains proteins of which a ZP can also be detected. While dilution, the surfactants desorbed from the particle surface due to their weak binding, and might make room for the adhesion of substances from the cell culture medium such as amino acids, sugar and ions. With SDS, equilibrium seemed to be reached much faster, as the ZP value changed by 2 mV within one hour but remained at the same level of -10 mV after another 15 h. The reason for this could be the small molecular size and thus few contact points on the particle surface. In contrast, the ZP of Tween 80-stabilized NC showed its highest change after more than one hour and only a slight change within one hour (**Figure 18**).

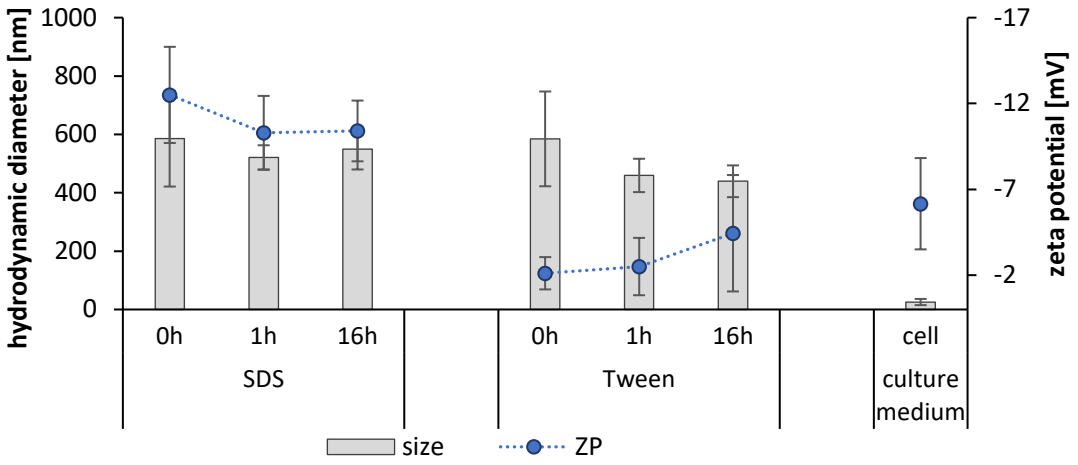

Figure 18: *Particle size and zeta potential of differently stabilized BI-6C9 NC in cell culture medium over the incubation time as well as the particle size and zeta potential of the cell culture medium itself for comparison.*

4.1.3 Determination of antioxidant capacity

In the following, an increase in efficiency caused by transformation into an amorphous state or by nanonization should be analyzed. An established cell model dealing with ROS-induced mitochondrial cell death pathway by BID activation was performed for this purpose. Spindle-shaped mouse hippocampal HT22 cells were used to investigates oxidative neuronal cell death [33]. The addition of glutamate leads to blockage of the cysteine/glutamate antiporter system located on the cell surface so that no further cysteine can be transported into the cells [35]. Consequently, the intracellular concentration of cysteine decreased. Cysteine plays a key role in the glutathione synthesis and this is crucial for the function of the glutathione peroxidase 4. Its depletion is associated with increased 12/15-LOX activity by accumulated ROS, leading to a chain reaction for a high production of soluble and lipid ROS [194]. In consequence, the pro-apoptotic BID is translocated to the mitochondrial outer membrane, where a further chain reaction initiates cell death. Therefore, if BI-6C9 inhibits the BID protein after successful cell uptake, the cell is rescued from death [33].

By adopting the cell test, a classical *in-vitro* dissolution study in a vessel can be omitted that aims to verify the enhanced solubility and to characterize the dissolution profile. Since only dissolved drugs can affect the target, a corresponding survival rate represents not only the effectiveness of the substance but also its dissolution behavior because the efficacy of BI-6C9 has already been proven [33,35]. Thus, the impact on the cell model clearly predominates the simple information about the dissolution rate in this study.

4.1.3.1 Effect of loaded aeroperls

Formulating amorphous systems is one of the most efficient approaches to improve the bioavailability of poorly soluble APIs. However, due to their high free energy, compounds in an amorphous state tend

to recrystallize. Thus, mesoporous silica aeroperls loaded with BI-6C9 have been used as a stabilizing formulation principle for an amorphous system. The use of aeroperls was used to provide another approach to improving the solubility. Like the SDS-stabilized formulation, they can be administered orally instead of i.v.

By Investigating the possible harmful potential in a cell culture model, the unloaded pure aeroperls (vehicle) as well as the loaded aeroperls did not negatively affect the viability of non-stressed cells (**Figure 19**). However, by stressing the cells by adding glutamate this formulation did not exhibit any protective effects either (**Figure 19**).

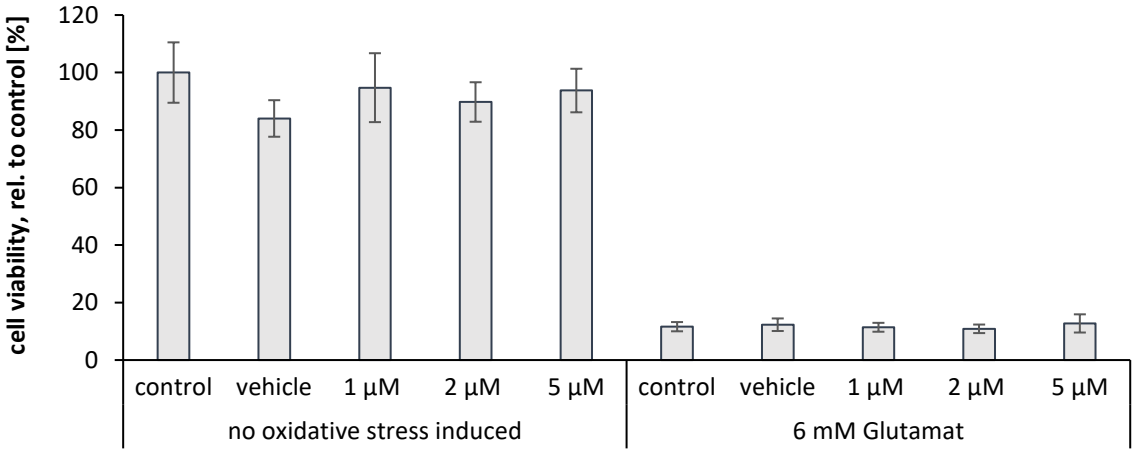

Figure 19: *Activity of amorphous BI-6C9 formulated as loaded aeroperls. By performing an MTT-assay to investigate the cell viability, neither toxicological (left) nor protective effects against glutamate-induced oxidative stress (right) on HT-22 cell line could be observed. Cells were incubated without aeroperls (control), empty aeroperls (vehicle) and BI-6C9 incorporated aeroperls in different concentrations (1, 2 and 5 µM). Cell viability was normalized to non-treated control (100%).*

As suspected by microscopy, it can be concluded that the BI-6C9 molecules were tightly packed in the aeroperls and probably block the mesopores so that they did not dissolve, or only to a very limited extent. At the same time, a hydrophobic layer of the API could have formed around the aeroperls.

In general, inhibition of crystallization within the mesoporous silica is explained by the molecular interaction between functional groups of the API and the silica surface. The large surface area within the mesoporous silica is providing additional surface free energy. Thus, the adsorption of the drug as a monolayer in amorphous form is thermodynamically favorable due to the lower state of free energy compared to its crystalline state. Therefore, the amorphous state can be considered highly physically stable [195]. The energetically favored state could be simply used to explain why the solubility and thus the bioavailability was insufficient. It plays also an important role in how deep the molecules are located in silica particles. For example, in a study by Ahern et al. a release plateau was observed at 80% due to the surface tension effect that hindered diffusion of the dissolution fluid [196]. The incomplete release was also explained by a dynamic adsorption equilibrium from the silica surface between

dissolved and adsorbed API molecules. Likewise, reverse dissolution was observed when adding blank mesoporous silica to an *in-vitro* dissolution experiment, i.e. the concentration of dissolved API was reduced [137]. Nevertheless, the assumptions could only be transferred if a monolayer development was expected. If the surface is completely covered with the API and an excess amount is present in the system a second layer may develop on top of the initial one [197]. However, the crystallization process inside should be hindered because the diameter of the mesopores is smaller than the critical crystalline core of the drug.

In this study, purely isolated BI-6C9 crystals outside the aeroperls were not observed, indicating a full coverage within the mesoporous silica, whereas many empty aeroperls were discovered beside them. Due to this high number of unloaded aeroperls, the filling degree of the loaded aeroperls must have exceeded the theoretical coverage of 100%. In other words, a multilayer inside or outside the silica particles could be created. A recent study by T. Le et al. demonstrated the development of furosemide NC on the exterior surface of the mesoporous silica at a drug load of 300% [136,137]. They were visualized by scanning electron microscopy and confirmed by DSC measurements, whereby a significant increase in dissolution profile was detected. In contrast, other studies are describing the opposite effect: an increase in drug load caused a decrease in release [137,198]. Reduced access of water molecules to the drug-silica interface, which is necessary to displace the drug molecules into solution, could account for reduced drug release and diffusion flux when drug loading exceeds the monolayer coverage. The combined effect of the sticking properties and the overloaded aeroperls hence result in poor solubility performance.

4.1.3.2 Effect of nanocrystals

The next formulation approach was the investigation of the drug NC. Both preparations stabilized with SDS and Tween 80, were compared to the classical application principle of poorly soluble API: dissolved in a solvent (DMSO) followed by diluting in the cell culture medium. In general, dissolving the API in solvents represents a perfect feature for obtaining first insights into how effectively the API penetrates into the cells and cell organelles or binds to the target molecule. Nevertheless, when transferring from *in-vitro* to *in-vivo* systems, the use of solutions containing toxic solvents, e.g. DMSO, might be a challenge. According to this, the claim was to develop a non-hazardous alternative applying to both, *in-vitro* and *in-vivo*. This should be realized with the NC production as they were able to increase the kinetic solubility, too.

Both BI-6C9 NC formulations (stabilized with Tween 80 or SDS) behaved identically to each other as well as to the DMSO-dissolved control (**Figure 20**). In other words, the NC showed no toxic effects and protected cells against induced oxidative stress in the same manner. With increasing concentration of BI-6C9, the protection effect increased as well, up to complete protection at a concentration of ≥5 µM. Significant protective effects were achieved at a concentration of ≥2 µM (**Figure 20**).

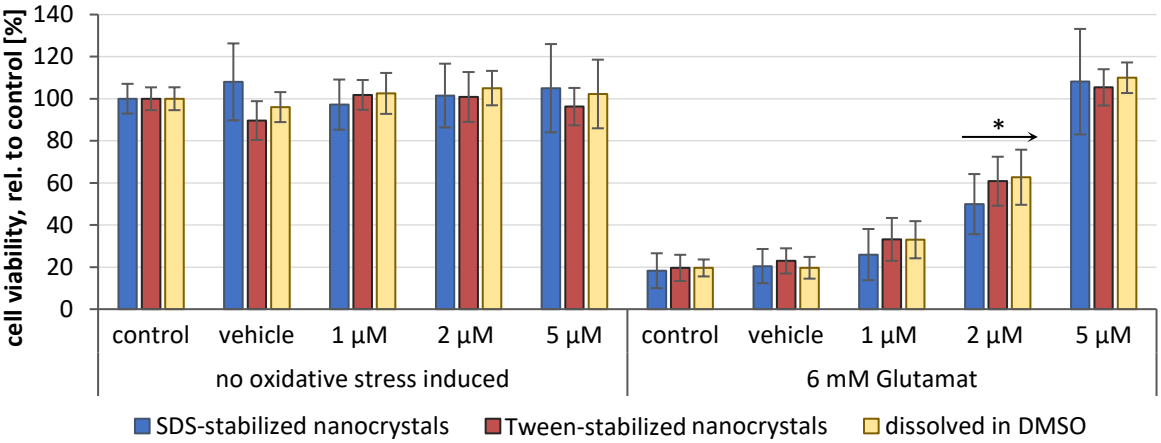

Figure 20: *Activity of NC formulations and dissolved active on HT-22 cell line. A dose-related increase in cell viability (MTT assay) despite glutamate-induced oxidative stress demonstrates the protective effect of the BID inhibitor BI-6C9 both as a nano-formulation and dissolved in solvent (DMSO). Incubated without any formulation (control), the API-free dispersant or solvent (vehicle) and the formulations in different concentrations (1, 2 and 5 µM) were treated either with nothing else (left) or with glutamate simultaneously (right) inducing oxidative stress. Cell viability is expressed relative to the non-treated control which is set to 100% for each formulation. * indicates statistical significance to treated control ($p \leq 0.05$, ANOVA)*

The similar efficacy of the DMSO solution and the nano-formulations could be explained by different effects. The NC possess an increased kinetic solubility of the NC and they are distributed evenly in the cell culture medium. This in turn increases the number of contact points onto the cells. In combination with the high adhesiveness, a large interface area was covered. As a result, a large API gradient was created between the outer and inner cell membrane. Small but continual dissolution of the NC forced an uptake to a certain extent (**Figure 21**).

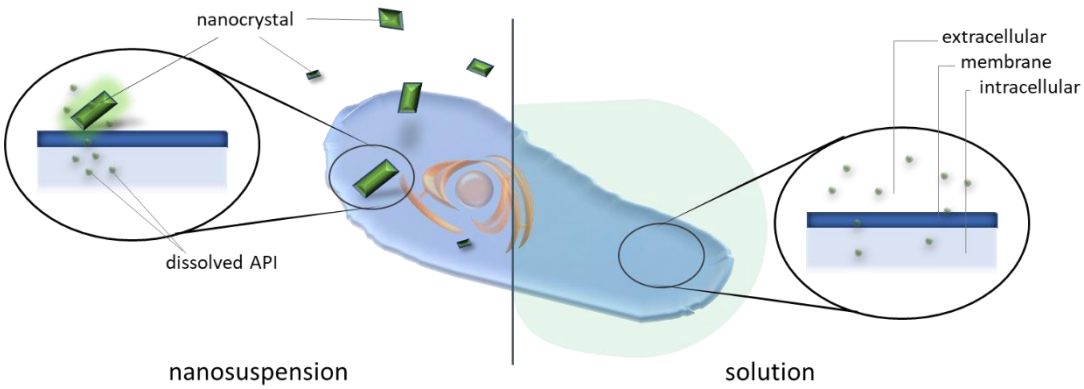

Figure 21: *Schematic model of the different effects of NC (left) and the solution (right) on the cells. Some NC reaching the membrane generate a large concentration gradient, which led to a high uptake into the cells, whereas the smaller gradient distributed over the entire cell leads to an equally high uptake for the solution formulation.*

Nevertheless, the DMSO-solution should be more effective since BI-6C9 is completely dissolved in the cell culture medium. On the other hand, the dissolved molecule must first have reached the cell surface by diffusion to be absorbed. The API-gradient between the cell interior and exterior is then smaller compared to the NC covered onto the cells (**Figure 21**). Additionally, by adding the DMSO solution to water, the solubility can be reduced below the saturation concentration and the very hydrophobic API would precipitate. Such precipitations do not always have to be visible immediately but could lead to uncontrolled crystal growth. In the case of BI-6C9, sticky aggregates might be formed. Anyhow, the concentration of dissolved molecules in the cell culture would decrease and jeopardize the effectiveness of the drug solution.

The beneficial effect of NC and the adverse effect of precipitation from the solution could explain why both concepts shared a similar efficacy. Due to the *in-vivo* applicability, the possible precipitation from the solvent as well as the environmental awareness for the reduction of solvents, the NC is therefore superior to the solution.

4.2 Hesperetin nanocrystals for the treatment of Alzheimer's disease

Alzheimer's disease is a slowly progressive brain disorder characterized by the destruction of neuronal cells and nerve contacts, which leads to problems in memory, orientation, speech, thinking and judgment as well as personality changes. In the brain of patients with Alzheimer's disease typical accumulation of intraneuronal and extracellular filamentous protein aggregates with the main protein Aβ lead to increased intracellular calcium levels, impaired mitochondrial redox activity and increased production of free radicals. Recent studies showed H_2O_2 accumulation in hippocampal neurons and neuroblastoma cultures as well as lipid peroxidation in gerbil synaptosomes. Thus, aggregated Aβ is associated with the production of ROS which alters endothelial structure and function resulting in neurotoxicity of enzymes and cell membranes. Despite many studies and the deep understanding, the disease is still only treatable and not completely curable, up to now.

Therefore, one therapeutic approach is to reduce oxidative stress. This can be achieved by the use of antioxidants such as flavonoids, e.g. quercetin, apigenin and hesperetin. Recently, hesperetin revealed ROS level reducing effects in an in-vivo Aβ-injected mouse model [112]. Nevertheless, its low solubility has so far hampered the use of adequate oral therapy.

For this reason, this section of the work aimed to improve the solubility of hesperetin by rendering the API into NC. For ascribing the positive profits to nanonization and gaining deeper insight into the influence of size on the physical and biological effects, the particles were produced in different sizes, i.e. tailor-made, by using different production methods such as BM and HPH under varying pressures and cycles. These tailor-made NC were investigated regarding solubility and dissolution velocity in an *in-vitro* dissolution study as well as an its antioxidant activity both *in-vitro* and in a cell culture model for AD. The *in-vitro* assay will be modified to account for the increased dissolution velocity by analyzing the time and concentration dependence.

4.2.1 Production of hesperetin nanocrystals with tailor-made sizes

The first part of this section focus on the production of tailor-made hesperetin NC. By varying the production techniques and parameters, hesperetin NC with different sizes were obtained. Measured by PCS, the hydrodynamic diameter ranged between approximately 200 and 800 nm (**Figure 22** upper). The application of very low pressures (formulation A) did not result in submicron particles which could thus not be analyzed due to the detection limit of the PCS. In contrast, by applying a few homogenization cycles more at slightly higher homogenization pressures (formulation B) NC with a size of about 800 nm were obtained. Medium pressures of 500 bar (formulations C-E) yielded particle sizes between about 520 and 660 nm, and a further increase in pressure to 700 and 900 bar could further reduce the particle size to about 500 and 400 nm (formulations F and G). Applying additional 20 HPH cycles at 1,500 bar upon formulation G resulted in formulation H, where no further decrease

in average particle size was observed, but particle sizes were similar to those of formulation G homogenized at 900 bar only. The smallest particles and the narrowest size distributions were obtained by the BM process (formulation I). The same trend was observed of the particle size distribution, expressed as PdI, that was lower with harsher HPH process conditions and was the lowest using the BM procedure (**Figure 22** upper).

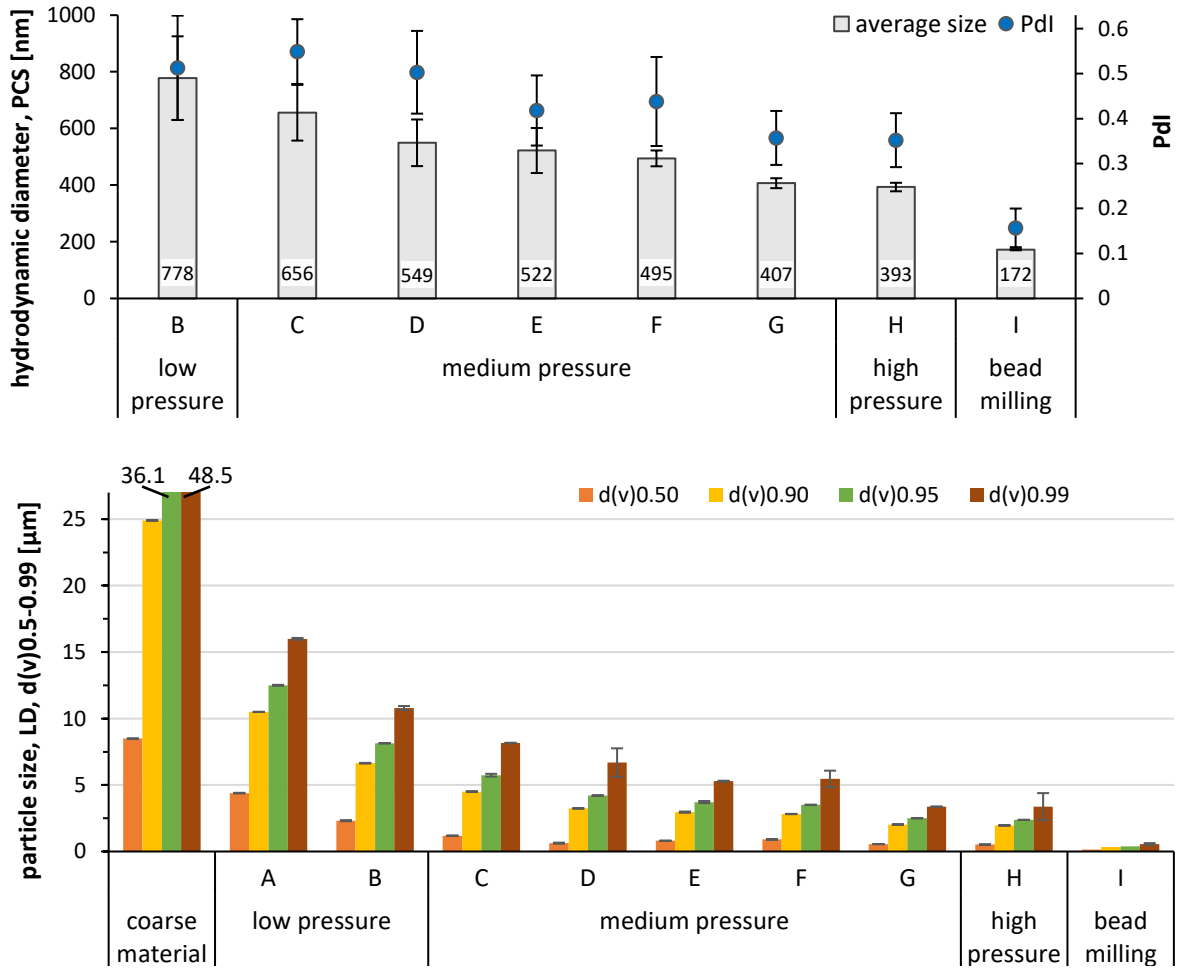

Figure 22: *Hydrodynamic diameter and polydispersity analyzed by PCS (upper) and median particle size diameter by LD (lower) of the hesperetin NC at the day of production depending on the production conditions applied: formulations A – H were produced by modified HPH with increasing number of homogenization cycles and pressure; formulation I was obtained by a small scale BM process. Formulation A is not displayed in the upper graph due to the detection limit of PCS.*

These results of decreasing particle size and distribution with increasing homogenization pressures and cycles were confirmed by LD measurements (**Figure 22** lower). Applying five homogenization cycles at 200 bar (formulation A) reduced the particle size by about 50%, while five further cycles at 300 bar (formulation B) almost caused a quartering in comparison to the initial size of the coarse material for the d(v)0.95 values. Thus, medium pressure was sufficient to produce hesperetin NC. Reasons for this might be a relatively low hardness of the material, which was already reported for other flavonoids

[167]. On the other hand, it can also be observed that the reduction in particle size from the formulation E to F and then to G was relatively small, indicating that the energy was not sufficient to further break up the larger particles. The nanonization procedure is characterized by breaking up the (micro-)particles at their weakest points as a result of cavitation forces. If all weak points are exploited by repeating the homogenization cycles at the same pressure, there can be practically no further breakage. As soon as the pressure and thus the energy is enhanced (formulation G), however, a more efficient particle size reduction was achieved. Interestingly, this process condition seemed to already provide the maximum effect, since no further improvement regarding particle size could be achieved by further increasing the pressure. In other words, performing the HPH process at medium pressure up to 900 bar for 33 cycles was sufficient to produce a hesperetin nanosuspension, i.e. the largest particles were smaller than 5 µm and the average size was about 400 nm. In this way, comparable nanosuspensions regarding particle size could also be produced using medium pressure homogenization if high pressure is technologically not feasible. However, smaller particles could only be produced by using the BM method, in which the largest particles (d(v)0.99) with a size of 0.56 µm were smaller than one micrometer (**Figure 22**, formulation I). Hence, BM proved to be the best method for producing the smallest possible NC, which is also easier to handle because it does not require 30 cycles with strict cooling in between.

The fact that the higher number of cycles at the same pressure yielded a low efficacy in diminution, was also visualized microscopically (**Figure 23**). Furthermore, it was observed that the number of loose agglomerates became smaller. The reason is the greater coverage with surfactants. Homogenization not only causes breaking but also permits deagglomeration. Thus, with each cycle, the chance is raised for the surfactants to be absorbed onto the surface that otherwise competes with particles. As discussed directly afterward, the similar ZP values might indicate a sufficient and comparable coverage of the particles (c.f. section 4.2.2.1). It could be, therefore, concluded that with a high number of cycles, even at low pressures, a higher stability could be achieved despite comparatively large particles, i.e. creating tailor-made NC.

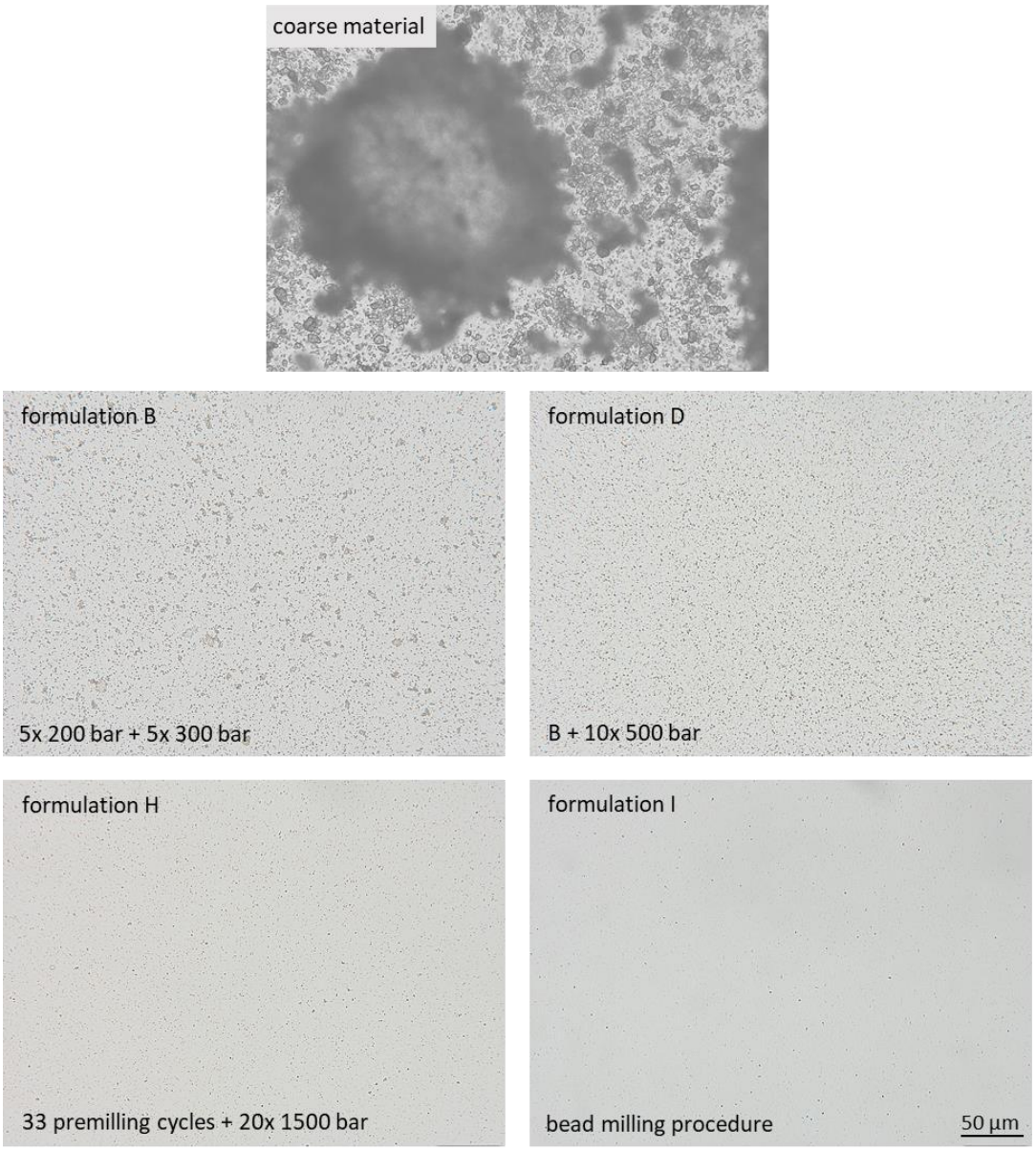

Figure 23: *Microscopic images of the hesperetin coarse bulk material and after nanosizing by different HPH production conditions (formulation B, D and H) and by BM (formulation I), 400-fold magnification for all images. Larger particles and more agglomerations can be observed with fewer homogenization cycles and at lower pressures.*

In the studies by L. Al Shaal et al. [104] and P.R. Mishra et al. [105], hesperetin NC with an average size of about 330 and 300 nm were obtained after 20 and 30 cycles of HPH, respectively. Although they also stabilized with PLC and performed 20 cycles at 1,500 bar each, the resulting average particle size in the present thesis was about 60 nm larger. The main difference, which seemed to play a key role, is the number of pre-milling homogenization cycles at low pressures, i.e. 33 cycles in the present thesis compared to 5 cycles in the recent works [104,105]. The influence of the number of homogenization cycles could be explained as follows: Even a medium pressure is sufficient to produce NC (**Figure 22**), which should exhibite an increased solubility. By further applying cycles, the temperature is briefly increased that additionally favors the solubility of the API and especially of the smallest particles. After

cooling, the supersaturated solution recrystallizes on existing larger crystals, preferably on "gaps", to ensure a small surface area. These gaps, on the other hand, are the imperfections necessary to break the crystals into nanosized fragments. In other words, the application of several cycles could strengthen the crystals due to Ostwald ripening, thus resulting in larger NC on average. For future developments, the process condition should be modified so that the pre-milling is as short as possible but also efficient to produce the smallest possible NC.

To conclude, the application of many HPH cycles at medium pressure is a good alternative when the HPH device could not reach higher pressures. For more effective nanosizing and more time-savings, HPH should be applied at high pressures in combination with a low number of pre-millings. The best method to produce NC was the BM method which led to the smallest NC with with the least effort such as manually cooling or performing cycles.

In addition to particle size and handling, the physicochemical properties of NC may differ due to manufacturing methods, which is investigated below.

4.2.2 Determination of physico-chemical properties

4.2.2.1 Zeta potential and crystallinity

The ZP measurements were performed in distilled water related to the Stern potential and in the original dispersion medium for characterizing the diffuse layer [180]. In general, the use of non-ionic polymer stabilizers yields low ZP values as the large loops on the particle surface shifts the shear plane [105,180]. If measured in the original medium. i.e. adding more stabilizers to the dispersion, the ZP could slightly approach zero as the surfactant layer becomes thicker. When adding water, no change in the ZP might be observed since the large polymer molecules are tightly bound to the surface via multiple contact points. In this study, PLC was used as stabilizer. It is a small non-ionic surfactant but known to form electrostatically charged micelles [199], thus leading to a combination of steric and electrostatic stabilization mechanisms and relatively high ZP values [200]. Also, in this study high ZP of > |30mV| were obtained for both media (**Figure 24**), indicating excellent electrostatic NC stabilization.

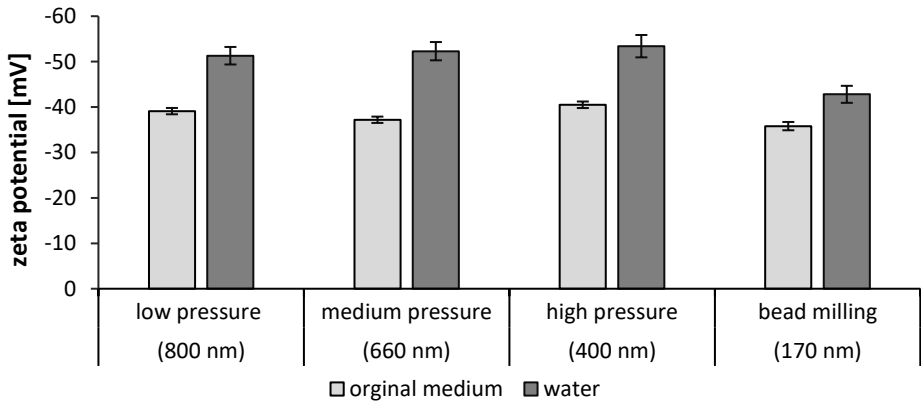

Figure 24: *Zeta potentials of the differently produced hesperetin NC. Measurements were performed in the original medium (surfactant solution) or in water (conductivity 50 µS/cm).*

Analysis in water “dilutes” the particles, and surfactant loosely bound to the surface of the particles can desorb. Thus, by comparing the ZP values obtained in water and original dispersion medium, it is possible to assess how strongly the surfactant layer has adhered to the surface of the particles as follows: the smaller the ZP difference, the stronger the interaction between surfactant and surface and consequently, the more pronounced is the stabilization efficacy [104].

Concerning the hesperetin NC obtained by HPH, the ZP values were similar despite different production conditions and the resulting various particle size and distribution. Relevantly, for the measurement of the ZP only particles with a size of < 1 µm can be detected. The same nanonization procedure led to NC being identically in shape, charge, and coverage. Thus, large particles found in the nanosuspension obtained by low and medium pressure had no influence on the zeta potential but the presence of some small NC. Analysis of the ZP in the original dispersion media is believed to represent the real charge of the particles during storage and is important to predict the physical stability of the particles during storage [180].

In contrast, NC prepared with the BM technique exhibited slightly lower ZP values when analyzed in water compared to those obtained by the HPH technique, whereas no differences in ZP analysis were found in the original dispersion media. This might indicate that the surface of the NC produced by BM and HPH exhibited different properties. One possible explanation for this observation would be the formation of an amorphous hesperetin layer around the crystalline core of the NC due to the milling, which was already reported previously for various other API [160]. To prove or disprove this theory, X-ray diffraction patterns were performed for all formulations (**Figure 25**).

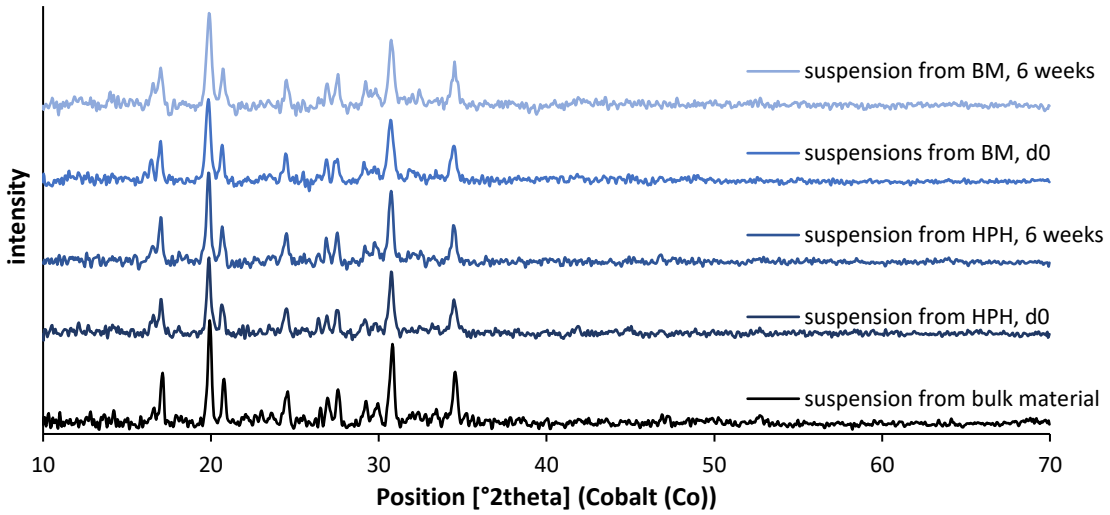

Figure 25: *X-ray diffraction patterns of the differently produced hesperetin NC at the day of production and after 6 weeks storage as well as the bulk material. Formulation H (high pressure, 400 nm) are compared with formulation I (BM, 170 nm).*

Peaks in intensity stand for crystalline structures, i.e. a straight line would represent an amorphous form. Also, a flattening of the intensity or the absence at certain angles indicates a partly amorphous state. Results did not show any differences between the NC formulations to each other and the coarse bulk material. Hence, it can be assumed that the differences in ZP are not due to changes in the crystalline state but are related to other circumstances. The most likely explanation for the differences in ZP would, therefore, be different surface properties, which are related to the different diminution principles. For this, the HPH process mainly uses cavitation forces, whereas BM uses mainly shear forces. Hence, depending on the diminution technique used, the crystalline lattice of the crystals will break in different directions, thus leading to different newly created surface properties, e.g. changes in lipophilicity or orientation of functional groups. Consequently, changes in ZP values could occur. On the other hand, even if the X-ray analysis revealed the same crystallinity, its sensitivity could be overestimated. It has been demonstrated in the study by P.A. Priemel et al. that although the use of X-ray pattern, in contrast to DSC and FT-ATR-IR measurements, recorded a higher degree of amorphization, they detect clear peak signals whenever the surface re-crystallized [201]. The reason lies in the deeper penetration depth of the light wavelengths [202], namely in the order of hundreds of microns, which permits a larger proportion of nanoparticles to be scanned. This, combined with the low surface disturbance in relation to the entire particle body, must have led to the observation of an apparently pure crystalline suspension. In other words, X-ray analysis was not able to explain the differences in zeta potential found between the nanosuspensions being produced by HPH and BM, respectively. At least, it could be proven that the crystallinity in all samples basically retained the same modification.

4.2.2.2 Dissolution profiles of hesperetin

In the next step of this work, the dissolution rate and the kinetic solubility of the differently sized hesperetin nanosuspensions were determined and compared to the large sized bulk material. The solubility of the hesperetin bulk material in water at 37 °C was determined to be 26.4 mg/L, which was well in between the values previously published [203,204]. Tailor-made NC were investigated in a dissolution study conducted at a final concentration of 27.3 mg/L, i.e. above the saturation solubility of the bulk material. The idea behind this was to point out the solubility increase of the NC among each other and compared to the bulk. Also, it should be able to differentiate solubility velocity visibly.

Results revealed no significant differences in dissolution velocity and kinetic solubility between bulk material and NC with sizes > 500 nm (**Figure 26**), and only small differences were found in the total amounts of dissolved active.

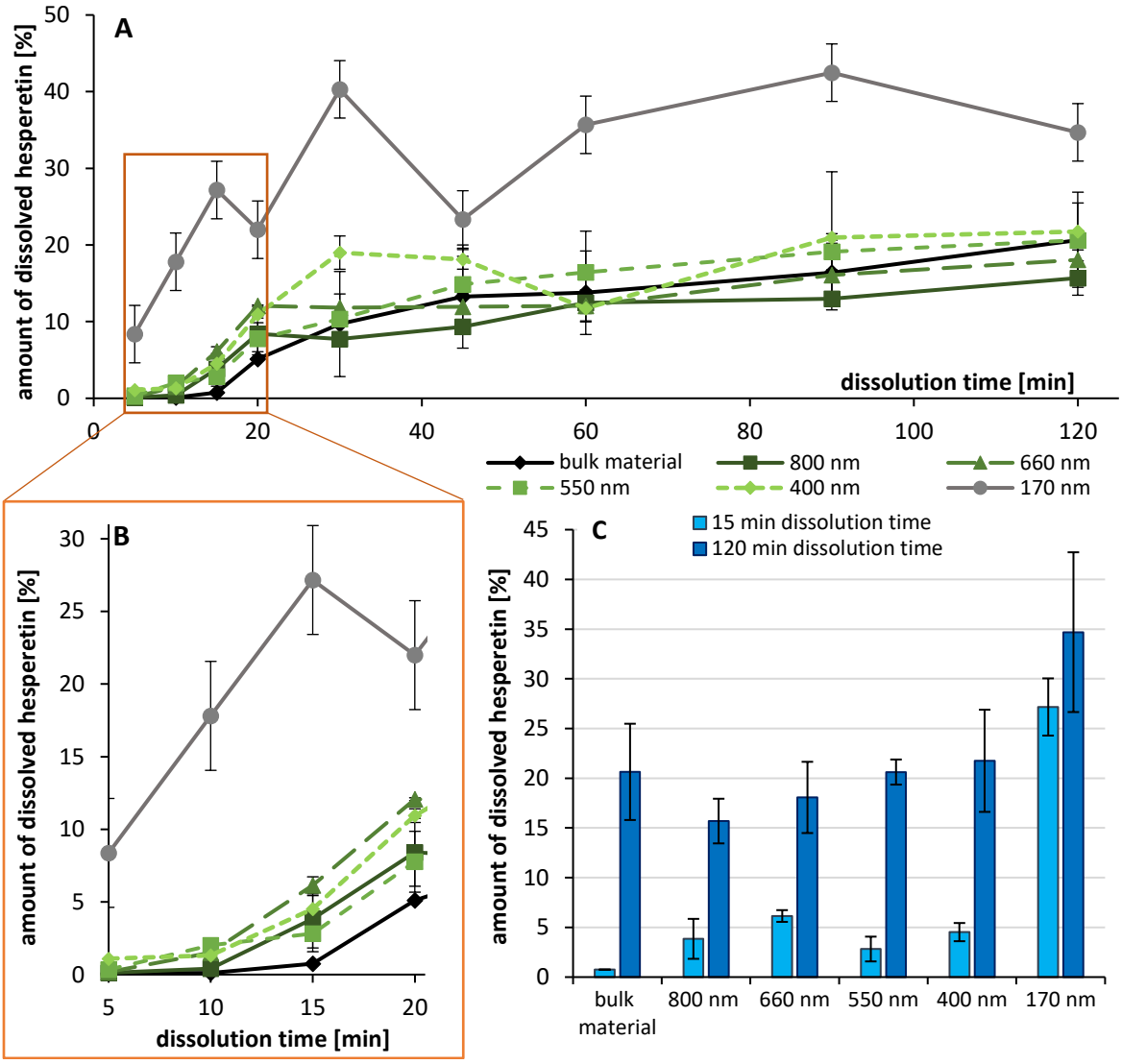

Figure 26: *Dissolution profile of the differently sized hesperetin NC in comparison to its large sized bulk material. Dissolution study was performed for 120 min (A), zoomed in the first 15 minutes of dissolution time (B), and their resulting solubility after 15 and 120 minutes were compared (C).*

Especially in the beginning, the dissolution velocity of nanosized hesperetin was higher than that of the larger sized bulk material. A significant increase in both, dissolution velocity and solubility, was observed for 170 nm sized particles, i.e. NC produced by BM. During the first 15 minutes of the dissolution study, the amount of dissolved active was almost 5 times higher for the smallest sized NC (170 nm) than the larger sized particles (**Figure 26 B, C**). This means that after 15 minutes about 27%, 6% and 1% of the given hesperetin was dissolved that possessed an average size of 170 nm, 660 nm, and the bulk material, respectively. For the 170 nm sized NC, interestingly, after 15 minutes a decrease in the amount of dissolved active was observed, which increased again during the next minutes of the experiments and subsequently decreased again. The observation can be explained by the increased kinetic solubility of the small sized NC (170 nm), which results in a pronounced dissolution rate at the beginning of the experiment. The fast dissolution led to a supersaturated solution of hesperetin in

which the amount of dissolved drug is above the thermodynamic solubility of bulk hesperetin in water. Consequently, as this supersaturated solution is not thermodynamically stable, re-crystallization of the supersaturated API is highly likely to occur. Re-crystallization leads to a decrease in the amount of the dissolved API and thus explains the observation for the NC with sizes < 200 nm. The same effects to a much less pronounced extent and later in the dissolution study were also observed for the NC with a hydrodynamic diameter of 400 nm but were not observed for the NC with sizes > 500 nm. Such an observation was also reported for Q_{10} NC, where a slowly adjusting imbalance in dissolution and precipitation was used to describe the kinetic process [205]. These results demonstrated the size-dependent increase in dissolution rate and kinetic solubility. However, results could also imply the hazard that the created supersaturated solutions might lead to re-crystallization of the API and thus to a loss of the special NC properties. Nevertheless, even though some re-crystallization might have occurred for the 170 nm sized NC, their all-over kinetic solubility was about 1.5-fold higher when compared to bulk material and the larger sized NC (**Figure 26 C**).

Due to the small and almost negligible differences in saturation solubility after 2h between the larger sized (> 400 nm) formulations, only the 660 nm formulation was selected for all further experiments. In summary, the formulations with 170 and 660 nm NC and the bulk material were used for the determination of the antioxidant capacity, which was determined *in-vitro* and in the Alzheimer cell culture model.

4.2.3 Determination of antioxidant efficacy

4.2.3.1 Antioxidant capacity by DPPH assay

Using the DPPH assay allowed the determination of the IC_{50}-value, where low values indicate a high AOC. The IC_{50} is related to the amount of dissolved API, because only the discrete molecules can react with their specific target. Today, in most biological assays, poor solubility is overcome by simply dissolving the API in organic solvents, e.g. DMSO or alcohols. Therefore, to differentiate the AOC between a standard formulation (solution in organic solvent) and the nanosuspensions, not only the selected suspensions but also an ethanolic hesperetin solution were used for the determination of the IC_{50}. The standard protocol specifies to perform the assay in an ethanolic or methanolic solution and for this reason, all formulations have been diluted to the appropriate concentration with ethanol prior to the performance.

In the first step, bulk material dispersed in water to a final concentration of 5% was prepared and then diluted with ethanol to determine its IC_{50} value. This was compared to the IC_{50} values of the ethanolic solution, i.e. without any amount of water (**Figure 27**). In other words, investigations were performed in ethanol and revealed a higher IC_{50} (lower AOC) for the hydrated bulk material. Over time, the AOC increased for both formulations and after 45 min almost no differences in AOC were determined

between both formulations (0.16 vs. 0.19 mg/mL, Figure 27). Results were expected and can be explained as follows: The DPPH assay is a chemical reaction, hence the number of free radicals scavenged by the added antioxidant increases over time, which results in a decrease in IC_{50} value over time. The effect can be seen for the ethanolic hesperetin solution. In contrast, the hesperetin suspension contained less dissolved molecules and thus, less DPPH radicals can be scavenged at the beginning of the assay. Consequently, higher IC_{50} values must be observed when compared to the ethanolic solution. Over time hesperetin dissolved, leading to a decrease of the IC_{50}. After 45 min of reaction time probably all hesperetin particles are dissolved, but the time for the reaction was less and thus the IC_{50} values are still slightly higher than the values obtained for the ethanolic solution.

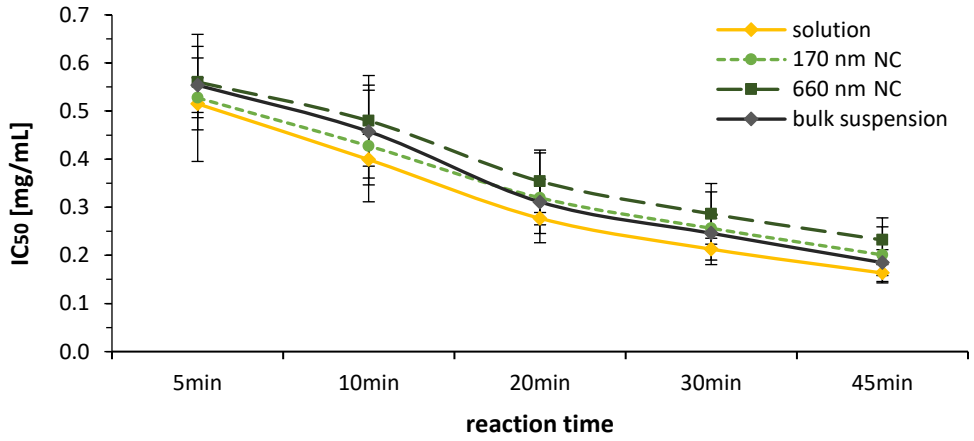

Figure 27: *Determination of antioxidant capacity expressed as IC_{50} by DPPH assay in dependence on different reaction times. Samples were diluted in ethanol to fulfill the standard protocol before adding the DPPH radical. An ethanolic hesperetin solution as well as its aqueous bulk dispersion served as references.*

Likewise, the IC_{50} values for the NC (170 and 660 nm) were determined. In the beginning, the small sized NC (170 nm) were found to possess similar IC_{50} values to the ethanolic solution, whereas the larger (660 nm) possessed IC_{50} values being similar to the values obtained for the bulk material. As discussed earlier, the IC_{50} value is related to the amount of dissolved active and thus the results obtained correlated well to the solubility data obtained in the previous part of the study (c.f. section 4.2.2.2). With increasing time, the IC_{50} values of the NC decreased more slowly than the values for the bulk material and the solution. Reasons for this might be the surfactant and the encapsulation of the active into micelles and/or agglomeration of the NC in the ethanolic environment, leading to a reduced solubility of hesperetin.

In case of the NC, the surfactant cannot be omitted but can be added in similar amounts to the bulk material. Therefore, the test was also conducted with bulk material containing surfactant as the NC to elucidate the function of the stabilizer on the reaction kinetics. It was found that the surfactant did not interfere with the radical scavenging reaction, i.e. neither the reaction velocity nor its extent (IC_{50})

differs from the pure bulk material (**Figure 28**). Accordingly, the use of PLC as surfactant cannot be an excuse for the slightly weaker antioxidant effect compared to the ethanolic solution. Anyhow, it must be noted that all formulations have very similar IC_{50} values after corresponding reaction times and that there is no statistical difference. This was expected because the reaction took place in an ethanolic medium in which hesperetin dissolves well.

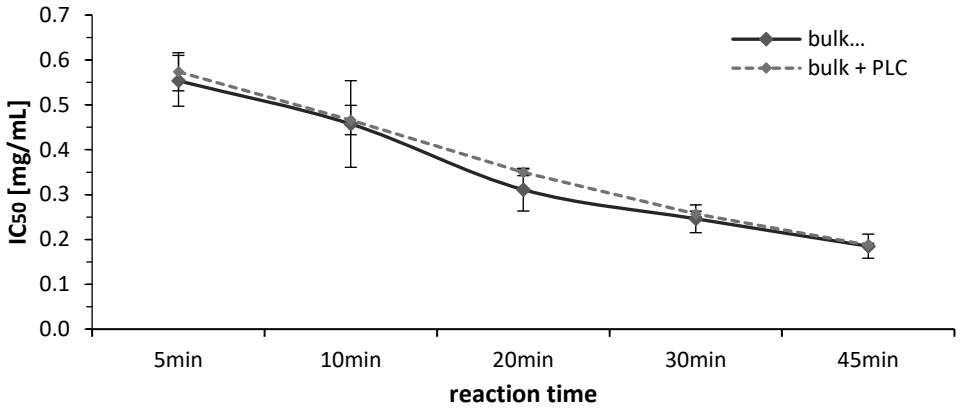

Figure 28: *The comparison of the aqueous bulk suspensions with and without PLC in terms of their antioxidant capacity (IC_{50}) by varying the reaction time.*

Again, the assessment of the IC_{50} in an ethanolic medium was performed to gain details about the reaction mechanism and to comply with the standard protocol [181]. Such a condition applied, however, does not reflect the environment presented in *in-vivo* studies. For this reason, in the next step, the IC_{50} was determined in aqueous media (**Figure 29**). As DPPH required a medium in which it can dissolve in, an ethanolic DPPH solution was added to the aqueous formulation in a ratio of 1:1. Hence, as the formulations were previously diluted with ethanol to the final concentration, the ethanolic hesperetin solution and the formulations were adjusted to the final concentration (0.01 – 0.70 mg/L) with water.

The AOCs determined in water (**Figure 29**) were almost opposite to the results obtained in the ethanolic medium (**Figure 27**). In the beginning, the highest AOC was found for the NC, the second-best AOC was found for the bulk material and the lowest AOC (highest IC_{50} value) was found for the ethanolic solution, when investigated in a semi-aqueous medium. Over time, the differences became smaller and canceled out after 45 min of reaction time. The differences between bulk material and NC can be explained with the increased dissolution velocity and improved kinetic solubility of the NC (**Figure 26**).

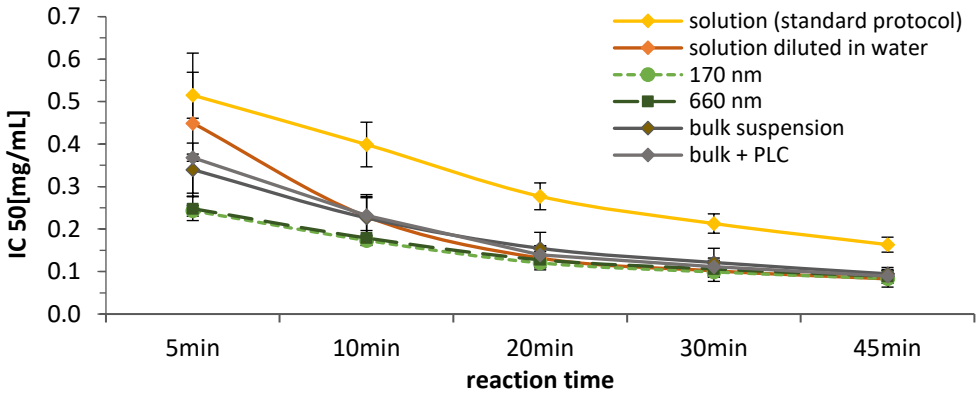

Figure 29: *Antioxidant capacity (IC_{50}) by a DPPH assay in dependence on different reaction times. Samples were diluted in water before adding the ethanolic DPPH solution. Also, the ethanolic hesperetin solution diluted with ethanol, already shown in Figure 27, was included for comparison.*

However, the poor AOC of the ethanolic hesperetin solution was not expected and can only be explained by precipitation of the dissolved molecules upon the addition of the aqueous reaction medium. The concentration of hesperetin used in the assay ranged from 0.66 – 2.67 mmol/L. The solubility of hesperetin is about 73 mmol/L in ethanol but only 87 µmol/L in water. Hence, hesperetin concentrations above the saturation solubility of hesperetin were used. As the DPPH assay was performed in small quantities in a 96 well plate, possible precipitation of the API might not be reliably detected in the small vessels of the plate.

Therefore, to investigate whether precipitation was taking place, the test setup was simulated in a larger volume. For this, the ethanolic hesperetin solution was added to water to yield a mixture containing about 0.1% ethanol, 10µmol/L hesperetin and water. The mixture was prepared *in-situ* by adding the ethanolic solution to water, which itself was already contained in the small volume dispersing unit of the laser diffractometer (LD). So, after adding the ethanolic solution, LD measurement was directly performed which is an ideal feature to discover particles inside a sample. In consequence, this procedure allowed the analysis of possible precipitated hesperetin crystals in the mixture. As result, the formation of large particles with sizes up to 2,300 µm was detected (**Figure 30**). The particle size decreases rapidly with ongoing size analysis and results in sizes in the lower micrometer range after 10 measurements. Conclusively, the assumption that precipitation of hesperetin was taking place after the ethanolic solution is added to the aqueous test medium could be confirmed by this measurement and the low AOC of the ethanolic hesperetin solution could therefore be partially attributed to this phenomenon.

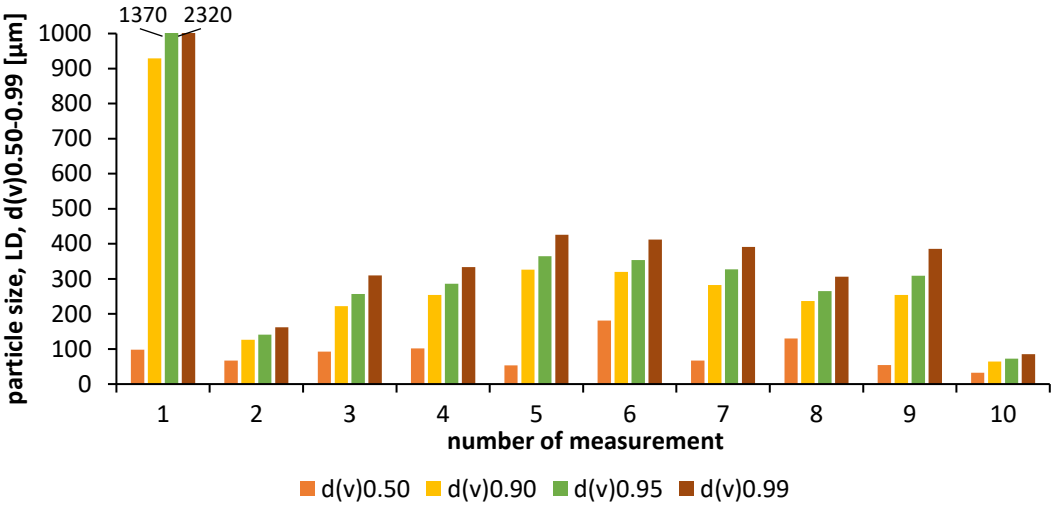

Figure 30: *Particle sizes analyzed by LD measurement, caused by adding an ethanolic hesperetin solution to the dispersion unit filled with water. The data represent the sizes obtained from 10 sequential measurements, where one measurement takes 20 s.*

Moreover, by comparing both test conditions, all hesperetin formulations exhibited higher AOCs when performed in a semi-ethanolic test medium compared to pure ethanol. This suggests that water played a crucial role in this reaction kinetic and seemed to increase the reaction velocity. Performing in ethanol the reaction was apparently not completely exhausted after 45 minutes, whereas in semi-ethanol the reaction proceeded hardly at all after 30 minutes. The benchmark was the change in IC_{50} values over time and the final IC_{50} values themselves, i.e. from 0.11 (30 min) to 0.09 mg/mL (45 min). Water cannot be considered a radical scavenger but could act as an intermediate for the transmission of the H-atom.

In simplified terms, the reversible reaction proceeds as follows:

$$DPPH\cdot + AH \leftrightarrow DPPH_2 + A\cdot$$
$$A\cdot + A\cdot \rightarrow A\text{-}A$$
$$A\cdot + DPPH\cdot \rightarrow DPPH\text{-}A$$

where DPPH· is the radical and AH represents a compound that easily emits a proton and electron, e.g. hesperetin and water. In case that water is oxidized by DPPH·, a hydroxyl radical (HO·) will be formed, which in turn reacts within nanoseconds to hydrogen peroxide (H_2O_2) or removes hydrogen atoms from organic molecules such as hesperetin. The data suggest that hesperetin is much more effective at reducing H_2O_2 than scavenging organic radicals, which was also revealed in a study by A.H. Esmaeili and co-workers [206]. This is in good agreement with various studies in which hesperetin reduced the cellular oxidative stress by neutralizing H_2O_2, HO· and superoxide ($\cdot O_2^-$) [102,109].

Overall, it can be concluded that hesperetin NC, regardless of the production technique, retains its AOC and is comparable with the AOC of a freshly prepared solution.

4.2.3.2 Antioxidant efficacy in cell studies

Following the successful development of differently sized NC and the demonstration of their very good dissolution and antioxidant properties, the focus is subsequently on identifying how effective they are in an Alzheimer cell culture model. For this purpose, the formulations were kindly tested by the working group of Prof. Dr. G.P. Eckert (Department of Nutrition in Prevention & Therapy, University Gießen, Germany) in a previously developed cell model of the initial phase of sporadic AD, where SH-SY5Y-AβAPP$_{wt}$ cells produce relatively low levels of neurotoxic Aβ and show impaired mitochondrial functions AD [207]. To simulate a more progressed stage of AD, cells were additionally treated with rotenone, a specific complex I inhibitor. Complex I, the first large protein complex of the respiratory chains, is responsible for the development of the electrochemical potential difference that in turn is used to produce ATP. It was recently shown that the addition of rotenone only slightly increased the ROS level, whereas synergistic effects with Aβ toxicity enabled a 5-fold increase in ROS [208]. Therefore, the Aβ-producing neuronal cells in combination with rotenone represent an ideal model to investigate the antioxidant efficacy of hesperetin NC in comparison to its solution.

Adding the ethanolic hesperetin solution to SH-SY5YAßAPPwt cells increased the ATP levels in a dose-dependent manner (**Figure 31 A**). Significant effects were observed at a concentration of 1 µM. Both hesperetin NC formulations (with a hydrodynamic diameter of 170 and 660 nm) also increased ATP levels in dependence on the dose and, in contrast, they showed significant effects for all concentrations tested (**Figure 31 B, C**). Nanocrystals with a size of about 170 nm and a concentration of 10 µM increased the ATP level by 12% compared to control, which comprised the best efficacy.

Incubation with rotenone reduced the ATP levels by 50% compared to the control. However, the treatment with hesperetin solution did not affect this insult, whereas both NC formulations were able to increase the ATP level at the concentrations of 1 and 10 µM, respectively (Figure 31 D-F). The successful application of hesperetin in neuronal cells agrees with previous studies [111]. Additionally, hesperetin recently revealed ROS level-reducing effects in an *in-vivo* Aβ-injected mouse model [112]. The working group demonstrated that “hesperetin efficiently reversed the pathological outcomes of Aβ treatment in mice and in cells, mainly by inhibiting oxidative stress via the regulation of Nrf2/HO-1, neuroinflammation via the regulation of TLR4/NF-κB and apoptotic cell death via the regulation of Bax/Bcl-2, caspase-3 and PARP-1” [112]. Again, in this study, the effect of hesperetin seemed to be improved by transforming it into a NC formulation, which should be applied orally as well as intravenously without using harmful solvents or excipients.

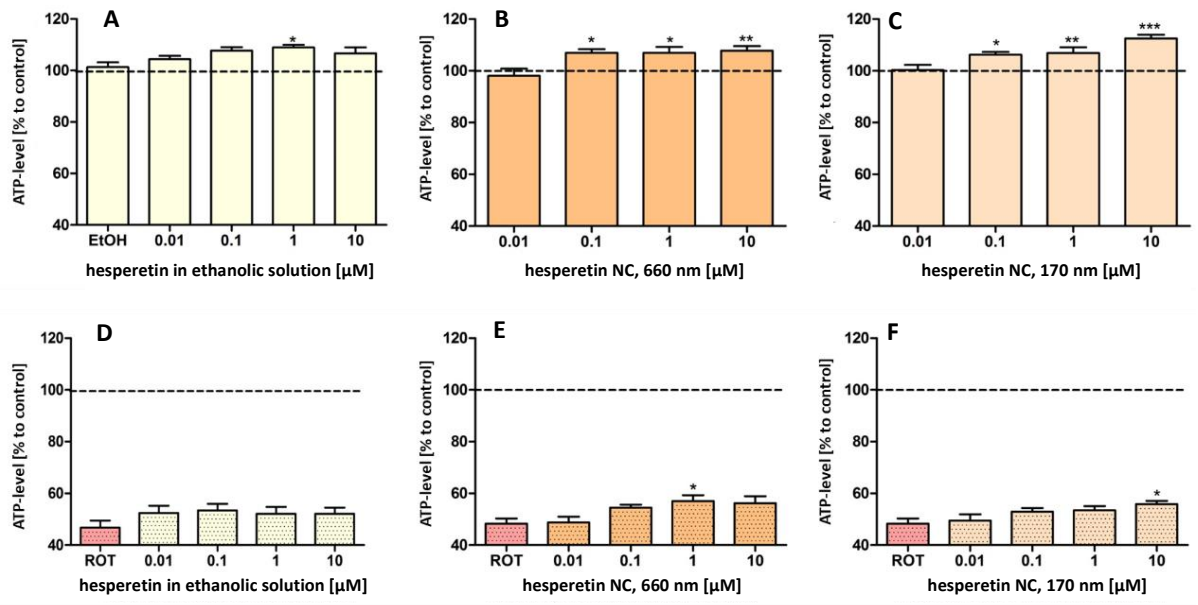

***Figure 31**: Basal ATP level of SH-SY5YAßAPPwt cells after 24 h incubation with different concentrations (0.01–10 µM) of ethanolic hesperetin solution (A), hesperetin NC with a hydrodynamic diameter of 660 nm (B) and 170 nm (C). ATP levels of SH-SY5YAßAPPwt cells after preincubation with the different hesperetin formulations (solution (D), 660 nm sized NC (E) and 170 nm NC (F)) for 1 h and insult with rotenone (ROT, 25 µM) for 24 h. Cells treated with cell culture medium served as control (100%); cells treated with the respective ethanol concentration did not show significantly altered ATP levels (left); n = 8; mean ± SD; t-test; ∗p < 0.05; ∗∗p < 0.01, ∗∗∗p < 0.001.*

The enhanced biological effects seemed to be higher for the small sized NC that possessed the highest solubility. However, at closer examination, differences in efficacy between the different formulations can be observed (**Figure 32**). Using the hesperetin solution increased the ATP level at concentrations of 0.01 to 1 µM and reduced the ATP level at a higher dose (**Figure 31 A** and **32**).

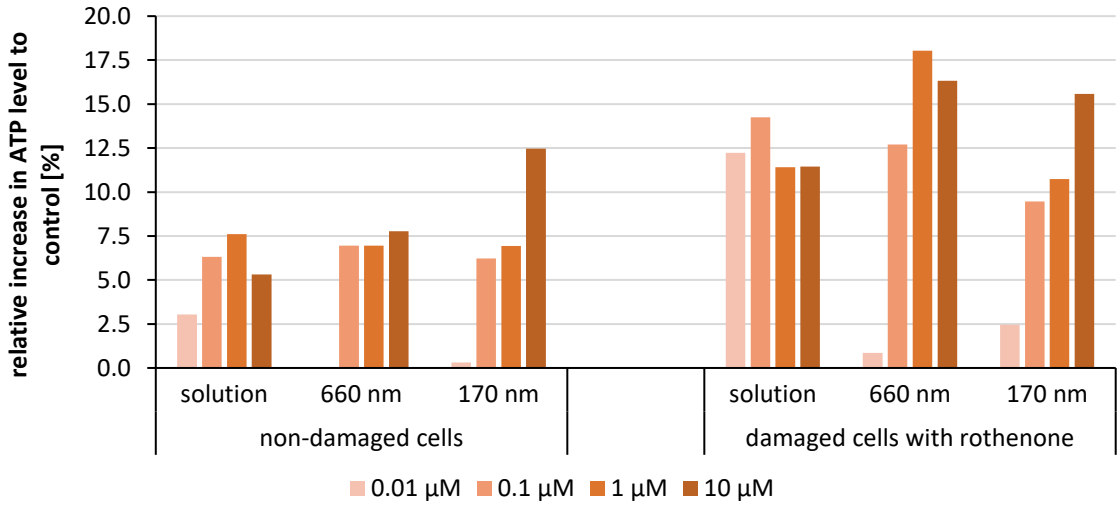

***Figure 32:** Determination of the increase in ATP levels in relation to the untreated control in an Alzheimer's disease cell culture model. Non-damaged cell represents the model for the early stage of AD, rotenone is used as model for the progressed stage of AD.*

One possible explanation would be a non-linear dose-response-curve, which was often reported for antioxidants [209,210]. Hence, data could indicate an antioxidative potential of hesperetin at lower doses but pro-oxidative effects at higher doses, i.e. hesperetin might be another member of compounds that are known to undergo hormesis effects [211,212]. Pro-oxidative effects were found for example in a study by G. Yen et al. [213] and by J. Zhang et al. [214], where hesperetin increased the ROS levels at concentrations > 100 µM in lymphocyte cells and hepatocellular carcinoma cells, respectively. It was furthermore shown that some flavonoids are capable of auto-oxidize while simultaneously producing the superoxide anion, hydrogen peroxide, and hydroxyl radical resulting in metabolism disorder and DNA damage and, consequently, cell cytotoxicity [215,216].
In contrast, data in this work showed, that the small sized NC were most effective and led to the most pronounced increase in ATP in SH-SY5YAβAPP_{wt} cells, also at higher hesperetin concentrations. So, if it is assumed that hesperetin as NC - at least in the concentration tested in this study - has no pro-oxidative properties at higher doses, this would indicate that small NC, which showed the highest solubility, lead to the most pronounced biological effect. After rotenone treatment, only a slight additional mitochondrial protection was detected after incubation with hesperetin NC, while the hesperetin solution showed no significant protection at all. The larger sized NC yielded already a significant elevation at the small concentration of 1 µM, whereas the small sized NC showed a significant increase of ATP at 10 µM.

The data were not expected and seemed to be not conclusive at the first glance, because initially it was expected that differences would only be observed depending on the dose, but not between the different formulations at the same concentration. This was assumed, because it was expected that all active - independent on the formulation used - can be dissolved in the cell culture experiment, leading to similar amounts of dissolved active and thus to similar cellular *in-vitro* effects. Nevertheless, the weaker performance of the ethanolic solution compared to the NC regarding antioxidant activity in a cellular system echoes the *in-vitro* DPPH assay. As a logical consequence, it needed to be analyzed whether re-crystallization occurred. Since the cell medium contains, among other compounds, proteins that impair the LD measurement, a microscopic characterization was carried out. Indeed, microscopic observation revealed the presence of particles with sizes in the range between 1-10 µm (**Figure 33 A**). The same procedure was carried out in an isotonic saline solution with NaCl, which corresponds to the classic *in-vivo* application where even more and larger precipitates were found (**Figure 33 B**). This could be explained by the salting-out effect, where an electrolyte – non-electrolyte interaction yields less solubility of the non-electrolyte. This effect could be attenuated in the cell medium by the presence of complex polyvalent ions and organic molecules.

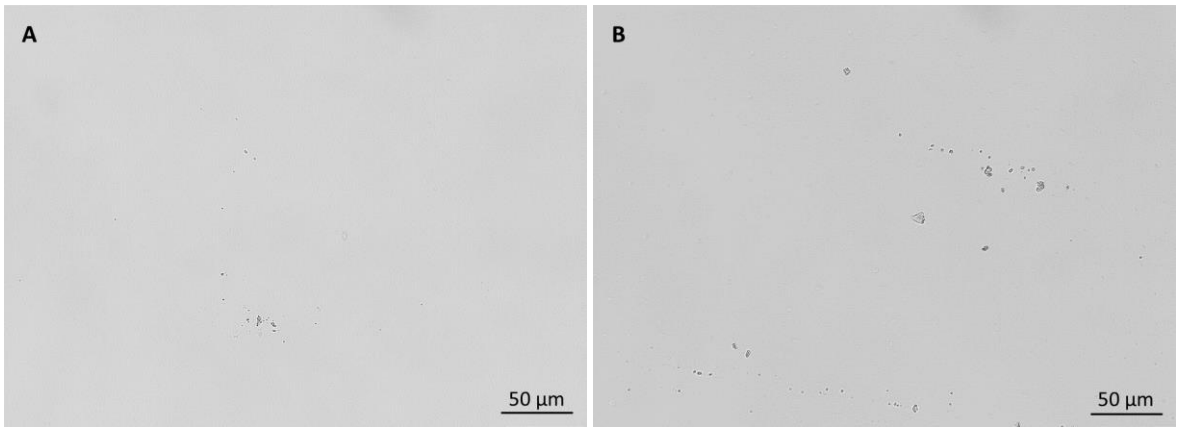

Figure 33: *Microscopic images of ethanolic hesperetin solution dispersed in A - cell culture medium, B - 0.9% NaCl solution.*

Due to the unexpected results obtained for the ethanolic hesperetin solution, which could be explained by a partial precipitation of the active and thus the reduction of dissolved molecules and lower biological activity, also a more detailed interpretation of other results seemed to be necessary. Hence, it was aimed to investigate if also for the differently sized NC a reduction of freely dissolved molecules might have occurred during the cell culture tests. In the case of NC, a reduction in solubility is possible due to re-crystallization and/or agglomeration of particles. Both phenomena result in the formation of larger particles, and consequently lead to a reduction in kinetic solubility and dissolution velocity. Therefore, to investigate the formation of larger particles during the cell culture experiments, the cell culture experiments were simulated by adding the formulations to the cell culture medium. Possible changes in size were monitored over time by analyzing the size by both, PCS and LD. It should be noted that proteins can also be detected in the cell culture medium, which could bias the particle size of the NC. For this reason, only the change in particle size over 4 h was considered. In addition, the zeta potential of the particles was analyzed in cell culture medium and compared to the ZP obtained in water and original dispersion medium.

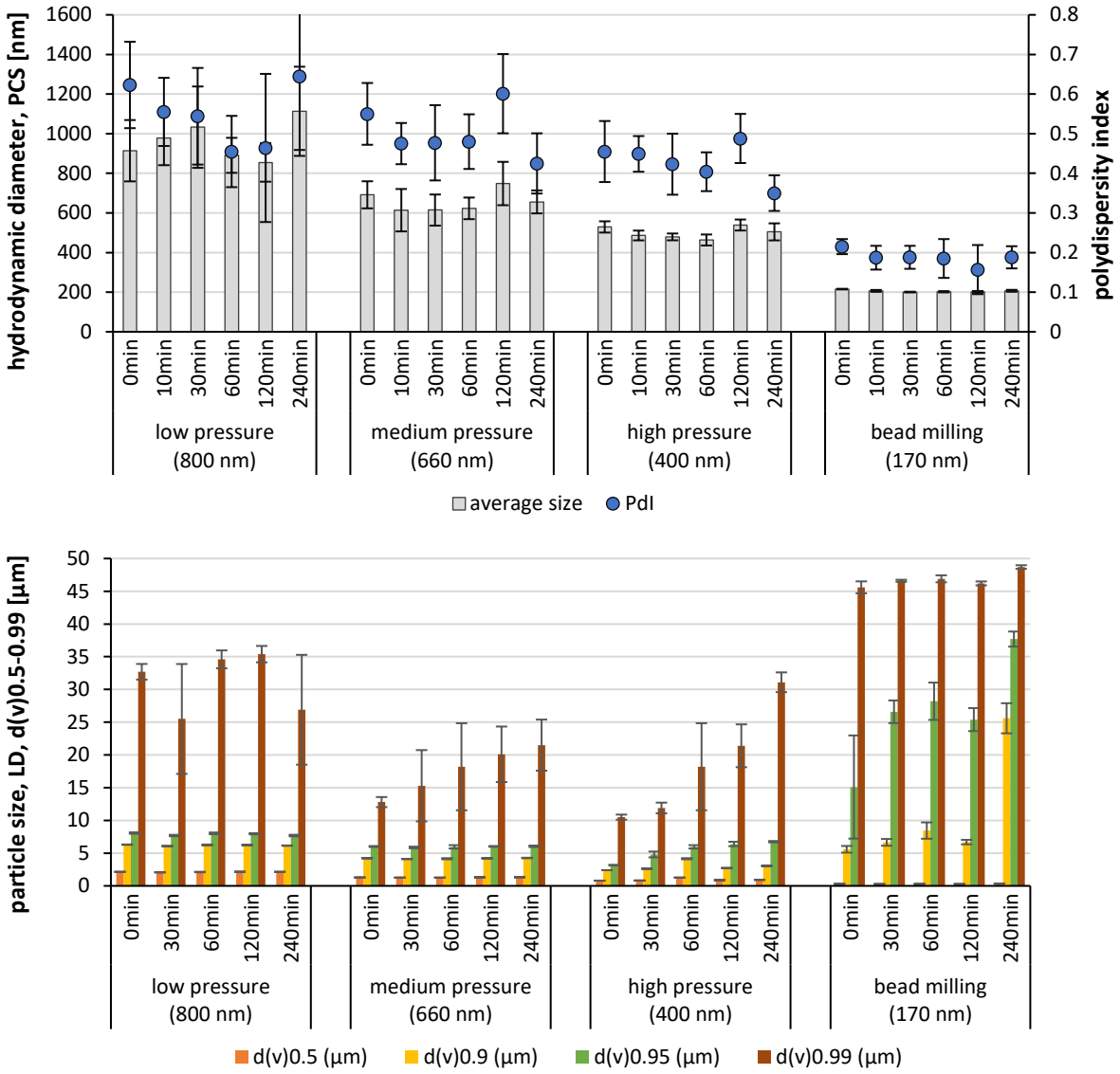

Figure 34: *Change in particle size of the hesperetin NC in the cell culture medium, measured by PCS (upper) and LD (lower). Formulations were dispersed in cell medium and directly measured afterward (0min) and in defined time intervals (10-240 min).*

Size analysis revealed no changes in the particle size for all NC when analyzed by PCS (**Figure 34** upper). However, when looking at the sizes obtained by LD measurements (**Figure 34** lower), clear changes in size become obvious. Changes in particle size were not detected for the d(v)0.50 values. Hence, data confirm results obtained from the PCS analysis and prove that the mean size was not affected by the addition of the cell culture medium. However, pronounced changes were detected for the d(v)0.99 values. Hence, in all formulations about 1% of the volume of the particles processed sizes between 20 and 50 µm. The d(v)0.90 and d(v)0.95 values of the larger sized NC, produced by HPH, were not affected by the addition of the cell culture media, i.e. the particle sizes remained unchanged and did not show any particle growth. In contrast, the d(v)0.90 and d(v)0.95 values of the smallest sized NC produced by BM, were strongly affected by the cell culture medium and resulted in d(v)0.9 values > 25 µm. This means that, in contrast to the larger sized NC (> 400 nm), where only < 1% of the particles

possessed sizes > 25 µm, the 170 nm NC contained at least 10% of aggregated hesperetin particles in the micrometer range. As a result, a lower number of NC would be practically available and then less dissolved active was available in the initially small sized NC formulation than for the larger sized one. Consequently, a similar efficacy despite different size and solubility, which were not conclusive at the beginning, became logical when considering the size changes upon the addition of the cell culture medium.

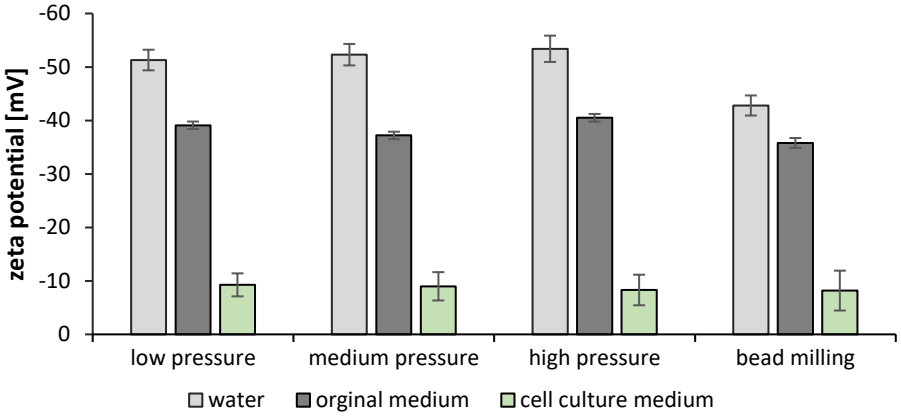

Figure 35: *Determination of zeta potentials of differently produced hesperetin NC measured in cell culture medium in comparison to the ZP in water and original dispersion medium.*

Reasons for the more pronounced increase in size for the 170 nm NC in the cell medium might be explained by the production method and the resulting differences in zeta potentials. Only the small sized NC were produced by BM, whereas all larger sized NC formulations were produced by HPH. Again, zeta potential analysis in water revealed lower values for the NC that were produced by BM. In contrast, the same ZP were found for all formulations when analyzed in the original dispersion medium or cell culture medium (**Figure 35**). Zeta potential analysis in cell culture media was performed to determine the influence of the cell culture medium on the physical stability of the particles. Results revealed a strong decrease in ZP for all formulation to < |10| mV, implying thus a strong impact of the cell culture medium on the physical stability of the hesperetin NC. Hence, the differences in physical stability between both production methods cannot be explained from this data set. Also, no differences in ZP were obtained when the particles were analyzed in the original dispersion medium, which indicates that the surfactant layer around the particles is similar for both particles. However, the differences in ZP analyzed in water could give a hint that the small sized NC possess a more hydrophobic (less polar) surface than those produced by HPH. Again, ZP analysis in water means that the particles are diluted for the measurement and the surrounding surfactant layer is washed off, when not firmly bound to the surface of the particles, that in turn resulted in the determination of the Stern potential, which is strongly related to the Nernst potential of the particles [180] (**Figure 36**).

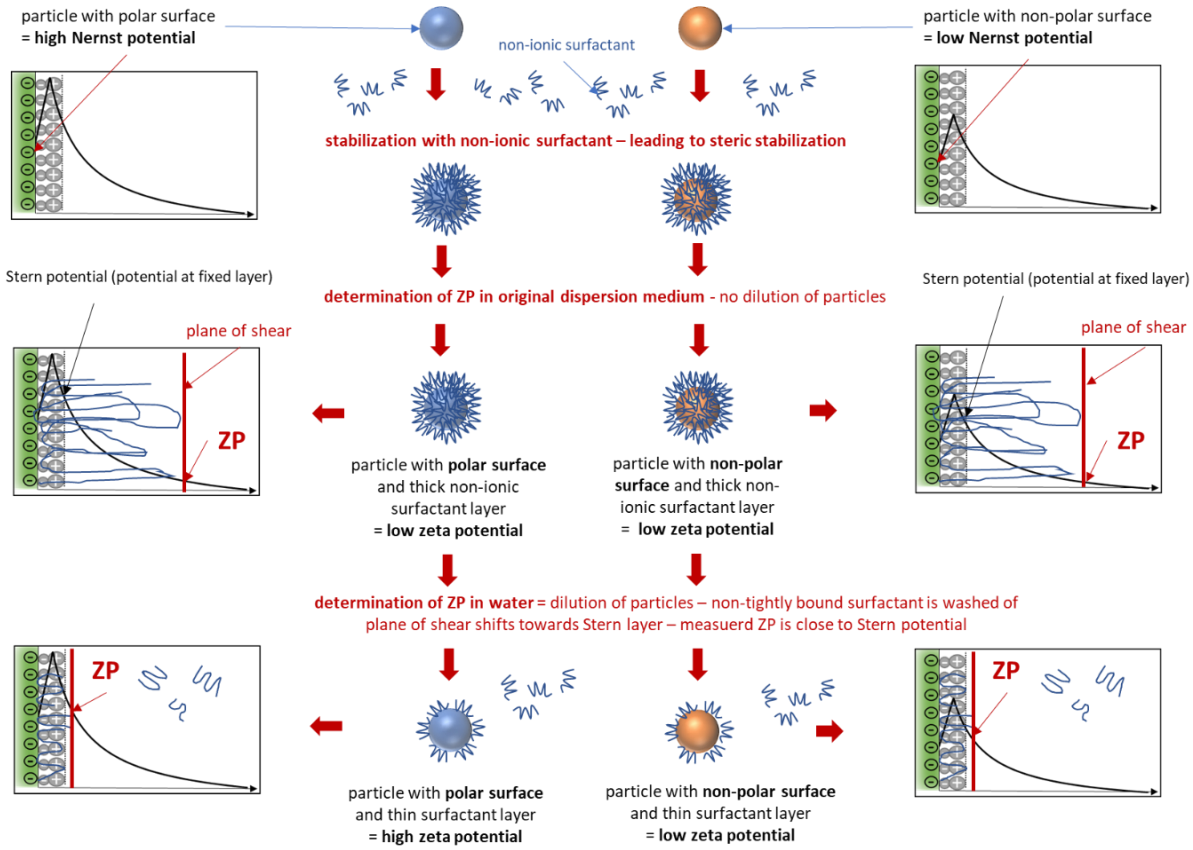

Figure 36: *Scheme of zeta potential analysis of nanoparticles in different dispersion media. Upon addition of a non-ionic stabilizer, a thick polymer layer is formed around the particles. Analysis in original dispersion medium analyzes the charge of the particles in original state. Analysis in water analyzes the charge close to the Stern layer (fixed layer). As the Stern potential is closely linked to the Nernst potential, differences in surface polarity of the particles can be discriminated.*

Based on this observation it can be assumed that dilution with cell culture medium – which will also lead to this wash off effect and a subsequent rearrangement of the surfactant layer – will cause a more pronounced agglomeration and particle growth of the small sized particles with hydrophobic surface than for the particles with a more hydrophilic surface. The reason is, that the free interfacial energy is higher for the hydrophobic surface and accordingly also the tendency to reduce the total surface.

In section 4.1.2.3, the washing off from surfactants by substances contained in the cell culture medium was observed over time as the ZP approached that of the medium (**Figure 18**). It was proposed that the adjustment of the ZP was faster for the smaller stabilizer molecules. As the decyl glucoside, PLC, can be considered as a small molecule, fast desorption from the particle surface was also expected in this case. The surfactant would be replaced by other small cell culture substances such as sugars or amino acids, or entrap them and proteins in micelles. Indeed, the zeta potentials of hesperetin NC in cell culture medium adjusted immediately and remained within the same range for 24 h (**Figure 37**).

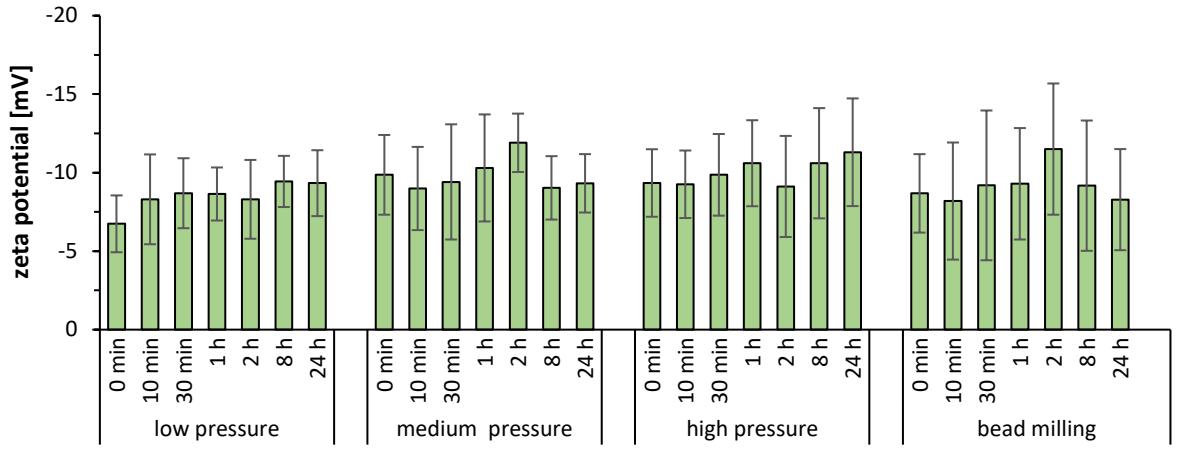

Figure 37: *The ZP of differently produced hesperetin NC measured in cell culture medium at various time points over 24 h of storage.*

The immediate change and weakening of the surface shielding, resulted in fast agglomeration, i.e. at the moment when particles come into contact with the medium, the surfactants are washed off, which causes agglomeration of the particles immediately to reduce the high surface energy of the smallest particles. On the other hand, the ZP measurement indicates long-term stability. It was therefore assumed that NC will not be stable in the medium for all formulations over weeks. Again, the small particle fraction has the highest surface energy, which the system aimed to compensate by the formation of aggregates. This probably happened faster and to a greater extent and would occur also for larger sized particles after a certain time.

Based on the observations, that both – ethanolic hesperetin solution and nanocrystals – changed their physico-chemical properties during the cell culture experiments, it needs to be concluded that the real potential of hesperetin for the prevention and treatment of AD could not fully be exploited in this study. Nonetheless, results demonstrate the great potential of this API and the superiority of the NC for the treatment of AD.

Results also demonstrated the urgent need to characterize the physico-chemical properties of all samples that are used in the biological test assays, not only *in-vitro* but also in the biological test media itself. Solutions of active compounds in organic solvent are likely to precipitate in the aqueous cell culture media, especially if high concentrations and/or poorly water-soluble actives are used. As seen in this work, such precipitations could be easily overseen by the naked eye, because only structures in the lower micrometer range are formed. As only particles with sizes > 150 µm are regarded to be visible [217], smaller non-visible particles can only be detected by using for example light microscopy. So, once organic solutions of API are used in cell culture tests, light microscopy should be used to prove that no precipitation of the API occurred in the cell culture medium. The same is recommended, whenever organic solutions are tested in other biological media such as artificial blood, i.e. isotonic

NaCl solution. Due to the clear appearance of the NaCl solution the formation of crystals is easily detectable (**Figure 33 B**). Tests of this kind should be considered in the future to avoid false conclusions or misinterpretations of biological test models.

Moreover, in this study, not only the organic solution was found to undergo changes in size, but also the NC were shown to agglomerate to some extent. The agglomerates were not detected when DLS measurements were performed as a stand-alone technique for the characterization of the particles, and only the use of an additional technique, i.e. laser diffraction, could reliably detect the changes in size. Hence, data demonstrated again, that size analysis is only meaningful if different and independent methods are used [179,218]. Finally, only the combination of different techniques for particle size characterization of the final formulations allowed a conclusive explanation of the results obtained. In conclusion, it means that the development of a nanoparticular formulation should include not only the determination of physical stability under storage conditions but also the testing of physical stability in biological test media. Consequently, only the formulations being physically stable in the biological test medium should be used for all biological experiments. The optimal formulation should of course possess both, sufficient physical stability during storage and in the biological test setup.

To sum up, the aim in this chapter was to develop tailor-made hesperetin NC by different methods and conditions in order to investigate a size-dependent effect regarding dissolution velocity and efficacy in a cell culture model. NC populations ranging between 170 – 800 nm were successfully produced. It has been demonstrated that the smallest NC population exhibits the fastest dissolution rate in the saturated medium. Larger NC showed a slower dissolution rate, which decreased with increasing amount of microparticles, so all tailor-made NC were improved compared to the coarse bulk material. A size dependency became more evident the higher the concentration of the formulations used, with a significant increase the smaller the particles. Therefore, if drug NCs are intended to be developed, future studies should focus on producing them with the smallest possible size.

4.3 Development of rutin nanocrystals in a pulmonary formulation for treating COPD

Worldwide, three of the top five non-infectious diseases caused death are related to lung diseases such as chronic obstructive pulmonary disease (COPD). This term covers various diseases of the lungs that are caused by inflamed and permanently narrowed airways and bronchi. Their symptoms involve chronic coughing, sputum, shortness of breath, and a significant reduction in performance. Up to now, COPD cannot be cured but only treated which ultimately causes the patient to die under respiratory distress [66]. Inhalation of cigarette smoke and environmental pollutants induces the alveolar macrophages in the lung epithelial cells to produce an excess of reactive oxygen and nitrogen species leading to oxidative stress [49,50]. Thus, oxidative stress plays the most important pathological mechanism in COPD [53,54]. Furthermore, it might result in acute or chronic inflammation, climaxing in a process of lung repair and it is highly associated with a decrease in lung function [66].
Flavonoids have been widely used in folk medicine and, as aforementioned, are attributed with anti-inflammatory and antioxidant activity. For example, an *in-vitro* and *in-vivo* mouse study by Lim et al. demonstrated the reduction of inflammatory cells, TNF-α, IL-6, and NO production in lung macrophages [219]. The isolated flavonoid, rutin, is also associated with great benefits in the treatment of inflammation and oxidative stress found in COPD, which qualifies rutin as a promising candidate [97,98]. Due to its low solubility in water and the difficulty to address the specific target, namely the lung macrophages, technological application strategies are required that combine both in one.

Therefore, the aim was to develop a sophisticated and easy-to-use formulation with rutin to reduce oxidative stress and its causes in the lung. For reaching this, three sub-aims were defined:

I. Rutin as a poorly water-soluble antioxidant must be produced to stable nanosuspensions from which,
II. the most pronounced formulation must be transferred to an inhalable dry fine powder, that in turn
III. should demonstrate enhanced antioxidative and dissolution properties *in-vitro*.

4.3.1 Production of rutin nanocrystals

For the development of a physically stable rutin nanosuspension with the aim of a pulmonary application, the following requirements must be fulfilled: the presence of a suitable stabilizer that not only protects the NC from agglomeration but is also harmless and approved for the administration into the lungs. Furthermore, since the special properties of NC are also related to their size (c.f. chapter 4.2), the first step of this chapter focused on the production of the smallest possible NC using HPH.

Afterward, the stability of the nanosuspension will be assessed and the most promising ones will be investigated in a scale-up process. It was assumed that the most stable nanosuspension would be also more resistant to further stress by formulation development studies. The scale-up investigation is needed to address industrial application issues but also to obtain enough material for additional investigations, such as *in-vitro* characterization, formulation optimization and cell culture studies.

4.3.1.1 Characterization of the nanocrystals

4.3.1.1.1 Particle size

Rutin NC were produced by HPH. Besides the production parameters, e.g. temperature, number of homogenization cycles, and power density (homogenization pressure), the stabilizer used also affects the resulting particle size, size distribution and especially the physical stability [155,220]. Hence, in this study, five different stabilizers were used. These were selected from a pool of surfactants being suitable for inhalation or are proved to be safe for a lung administration, i.e., they possess the GRAS (generally recognized as safe) status and are introduced in terms of chemical properties in **Table 6.**

***Table 6**: Chemical properties of the stabilizers used to produce rutin NC. The degree of the hydrophilic and hydrophobic groups is empirically expressed by the HLB (Hydrophilic Lipophilic Balance), where a higher value represents a more hydrophilic character. Lecithin consists of a mixture of polar and non-polar lipids with a predominant group of glycerophospholipids, e.g., phosphatidylcholine, so that a fixed HLB value can only be estimated.*

stabilizer	macro-structure	HLB value	charge	water-solubility
bovine serum albumin	polypeptide	-	zwitterion	40 g/L
Tween 80	polysorbate	15	nonionic	100 mL/L
Poloxamer 188	triblock copolymers	> 24	nonionic	soluble, > 100 g/L
Lecithin S75 Lecithin E80	phospholipids	6-10	zwitterion	practically insoluble < 0.1 g/L

The stabilizers were used solely or two of them are combined (co-stabilized) with the aim of increasing the physical stability of the resulting rutin nanosuspension. By doing so, 12 different formulations were produced (**Figure 38**). The production parameters were the same for all formulations, that means in detail that all formulations consisted of 5% (w/w) rutin and 1% (w/w) surfactant or surfactant mixture, they were prepared with 20 homogenization cycles at 1,500 bar, and strictly cooled down to a temperature < 10 °C between the cycles.

As result, the hydrodynamic diameter of the particles analyzed by PCS ranged from 300 nm for BSA-stabilized rutin NC to 430 nm for Lecithin S75-stabilized one (**Figure 38**). One sub-aim was the production of NC as small as possible, preferably < 400 nm, which was achieved for most formulations. In general, formulations with average particle sizes (hydrodynamic diameter) larger than 400 nm were obtained when using lecithin as a stabilizer or co-stabilizer (**Figure 38**).

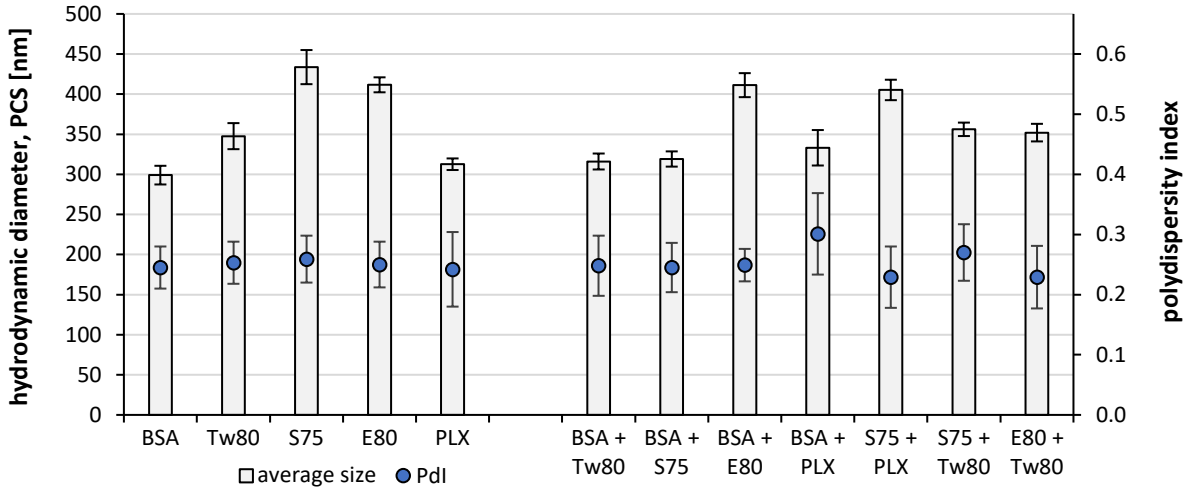

Figure 38: *The hydrodynamic diameter and size distribution by PCS of the rutin NC at the day of production depending on the stabilizers used: BSA – bovine serum albumin, Tw80 – Tween 80, S75 – Lecithin S75, E80 – Lecithin 80, PLX – poloxamer 188. Formulations were produced by HPH for 20 cycles at 1,500 bar.*

Moreover, in this study, particle sizes were slightly smaller than in other previous studies in which particle sizes of about 700 nm were obtained by HPH [221]. The reduction of the particle size using HPH was improved by strict cooling during the whole homogenization process and by a suitable ratio of rutin, stabilizer and water. Further diminution of the particle size would not be reached by HPH. After application of the first main homogenization cycle, the average particle sizes ranged between 470 and 344 nm. Application of additional 19 cycles reduced particle size by approximately 40 ± 30 nm, with the most efficient size reductions observed within the first cycles (**Supplementary Figure S1-S12**). This is in good agreement with a study by V. Martena and co-workers [222]. They also demonstrated that increasing the number of homogenization cycles up to 30 even increases the average particle size due to the formation of agglomerations [222]. Such agglomerations are driven by the insufficient stabilization effect of the drastically increased surface energy in total [147]. On the other hand, a recent study showed that doubling the homogenization pressure from 2,000 bar to 4,000 bar has only a minor effect on the particle size, too [156]. Another approach to producing smaller NC is a combined technique of BM and subsequent HPH (smartCrystals®) that was used in a recent study and resulted in rutin NC of about 300 nm in hydrodynamic diameter [223]. Therefore, the particle size obtained in this thesis seemed to be the smallest possible by HPH and even smaller particles could not be obtained. However, performing the small scale BM technique might lead to smaller particle sizes (c.f. chapter 4.2) but this was not an option in this study because a higher quantity of rutin NC was required for subsequent investigations and formulation steps.

Besides the small particle size, its size distribution should be small at the same time otherwise the Ostwald ripening is facilitated [193]. The polydispersity index (PdI) is a measure of particle size distribution and was about 0.25 (**Figure 38**), indicating a rather broad size distribution.

In general, it has been shown that NC formulations produced by HPH can have PdI values between 0.20 and 0.25 [167,221,224]. The reason for the relatively high dispersibility can be attributed to the production process of the NC. Due to the cavitation forces, the crystals are broken in their fragile points in the particle structure, so-called imperfection. As result, very small particle or molecule aggregates are split off from the parent crystals that in turn remain as “larger fragments” in the suspension. Increasing the number of cycles increases the number of NC due to many splits from the imperfections and the resulting size reduction of the parent crystal. As consequence, the crystals become more and more perfect, where further reduction is no longer possible [155]. At the same time, the split-off fragments might vary in size depending on the imperfection location at the parent crystal.

The presence of those larger "perfect" crystals and thus the broad particle size distribution could be confirmed by LD measurements, where particles up to 3.2 µm in size were detected (**Figure 39**).

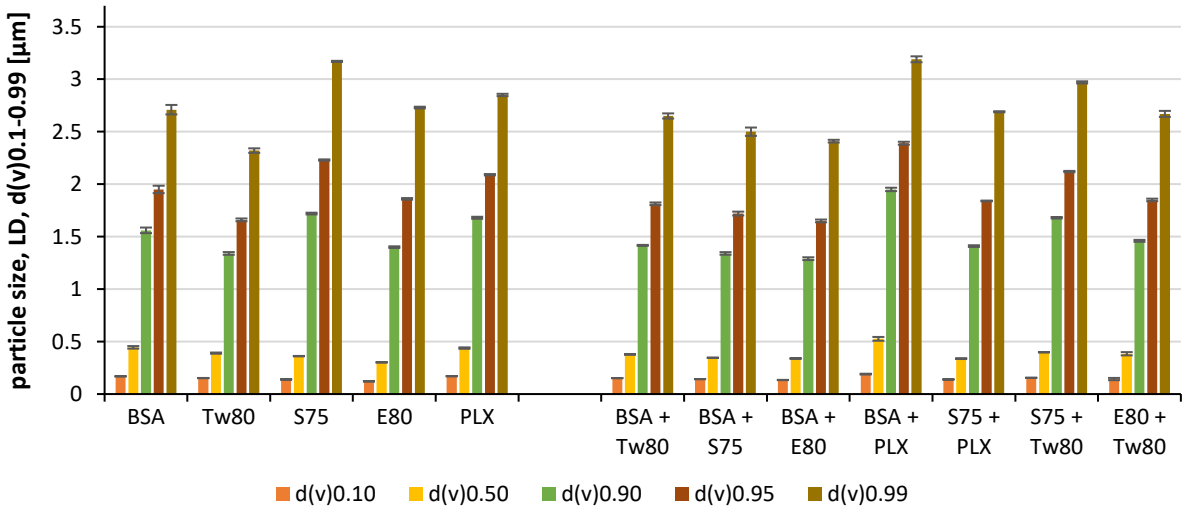

Figure 39: *Particle sizes by LD measurements at the day of production depending on the stabilizers used: BSA – bovine serum albumin, Tw80 – Tween 80, S75 – Lecithin S75, E80 – Lecithin 80, PLX – poloxamer 188. Formulations were produced by HPH for 20 cycles at 1,500 bar.*

The polydispersity can also be expressed by calculating the span from LD-Data as

$$\text{span} = \frac{\text{d(v)0.90} - \text{d(v)0.10}}{\text{d(v)0.50}}$$

[220]. This equation shows that the narrower the d(v) values are relative to each other, the smaller the resulting span value and thus the smaller the polydispersity. Similar to the PdI by PCS the values should be as small as possible. In **Table 7** the PdI values and the calculated span values are compared. Interestingly, there are large differences in the highest and lowest values for the polydispersity, based on the method used. For example, Tween 80-stabilized formulation showed the smallest, whereas Lecithin S75-stabilized NC the largest span value. In contrast, the surfactant mixtures of Lecithin S75

and PLX, as well as Lecithin E80 and Tween 80 had the smallest and the mixture of BSA and PLX the largest PdI value.

Table 7: *Comparison of the particle size distribution by the approximation via PCS and the calculated one via LD data. The green and red highlights display the smallest and largest value in the column, respectively.*

stabilizer	span	PdI
BSA	3.13	0.25
Tw80	3.05	0.25
S75	4.38	0.26
E80	4.24	0.25
PLX	3.45	0.24
BSA + Tw80	3.35	0.25
BSA + S75	3.46	0.25
BSA + E80	3.41	0.25
BSA + PLX	3.35	0.30
S75 + PLX	3.76	0.23
S75 + Tw80	3.83	0.27
E80 + Tw80	3.43	0.23

The question now is why the stabilizer influences the particle size directly after production. After leaving the homogenization gap, the particles were able to agglomerate if the stabilizing effect was not fast enough. This depends on the molecular weight of the stabilizer (the diffusion is faster the smaller the molecular weight) and on the de-aggregation velocity from the surfactant micelle to the monomer. For this reason, it was expected that a surfactant mixture of a low and a high molecular weight surfactant would lead to an advantageous synergistic effect. Interestingly, the highest PdI by PCS and the largest particles by LD (d(v)0.90-0.99) were found in the same formulation, that was co-stabilized by the highest molecular weight surfactants, BSA and PLX (**Figure 38** and **39)**.

4.3.1.2 Zeta potential

As already mentioned, the zeta potential measurement, representing the physical long-term stability, was used to study the stabilizer's effectiveness and suitability, which in turn plays the deciding role for further investigations. The ZP measurements were performed in water and in the original medium (corresponding surfactant solution) to assess how tight the surfactants were bound onto the particle surface. For non-ionic surfactants (PLX and Tween 80) the difference between both measuring media should be nearly zero as the layer remained unchanged onto the particle surface, whereas for ionic surfactants (lecithins and BSA) the difference could be high due to the additional absorption of ionic charge.

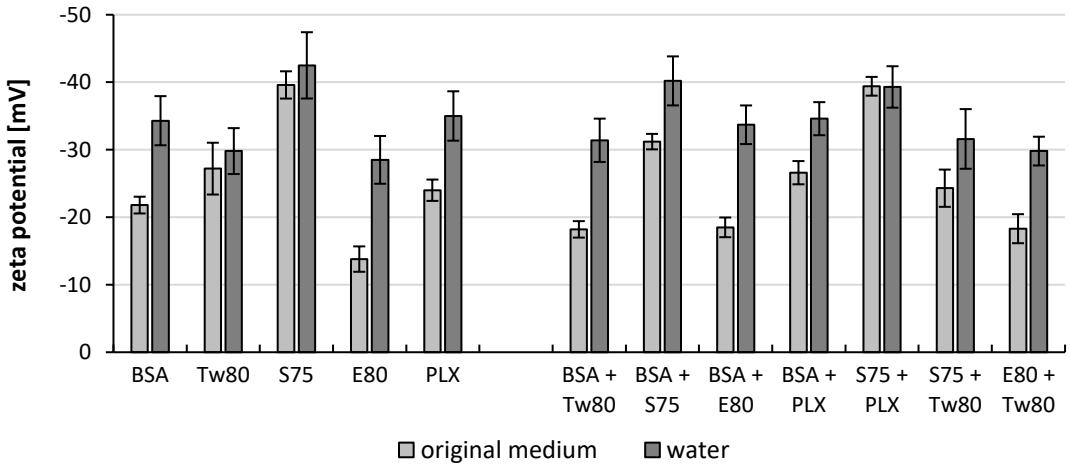

Figure 40: *Zeta potential measurements of each rutin nanosuspension in water (adjusted to a conductivity of 50 µS/cm by using sodium chloride solution) and the original media (obtained by a 1% (w/w) stabilizer solution). Data expressed as mean ± SD.*

Measured in water, all ZP values ranged around -30 and -40 mV, which is associated with good stability (**Figure 40**) [180]. For all mono-stabilized nanosuspensions, formulations with Tween 80 and Lecithin E80 seemed to be the most promising non-ionic and ionic stabilizers, respectively. Concurrently, the ZP values of the mono-stabilized formulations without lecithins and measured in the original medium were around -25 mV, while those mono-stabilized with Lecithin S75 and E80 differed significantly with ZP by about -40 and -15 mV, respectively.

However, it must be considered that surfactants were able to additionally form micelle structures with their own detectable surface charges. If such surfactant micelles are present along with the NC, they would be involved in the ZP measurement and thus influence the resulting ZP value. In terms of lecithin, even vesicles could be developed. Due to their poor aqueous solubility, it was assumed that lecithin molecules diffuse more slowly to the particle surface during the NC production and instead develop nanostructures among themselves, e.g. micelles or vesicles.

Therefore, the next step was aimed to investigate whether and how easily such lecithin micelles or vesicles can form. For this purpose, a 1% (w/w) suspension of Lecithin S75 or E80 itself in purified water was prepared by HPH for 3 cycles at 500 bar and then their zeta potentials were measured. Indeed, it was possible to form detectable structures that confirm the difference in the ZP (**Figure 41**). Moreover, these ZP values did not change even when other surfactants are involved in an equal ratio of 1:1. In other words, the presence of lecithin seemed to be a key factor in determining the value of the ZP and cannot be changed by other non-ionic surfactants and probably only slightly by other neutral compounds like rutin. This observation might explain why the ZP of NC stabilized with Lecithin S75 and E80 were significantly different compared to the otherwise-stabilized rutin NC (**Figure 40**).

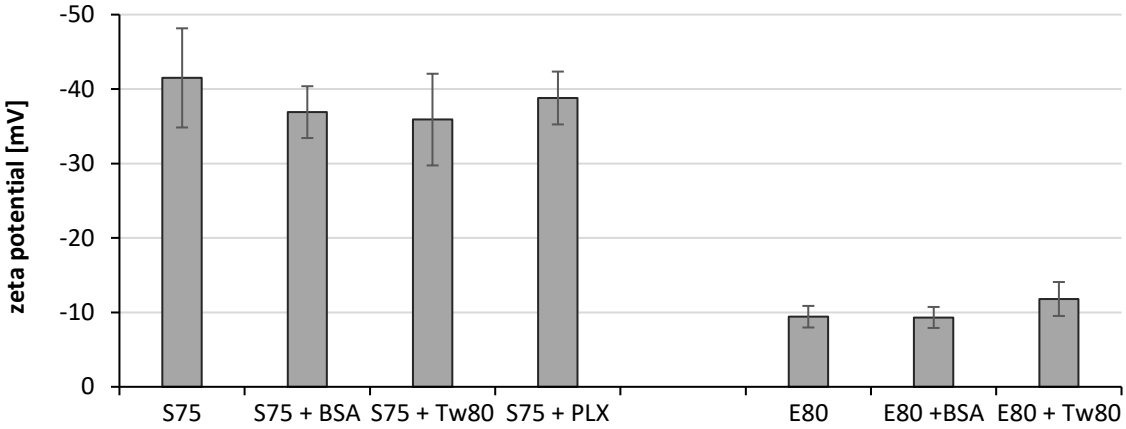

Figure 41: *Zeta potentials of the developed micelle structures generated by HPH of a 1% (w/w) aqueous surfactant dispersion.*

Lecithin consists of a mixture of polar and non-polar lipids with the main compound glycerol-phospholipids, e.g. phosphatidylcholine. Lecithin E80 is obtained from egg and contains 80% (w/w) of phosphatidylcholine while Lecithin S75 from soya contains 70% (w/w). Also, depending on the source they vary a lot for the fatty acid chain length and degree of unsaturation as well as for the type of polar head groups most favored. On the other hand, both lecithin types showed no differences in viscosity, surface tension, and spray angle [225]. In fact, when using lecithin, not only one or a few chemical structures could cover the nanoparticle by absorption, but instead many, sometimes completely different structures were adsorbed onto the surface. Thus, lecithin can be considered as a highly interacting and potent complex emulsifier. The different compositions, therefore, resulted in the different ZP of the rutin NC and the nanostructures (**Figure 40** and **41)**

Also, different surfactant combinations were tested to elevate the effectiveness of possible synergistic effects. Formulations measured in water showed values being the mean of the corresponding mono-stabilized formulation, whereas measurements in the original medium indicate no tendency (**Figure 40**). In-depth investigations dealing with the interaction of the surfactants on the rutin surface would be necessary to determine the shielding potential. To this point, a mixed and complex surfactant layer on the surface could have formed, whose interpretation regarding the physical stability would only be a vague assumption at this point of the study and shows the need for monitoring the long-term stability. So, the influence of interaction and stability of the co-stabilization between two surfactants will be discussed in detail next.

4.3.1.3 Storage stability of the rutin NC

During the storage, the developed nanosuspensions can undergo biological, chemical, and physical degradation. In general, the aqueous media are susceptible to uncontrolled microorganism growth, investigated in more detail in section 4.3.1.5. Examples of chemical decay are oxidation or hydrolyzation which are discussed in section 4.3.1.6. The physical instability of nanosuspensions such as agglomeration and Ostwald ripening is subsequently focused.

4.3.1.3.1 Physical stability

So, for determining the physical stability, the particle size of the 12 rutin nanosuspension was monitored over 12 months by storing them in 50 mL screw cap flask in the fridge (5 ± 3 °C). That means that the particle sizes were analyzed after 1, 7, 14, 28, 60 and 90 days as well as one year after the day of production.

For a better overview, the results of the first 28 days of storage will be discussed separately at the beginning. **Figure 42** shows the alteration of the particle size measured by PCS and LD. These data give a short overview and detailed results are attached (**Supplementary Figures S1-S12**). All formulations, except three, namely those stabilized with Tween 80, Lecithin S75, and the combination of Lecithin S75 with PLX, were physically stable over four weeks of storage regarding particle size (**Figure 42** upper). Interestingly, the NC stabilized or co-stabilized by BSA are characterized by a smaller average particle size which remained unchanged during the storage time of 4 weeks. So, they seemed to be promising at the first glance. In contrast, it can be seen that the formulations stabilized with Tween 80 and co-stabilized with a lecithin led to the development of agglomerates because the d(v)0.99 value increased strongly whereas the average particle size decreased at the same time (**Figure 42** upper). However, this is typical and can be explained as follows: If particles agglomerate, they are recognized as large structures in the LD, while PCS cannot see them due to the detection limit. As result, the larger fragments are overlooked by PCS, and the huge number of small particles shifts the hydrodynamic diameter to a smaller average size [178].

In contrast, nanosuspensions stabilized with the mixture of PLX and Lecithin S75 seemed to possess a slight particle growth, where the smallest particles dissolved and re-crystallized at larger particles (**Figure 42** upper). However, this process should be slow as the d(v)0.99 value gives no hint. Usually, the largest particles grow according to Ostwald riping, thus the d(v)0.99 value should be increased preferably. By investigating the most pronounced formulations for the scale-up process as well as for the subsequent drying step, the nanosuspensions were stored and monitored meanwhile for at least one year (**Figure 42** lower).

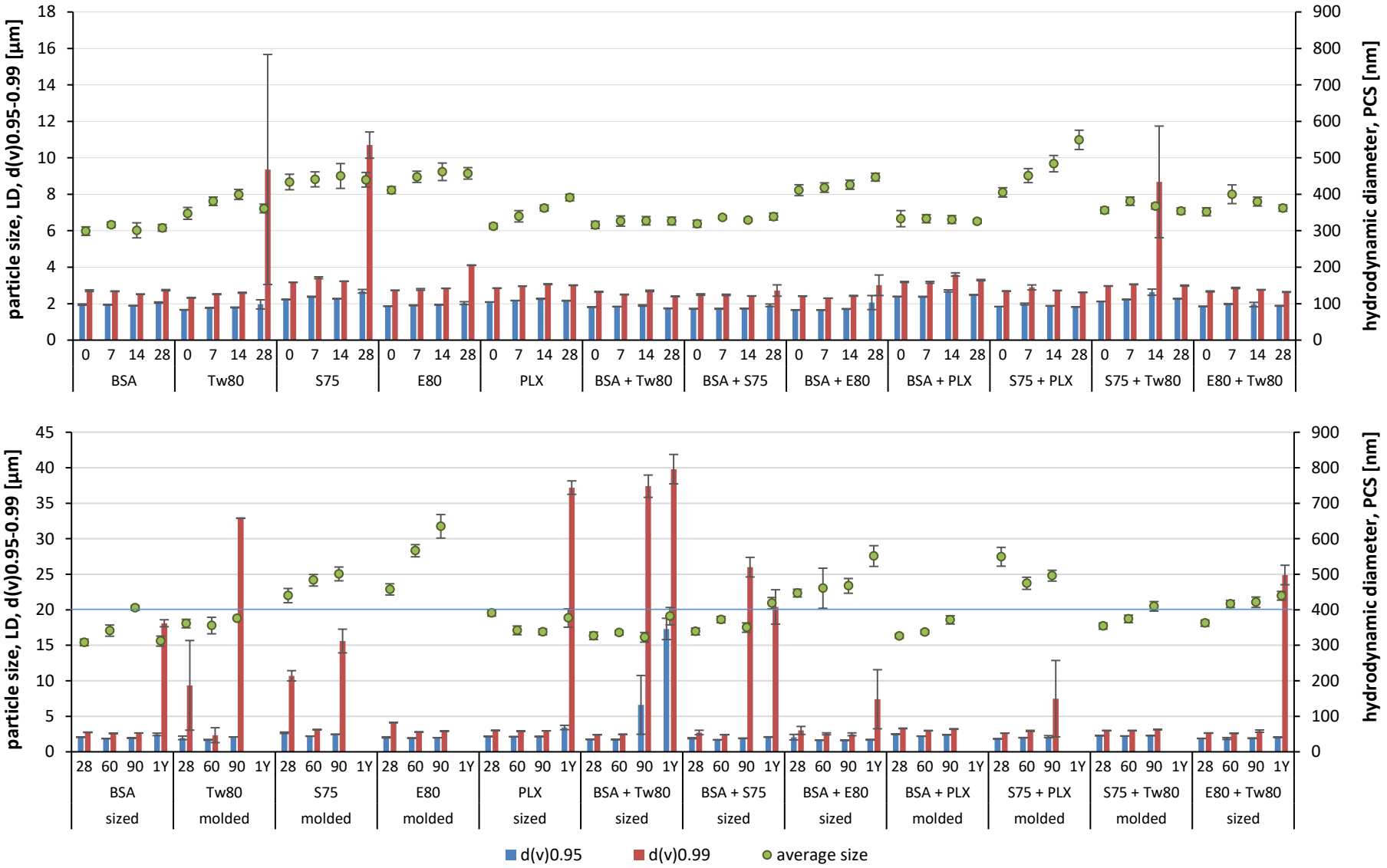

Figure 42: *Particle sizes of rutin NC measured by PCS and LD in dependence of stabilizer and stabilizer mixture, upper: at the day of production (0), and after 7, 14 and 28 days of storage, lower: after 28, 60 and 90 days as well as after one year (1Y) of storage.*

Based on the results obtained after a storage time of one year, the twelve nanosuspensions produced can be distinguished into two groups. One group displays formulations in which mold has grown during the storing time, i.e. they are microbiological unstable. These formulations were stabilized with Tween 80 or a lecithin, and with the combinations of BSA and PLX, Lecithin S75 and Tween 80, Lecithin S75 and PLX (**Figure 42** lower). The second group refers to nanosuspensions that are physically unstable, which means that the particle size has increased enormously including formulations stabilized with BSA or PLX and with combinations of BSA and Tween 80, BSA and lecithins, Lecithin E80 and Tween 80 (**Figure 42** lower).

Up to this point, no preparation seemed to be perfectly stable over one year of storage. So, this study demonstrated that a pulmonary application via a nebulizer could be rather impractical, as the stability would be too low considering the time of transportation and storage before the sale or at the patient's home. A drying process to stabilize against crystal growth or agglomeration could be a feasible approach to solve the issue. Therefore, the one-year storage study was conducted to get an idea of the resilience if other processes, like drying processes, would be applied and which surfactant or surfactant combination was best suitable to stabilize the rutin NC. However, before such improvement can be carried out, the factors responsible for the low physical stability should be analyzed.

Further information about the kind and extent of the physical instability was visualized by microscopy. The formation of agglomerations was observed in all formulations, which were microbiological stable over one year of storage (**Figure 43**). Reasons for the particle growth observed are already discussed previously.

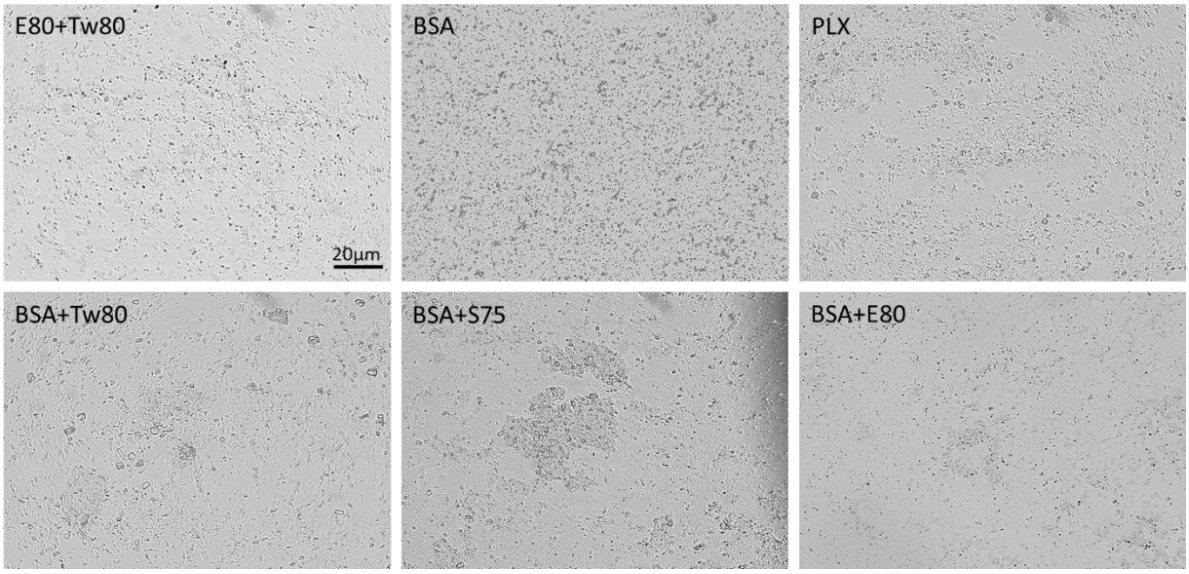

Figure 43: *Microscopic images of the rutin NC after one year storing in the fridge. Larger inhomogeneous structures represent agglomeration such as predominantly present in the formulation with serum albumin and Lecithin S75 (BSA+S75), while large crystals caused by Ostwald ripening can be seen in formulation with serum albumin and Tween 80 (BSA+Tw80).*

Additionally, crystal growth caused by Ostwald ripening was found in formulations with Tween 80 and to a lesser extent with PLX (**Figure 43**). This could be explained by the fact that surfactants are usually capable to increase solubility, which in turn would favor Ostwald ripening [193,226]. conventional non-ionic surfactants usually form classical micelles at lower concentrations. The surfactant PLX, however, develops monomer-micelles due to a change in configuration. Indeed, the critical micelle concentration (CMC), i.e. the concentration above which micelle can be produced themselves, is about 0.0015% (w/w) for Tween 80 [227], and 1.3 – 10% (w/w) for PLX depending on referring source [228–230]. Lecithin does not typically form micelles because it is poorly soluble in water and tends to form vesicles instead. After exceeding the CMC, the PLX monomers merge to aggregates of various sizes being able to solubilize drugs. Above the CMC the saturation solubility of hydrophobic APIs such as rutin is enhanced by entrapment (adsorbed or dissolved) in the micelle cores. Before reaching the CMC the API's solubility almost does not increase whereas from CMC onwards the solubility increases linearly with the surfactant concentration, indicating that solubilization is correlated to micellization [231]. Hence, the CMC is the lowest surfactant concentration needed for solubilizing a poorly aqueous soluble API. Consequently, as Tween 80 forms significantly more micelles, the solubility of rutin may be increased in Tween 80-stabilized formulations. On the other hand, not only the number of micelles determines the extent of solubilization but also the specific solubilization capacity, micelle-water partition coefficient and the shape of the micelle due to the loci (inner core, outer core, on polyoxyethylene/ -propylene or CH_2 chains and intermediate positions) [232]. This means that the chemical structure of the surfactant micelles and the resulting interaction potential of the API plays also a role in the solubility enhancement of the API.

In order to decide which formulation would be eligible for further processing steps, the non-molded formulations were compared and illustrated in **Figure 44**. The average particle size increased over time in all formulations, highlighted by a green trend line (**Figure 44**). Interestingly, the average particle size increased fastest where the d(v)0.99 values changed least and vice versa. For example, within one year of storage the hydrodynamic diameter and the d(v)0.99 value of rutin NC stabilized with a mixture of BSA and Lecithin E80 increased from 410 to 550 nm and 2.4 to 7.4 µm, respectively. Once again, it needs to be considered that the d(v)0.99 value represents only 1% of the particles by volume, i.e. the correlated number of particles is even many times lower. View differently, the smallest particles also have the smallest volume and thus a lot of them are needed to represent the volume of one larger NC. Therefore, most non-molded formulations could be considered to be stable, with the exception of the rutin NC stabilized with a mixture of BSA and Tween 80. In the nanosuspension stabilized with PLX, a slight change in the average particle size was observed on the day of production which was maintained over one year (**Figure 44**).

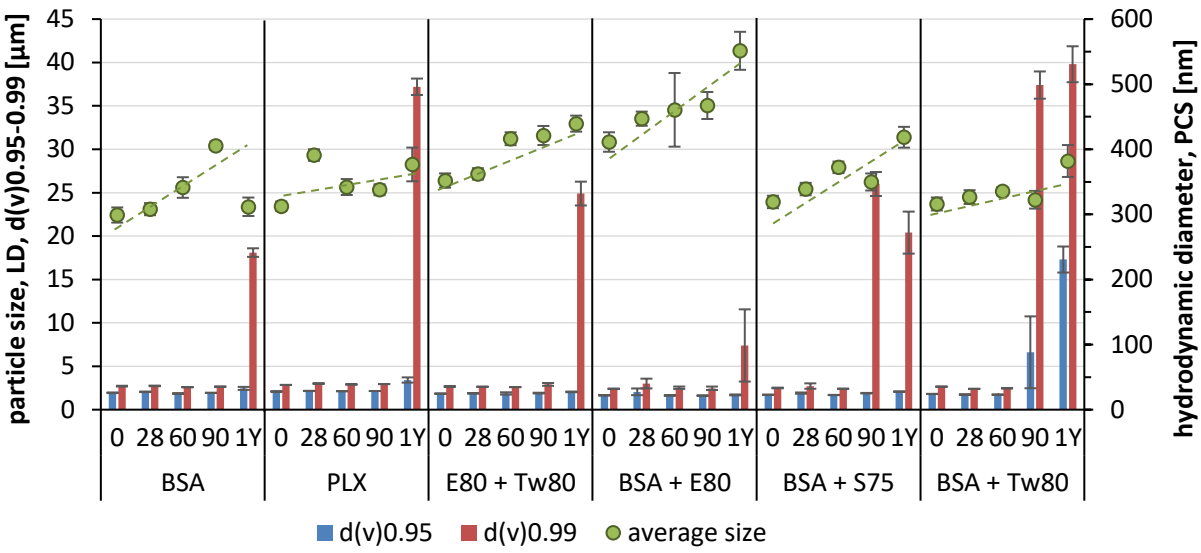

Figure 44: *Particle size of rutin nanosuspension characterized by PCS and LD over a storage period of one year in the fridge. The dotted line reflects the tendency by PCS.*

4.3.1.3.2 Influence of lecithin vesicles

When adding lecithin, the average particle size enlarged most (**Figure 44**). To explain this, it needs to be considered that lecithin nanostructures could be formed during the NC production. A formation of those has been confirmed previously (c.f. 4.3.1.2). As the PCS can only detect the smaller particles and can oversee larger particles within a mixt population, the lecithin vesicles formed on the day of production got a higher influence due to their large amount [178]. After a certain storage time, the vesicles can degrade. Hence, one explanation could be that the measurable average size slowly approached the real average size of the rutin NC, besides the agglomeration and crystal growth that could occur, too.

Therefore, the next step was to confirm or disprove the theory of generated lecithin vesicles that merge over time into larger aggregates. For this purpose, pure lecithin vesicles without an active ingredient or other excipients were prepared in a final concentration of 1% (w/w) in water by applying HPH with three cycles at 500 bar. The structures obtained were characterized and monitored regarding size and zeta potential for one year (**Figure 45**). In other words, the original dispersion medium without rutin was investigated regarding particle characterization.

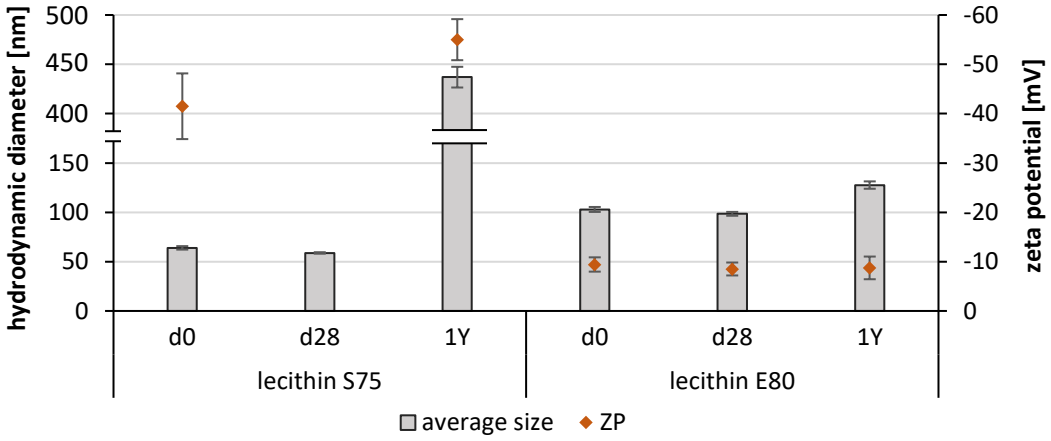

Figure 45: *The hydrodynamic diameter by PCS and ZP of pure lecithin vesicles obtained by HPH and stored over one year in the fridge.*

The size of vesicles derived from Lecithin S75 differed substantially from those of Lecithin E80 with about 60 vs. 100 nm, as well as the regarding zeta potential (-42 vs. -9 mV) (**Figure 45**). Interestingly, only based on the size, lecithin liposomes could have been created, as they are typically about 50 - 200 nm in diameter and are known to degrade [233]. After one year, the size of the Lecithin E80 vesicles grew only slightly and the zeta potential remained also almost unchanged, whereas the Lecithin S75 vesicles were fully aggregated to 440 nm sized lumps. Those lumps were observed macroscopically as sedimentation was obtained. Both effects were unexpected, the fact that the vesicles with a very low zeta potential were more stable and the fact that the vesicles were kind of stable for at least one year. In general, vesicles are unstable for thermodynamic reasons as they tend to reach the lowest energy state by partially losing their formation. The instability of lecithin vesicles can also be caused by chemical alteration due to the formation of hydroperoxide as well as other polar oxidation intermediate and end products, e.g. aldehydes. An accumulation of oxidation products inside the vesicles or liposomes enhances the osmotic pressure leading to water intake [234]. The higher number of double bonds in the fatty acid chain of soy lecithin makes it more vulnerable to oxidation, which is more prevalent with increasing storage temperature [235].

It was thus believed that if such chemical alterations have occurred in this study, a pH shift and/or an increase in conductivity could be detected. Therefore, the pH value and conductivity of all lecithin-stabilized formulations were measured and compared with these of the original medium, i.e. 1% (w/w) surfactant solution produced by 3 cycles of HPH at 500 bar (**Table 8**).

Table 8: *The pH value and conductivity of the corresponding stabilizers measured in the rutin nanosuspension, and their pure dispersion or solution meaning the original medium.*

formulation	nanosuspension		original medium	
	pH	conductivity [µS/cm]	pH	conductivity [µS/cm]
S75	5.9	700	7.7	130
S75 + Tw	5.5	730	7.0	40
S75 + PLX	5.2	770	7.1	70
E80	5.6	900	7.2	220
E80 + Tw	5.4	810	7.0	100

As result, the pH values of the NC formulations ranged between 5 and 6, and between 7 and 8 for the original medium (**Table 8**). These values remained constant for over four weeks of storage. Again, monitoring of possible pH shifts or changes in conductivity was performed to assess whether instabilities could be detected in advance, which was not observed in this case. Finally, the conductivity – as a function of the number and size of the ions – was higher for the Lecithin E80-stabilized formulation than for the Lecithin S75-stabilized. This indicates a higher number of ions in the solution and probably as part of the electrostatic shielding of the vesicles, which could explain the better physical stability.

4.3.1.3.3 Identifying the appropriate formulation

By developing nano-formulations, the major question always arises at the beginning as to which stabilizer works best for this purpose. Therefore, regardless of the production method, a careful evaluation of the type and concentration of the stabilizer is required. The optimal stabilizer is the one that interacts strongly with the particle surface and is therefore tightly bound to it. In this way, it can effectively create a steric shielding or an electrostatic repulsion that prevents another particle from approaching too closely and agglomerating irreversibly. Many studies were performed in the past to find a rational correlation between drug compound characteristics and stabilizer's behavior. Different drugs and stabilizer combinations were produced to NC and the resulting stability and particle size were evaluated. As result, neither the physico-chemical properties of the drug molecule (molecular weight, solubility) nor bulk properties (melting point, density) influence the success rate for developing a nanosuspension because these parameters do not reflect the surface properties of the NC [220]. There is a hint that a low drug enthalpy formulation, i.e. the strength of intermolecular interactions, may undergo agglomeration with time. Lyophobic surfaces can result from particle fraction or are already present due to a high logP value of the API. It was found that higher surface hydrophobicity causes an enhanced tendency for particle agglomeration. On the other hand, a more hydrophobic stabilizer has therefore a greater affinity to the particle surface and can cover it better. Fully synthetic compounds such as PVA or PVP are preferable to semi-synthetic polymers like HPMC, HEC, or Na-

alginate, while co-polymers with a pronounced hydrophilic and hydrophobic region as PLX or Kollicoat® (Polyvinyl alcohol-polyethylene glycol graft-copolymer) are even more advantageous for stabilization [159,220]. The degree of surfactant's hydrophilic and hydrophobic groups is empirically expressed by the HLB (Hydrophilic Lipophilic Balance), where a higher value represents a more hydrophilic character. Hence, the HLB could serve as a rough and quick tool for predicting its efficacy in stabilizing NC.

Up to now, only a rough tendency can be provided as to which surfactant group is most suitable. Rutin with its logP value of -1.97 should be suitable for the group of more hydrophilic surfactants [236]. The correlation between the HLB value of surfactants used and the resulting stability was then evaluated by comparing the alteration in particle size distribution and the absolute maximal particle growth. For this purpose, the calculated span values after 28 and 365 days of storage were differentiated from the span value (Δ span) obtained from the day of production. The difference was also calculated for the d(v)0.99 values (Δ d(v)0.99) and regarded as a measure of absolute particle growth. The results are summarized in **Table 9**.

Table 9: *Comparison between the HLB value of the stabilizers used and their resulting effectiveness in stabilizing the rutin nanosuspension. The stability effectiveness was expressed as the change in span and d(v)0.99 values by LD after four weeks and one year of storage compared to its values at the day of production. A negative sign means a decrease of the span from d0 to d28 and d365, respectively. Blank fields are caused by unavailable data due to mold.*

Stabilizer	HLB	Δ span		Δ d(v)0.99 [µm]	
		4 weeks	1 year	4 weeks	1 year
PLX	>24	0.20	0.08	0.16	34.35
Tween 80	15	0.31		7.04	
Lecithin S75	6-10*	0.05		7.53	
Lecithin E80	6-10*	0.07		1.38	
BSA	N/V	-0.68	-0.17	0.03	15.39
PLX + S75	>15	-0.23		-0.07	
Tw80 + S75	>10	-1.05		0.02	
Tw80 + E80	>10	-0.12	0.24	-0.03	22.23
BSA + S75	N/V	-0.59	0.17	0.22	17.90
BSA + E80	N/V	0.50	-0.02	0.60	4.99
BSA + PLX	N/V	-0.32		0.10	
BSA + Tw80	N/V	-0.26	12.23	-0.25	37.15

** Lecithin consists of a mixture of polar and non-polar lipids with a predominant group of glycerophospholipids, e.g. phosphatidylcholine, so that a fixed HLB value can only be estimated.*

An increase in the Δ span value means that the particle size dispersion has enlarged, i.e. the d(v)0.90 value has increased. In contrast, a negative sign in the Δ span values means mathematically, that the d(v)0.10 and/ or the d(v)0.50 value increased. Mathematically, the d(v)0.90 could also decrease, which

is theoretically and practically improbable. In total, a negative sign in the Δ span values needs to be considered more critical as it directly reflects a decrease in the small particle population and hence a shift to a larger median, i.e. d(v)0.5 values. Regarding the stability in terms of agglomeration and particle growth (Δ d(v)0.99) after four weeks of storage, this could be significantly improved by a combination of two surfactants (**Table 9**). For example, NC stabilized with Tween 80 showed a particle growth of about 7 µm, which was completely avoided - meaning that no particle growth occurred - when BSA or lecithin was added. In fact, the formulation stabilized with the mixture BSA and Lecithin E80 was found to be the most long-term stable regarding particle size. This was unexpected because in each case as solo-surfactant and as a mixture the stabilizing effects proved not to be superior after four weeks of storage. On top, an average particle size of about 410 nm at the day of production was obtained and thus this formulation showed the second-largest hydrodynamic diameter (**Figure 38**). One feasible explanation for the larger size could be that Lecithin E80 together with BSA formed a super complex where lecithin-stabilized partially the NC as well as BSA which is absorbed onto the surface. As result, lecithin additionally stabilized BSA against degradation. Likewise, a larger surfactant layer was developed that enlarged the hydrodynamic diameter. The great mixture of different lipids and phospholipids led to the ideal electrosterical repulsion. This is not inconsiderable because NC have already been successfully stabilized with amino acid co-polymers [237], and BSA itself can also be stabilized by lecithin and vice versa [238]. Other studies are suggesting a greater potential for the combined use of ionic and polymeric surfactants [239]. For example, the study by C. Jacobs and R.H. Müller demonstrated the beneficial effect of the surfactant mixture of lecithin and tyloxapol (non-ionic polymer) in stabilizing budesonide NC for one year [240].

By comparing the mono-stabilized NC, PLX was found to be preferable and BSA could be used as an alternative. This is in good agreement with other successfully PLX-stabilized NC studies produced by HPH [241,242] and BM [243]. However, it must not conclude that PLX is universally compatible as it has been shown to fail the stabilization with miconazole [190]. The less successful stabilizer for rutin NC was soy lecithin and surprisingly Tween 80 which could be explained as follows: the key factor for stabilization is the affinity of the stabilizer to the surface and the resulting steric or electrostatic repulsion. Lecithin and Tween 80 contain fatty acids as a lipophilic chain whereas the hydrophobic chain of PLX consists of a PPO-chain that would be more likely to be adsorbed onto the hydrophobic nanoparticle surface. Also, BSA featured only hydrophobic domains due to the order of hydrophobic amino acids or side chains that are carried to the outside and not as lipophilic as the pure C-C-chain of a fatty acid. Further studies for this hypothesis are urgently needed. Nevertheless, it can be confirmed that the HLB is less suitable as a basis for a possible explanation and prediction of the NC stabilization.

To sum up, a small surfactant is needed whose hydrophobic side chain fits chemically optimally to the particle surface and covers it fast. However, it would be too hydrophobic for the aqueous environment

alone. Therefore, a long hydrophilic or electrostatic shielding is necessary at the same time for more hydrophilicity to the periphery. Otherwise, the composition would be poorly assimilated by the water and cause agglomeration. It has been shown that a second surfactant, which was too hydrophilic when used as a mono-stabilizer, can be profitable in this case. Hence, two surfactants, which are not very suitable individually, can be excellent in combination. At the end of one year of storage, the rutin NC stabilized with a mixture of Lecithin E80 and BSA was identified as the most stable.

4.3.1.4 Scale-up process

4.3.1.4.1 Particle size

For further investigation but also for a feasible production of a clinical batch size, it is important to produce a higher amount of a physical and microbiological stable nanosuspension. For this purpose, a scale-up process was performed using HPH by ARTcrystal® technology by P. Scholz and K.M. Keck [167]. Larger amounts of nanosuspension need to be stable at least for the time until they are end-formulated and applied *in-vitro* and *in-vivo*, respectively. Therefore, suitable storage conditions were studied including the storage container, which is discussed in the following as well as the storage temperature, which is focused on in section 4.3.1.4.4. The rutin NC formulation stabilized with the mixture of PLX and BSA seemed to be promising after four weeks of storage and was thus used for this scale-up (**Figure 42**). After their scale-up production, the nanosuspension was subsequently fractionated in different bottles, i.e. a plastic tube, brown glass and white glass bottle. All nanosuspensions were stored in the fridge (5 ± 3 °C) for 90 days and samples for analysis were withdrawn at the day of production (d0) and after 1, 7, 14, 28, 60 and 90 days (d1 - d90) of storage.

Directly after the production (d0), a hydrodynamic diameter of about 380 nm of the rutin NC was detected when produced by the continuous scale-up process using the ARTcrystal® technology with a batch size of 300 mL. This was slightly larger compared to the discontinuous HPH process in 40 mL batch size (pilot-scale) with about 330 nm (**Table 10**).

During the HPH process, the temperature of the dispersion rises, and the large volume means that the cooling time takes much longer. As result, after each cycle, a higher amount of rutin is dissolved with enough time to re-crystallize completely during cooling. Re-crystallizations tend to occur on larger crystals and can also fill imperfections, hampering further comminution at these positions. Both effects might lead to larger particles that were detected by laser diffraction (**Table 10**). Thus, the particles were enlarged to 2.69 and 3.63 µm (vs. 2.39 and 319 µm) for the d(v)0.95 and d(v)0.99 values, respectively. Consequently, the PdI also increased slightly from 0.30 to 0.32.

Table 10: *Comparison of the rutin nanosuspension regarding the particle size of the pilot-scale by HPH in discontinuous 40 mL batch size and the scale-up process. Particles were stabilized by a mixture of BSA and PLX.*

	$d_{hydrodynamic}$ [nm]	PdI	d(v)0.10 [µm]	d(v)0.50 [µm]	d(v)0.90 [µm]	d(v)0.95 [µm]	d(v)0.99 [µm]
pilot-scale	333 ± 22	0.301 ± 0.07	0.19 ± 0.01	0.53 ± 0.02	1.95 ± 0.02	2.39 ± 0.01	3.19 ± 0.03
scale-up	376 ± 25	0.320 ± 0.09	0.19 ± 0.01	0.53 ± 0.03	2.16 ± 0.05	2.69 ± 0.05	3.63 ± 0.08

The differences observed played only a minor role due to the small quantity of larger NC. Otherwise, the number of NC responsible for special properties, i.e. particles < 1 µm in size characterized by enhanced dissolution rate, solubility and adhesiveness, could be marginally reduced as a consequence. This could not be confirmed because at least 50% of the volume-based particles possessed the same size, i.e. the d(v)0.50 value is completely the same for both production processes (**Table 10**). Therefore, there was a negligible difference in the results between the production processes of the discontinuous small batch size and the continuous scale-up process regarding size at the day of production. In other words: the scale-up could be used as a good approximation to produce comparable rutin NC at the day of production. Next, the physical stability of the scale-up NC should be investigated and compared to those of the pilot-scale. Not only this, but the nanosuspension was additionally divided into three vessels of different materials and the particle size was monitored over 90 days (**Figure 46**).

4.3.1.4.2 Physical stability depending on the storage container

Over this period, only a small increase in the hydrodynamic diameter measured by PCS can be found in all containers, whereas the extent was found to be higher when stored in a glass bottle (**Figure 46** upper). On the contrary, a beginning instability after 28 days was detected by LD measurements (**Figure 46** lower). These manifested mainly when storing in plastic tubes and brown glass, while the use of white glass provided stability of the NC for 90 days. The stabilizer mixture of BSA and PLX was used due to its excellent stability found in the small batch (pilot-scale) when stored in a plastic tube over at least 28 days of storage(**Figure 42**) and was not observed at the scale-up process (**Figure 46**).

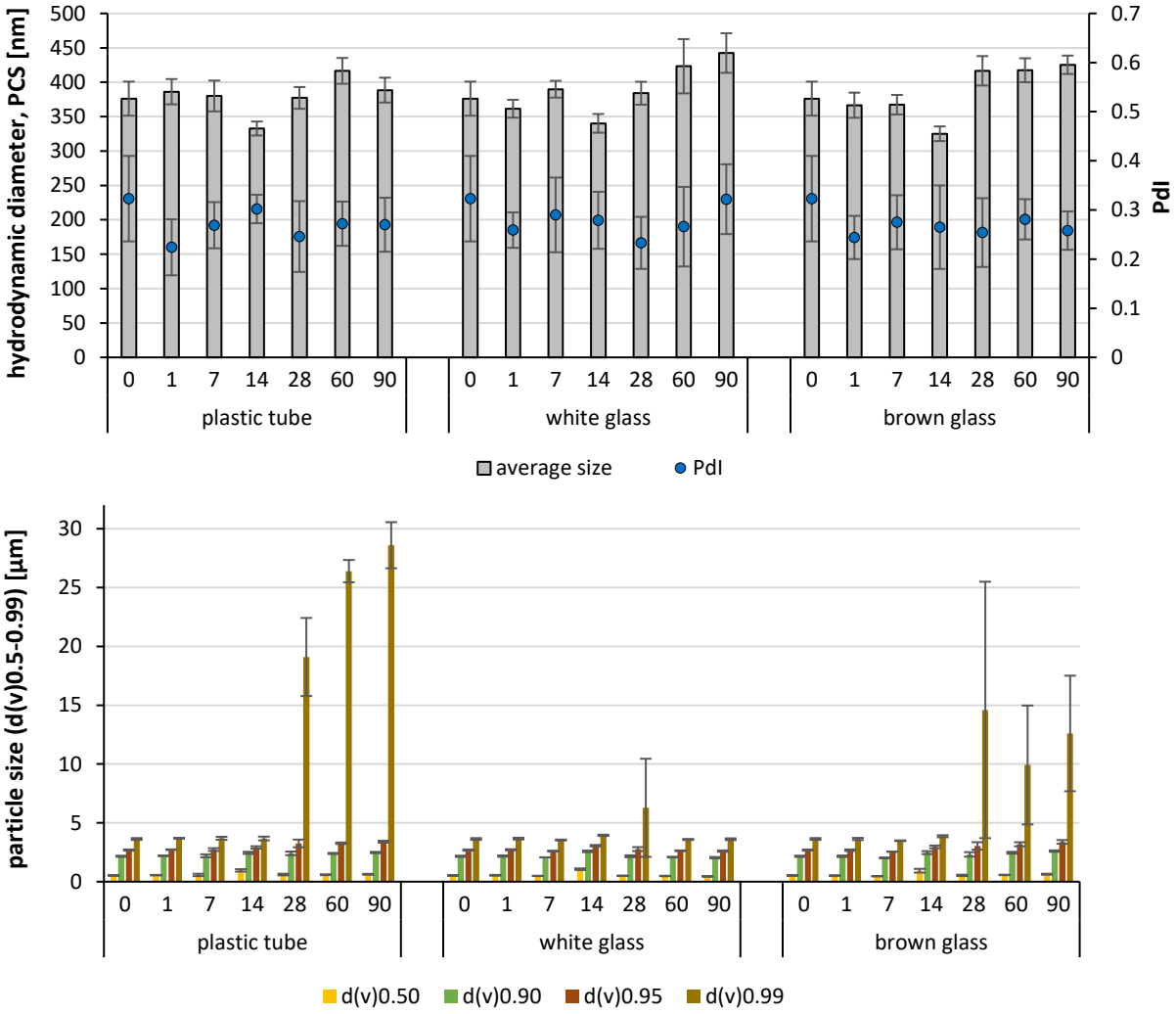

Figure 46: *Particle size characterization by PCS (upper) and by LD (lower) of rutin NC co-stabilized by PLX and BSA depending on storage container over 90 days of storage. Nanosuspension was produced by a continuous scale-up process.*

A possible explanation could be, that BSA formed protein-protein or even protein-NC aggregates, which had been promoted by the prolonged heat exposure during the process. In general, the thermally induced aggregation pathway of BSA follows the kinetics of the second order reaction [244]. Thus, the number of irreversible formed BSA-aggregates must be elevated at the initial phase. Under the assumption that BSA contributed significantly to the stabilization of the rutin NC and that the proportion was rapidly decreased, the logical consequence must be an early instability. Even if the stability has declined, the nanosuspension was more stable than mathematically estimated, probably due to the additional surfactant, PLX. Surfactants can do both, stabilize but also destabilize proteins. If the proteins contain hydrophobic pockets such as serum albumin, the hydrophobic part of the non-ionic surfactants will bind to them. This results in more hydrophilic groups being exposed in the medium, and consequently, the surfactant-protein complex becomes more hydrophilic and the effective increase in solubility of the complex prevents the formation of higher order aggregates

[245,246]. In contrast, non-ionic surfactants are able to dissolve protein aggregates without changing greatly the protein conformation [247]. However, assuming that the d(v)0.99 values represent only a small percentage of the entire particle population and that the d(v)0.95 values remained constant, the detected physical instability occurred to a tolerable extent.

Besides a slight physical instability, it was also assumed that the container used might affect the stability because of NC interactions with the material or the release of ions or other compounds from the containers. However, this assumption could not be confirmed in this study. One feasible reason would have been the diffusible parts of the container impacting the suspension such as plasticizers in the plastic tube. For example, a recent study analyzed the migration kinetics of plasticizers in infusion medical devices where 1-2% of the declared content were released within 24 h [248]. In order to be able to assess whether interfering chemicals diffuse into the suspension, the ZP values were compared after one week of storage in the corresponding container (**Figure 47**). It was found that the ZP values were completely identical, which reflects the similar behavior of the storage stability.

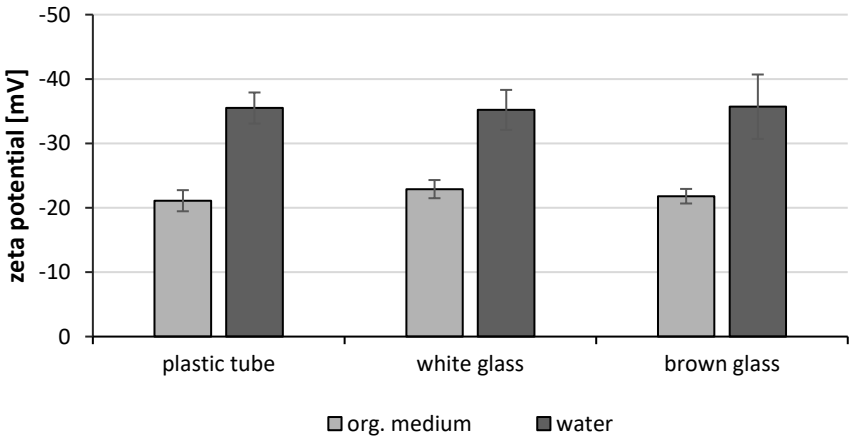

Figure 47: *Zeta potential of the rutin nanosuspension stabilized by BSA and PLX, produced by a continuous scale-up process, and stored one week in different containers, i.e. in a plastic tube, white and brown glass. Measurements were performed in water with a conductivity adjusted to a conductivity of 50 µS/cm and the original medium freshly prepared with the stabilizers (1%, w/w).*

Interestingly, the ZP from the scale-up process measured in the original medium differed remarkably from that of the small batch production process (-21 vs. -27 mV). Due to the large molecule with hydrophobic and hydrophilic partial structures as well as the charges within the complex protein skeleton, the classical rule of stability prediction cannot be applied. A further complicating factor for prediction is caused by adding a large non-ionic surfactant. The question now is whether the lower or the higher ZP would lead to better physical stability. Anyhow, the lower ZP value could be an indication that the surfactant layer became thicker, i.e. the combined layer structure as observed in the pilot-scale might be differently constructed in this case. In both production approaches (small and scale-up)

the same amount of surfactants was added, which should lead to a similar layer on the particle surface. A reduced ZP after adding further surfactants (through dilution with the original medium) indicates that the surfactant layer in the scale-up approach was more hydrophobic towards the outside, or the surfactant layer was formed irregularly, i.e. with gaps and accumulations. However, in both cases, more surfactants can attach and expand the layer. In other words, the layer was built in such a way that the adherence of the small NCs might be more facilitated, which in turn led to the observed agglomeration.

To prove this, the zeta potential in dependence on the BSA concentration and contact time with NC were investigated. For this purpose, a BSA solution was added to a PLX-stabilized rutin NC yielding a final concentration of 0.5, 1 and 2%, i.e. half, equal, and double concentrated to the scale-up batch. Additionally, the ZP of a pure BSA solution in water or PLX was examined.
Interestingly, as a result, the zeta potential of the PLX-stabilized rutin NC did not change significantly with increasing BSA concentration nor with more incubation time (**Figure 48**).

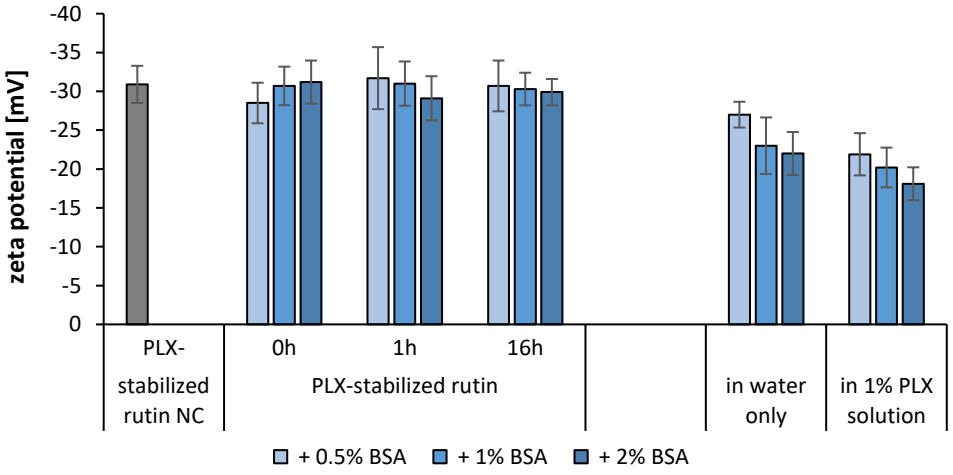

Figure 48: *Zeta potential of a PLX-stabilized rutin nanosuspension enriched with different concentrations of BSA. In comparison, ZP measurements were performed with BSA only solved in water or a PLX solution. All specifications refer to the resulting final concentration.*

It was expected that the surfactant layer on the particle surface adapted over time to a thermodynamically stable state, which would approach the same layer structure, and thus the zeta potential would reach the same value as the NC produced directly with BSA and PLX together. In contrast, the zeta potential has not altered over time or with changes in the concentration. This supports the theory that large non-ionic stabilizers are tightly and practically irreversible bound on the surface due to Van-der-Waals forces. PLX is a block copolymer of polyethylene oxide – polypropylene oxide – polyethylene oxide type, PEO–PPO–PEO, where the hydrophobic PPO block forming small loops on the surface is attached with serval contact points on the particle surface (**Figure 49**). As result, the

added BSA molecule remained in the dispersion. There was only a minor decrease in ZP compared to the PLX-only-stabilized suspension because the BSA solution possesses a zeta potential ranging from -27 mV up to -22 mV for 0.5 - 2.0 % solutions (**Figure 48**). The number of BSA molecules or aggregates with its own ZP was smaller than the huge amount number of NC being in suspension. By adding BSA and PLX the resulting ZP is even smaller with -22 to -18 mV for (0.5 to 2.0 % BSA solution), which means that PLX formed a layer on the BSA structures. Additionally, these results give a hint that different ZP values were more likely caused by the shape of the NC, which is due to a difference between the scale-up and pilot scale. Since the comminution principle, cavitation forces, is identical for both, the temperature or cooling time seemed to play the main role.

The longer cooling time allowed the particles to re-crystallize more "perfectly". This means that imperfections are filled and hydrophilic partial structures caused by cavitation forces and crushing are re-shaped to hydrophobic ones. Also, this might be a possible explanation why the surfactant layer formed differently, detected by ZP measurements (**Figure 47**).

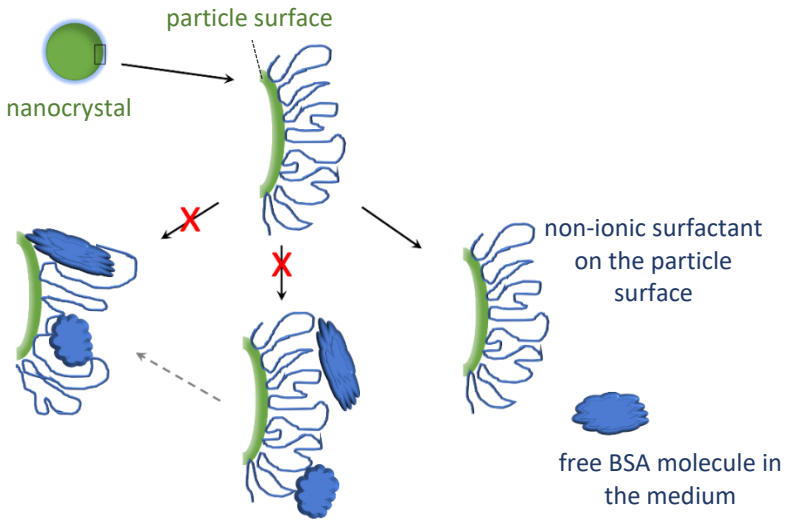

Figure 49: *Schematic representation of a particle surface to which PLX adheres with characteristic loops. Three possible scenarios would be possible by adding BSA as a further stabilizer: incorporation of the BSA into the loop structure, as in the co-stabilized formulation (left), adhesion to the loops with expansion of the shear plane (middle) and no interactions (right).*

Based on the results, it can be assumed that the ZP measurement gives a great indication of predicting the stability when another process was applied. To confirm this theory and to ensure that NC produced continuously in a scale-up were not significantly less stable, rutin NC without adding BSA - meaning stabilized by PLX only - were produced in the same way. Besides setting the same process parameters, the nanosuspensions obtained were separately stored in a plastic tube and glass bottle as well.

Detailed comparison of particle characterization of the PLX-only-stabilized rutin NC at the day of production is summarized in **Table 11** and the stability data are shown in **Figure 50**.

Table 11: *Comparison of the rutin nanosuspension regarding the particle size of the pilot-scale by HPH in discontinuous 40 mL batch size and the scale-up process. Particles were stabilized with PLX.*

	$d_{hydrodynamic}$ [nm]	PdI	d(v)0.10 [µm]	d(v)0.50 [µm]	d(v)0.90 [µm]	d(v)0.95 [µm]	d(v)0.99 [µm]
Pilot-scale	313 ± 7	0.24 ± 0.06	0.17 ± 0.01	0.44 ± 0.01	1.68 ± 0.01	2.09 ± 0.01	2.85 ± 0.01
scale-up	437 ± 10	0.25 ± 0.04	0.20 ± 0.01	0.57 ± 0.05	2.16 ± 0.07	2.67 ± 0.06	3.56 ± 0.09

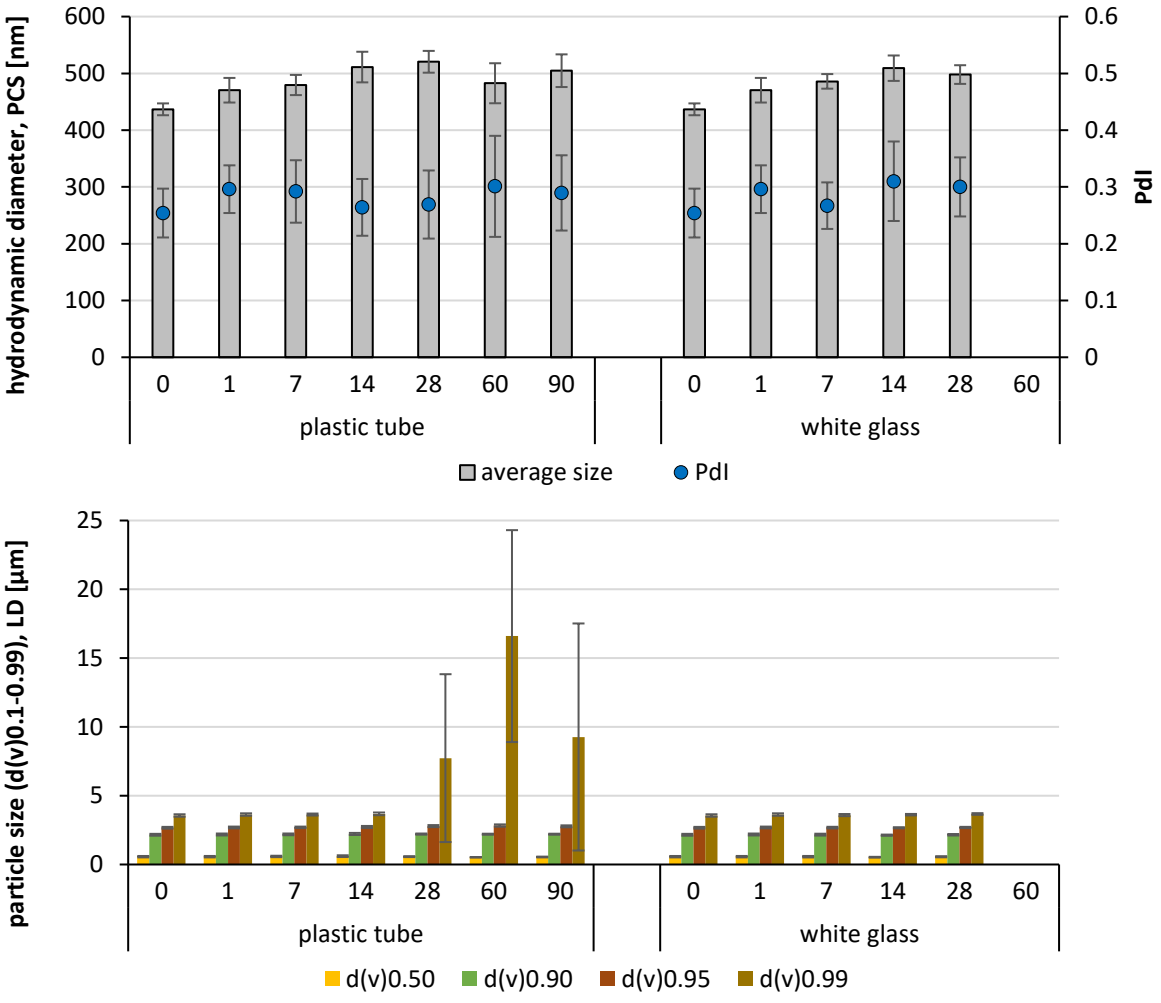

Figure 50: *Rutin nanosuspension produced by scale-up process and characterized by PCS (upper) and LD (lower) over a time of 90 days. Preparation was separated into two fractions, where one was stored in a plastic tube and the other in a glass bottle, each in the fridge.*

In general, it can be said that the trend of the result is similar, that means in detail that

(I) particles at the day of production obtained by scale-up process were larger compared to those produced by a 40 mL batch size (313 vs. 437 nm),

(II) the average particle size increased slightly over the storage time of 90 days in both plastic falcon tube and white glass and

(III) first particle agglomeration was found after 28 days of storage in a plastic tube (**Figure 50**).

In contrast, the nanosuspension stored in white glass exhibited no particle growth at all but formed mold growth when stored for more than 4 weeks (**Figure 50**).
Based on the fact that the results are similar compared to the respective pilot scale, It can be presumed that the observed lower physical stability after using the scale-up is rather related to the production process than to the storage container.

Furthermore, the zeta potential measured in water was slightly lower but not significant compared to the pilot-scale (**Table 12**). The zeta potential depends on the size and shape of the particles, among other factors such as charges. Therefore, the shape might be also different due to the changed production method. In the end, this difference would affect the ability of surfactants to adhere to the particle surface and thus decrease their steric shielding force. The main theory assumes that the ZP of steric stabilizers should be as small as possible, but also that the difference between the measuring media should be almost zero. In this case, the scale-up resulted in a smaller difference which, however, did not agree with the lower stability. Thereafter, the most relevant indicator for the lower stability was the larger particle size obtained by scale up the HPH.

Table 12: *Zeta potential of the PLX-stabilized rutin nanosuspensions obtained by the discontinuous 40 mL batch size (pilot-scale) and the scale-up process in continuous mode. Measurements were performed in water (50 µS/cm) and the original medium (surfactant solution).*

	original medium	water
scale-up	-25 ± 3 mV	-29 ± 3 mV
pilot-scale	-24 ± 2 mV	-35 ± 4 mV

On the other side, performing only two studies in which both contained the same stabilizer, PLX, cannot be used to allow a universal assumption. For this reason and to verify BSA as a feasible co-surfactant, a third investigation was performed with a mixture of Tween 80 and BSA as stabilizer. Additionally, it was expected that the presence of larger particles could play a role in the lower stability. Therefore, the stability of nanosuspensions containing larger particles caused by a lower number of homogenization cycles was investigated as well. Hence, tailor-made rutin NC were produced.

4.3.1.4.3 Storage stability depending on particle size

The scale-up process was performed with 20 HPH cycles to produce a nanosuspension stabilized with BSA and Tween 80. Samples were withdrawn every 5 cycles and characterized regarding at the day of production and 1, 7 and 15 days after the production. In addition, the formulation prepared with 20 cycles was stored for 90 days to compare its stability with that prepared at pilot-scale.

As a result, applying further homogenization cycles from 5 to 20 reduced the hydrodynamic diameter from 500 nm to 380 nm, respectively (**Figure 51** upper). The same trend was found using LD measurements: the larger particles detected for the d(v)0.99 were reduced by about a third from 10.6 to 6.7 µm after increasing the homogenization cycles from 5 to 20 (**Figure 50** lower). By storing these nanosuspensions in a plastic tube at 5 ± 3 °C, the particle size increased slightly, which was more pronounced for suspensions produced with 10 and 15 homogenization cycles. Small changes were observed for the average particle size of the rutin NC produced with 20 cycles over 90 days of storage, which reflects the usual production process at pilot-scale and scale-up, too. Physical instability was found after 60 days of storage, where the d(v)0.99 value was about 34 µm. Compared to the nanosuspension produced by the pilot-scale, the particle sizes were larger at scale-up with 330 vs. 370 nm by PCS and 2.7 vs 6.7 µm at d(v)0.99 by LD. Again, the scale-up nanosuspension was physically stable for only 60 days, whereas the nanosuspension produced by the pilot-scale was stable for at least 90 days. A direct relation to the particle size could not be shown, because the larger particles from a 5-cycle batch displayed a similar performance to the 20-cycle batch within 15 days of storage. Nevertheless, the findings strengthen the theory that the scale-up process impairs the physical stability of the nanosuspension because a longer storage time caused agglomerations earlier (**Figure 42** and **51**). This could again be explained by the longer temperature rise and thus the tendency to form more perfect crystals along with a more hydrophobic particle surface.

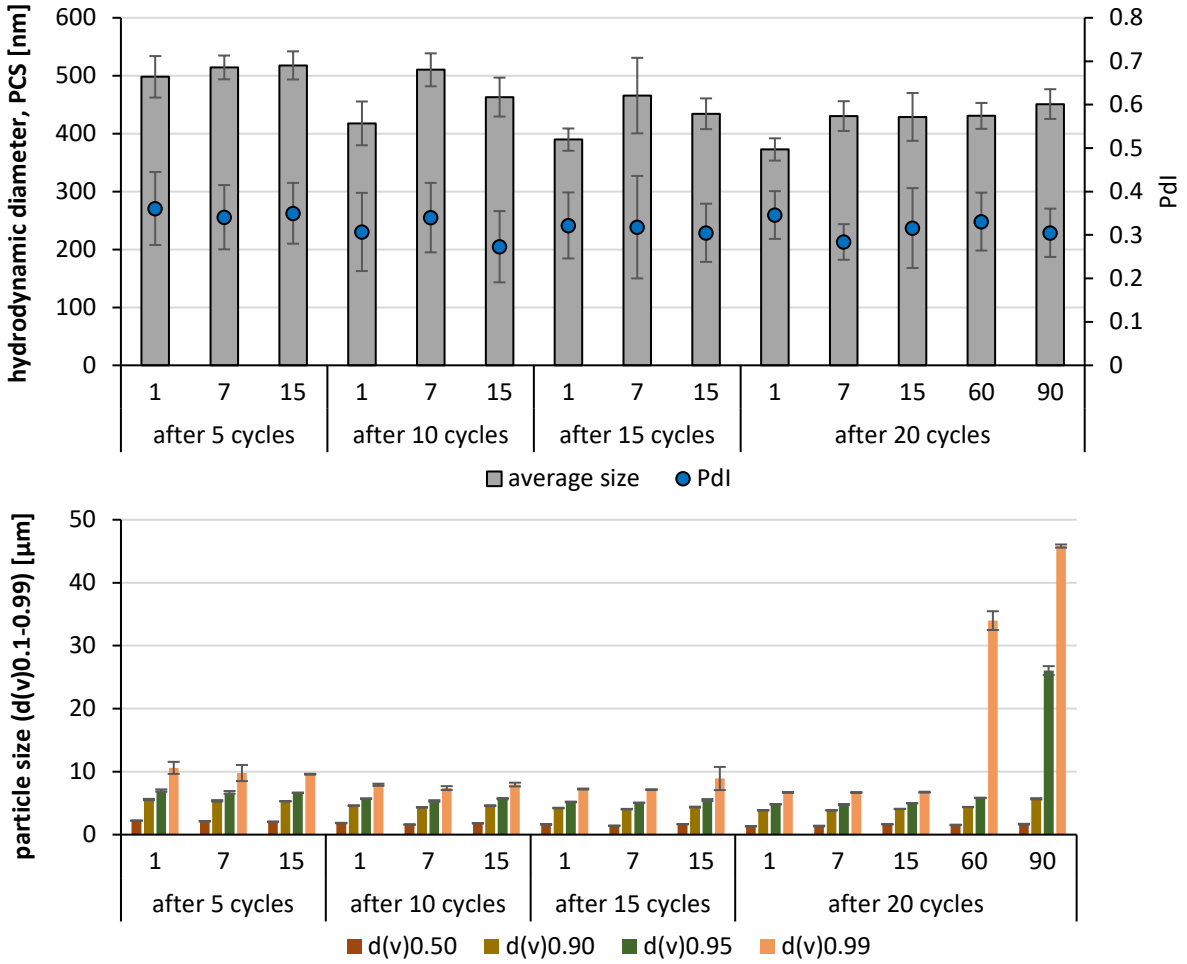

Figure 51: *Rutin nanosuspensions stabilized by a mixture of BSA and Tween 80 were produced by varying the number of homogenization cycles in the pilot-scale. Particle size was characterized by PCS (upper) and LD (lower) over 15 and 90 days.*

Also, ZP measurements of all scale-up batches were performed to assess to what extent this can be used to predict stability in comparison to the pilot-scale batch. First, the ZP remained identical with an increasing number of homogenization cycles for the scale-up batches (**Figure 52**). This was expected because some NC, i.e. particles < 1 µm, were produced after passing the homogenization gap and only these NC can be detected by zeta potential measurements. Hence, with a higher number of homogenization cycles the amount of NC being < 1 µm increases. In contrast, the characteristic shape, structure and surfactant layer caused by the cavitation forces and the temperature difference were retained throughout all cycles. Again, BSA used as co-surfactant is prone to degradation in a time- and temperature-depending kinetic. Such unfolded protein structures adsorbed on the particles could render the surfactant layer more hydrophobic and alter the surfactant charge toward the outside, or the surfactants could be irregularly arranged. In all cases, more surfactants from the original medium can adhere to extend the surfactant layer on the particles. The same effect was described for the scale-up approach stabilized with BSA and PLX (**Figure 47**). For this reason, it was to be expected that the ZP

values of the pilot-scale were higher than those of the scale-up. This strengthens the thesis that ZP measurements help also to assess the stability of nanosuspensions prepared by different methods.

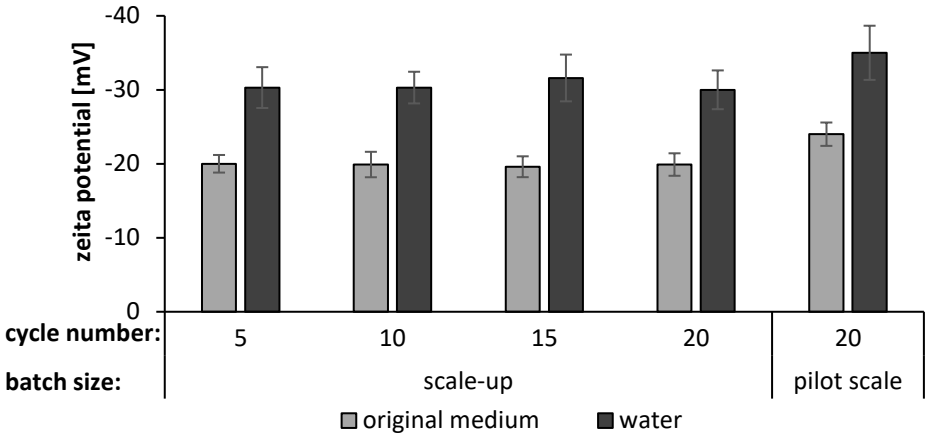

Figure 52: *Zeta potential of the differently produced rutin NC stabilized by a mixture of BSA and Tween 80.*

Besides the ZP measurements, the lower stability compared to the pilot-scale batch could also be predicted by microscopy. In all cases, i.e. after 5, 10, 15 and 20 cycles, the nanosuspensions showed clouds of particles representing an indication and forecast for the enhanced formation of agglomeration (**Figure 53 A-D**). Such accumulations of particles allow overcoming the energy barrier of maximum potential after DLVO theory, and aggregation occurs (**Figure 53 G**). At the same time, it shows that the attraction between the particles seems to be too high.

It can be concluded that the surface properties of the particles have changed compared to the pilot scale. The surfactant layer revealed a lower shielding efficacy in three cases and therefore or additionally the particles are more hydrophobic. Hydrophobic particles are more difficult to disperse in the hydrophilic aqueous medium, which facilitates separation and thus an easier approach between the particles with the result of a faster agglomeration. In other words, this slight difference in particle surface texture is related to the scale-up process. The take-home message for future studies is that an initial stage surfactant screening cannot be easily transferred to the scale-up, even if the comminution method, HPH, is the same.

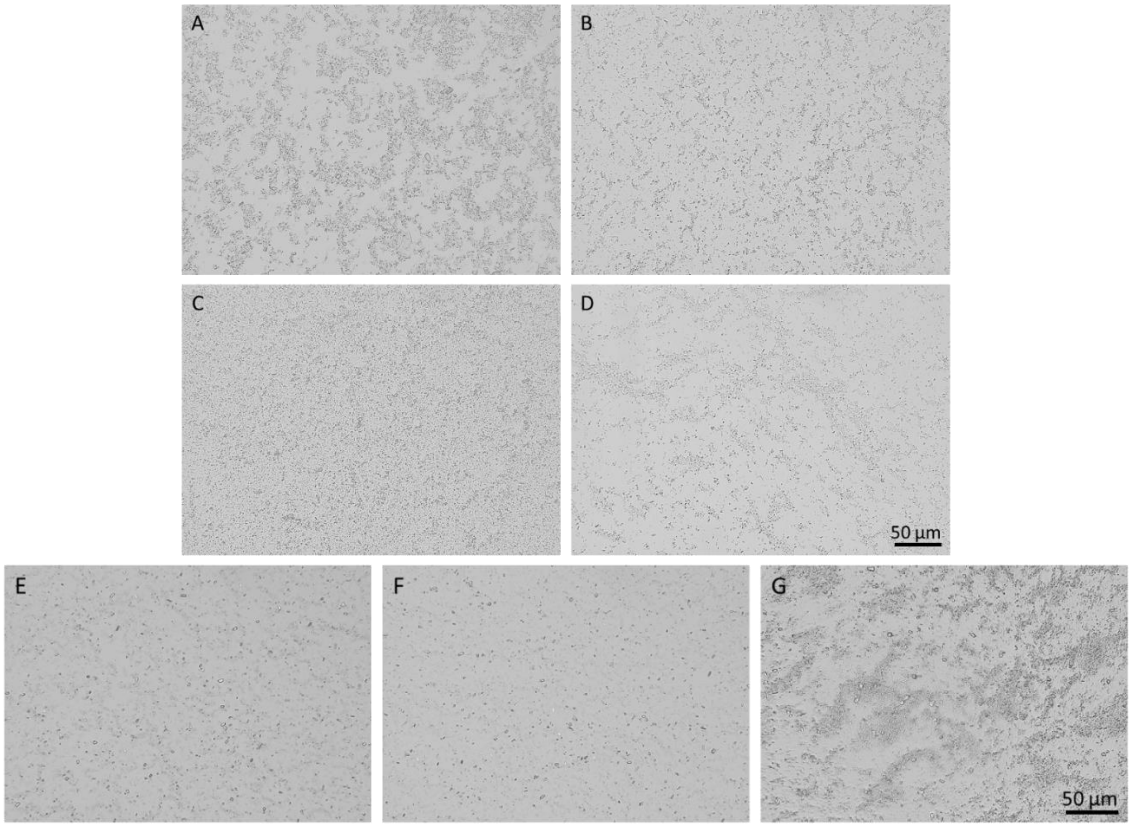

Figure 53: *Microscopic images of the rutin nanosuspension stabilized by a mixture of BSA and Tween 80 and produced by a scale-up batch with 5 (A), 10 (B), 15 (C) and 20 (D) homogenization cycles one day after the production as well as the latter after 7 (E), 15 (F) and 60 days (G) of storage.*

4.3.1.4.4 Prolongation of storability

So far in this work, the physical stability has been optimized by using the most appropriate stabilizer and storage container. However, the physical and microbiological stability has not been observed in any formulation for longer than one year. Microbiological stability, in particular, is a problem since on the one hand no information can be drawn about physical stability and on the other more critically hand, the treatment is jeopardized by infection. Bacteria and fungi grow faster at higher storage temperatures. Also, higher storage temperatures are believed to reduce physical stability by facilitating Ostwald ripening and agglomeration due to increased solubility and faster particle movement.

For these reasons, this section addressed the influence of storage temperature and the use of preservatives in terms of microbiological and physical stability. The addition of preservatives is usually not used for physical stabilization investigations but is often used to guarantee microbiological stability during the whole procedure. Nevertheless, preservatives are usually small molecules with the possible ability to adhere to the particle surface. Hence, the possible influence for a physical stabilization or destabilization should also be investigated. For this purpose, the suitable representative, Euxyl PE9010,

was selected which has already proven its worth in stabilizing nanosuspensions when adding after the NC production [104].

The question has also been how effective the physical stabilization is depending on the storage temperature. In the scale-up study, it was already shown that a longer duration of higher temperature in the manufacturing process led to changes in the stability of the nano-formulation. It is therefore conceivable that the preservative could also show different effects at different storage temperatures. When considering the storage temperature, storage in a refrigerator is preferred, but what if an even lower temperature is used, i.e. the suspension is stored in a frozen state?

To answer these questions regarding physical stability, the experimental set-up was carried out as follows: Rutin NC stabilized with PLX were produced using pilot-scale HPH and then divided into two groups, where one was enriched with Euxyl PE9010 as preservative and the other rested as non-preserved reference. Both groups were then divided again and stored at different temperatures, i.e. in a frozen state at -20 °C, in the refrigerator at 5 ± 3 °C, at 21 °C room temperature and in the climatic chamber at 30 °C. The frozen samples were separately filled directly after production into 1.5 mL safe-lock microcentrifuge tubes and placed in the freezer for a rapid freezing process. Likewise, the thawing process was carried out quickly by placing the tube in an ultrasonic bath pre-heated to 40 °C. Thereafter, the frozen-thawed samples were immediately characterized and only used at the day of characterization to allow reliable characterization of feasible microbial growth or physico-chemical instabilities during the storage. However, all nanosuspensions were characterized regarding particle size by PCS, LD and microscopy and by ZP measurements, with samples drawn at the day of production and 7, 14, 28, 60 and 90 days after the production. The microbiological stability of the four nanosuspensions was investigated after 1, 2 and 3 months of storage at four different temperatures (-20, 5, 21 and 30 °C) and discussed afterward (c.f. section 4.3.1.5).

At the day of production, rutin NC possessed a hydrodynamic diameter of about 410 nm that did not change upon the addition of the preservatives (**Figure 54**). Also, the particle size measured by LD revealed no differences in particle size after the addition of the preservative. In contrast, differences were found when stored at different storage temperatures. While the non-preserved formulation was stable at least 90 days at -20 and 5 °C and at least 60 days at room temperature, higher temperatures reduced the physical stability. Consequently, the least stable formulations were obtained when the formulations were stored at 30 °C (**Figure 54** upper). At higher temperatures, an accelerated particle growth follows due to the Ostwald ripening. There are two principal explanations for this: At first, solubility increases with the temperature that favors the supersaturated environment around the larger particles and this in turn re-crystallization, i.e. particle growth. Second, enhanced hydrophobic interactions between particles and the dehydration of polymer were observed with the consequence of a higher aggregation tendency [193,249]. The same trend was found for quercetin NC where the

highest storage temperature (40 °C) resulted in aggregation and particle growth, while lower temperature ensured physical stability for 180 days [250]. As an explanation the authors suggested the increase of the diffusion constant according to the Stokes-Einstein equation as well as an easier overcoming of the energy barrier owing to higher kinetic energy.

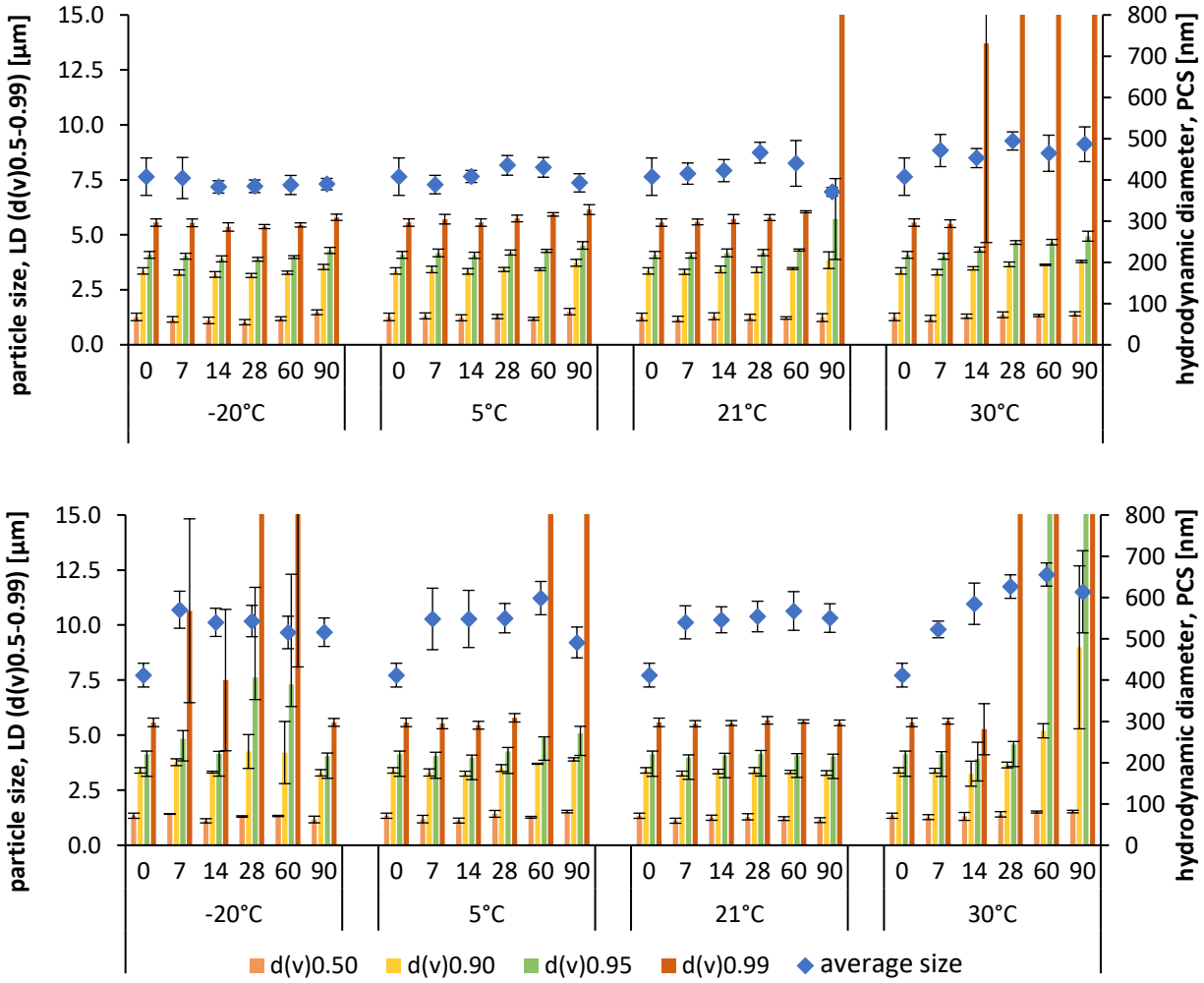

Figure 54: *Hydrodynamic diameter (PCS) and particle size by LD of the rutin nanosuspensions stabilized by PLX stored over 90 days under varying temperatures. They were left as they are (upper) or preserved with Euxyl 9010 directly after production (lower).*

Interestingly, the addition of the preservative Euxyl PE9010 completely changed the physical stability at different temperatures (**Figure 54** lower). While the formulation remained stable when stored at room temperature for at least 90 days, higher and lower storage temperatures are accompanied by a loss of physical stability after four weeks and freeze-thawing was even impossible to deal with (**Figure 54** lower). The destabilization seemed to be directly associated with the presence of the preservative, which was added to the samples at room temperature. Changes in the temperature might affect the preservative-particle as well as the preservative-surfactant interaction and thus the stability. Further hints for the destabilizing potential could be shown by microscopy (**Figure 55**).

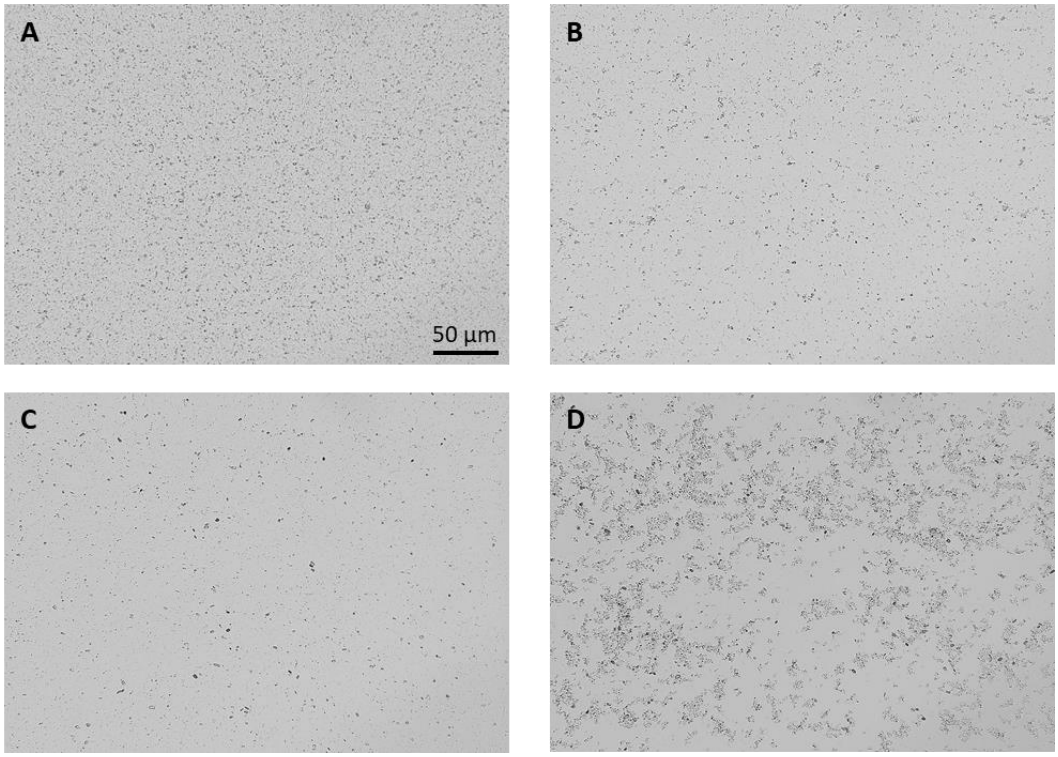

Figure 55: *Microscopic images of the rutin NC after the production (A), and with the presence of the preservative Euxyl PE9010 (B). Samples were freeze-thawed without (C) and with (D) addition of the preservative. (Magnification 400-fold).*

Non-preserved rutin NC were microscopically characterized as loose, finely distributed nanoparticles, whereas subsequent addition of the preservative led to slight accumulations of loose agglomerations (**Figure 55 A and B**). Again, the rutin nanosuspension was preserved after production and hence the stabilizer acted quickly as the images were taken shortly after production. This means that the preservative immediately destabilized the nanosuspension, as the agglomerates were visible under the microscope within minutes. A fraction of each formulation (preserved and non-preserved) was also frozen immediately after preparation and then thawed for particle characterization by microscopy. As result, the formulation with preservative was characterized by pronounced aggregates while the non-preserved one remained finely dispersed (**Figure 55 C and D**). In other words, the destabilization observed at the beginning was enhanced by the stress during freezing and thawing. The loose agglomerations observed by microscopy at the day of production were destroyed due to the stirrer motion during the LD measurement and thus not detected. However, as these loose agglomerations were forced to develop into more stable aggregates after freezing, they were able to be detected by LD (**Figure 54** lower). By microscopy, it was possible to reveal the first signs of a physically destabilizing effect caused by the preservative.

Microscopy is not the only great feature for identifying stabilization problems in advance. Carrying out the relatively short approach of freezing and thawing within a few hours could be an alternative method or an additional method, e.g. when the results by microscopy are inconclusive. In contrast, the

freeze-thaw process for the non-preserved formulation was stable throughout the storage period of 90 days and also appeared to remain stable for much longer, as no interactions between particles could occur in the frozen state. Hence, suitable combinations of preservatives or other excipients with the nanosuspensions can be also investigated by freeze-thawing, as the formulation remained unchanged during the process.

To summarize, the freeze-thawing approach could provide both a physical stabilizing feature for nanosuspensions and a fast method for analyzing destabilizing effects. It is beneficial to identify the limited physical stability of suspensions if a study aims to investigate various excipients regarding long-term stabilizing and destabilizing effects. In this way, (de)stabilizing effects can be identified at an early stage and the time-consuming storage investigations can be dispensed with.

In the comparative studies by L. Al Shaal et al. [104] and by S. Kobierski et al. [157], it was demonstrated that the use of some preservatives added to a drug-surfactant formulation can sustain its stability, while others destabilize it immediately. In both previous studies, NC stabilized with PLC and preserved with Euxyl were found to be best. Therefore, the same procedure was repeated in this work using a rutin nanosuspension stabilized with PLC. The idea behind this was to generate a possible correlation between different stabilizing and destabilizing effects of storage conditions and preservatives on rutin NC. Additionally, possible differences between the surfactants should be identified (PLC vs. PLX).

As observed for the PLX-stabilized formulation, the stability over time of the non-preserved preparation with PLC decreased at higher storage temperature (**Figure 56**). Therefore, freeze-thawing resulted in the most stable formulation while the less stable one was obtained when stored at 30 °C. Due to its small molecule size and low number of contact points with the particle surface, it was believed that PLC could generally desorb easily and be replaced by other substances, such as the preservative Euxyl PE9010. In practice, however, it seemed rather as if the preservative contributed to the stabilization, which can be confirmed by microscopy (**Figure 57**). The non-preserved preparation exhibited a few loose accumulations that easily developed aggregates with time. By adding Euxyl PE9010 those accumulations were missing and thus a higher stabilization due to synergistic effects came into action. Consequently, Euxyl PE9010 possessed two positive effects: It improved the physical and microbiological stability of the PLC-stabilized formulation and can also be successfully frozen with it to further increase shelf life. In the frozen state, there is no molecular or particle motion. It could therefore be assumed that frozen nanosuspensions are stable for much longer than the storage period investigated.

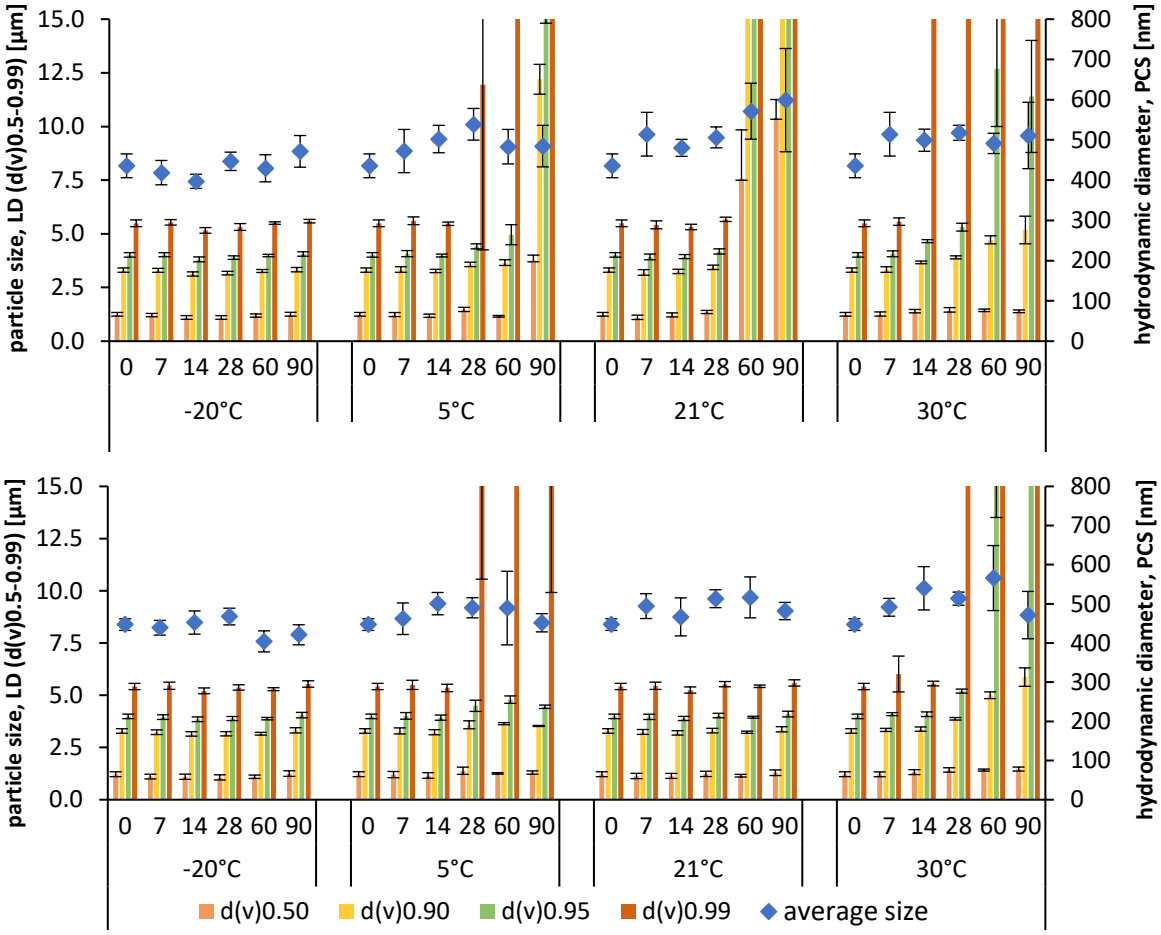

Figure 56: *Hydrodynamic diameter (PCS) and particle size by LD of the rutin nanosuspensions stabilized by PLC stored over 90 days under varying temperatures. They were left as they are (upper) or preserved with Euxyl 9010 directly after production (lower).*

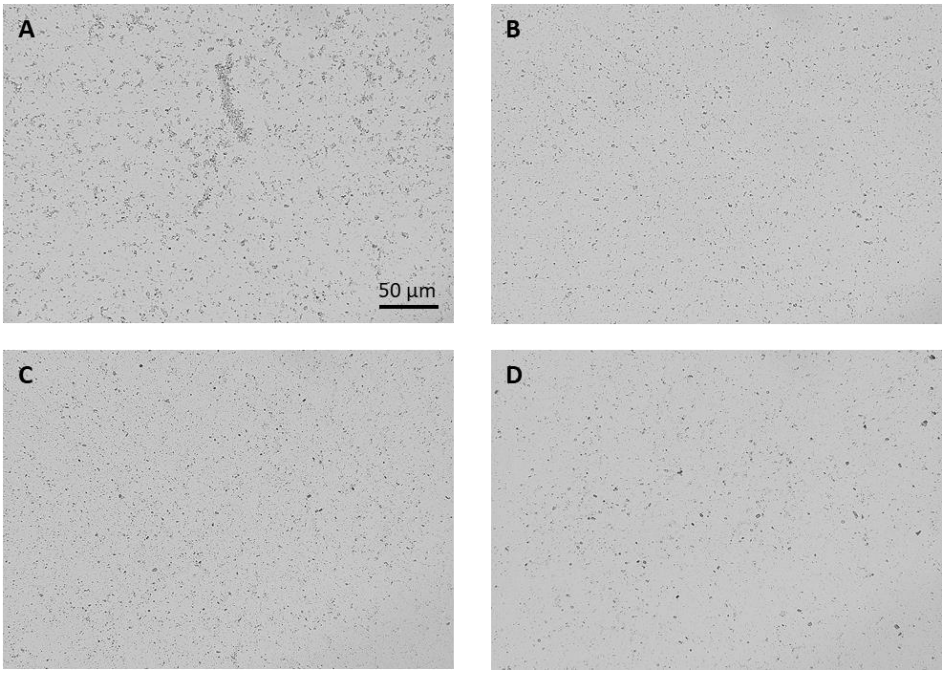

Figure 57: *Microscopic images of PLC-stabilized rutin NC after the production without Euxyl PE9010 (A), and with (B). Samples were freeze-thawed without (C) and with (D) addition of the preservative. (Magnification 400-fold).*

Another similarity compared to the PLX-stabilized rutin NC became apparent: the stability of the preserved formulation is best at room temperature, i.e. no agglomerations occurred within 90 days of storage (**Figure 54** and **56**). Furthermore, higher and lower storage temperatures, except freezing, led to less physical stability. This shared characteristic of the best stability at room temperature of both preserved formulations indicated a temperature dependency of action and interaction of Euxyl. Further investigations would be necessary to elucidate the mechanism in more detail.

A major difference between both preserved formulations (stabilized with PLX and PLC) is the tendency to aggregate after the freeze-thawing process. This supports the thesis that freeze-thawing could be seen as a catalyst for and the identification of possible disturbing effects and excipients, respectively. If a compound was added to the formulation that resulted in some physical instability at the beginning, freezing will fail and the suspension agglomerates. Conversely, if the suspension is intrinsically physically stable, this condition could be extended indefinitely by freezing.

In summary, the addition of Euxyl PE9010 was shown to decrease the physical stability of PLX-stabilized rutin-NC but increase that of PLC-stabilized one. It was hypothesized that the change in the surfactant layer played the main role in this observation. For this reason, the ZP was measured to determine whether changes in the surfactant layer onto the particles have occurred. If the preservative deposited into or onto the existing surfactant layer, it would shift the shear plane. Likewise, the preservative could interfere with the formation of surfactant micelles or even promote them due to interactions, such as Van-der-Waals force. Both the shift of the shear plane and the formation of a preservative-surfactant complex would lead to detectable changes in the zeta potential.

Interestingly, by comparing the zeta potential over time and against the preservation state, no changes were observed in this study (**Figure 58**). This suggests no interference of the preservative on the stabilization mechanisms of the NC surface.

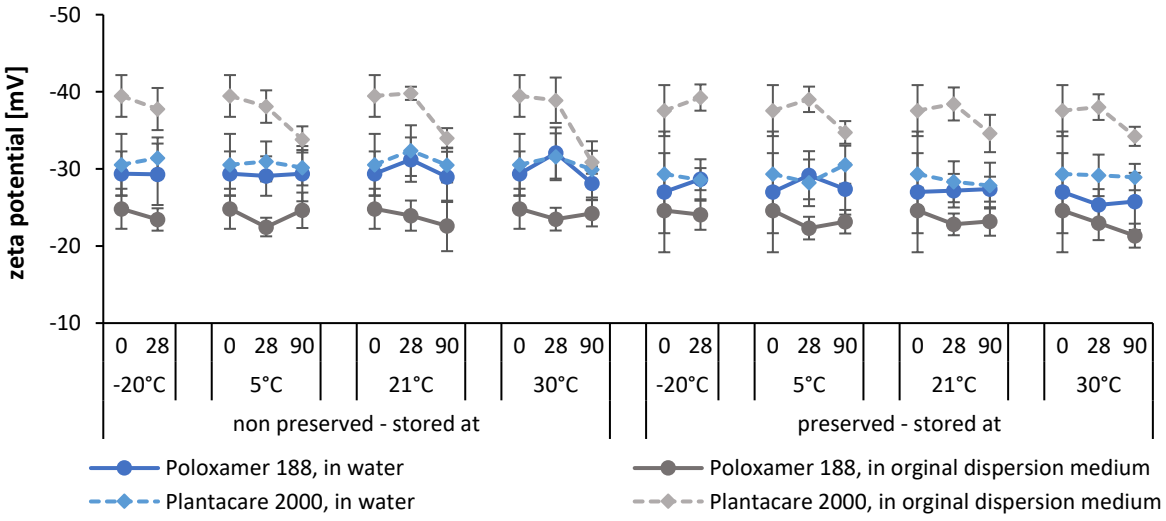

Figure 58: *Time-dependent ZP values of the differently stabilized and stored rutin nanosuspensions.*

For the formulation stabilized with PLX on the one hand, this was not expected with regard to the assessment of the hypothesis of changed surfactant layers. On the other hand, an exchange of the large surfactants with their many contact points at the particle surface would be atypical. This is also reflected in the dilution with water, where the ZP decreased only slightly compared to the dilution with the original medium (**Figure 58**). However, the destabilizing effect in a PLX-stabilized nanosuspension was also confirmed in a study by Beirowski and co-workers, who showed that some combinations of PLX and cryoprotectants were unsuitable for NC stabilization during a freezing process [251]. Hence, other mechanisms might account for the weaker stability of the preserved PLX preparation, e.g. a reduction of the steric shielding. Steric stabilization is mainly achieved by preventing surfactant's tail segments from interpenetrating because the resulting de-solvation is thermodynamically unfavorable [149]. Hence, if the preservative could favor such inter-penetration, agglomerations would result.

In contrast, the alkyl polyglucoside PLC, characterized as a smaller surfactant molecule, was believed to have easier "wash-off" after the addition of water or other small molecules. The reason is the presence of only one contact point to the particle surface and the desire for balancing the concentration in the dispersion medium. Indeed, the addition of water reduced the ZP from -40 to -30 mV (**Figure 58**). The addition of Euxyl PE9010, however, neither affected the ZP nor the tendency of a slight decrease after 90 days. The shear plane was not elongated whereas instead the density of stabilizers could be elevated by inserting the small preservative molecules in between. This resulted in a higher steric shielding efficacy.

In other words, in this study, the ZP measurements were insufficient to predict long-term stability, to explain the changed physical stability, and to determine possible interaction of the surfactant and particle with preservatives. Similar results were obtained in the study by L. Al Shaal and co-workers, where different preservatives did not significantly alter the ZP but led to very different stability performances which had been predicted microscopically [104]. Impairment degree can be explained by the nature of the stabilizer, hydrophobicity/ lipophilicity of the nanoparticle and the preservative. This determines how strongly and densely the stabilizers are bound onto the particle surface, how high the affinity of the preservative with the particle surface was in general, and finally what kind of stabilization might result, e.g. non-ionic small molecule with a weak steric shielding. In contrast, high differences in ZP and larger particle sizes compared to non-preserved formulations were detected when adding the preservative prior to the HPH process because the preservative is integrated into the surfactant layer. Due to its small size and/or uncharged nature, the stabilizing potential might be very low, which the stabilizers need to compensate for [157,252].

4.3.1.5 Determination of microbiological stability

To improve the microbiological stability, the same experimental setup as described above was adopted, i.e. rutin nanosuspensions were stabilized with PLX or PLC and each separated into a preserved and non-preserved group. These 4 groups were then subdivided again for storage at different temperatures (-20, 5, 21 and 30 °C). The growth of bacteria and fungi was determined for all formulations after 1, 2 and 3 months of storage by counting the colony forming units (CFU) on agar plates. One suspicion was the decrease in the stability due to the microbiological impact. On the one hand, the bacteria could be detected as individuals as they range in a detectable size, on the other hand, their metabolites could play a role in altering the medium. As shown in the previous section, the addition of another compound can strongly influence the physical stability without being able to be measured, e.g. via the ZP. For this reason, the influence of microbiological growth in the nanosuspensions on physical stability was studied. Furthermore, it is expected that the improvement of physical stability through the freeze-thaw process could provide additional microbiological benefits, which could omit the use of preservatives.

All preserved formulations showed excellent microbial quality as no fungi or bacteria were detected during the three months of storage. The evaluation is performed visually via agar plates, which are summarized in the appendix (**Supplementary Figure S13**). For the non-preserved nanosuspensions, the growth of microorganisms was temperature-dependent and was also slightly influenced by the type of stabilizer used (**Figure 59**).

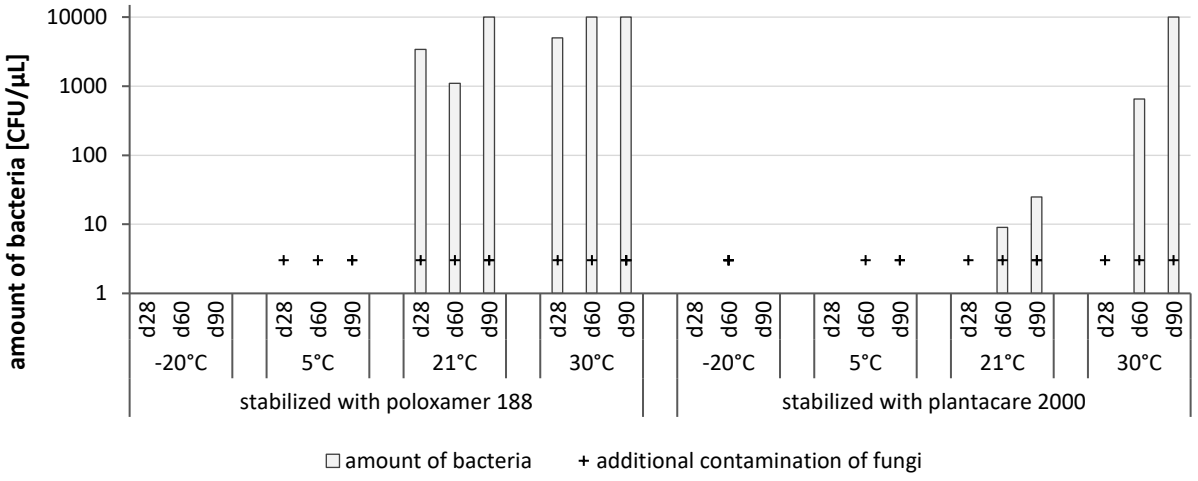

Figure 59: *After counting the colonies onto the agar plates, the bacterial density as CFU per microliter was plotted logarithmically. The microbial amount was monitored over three months of storage, expressed as a bar. + represents the contamination of fungi.*

Data indicate that for all formulations the number of bacteria was fairly low upon HPH, which is a well-described technique to reduce the number of bacteria in liquids [253], and that bacteria growth was mainly affected by the storage temperature. However, the formulations stabilized with PLC exhibited

less CFU, when comparing both formulations at the same temperatures. A possible reason for this observation could be the antimicrobial activity of the stabilizer PLC, which was already described in previous works [254,255]. Finally, it was found that no bacteria growth occurred in all formulations when stored in a frozen state at – 20 °C (**Figure 59**). Only in one frozen non-preserved sample, fungal growth was observed (d60, PLC-stabilized). The freeze-thaw process might not eliminate all fungal spores completely, nevertheless, it could drastically decrease their number. For example, it was found recently that yeast cells were able to survive freezing stress. Normally, freezing led to dehydration or ice formation inside the cell, which can be resisted depending on the phase (log or lag) [256,257]. Additionally, compared to non-frozen samples further growth was prevented. The fact that only one sample exhibited fungi growth can be explained statistically. A few fungi spores surviving HPH and the subsequent freeze-thaw process can be sampled with low probability. This theory is supported by the samples drawn after 90 days of storage, where no microorganisms were found. Hence, the hypothesis, that storing nanosuspensions after production in a frozen state might prevent microbiological growth during storage without the use of preservatives, could be confirmed. These findings are, so far, very promising and could enable a new concept to produce preservative-free nanosuspensions which can be stored over a longer period until further processing into final dosage forms.

Again, the use of preservatives protects the nanosuspension from microbial growth under common storage and transportation circumstances. However, based on the previous findings in this work, their use is also associated with possible impairment of physical stability. So, the work was also aimed at developing an alternative to preservatives and succeeded: Freezing preservative-free aqueous nanosuspensions represents a convenient formulation principle since potential interactions with preservatives and other excipients cannot occur. Also, allergies of consumers and/or regulatory hurdles can be circumvented with this concept. Furthermore, the freeze-thaw concept is simple and can be exploited not only in industry but also in early drug development, where nanosuspensions are often used for the early formulation of poorly soluble drug candidates. At present - due to the lack of microbial stability - nanosuspensions need to be prepared shortly before performing the experiments, i.e. assays, cell culture, or *in-vivo* studies. Any repeating of the tests or continued tests will require the production of new suspensions, which might possess slightly different properties, which in turn might then cause differences in the *in-vitro* and *in-vivo* data. By using thawed nanosuspensions from only one batch, these variations could be circumvented. In conclusion, the freeze-thaw concept is a simple method to prevent bacteria growth during the storage of nanosuspensions. It enables new possibilities for the use of nanosuspensions and thus can be seen as a highly promising concept, not only in pharma but also in food and cosmetics.

4.3.1.6 Determination of chemical stability

So far, this thesis focused on the physical stability of the rutin nano-formulations to ensure the main principle of nanoparticle's efficacy, namely the increased dissolution velocity and kinetic solubility. The effect of the active ingredient itself, however, is defined by its AOC. It was expected that a prolonged storage time and higher storage temperature promoted the oxidation of rutin which in turn would decrease its AOC. To investigate this assumption, the approach of differently stabilized and stored rutin NC - described in the section above - was adopted. This means that the rutin nanosuspensions were stabilized with PLX or PLC and used preserved and non-preserved, respectively. These 4 groups were then subdivided again for storage for 90 days at different temperatures (-20, 5, 21 and 30 °C), with samples drawn at the day of the production and 28, 60 and 90 days after the production. Hence, the influence of Euxyl PE9010 on the chemical stability of rutin nanosuspensions was investigated. The antioxidant capacity was measured by using the DPPH assay in which the IC_{50} is determined. If the same preparation reveals a reduction in AOC (higher IC_{50} values) over time, an oxidation process is indicated by the storage condition applied. A methanolic assay was used dissolving rutin completely to ensure that agglomerates would not delay the reaction.

In this study, the IC_{50} values for the different formulations over storage time did not change, independent of preservative, storage time, and storage temperature (**Figure 60**). As the AOC is an indirect measure for the chemical stability, the data indicate excellent chemical stability of all aliquots during storage. This is in good agreement with a recent study by L. Gao et al., where the authors could prove the chemical stability of a quercetin nanosuspension and the superiority against their solution [224]. In the comparison of the two differently stabilized rutin nanosuspensions, however, the PLC-stabilized one showed higher IC_{50} values indicating that the surfactant promotes the oxidation process. This could be caused by the shift in the pH value and thus the increased solubility. Rutin is a weak acid that is soluble in alkaline solutions and hence has a higher solubility in the weakly alkaline PLC solution. It seems that during the production process possible oxidation processes took place. If a higher concentration of rutin is dissolved during the process, the probability of an oxidation reaction is elevated. For this reason, the difference in IC_{50} values was higher between the differently stabilized NC at the day of production, than within the same formulation over the storage time (**Figure 60**). Thus, possibly physical or microbial instabilities of a nanosuspension has a much lower influence on the oxidation reaction than the medium created by the stabilizer. In this study, the test for AOC thus rather indicated the solubility in the medium, i.e. the influence of the surfactant on the degree of dissolution of rutin.

The formulation of NC represents a great feature that preserves chemical stability over longer storage times and higher temperatures. Thus, it requires only minor consideration of how soon further

processing must proceed, the transport conditions, or the general shelf life if the suspension is to reach the user.

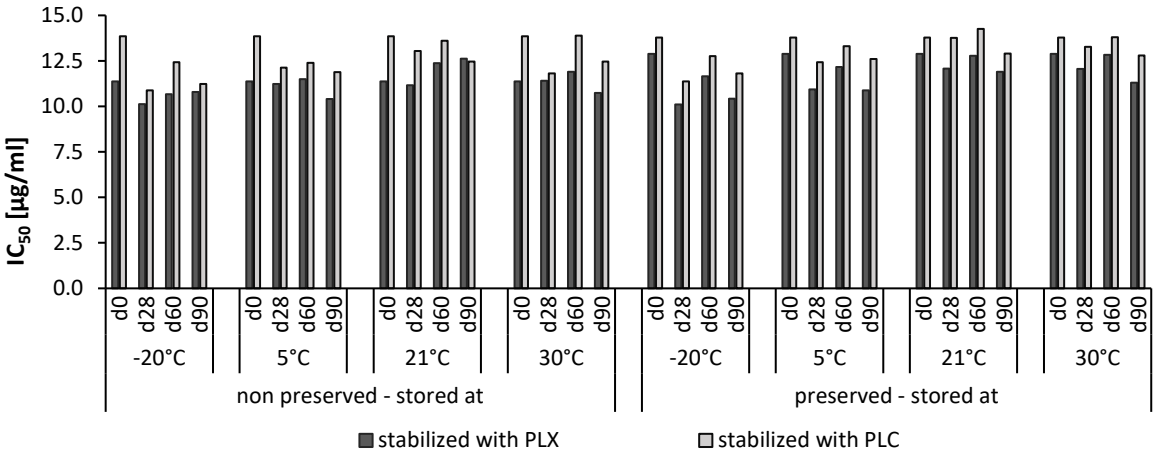

Figure 60: *Antioxidant capacity of the rutin nanosuspensions, expressed as IC_{50} values, depending on the stabilizer used, the addition of a preservative, and the storage duration and temperature. The lower the value the higher the antioxidant efficacy.*

Overall, rutin nanosuspensions were successfully produced and optimized regarding size, as well as physical, microbiological, and chemical stability. Of these, two points are not optimal: the best stability can be achieved by freezing the nanosuspension, resulting in further challenges for marketing. Second, the user must nebulize the nanosuspension himself if it is aimed to reach the lungs. To extend the shelf life and develop a more convenient application form, the next step of this thesis was to convert the aqueous suspension into a dry powder formulation for inhalation purposes.

4.3.2 Formulation of dried nanocrystals for inhalation

Up to this point of the study, stable rutin nanosuspensions were produced. Besides the challenges in preventing the stability of a suspension, a liquid formulation is not convenient for patients to apply. Disadvantages of a liquid spray inhaler, i.e. nebulizer include the requirement of an external power source leading to an in-house use only. Due to its size nebulizers are limited to clinical use and for a restricted patient population (young children and the elderly). Furthermore, the generated droplets differ depending on the atomization technique and of the formulation [258].

Those instability issues can be overcome by using the NC as a dry powder. Thereafter, the second sub-aim was to transfer the rutin nanosuspension into a flowable powder for use in a dry powder inhaler. To achieve this goal, two important biological and physiological aspects must be considered:

At first, the applied particles must have a size between 1-5 µm for reaching the deeper lung [186]. If they are smaller, they would be exhaled easily because they cannot settle and thus are kept in the air. If they are larger, they would be deposited on the upper lung area or on the oropharynx and then

swallowed into the gastrointestinal tract. Consequently, it means that the produced rutin NC would be too small if they were applied dried while remaining unchanged in size.

Second, the ciliated columnar epithelium in the upper airway emits secretes to catch and remove foreign particles by the mucociliary escalator. Avoiding the trap and clearance process can be achieved by inhaling very small particles or particles with suitable surface chemistry, e.g. covered with hydrophilic and neutrally charged polymers can help to prevent mucus adhesion [259]. Foreign particles reaching the deeper pulmonary alveolar region, are affected by macrophage clearance by phagocytosis. On the other side, macrophages are the main target for pulmonary antioxidative treatment. Therefore, the rutin NC must be dried in a biocompatible and degradable carrier with a size of 1-5 micron. After deposition in the deeper lung, these nano-in-micro structures dissolve and release the NC at their target. For that reason, harmless and approved adjuvants, i.e. amino acids and sugar (alcohols) were dried with the usual drying methods, meaning spray- and freeze-drying.

To reach the second sub-aim, spray- and freeze-drying processes should be investigated and optimized to successfully convert the rutin nanosuspension into a dry powder for inhalation. The optimizations include the determination of the process conditions, the development of the formulation, and the investigation of the application device.

4.3.2.1 Spray-drying

Spray-drying is a fast, simple, and scalable all-in-one process established in food, chemical, and pharmaceutical industry. Compared to other drying processes, spray-drying is continuous and capable to transform liquids into solid particles with adjustable size, distribution, shape, porosity, and density. In spray-drying, a liquid is atomized by a nozzle in a hot air stream. The resulting small droplets from the solution or suspension increase the surface area tremendously and thus lead to a fast mass and heat transport between the droplets and the carrier gas [260]. The airflow dries the liquid portion beside transport, which leads to a temperature reduction (inlet > outlet temperature). The drying of a single droplet takes less than one second. The resulting solids are deposited by centrifugal forces. As result, microparticles with a size of about 20-200 µm and narrow size distribution can be obtained usually [261]. The narrow size distribution results from the homogeneous generation of the droplets during atomization [260].

Thus, the nanosuspension is dried and, at the same time, carrier-based nano-in-micro particles with inhalable particle sizes might result. Therefore, this technique was used as the first method of choice. To allow a simplified definition and avoid confusion for the different particles, the nanoparticles continue to be referred to as NC while the resulting NC-in-carrier structures as microparticles. As explained in the previous section, the scale-up process to produce rutin NC stabilized with Tween 80 and BSA was used.

In the first trial, the rutin nanosuspensions were diluted with water before the spray-drying process. The idea behind this was that a high quantity of solids per milliliter liquid would adversely lead to heavier microparticles and microparticles with higher density, respectively. After the drying process, the re-dispersed NC were characterized regarding size by PCS and LD. The formulation and process conditions as well as the results are summarized in **Table 13**.

Table 13: *Overview of the composition, condition, and result of the spray-drying trials 1-4 (SD1-4). Rutin nanosuspension stabilized with a mixture of Tween 80 and BSA, diluted with water and enriched with mannitol (M) or lactose (L) as carrier, were dried with varying in-let and out-let temperature, while the airflow was constant at 160 L/min. Re-dispersed NC were characterized regarding size by PCS and LD with d(v)0.90 and 0.99 as a critical factor for identifying agglomerations and particle growth. The pure nanosuspension before processing was listed for comparison.*

N°	quantity [g] of			in-let [°C]	out-let [°C]	d(v)0.90 [µm]	d(v)0.99 [µm]	$d_{hydrodynamic}$ [nm]
	additive	water	NS					
SD1	2.5 (M)	27.5	20.0	63	48	4.0 ± 0.2	31.5 ± 6.4	346 ± 12
SD2	1.5 (M)	18.5	30.0	63	49	3.5 ± 0.1	30.5 ± 1.9	333 ± 22
SD3	1.5 (L)	18.5	30.0	63	50	4.1 ± 0.2	17.7 ± 8.8	321 ± 12
SD4	1.5 (L)	18.5	30.0	107	77	4.1 ± 0.1	12.3 ± 6.0	327 ± 4
pure nanosuspension:						3.9 ± 0.1	6.7 ± 0.1	386 ± 26

In all spray-drying tests of the first trial (SD1 to SD4) agglomerations were detected after re-dispersion by LD (**Table 13**). Small optimizations were achieved regarding the prevention of the NC-agglomeration by changing the process parameters and composition of the formulation from SD1 to SD4. While SD1 still formed huge agglomerations of about 32 µm, 12 µm sized NC-agglomerations were detected in SD4. Changing the formulation to a higher amount of solids per milliliter did not improve the final size of the resulting agglomeration, but the number of them, since the d(v)0.9 value could be reduced (from SD1 to SD2). A more pronounced improvement was achieved by adding lactose instead of mannitol and by increasing the drying temperature. The formation of agglomerations was also visualized by microscopy (**Figure 61**). However, the particle sizes detected by PCS decreased after the spray drying process in each case when compared to the initial nanosuspension. One reason for this might be the previous dilution with water, in which the smaller NC were partially dissolved. Another explanation could be that the agglomerations formed were outside the detection limit, shifting the average particle size towards the smaller ones. Similar observations were described previously in context with agglomeration formation at stability studies (c.f. sections 4.1.2.3 and 4.3.1.4.2).

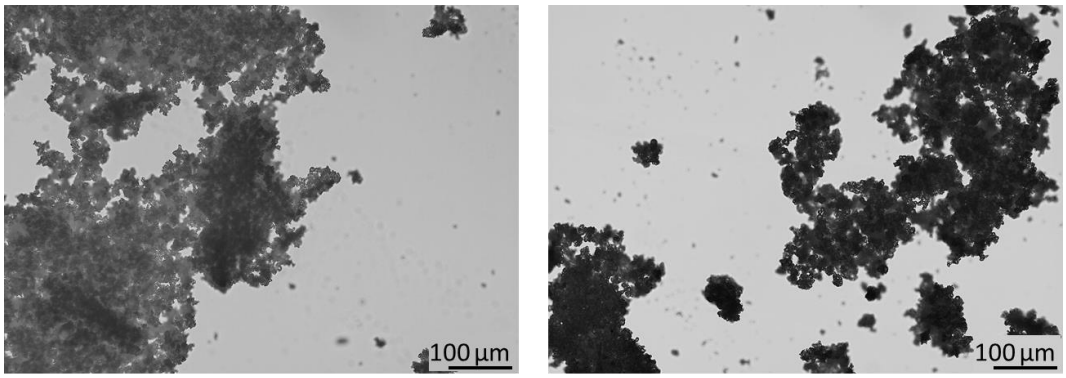

Figure 61: *Microscopic images of the spray-dried rutin NC formulations SD1 (left) and SD4 (right); magnification 200-fold.*

Besides maintaining the particle size of the NC, the more important aim was to develop a flowable fine powder for inhalation purposes. However, this was not achieved with these spray-dried formulations. Instead, a compact, coarse powder was obtained (**Figure 61**) which has been only sufficient for a few measurements due to a very low yield. Reasons for the low yield and the coarse structure are manifold and include the pre-formulation of the NC, such as the surfactants, to the applied process parameters. There are many studies concerning the optimal parameter to produce a spray-dried nanosuspension for inhalation [182,262]. One crucial factor was found to be the formulation itself. The formulations containing Tween 80 are critical as the melting point of the surfactant is much lower than the process temperature (and even the room temperature). Hence, Tween 80 is liquid during the spray-drying process including the particle separation within the cyclone. This circumstance in turn may favor inter-particle sticking and thus explains the resulting lumps. Problematic sticking on the chamber walls and between the particles was also observed in other studies [263,264].

For this reason, optimizations were carried out including modifications in the pre-formulation as well as for the process parameter. In terms of the formulation, a rutin nanosuspension was stabilized with a mixture of PLX and BSA, with both stabilizers have melting points above the process temperature. Moreover, additional water was omitted to reduce the total water content and the drying temperature was increased (**Table 14**). Both process modifications were aimed at shortening the drying time and thus at preventing wet microparticles from sticking to each other or to the chamber wall. In contrast, also in this trial (SD5 to SD7), only a very low yield of dried powder was obtained after drying due to adhesion to the chamber wall. However, the dry power separated in the collection vessel was re-dispersed and the NC were characterized regarding size.

Table 14: *Rutin nanosuspension stabilized with a mixture of PLX and BSA were enriched with mannitol as carrier before spray-drying at different set-up parameters such as the airflow and the in-let and outlet temperatures. The resulting particle sizes determined by PCS and LD are compared to the original nanosuspension before drying.*

N°	quantity [g] of		in-let [°C]	out-let [°C]	airflow [L/min]	d(v)0.90 [µm]	d(v)0.99 [µm]	$d_{hydrodynamic}$ [nm]
	mannitol	NS						
SD5	4.0	50.0	89	63	110	2.0 ± 0.1	3.4 ± 0.1	309 ± 24
SD6	4.0	50.0	151	101	102	17.8 ± 1.1	32.8 ± 3.4	785 ± 225
SD7	6.0	50.0	120	90	120	26.8 ± 1.3	45.1 ± 1.8	742 ± 170
pure nanosuspension:						2.1 ± 0.1	3.7 ± 0.1	349 ± 17

As a result, only a moderate drying out-let temperature of 63 °C combined with a mannitol concentration of 160% related to the rutin concentration was able to maintain the size of the rutin NC (SD5) (**Table 14**). Higher temperatures and mannitol concentration led to larger agglomerations. The first assumption for this was the degradation of BSA, which could promote aggregation and decrease thus the physical stability of the NC. On the other hand, the product temperature should be even lower than the out-let temperature due to the short drying time and the evaporation enthalpy at the droplets. This means, that the product temperature should be lower than the out-let temperature detected. Nevertheless, further general optimizations are required to find a basis from which an ideal outcome could be achieved by little step-by-step improvements. To investigate which factor caused the agglomeration of the rutin NC during the spray-drying process and also to further decrease the loss by adhesion on the chamber wall, the pre-formulation and process parameters were modified. For this purpose, the rutin nanosuspension was stabilized with PLX only and the process parameter applied are summarized together with the results in **Figure 62**.

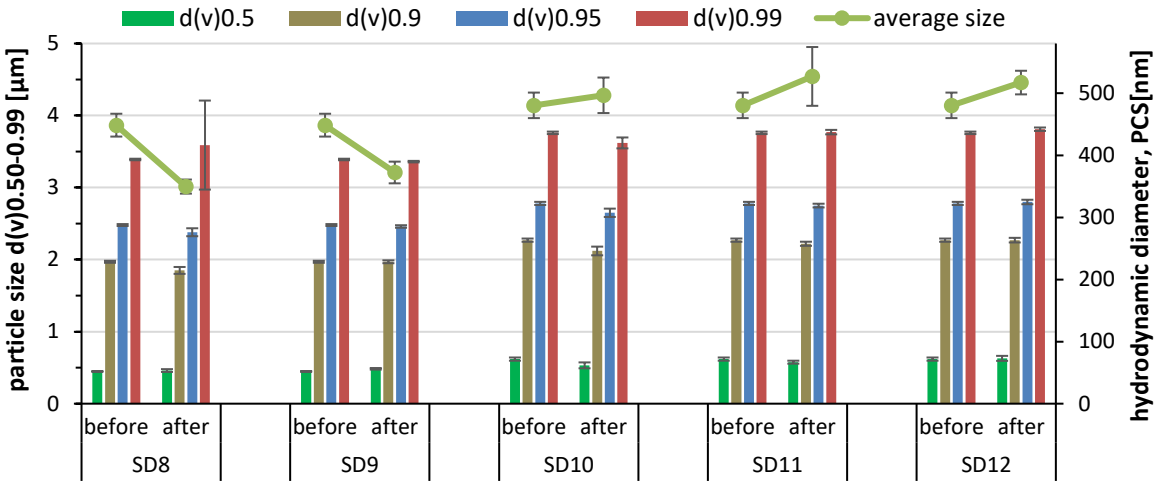

in-let	63	90	150	148	148	[°C]
out-let	52	66	101	100	100	[°C]
airflow	160	110	100	110	120	[L/min]
yield	low	low	31.3	26.2	29.3	[%]

Figure 62: *Particle size measured by PCS and LD of rutin nanosuspensions, stabilized with PLX, before and after the spray-drying process. The yield results from the measured mass in relation to the theoretical dry mass, which contains all solid components without water. Mannitol as carrier was added in a concentration of 8.0 in 100.0 g dispersion.*

By excluding BSA in the pre-formulation, sufficient stabilization of the NC could be achieved even at higher temperatures, i.e. that no agglomerations were detected after re-dispersion (**Figure 62**). The LD measurements showed no change in particle sizes, while PCS measurements revealed an increase in the hydrodynamic diameter with higher temperature. Below an out-let temperature of 100 °C the hydrodynamic diameter size decreased by about 90 nm and increased by about 35 nm above 100 °C out-let temperature, respectively. These harder conditions were necessary to increase the yield of the dried microparticles. Most of the loss happened through deposition on the wall of the drying chamber, which could be a consequence of high humidity. Although the residual moisture was not measured, it can be considered to be relatively high, because in all cases the result was a wet-looking lump instead of a fine, dry and flowable powder. In general, two approaches lead to a reduction in product moisture: increasing the air volume and increasing the temperature. By applying higher temperatures the yield was increased (SD8 to SD10), while increasing the airflow was not that successful to increase the yield (SD8, and SD10 to SD12). Despite these improvements, it was not possible to obtain a free-flowing dry powder. The resulting powders were visualized microscopically for size and shape (**Figure 63**). By doing so, larger structures with sizes of about 10-50 µm were observed. These structures appeared as composite substructures of the carrier, which could have been formed by the collision of microparticles that are too moist. These are retained by the adhesive power of the water layers and form crystal bridges from the carriers as they continue to dry. It is also visible that the NC are embedded in the carrier (**Figure 63**).

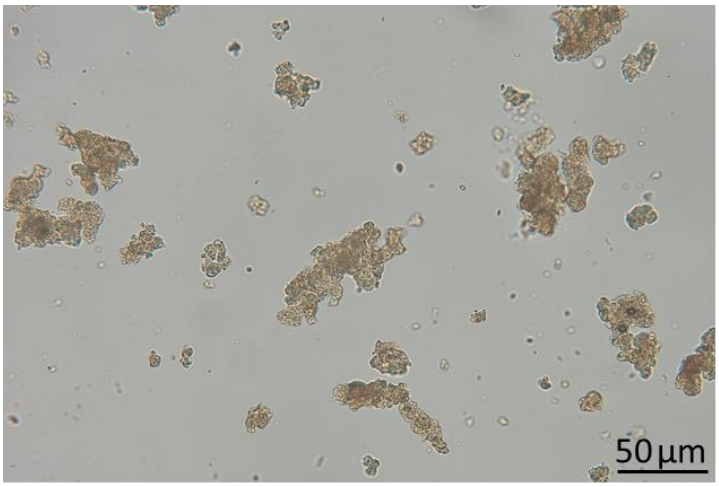

Figure 63: *Microscopy image of the spray-dried rutin nanosuspension SD12, magnification 400-fold.*

When comparing the microparticles obtained in the trials SD1 and SD4 to those of SD12, the carrier-NC structures became smaller (**Figure 61** vs. **63**). The reason for this is the higher temperature and adjustment of the formulation. Therefore, spray drying was improved in a manner that significantly smaller microparticles and a higher yield were achieved. In terms of the yield, however, no significant improvement seemed to be possible, since the temperature cannot be increased further and the change in the airflow did not play a crucial role in this trial (**Figure 63**). Nonetheless, these microparticles possessed a size of > 10 µm estimated by microscopic images. For a successful inhalation, this size would be too large. Consequently, another drying method was used to obtain a finely dispersed and freely flowable powder. Anyhow, the inhalability of the smallest particle population obtained by the spray-dried formulation SD12 is investigated and discussed by using the NGI afterward (c.f. section 4.3.2.3).

4.3.2.2 Freeze-drying

Since spray-drying was not successful and the resulting microparticles did not appear to be capable of self-dispersing into smaller fragments upon inhalation, a completely new approach had to be applied: freeze-drying. The use of the freeze-drying method results in a compact lyophilizate instead of a free-flowing powder, too. Nevertheless, it was expected that the lyophilizate would be promising, as its extremely highly porous structure could be easily crushed in a second step.

Rutin NC stabilized with different surfactants and surfactant combinations were supplemented with mannitol as classical cryo- and lyoprotectants in serval concentrations. These should prevent possible agglomeration of the NC during freezing and act as a matrix for including the NC. The particle size of the rutin NC were characterized before and after freeze-drying meaning after redispersion with the same portion of water that was previously removed from the formulations.

Regardless of the pre-formulation, i.e. the surfactants, and the concentration of mannitol added, the particle size remained unchanged (**Figure 64**). As expected, the NC also remained stable without adding

mannitol, which was also observed in the freeze-thawed studies described in section 4.3.1.4.4. If the stabilizer concentration and thus the steric stabilizer layer on the particle surface is dense enough, the NC were separated from each other during drying. Then, the formation of Van-der-Waals forces between the particles was not possible which consequently eliminates the need for additional cold protection during the drying process [251]. Thus, freeze-drying seemed to be also suitable for creating different pre-conditions for downstream process steps. This means that the power properties after the crushing steps could be adjusted in advance with different concentrations and compositions of the carriers added to the nanosuspension.

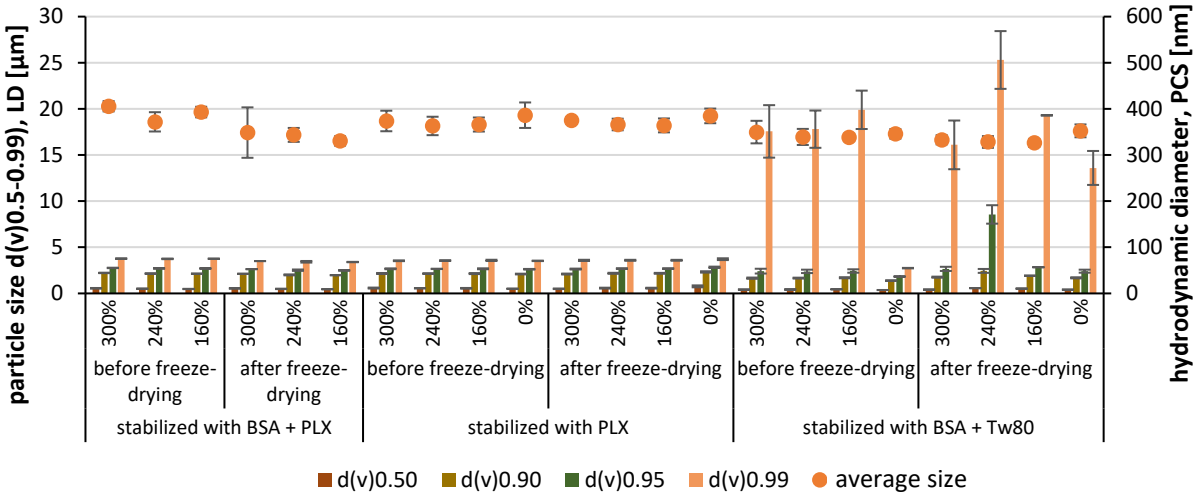

Figure 64: *Differently stabilized rutin nanosuspensions, supplemented with mannitol in a ratio of 0-300% to the rutin content of the suspension, were characterized regarding size (LD and PCS) before and after freeze-drying. Freeze-dried formulations were re-dispersed with the same amount of water that would theoretically have been removed.*

The only exception was found for the nanosuspension stabilized with a mixture of BSA and Tween 80. In this formulation, particles or aggregates were formed during the freeze-drying process, but also after the addition of mannitol prior to the freeze-drying step. These agglomerations showed a d(v)0.99 values by LD measurements of about 20 µm maintaining after the freeze-drying (**Figure 64**). One feasible explanation for the observed effect would be a salting-out of the BSA by adding a high amount of mannitol compared to the BSA concentration, which would cause the formation of protein aggregates. This is unusual at first glance because numerous studies are reporting that mannitol or other polyols protect proteins in solution from denaturation and kinetically delay aggregation [265]. Therefore, the reason for this is probably not mannitol itself but the instability of the formulation. For long-term stability studies, the nanosuspensions were stored at standstill. However, when adding mannitol, the suspensions were stirred and thus subjected to additional mechanical stress. Mechanical stress could induce protein aggregation due to the exposition of the protein to air-water interfaces, material surfaces and shear forces [266]. The hypothesis described above that the first aggregates

must already have formed due to the long heat exposure during the NC production, might be re-used at this point. The suspension stabilized with BSA and Tween 80 was prone to malformations anyway (c.f. section 4.3.1.4.2) and the further agitation (induced by stirring) might trigger further aggregations, between the BSA molecules, and also between the NC. Likewise, the agitation increases the probability for the NC to approach each other too closely, and feasibly for overcoming the energy barrier which leads to irreversible agglomeration. Freezing is also a stress factor that triggers protein aggregation, e.g. by the formation of ice-solution-interfaces or cryo-concentration of the protein and solutes [267]. Indeed, after freeze-drying the suspension without mannitol, larger agglomerates ranging about 18 µm were detected, which indicates that the formulation itself is susceptible and not stress-resistant.

After discovering that mannitol is suitable for some basic formulations at different concentrations, the experiment was repeated and an additional in-deep investigation regarding the stability for the PLX-stabilized formulation with cysteine, an amino acid, was carried out. Cysteine was selected because it also has antioxidant properties and - as a precursor of glutathione - it could provide additional benefits for subsequent cell and *in-vivo* studies. In all investigations, the lyo- and cryoprotectant were added resulting in a final concentration of 160% related to the rutin concentration (w/w). By using the combination of both, an equal weight of mannitol and cysteine was used. Also, the physical stability of the freeze-dried NC was monitored for one year (**Figure 65**). As a result, freeze-drying with the addition of cysteine was also successful, i.e. no changes in particle size were detected upon freeze-drying and re-dispersing (**Figure 65**). Hence, cysteine can be considered as a suitable cryoprotectant.

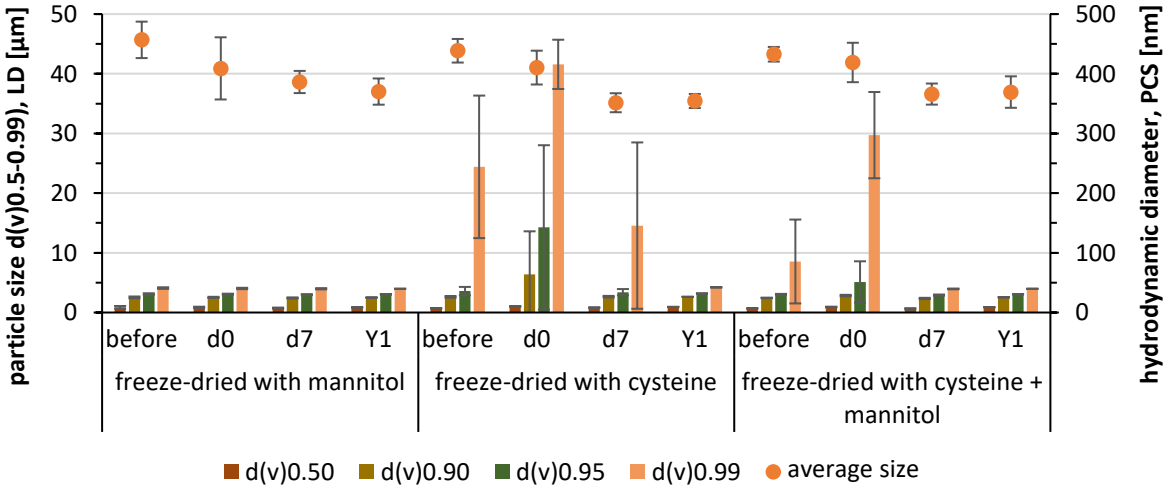

Figure 65: *Rutin nanosuspensions stabilized with PLX was enriched with mannitol, cysteine and a combination of both in a ratio of 50:50 (w/w). The formulations were freeze-dried, stored at room temperature for one year and characterized regarding size before freeze-drying, directly after (d0), after one week (d7), and after one year (Y1) of storage.*

Despite this, it was found that the hydrodynamic diameter measured by PCS decreased over the storage time of one year in all formulations (**Figure 65**). One possible explanation could be related to the freezing step, which is considered to be the most critical [268]. Some amorphous products like mannitol and glycine can form metastable glass due to incomplete crystallization during freezing. Some dissolved rutin molecules could also be partially embedded amorphously into this metastable glass form (**Figure 66**). Over time, such an amorphous complex would partially precipitate as crystals after falling below the kinetic solubility. With increasing storage time, more crystals could be developed in the solid matrix. Then, during redispersion, all rutin structures (nanocrystals, amorphous embedded co-crystals or discrete molecules) dissolve simultaneously until the saturation concentration was reached. However, amorphous rutin structures dissolve the fastest while the NC dissolves more slowly with increasing particle size. As result, the number of smaller particles increased that was measured by PCS and remained overseen by LD. Again, due to the thermodynamical instability of the amorphous embedded rutin molecules, crystallization might cause spontaneously upon the storage time. When redispersing the lyophlizates after one year, the initially existing NC and newly formed precipitates dissolved simultaneously, and consequently, the increased number of NC shifted the hydrodynamic diameter (**Figure 66**).

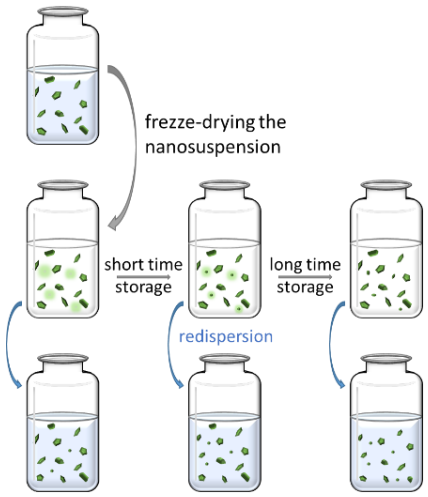

Figure 66: *Illustration of the amorphous rutin that could be formed during freezing in the carrier matrix. Crystallization processes would occur over time that increases the number of NC. After redispersion, shortly stored lyophilzates released fewer but larger particles, while longer storage time might result in more but smaller NC.*

Moreover, high d(v)0.99 values were observed by LD in the cysteine-containing formulations (**Figure 65**). The reason is, that cysteine dissolves very slowly, so that single non-dissolved cysteine crystals impaired the LD measurements. Performing longer redispersion time – as applied after one year of storage – demonstrated a necessary enlarged dissolution time for the correct assessment of

the NC's particle size. A closer look at the LD measurements confirmed that only the cysteine crystals are at the origin of the overestimated value (**Figure 67**). Each of the five measurements required just 20 s during which the particle sizes for the d(v)0.90-0.99 decreased significantly. Finally, after optimizing the measurement procedure, the particle sizes remained the same compared to the mannitol-containing formulation. Thus, it appeared that cysteine would have provoked flocculations, but this was not the case.

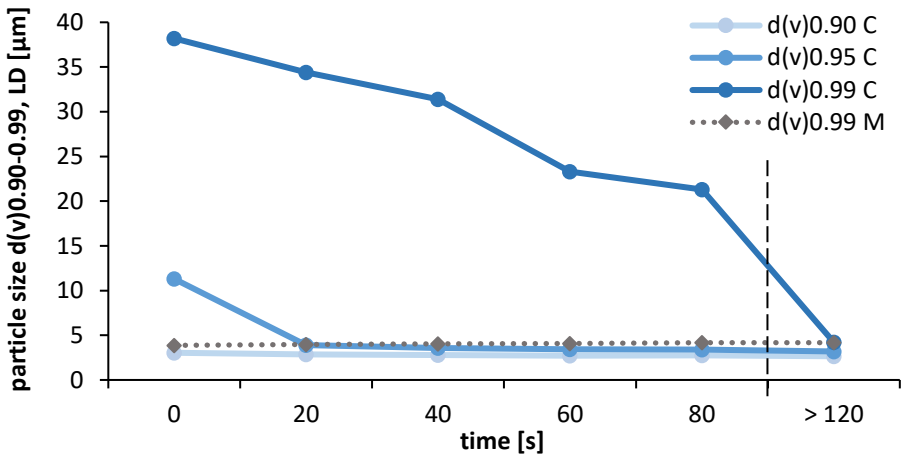

Figure 67: *Particle size of freeze-dried rutin NC with cysteine (C) and mannitol (M) were measured by LD as a function of the dispersion time.*

The excellent storage stability was also reflected in the zeta potentials (**Figure 68**). Neither the protectors (mannitol and cysteine) nor the entire freeze-drying process changes the zeta potential. Therefore, the NC surface remains unchanged, i.e. the stabilizers maintained their initial orientation and thus their function.

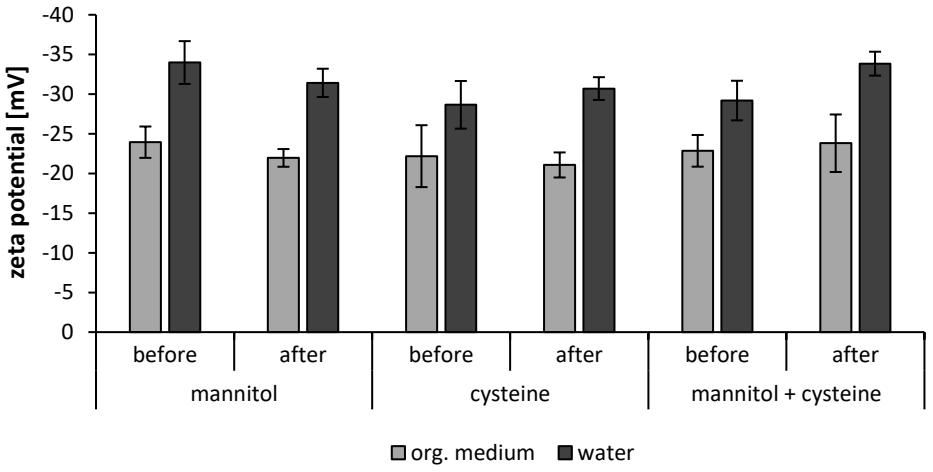

Figure 68: *Zeta potentials of the rutin nanosuspensions enriched with a protectant (mannitol, cysteine or its mixture) before and after the freeze-drying process.*

Apart from the challenges induced by cysteine, the NC as such remained intact even after at least one year of storage. This is extremely important and offers two advantages: From an industrial point of view, this not only allows the process to be time-independent but also to realize longer transport routes/ times to geographically separated further processing steps. From a marketing point of view, a product can be developed that can be offered for sale over a long period. In this way, one large production per year is sufficient instead of several smaller batches every few months.

Due to the two advantages that mannitol and cysteine suitably solidify rutin NC and should also possess antioxidant properties themselves, the resulting dry powders were used for further *in-vitro* and cell culture studies.

Again, freeze-drying was chosen as the pre-process for solidifying the nanosuspension, with the next step being the conversion into a fine powder for inhalation purposes. By using different excipients as matrix carriers for embedding the NC, it is feasible to vary crystallites, hygroscopicity and structures of the lyophilizates. Hence, further excipients were freeze-dried with PLX-stabilized rutin NC to develop the best formulation for transforming into an inhalable dry powder. As result, all excipients used were able to protect the rutin NC against agglomeration during freeze-drying but also for at least six months (**Figure 69**). Soy saccharide is poorly soluble in water and hence its non-dissolved particles were detected by PCS and LD, too. For this reason, the characterization of the soy saccharide enriched formulation by PCS and LD was not meaningful, and a determination about its physical stability could only be confirmed by microscopy (**Figure 70**).

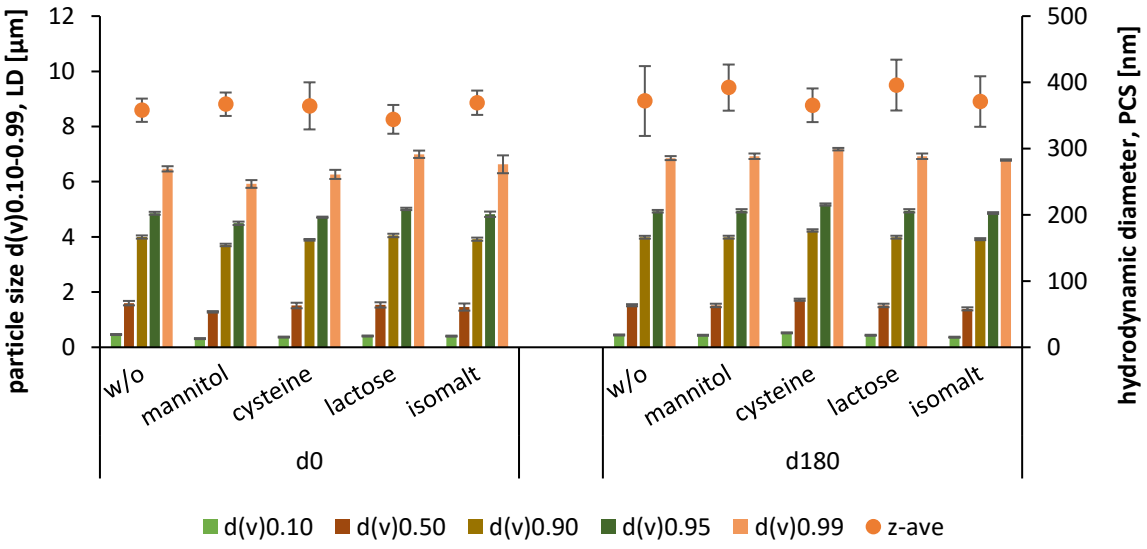

Figure 69: *Physical stability study of rutin NC freeze-dried without any (w/o) or with the additives mannitol, cysteine, lactose, isomaltose. Lyophilizates were re-dispersed with water directly after the freeze-drying process (d0) and after 180 days of storage (d180).*

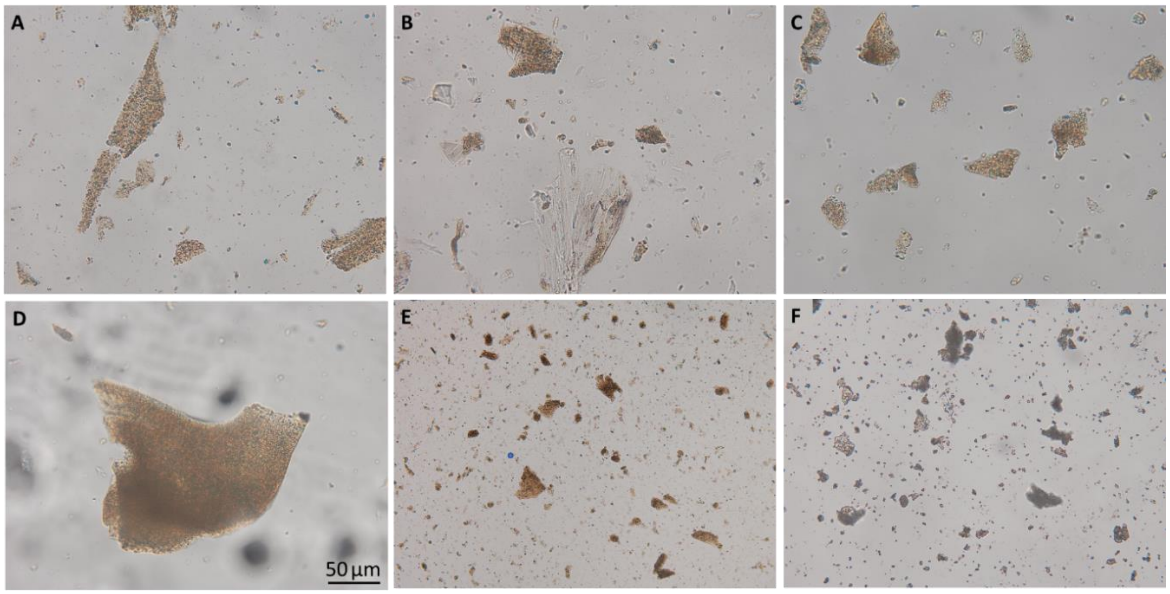

Figure 70: *Microscopic images of rutin NC freeze-dried with mannitol (A), cysteine (B), lactose (C), isomaltose (D), pure / without additive (E), and soy saccharide (F); magnification 400-fold.*

Compared to the formulation without any further additives, the microscopic images appeared to be identical to those with soy saccharide (**Figure 70 E** and **F)**. From this, it can be concluded that these NC have also maintained their size and physical stability. This was expected since freeze-drying was successful for the formulation without excipients and, consequently, the addition of a water-insoluble compound should lead to the same stability. However, it seemed that some NC covered the surface of the soy saccharides, which might represent an advantageous feature for subsequent crushing investigations. The microscopy was also used to characterize the structure of the matrix in which the NC were embedded. The NC were evenly distributed in a platelet-like structure when adding mannitol, lactose, and isomaltose, respectively (**Figure 70 A, C** and **D**). Those platelet-like structures seemed easy to break and might have a positive impact on the aerodynamic of the microparticles as similar to a bird's feather carried far with the airflow. The major difference was that isomaltose fragmented into much larger pieces and formed a generally firmer lyophilization cake. For this reason, isomaltose-containing freeze-drying cakes were not used in subsequent studies. By crushing the lyophilizates with the addition of cysteine three different and co-existing structures were found: platelet-like and cube-like structures with evenly distributed NCs in each, and cysteine crystals without rutin NC on or inside them (**Figure 70 B**). Together with its slow dissolution rate, it can be confirmed once again that the elevated d(v)0.99 values (**Figure 65**) are caused by pure non-dissolved cysteine crystals. These “extra-particles” being non-covered with NCs, represent an interesting feature for the subsequent crushing investigations. They could serve for hydrophobic or intra-particle shielding.

4.3.2.3 Crushing and Respiratory studies

Both, spray- and freeze-drying of the rutin nanosuspensions led to larger nano-in-microparticles, which exceeded the desired target size of 0.5 - 5 µm. To reduce the size, different crushing techniques were investigated in this part of the work. A simple particle size characterization would, however, not cover the flyability of the particles. Hence, the target size for a successful inhalation refers to the aerodynamic and not to the geometric diameter. The aerodynamic diameter is defined as the diameter of a sphere of unit density that reaches the same velocity in the air stream as a non-spherical particle of any density [269]. For this reason, the inhalability of the crushed microparticles was estimated using the next generation pharmaceutical impactor (NGI), which uses the deposition mechanism to determine the aerodynamic particle size. Two parameters can be identified: The fine particle fraction (FPF) indicates the proportion of particles smaller than 5 µm of the delivered dose, and the mean mass aerodynamic diameter (MMAD) indicates that 50% of the particle distribution based on mass are above or below this diameter. Both parameters represent a statistical measure of the batch particle population. In contrast to the Andersen-Impactor, the particles follow a horizontal airflow pattern within the NGI. The separation of the particles is achieved by impaction in a vertical direction such as in other test devices like the Anderson cascade impactor.

In order to prevent the particles from additional fragmentation and bouncing in the first stages (cups), the cups were coated. The coating is highly viscous with extremely low surface tension. This ensures that the coating remains form-stable during the airflow and that the particles do not rebound on the coating surface. Such a rebound is characterized by additional particle fragmentation and thus very small particles would be obtained. Hence, if rebound effects may occur, an increased concentration of API particles would be discovered in the "micro-orifice-collector" [270], corresponding to cup 8. This conversely means that if a larger quantity had been found in cup 8 (than in cup 7), the result could not be evaluated and the experiment would have to be repeated. However, this did not occur in any experiment in this thesis.

The NGI was operated at an airflow rate of 60 L/min and the cut-off diameters were calculated for each cup (**Table 15**). Thus, cups 2 - 5 are of particular interest for the target size between 1 and 5 µm.

Table 15: *The cut-off diameter on each cup of the NGI when applying an airflow of 60 L/min.*

cup number	**1**	**2**	**3**	**4**	**5**	**6**	**7**
cut-off diameter [µm]	8.06	4.46	2.82	1.66	0.94	0.55	0.34

As the spray-drying process should have generated fine microparticles that could already be inhaled, the most pronounced one, SD12, was used to study the inhalation capability. The freeze-dried formulations required an additional crushing step, which was carried out by using manually a mortar and a pestle. Cysteine and mannitol enriched lyophilizates, as well as the coarse pure rutin powder,

were used for this. Additionally, coarse mannitol was added as a filling agent before comminutions. All powders were then filled into capsules. The pulmonary application was simulated by using the Handihaler® inhalation device at the NGI, which characterized the aerodynamic properties of the formulations. The results obtained from the NGI analysis are shown in **Figure 71** and served as the first orientation for subsequent optimization studies.

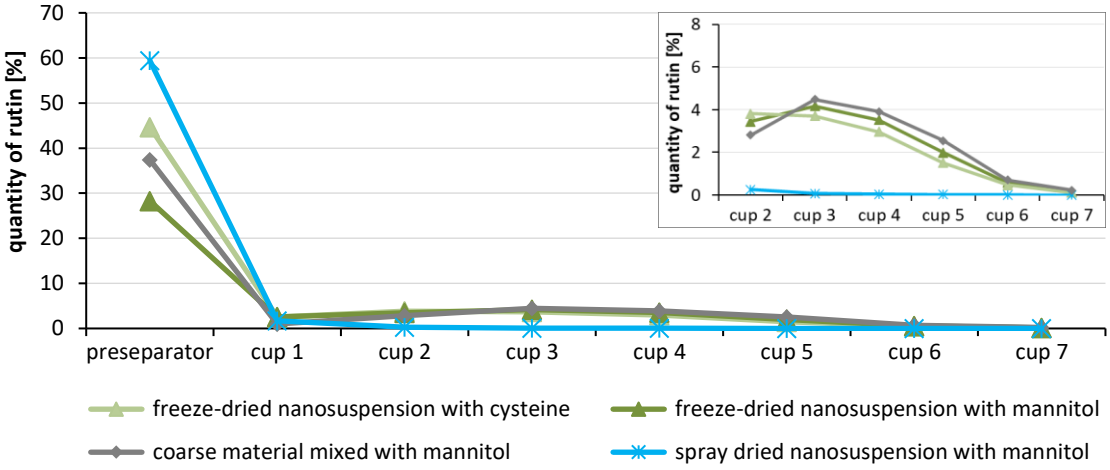

Figure 71: *Comparison of the powder dispersion among different drying methods by an NGI. The deposited amount between cups 2 and 7 is displayed enlarged.*

As expected, the spray-dried particles were mainly deposited in the preseparator and only a very small percentage of the particles reached the cups. The results for the freeze-dried products were significantly better, as about up to 3% of the given dose reached the cups 2 - 5 each. A slight difference can be seen between the formulations dried with mannitol and those dried with cysteine. Interestingly, the coarse material of rutin crushed with mortar and pestle performed similarly and seemed to be slightly better (**Figure 71**). In fact, by calculating from the deposition quantities, the best performance is obtained for the coarse material that possesses an FPF and MMAD of about 12.5% and 2.8 µm, respectively (**Table 16**).

Table 16: *The FPF and MMAD of the differently dried rutin NC formulations, calculated from the quantified amount shown in* ***Figure 71****.*

	FPF [%]	MMAD [µm]
coarse material mixed with mannitol	12.51	2.79
freeze-dried nanosuspension with mannitol	11.11	3.54
freeze-dried nanosuspension with cysteine	9.85	3.76
spray-dried nanosuspension with mannitol	0.19	22.10

The first trial showed that about a tenth to an eighth of a dose would reach the deeper lung expressed as FPF. Concerning the effort like the NC production and further processing, but also low available quantity per application, there is still room for further improvements. The average aerodynamic diameter already fulfilled the desired requirements of being between 1-5 µm. Although it might seem that the coarse material performed better than the lyophilizates, the differences were negligible. Furthermore, NC still possesses the enormous advantage of an increased dissolution rate and bioavailability. Again, in this work, the spray drying process was not successful in converting the nanosuspensions into a flowable powder, as the yield was too small and the resulting microparticles too large. Further optimization would demand additional process steps that would be too costly and time-consuming and not worthwhile. Therefore, freeze-dried formulations were focused on optimizations in the next trials.

Nowadays, many dry powder inhalation products are formulated with micronized API and larger lactose fragments serving as a drug carrier as well as a bulking agent. The feature of adding coarse material allows the small API particles to attach to and be detached from them by the force during aerosolization. The carrier and bulking fragments then reach the throat and finally the GIT whereas and the small API particles are transported with the airflow to the deeper lung. This should enable almost complete separation of the particles from each other without the risk of an irreversible accumulation of microparticles or at least a drastic reduction for the development of heavy agglomeration within the formulation [271].

In this work, this principle was exploited and coarse mannitol and lactose were added. Furthermore, the next trial aimed at applying different crushing methods to improve the MMAD and FPF of the dry powder formulations for inhalation. The focus was on crushing techniques that mainly industrialisable and scalable. Rutin nanosuspensions stabilized with PLX were used and admixed with coarse mannitol and lactose as a carrier and bulking agent. The crushing methods are summarized in **Table 17** and the results obtained by NGI are shown in **Figure 72**.

Table 17: *Alternative crushing methods of the freeze-dried rutin nanosuspensions.*

short name	detailed description
through 250 µm mesh sieved	With mannitol freeze-dried nanosuspension was crushed with a mortar and pestle with addition of coarse mannitol, the mixture was sieved through a 250 µm mesh sieve.
by vortex and beads	With mannitol freeze-dried nanosuspension enriched with lactose was placed in a falcon tube together with 1 mm zirconia beads and vortexed for a few minutes.
by turbula-mixer and beads	With mannitol freeze-dried nanosuspension enriched with lactose was placed in a 5 mL glass vial together with 1 mm zirconia beads, placed in turbula mixer for one hour.
by ultra-turrax, freeze-dried with mannitol	With mannitol freeze-dried nanosuspension enriched with mannitol and lactose crushed by using an ULTRA-TURRAX® disperser tubes (IKA, Germany).
by ultra-turrax, freeze-dried with cysteine	With cysteine freeze-dried nanosuspension enriched with mannitol and lactose crushed by using an ULTRA-TURRAX® disperser tubes (IKA, Germany).
by air jet mill without additional mannitol	After the usual procedure but without any additives, the mixture was milled by using an air jet mill.
coarse material minimized by air jet mill	The non-formulated coarse rutin material was milled by using an air jet mill.

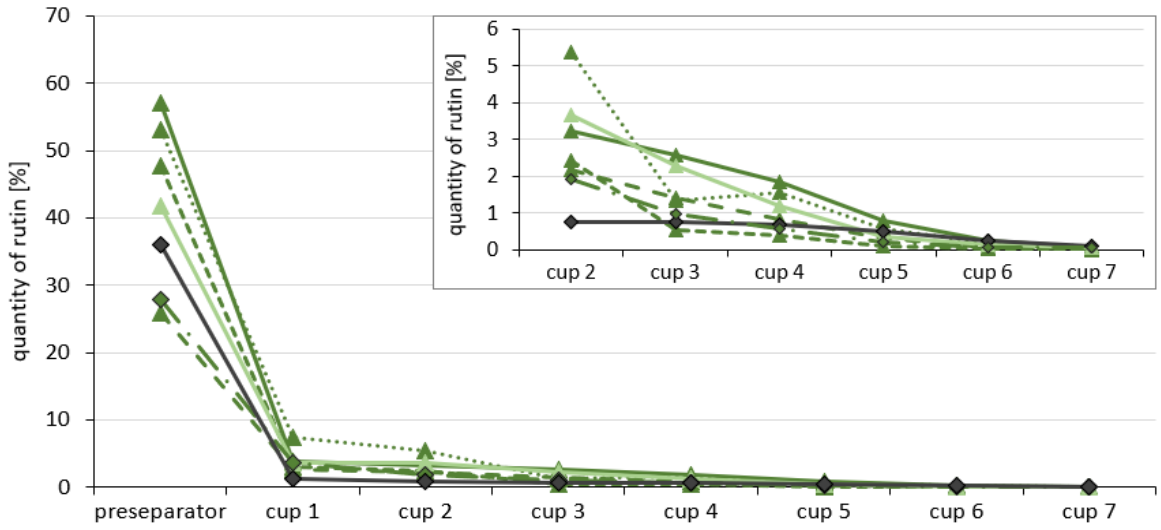

crushing process	FPF [%]	MMAD [µm]
through 250 µm mesh sieved	1.69	8.13
by vortex and beads	7.97	5.33
by turbula-mixer and beads	3.12	5.95
by ultra-turrax, freeze-dried with mannitol	6.18	5.16
by ultra-turrax, freeze-dried with cysteine	4.76	5.88
by air jet mill without additional mannitol	2.21	8.20
coarse material minimized by air jet mill	2.44	4.24

Figure 72: *Comparison of the efficiency of different crushing methods in terms of aerodynamic particle size and distribution. If not mentioned otherwise formulations freeze-dried with mannitol are used.*

As a result, the FPF ranged between about 1.7 and 8.0% with an MMAD of 4.2 – 8.2 µm (**Figure 72**). That means, that for all crushing methods applied in this trial, the inhalation performance of the dry powder has weakened compared to simply using a mortar and a pestle (first trial, **Figure 71**), i.e. the fine particle fraction has been reduced while the aerodynamic diameter was enlarged. Moreover, the type of particle distribution has changed. While in the first trial the classic maximum could be seen at cup 3, this was completely missing in this second trial (**Figure 72**). Instead, the curve flattens exponentially from the pre-separator to the last cup, indicating that the main population had a size > 8 µm when assuming a Gaussian distribution. Thus, the crushing methods were inappropriate.
The comminution processes can be distinguished into three main principles: Comminution due to impact forces by beads, collisions of particles with each other (by air jet mill), and grinding by mortar and pestle. The idea behind the use of grinding beads was that the beads should crush the particles, similar to in the milling process for the NC production (c.f. sections 4.1.2.2 and 4.2.1). In contrast, exactly the opposite seemed to have happened: the beads might compress the fine structures and highly porous lyophilizates back into a dense coarse powder. The resulting coarse structures then caused degraded performance with aerodynamic diameter > 5 µm and an FPF of < 8% (**Figure 72**). Also, the use of an air jet mill was not successful to obtain a powder that could be inhaled. Interestingly, after crushing with mortar and pestle, the percentage of FPF decreases from 11.1% to 1.7% when a sieve is used (**Table 16** vs. **Figure 72**). In summary, up to this point, the best crushing method to obtain a powder for inhalation was the simple use of a mortar and a pestle along with the addition of coarse mannitol. Further improving steps would include optimizing the formulation regarding the type and ratio of different excipients as coarse carrier and bulking agent to the lyophilizates but also during freeze-drying as cryoprotectant.

However, before performing such studies, it should first be determined whether the rather small FPF could result from external influences. One external influence could be moisture diffusing through the capsule shell to the powder. In this process, the hygroscopic microparticles would also gain mass with the water absorption and, at the same time, inter-particle interactions would build up due to water-induced capillary forces. Therefore, the capsule shell used in this work consisted of hydroxypropyl methyl cellulose and is thus designed to prevent the product from external moisture. On the other hand, due to their high hygroscopicity, lyophilizates quickly absorb water from the ambient air, which might occur during the comminution and filling processes. That in turn could increase the capillary force and thus the inter-particle adhesion. Other factors affecting the interaction between the particles within the airflow could be the dispersibility within the capsules and the inhalation device.

The aforementioned studies have been performed using the Handihaler®. It was believed that the Breezhaler® would improve the FPF of the dry powders for inhalation because the capsule rotates within it during the inhalation. Using the Breezhaler®, the microparticles are aspirated from the perforated capsules by the vacuum and centrifugal forces additionally remove the powder from the capsules and disperse it through impaction forces [271]. As result, even at lower airflow, the entire powder is released [272].

Moreover, the degree of filling could play a role in that the separating air stream whirls up the particles already in the capsule and carries them with it. If the filling level is too high, turbulence could not sufficiently occur and consequently, uniform microparticle agglomerations followed the airflow with little separation between the particles. Therefore, in the following trial, the capsule filling level and two different capsule-based powder inhalers were investigated according to the inhalation performance of the dry powder. For this purpose, either one single capsule was filled almost completely up with 60 mg or five capsules were filled with 12 mg powder each and applied one after the other using the HandiHaler® or Breezhaler® and analyzed by NGI.

As a result, neither the filling level nor the replacement by a more beneficial inhaler resulted in a significant increase of FPF or a reduction of MMAD. In this trial, the respirable fraction (FPF) remained at about 12% with an average aerodynamic particle size of less than 5 µm (**Figure 73**). Hence, external influences play a minor role for this powder, and a greater potential is to improve the formulation to reduce inter-particle interactions and facilitate desorption from the carrier.

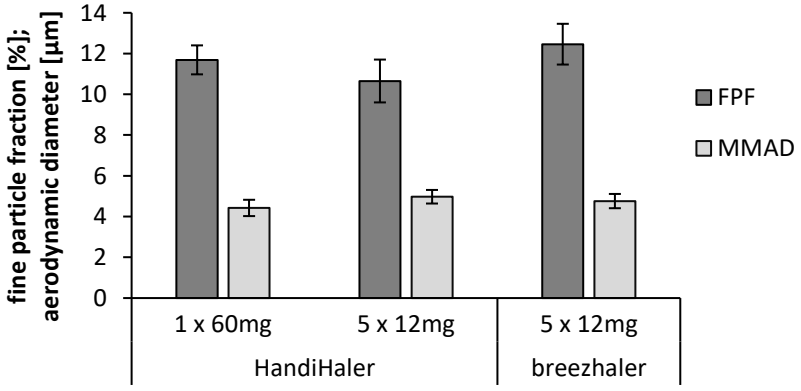

Figure 73: *Fine particle fraction and mass median aerodynamic diameter depending on the device and filling level. Rutin nanosuspension freeze-dried with mannitol and crushed by mortar and pestle was used.*

Thereafter, the next trial aimed at optimizing the formulation of the powder after the drying process. Both, the microparticles were too large and inter-particle forces were still too high. To solve both problems, a finer sieve with a 180 µm mesh was used, and magnesium stearate (Mg-Stearate) as an additional excipient was added. Although sieving is not an official method of comminution, the use of a finer sieve led to better results (**Figure 74**). By doing so, the nanosuspension freeze-dried without a

protectant/ additive, blended with mannitol, and sieved through a 180 µm mesh resulted in an FPF of 16%. Once compacted by a mortar and pestle, the microparticles and coarse mannitol seemed to be loosened by the sieve and a reformation of agglomeration might be thermodynamically guarded by the coarse mannitol. A better effect to reduce the particular interactions was achieved by adding Mg-Stearate to a final concentration of 0.2%, resulting in an FPF of almost 20% (**Figure 74**). In this case, the existing soy saccharide replaced the larger mannitol crystals. A further improvement in the FPF was achieved by the addition of lactose, which is often used commercially [271]. However, the combination of lactose and Mg-Stearate in a soy saccharide freeze-dried formulation led to an FPF of about 22% and an MMAD of 4.2 µm (**Figure 74**). This is a good result and will be discussed after the last optimizations, where these findings were the precursory basis.

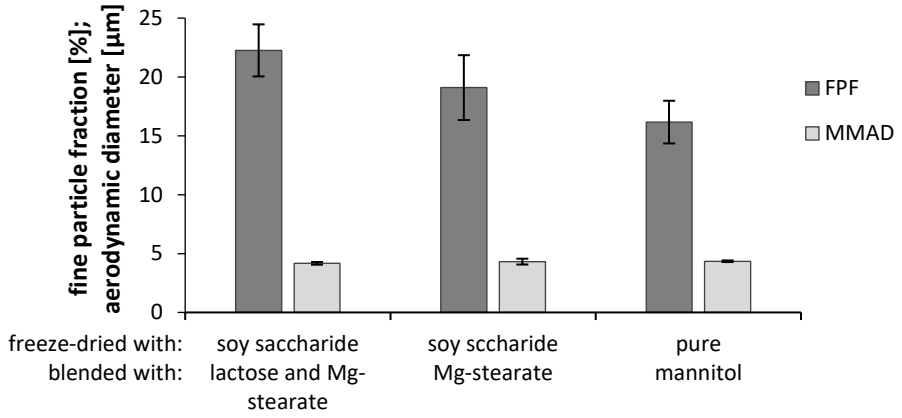

Figure 74: *Inhalation parameters after optimization of the production process by using a 250 µm sieve and adding excipients such as lactose and magnesium stearate.*

It can be concluded that the respirable amount of the dried powder was doubled after optimizing the formulation parameters. Additionally, when using a sieve, it was observed that the lyophilized microparticles were slightly sticky and easily deformed. In order to reduce the plasticity and enable simultaneously even more effective comminution, cryo-milling was performed, which could also be used for industrial demands. Likewise, a process for the industrialisable approach with mortar and pestle was realized with an automatic mortar grinder. The crushing methods and parameters used are summarized in **Table 18**. As demonstrated above, the addition of Mg-Stearate increased the percentage of FPF, and thus it was also admixed in both formulations after the comminution process and compared to the original formulation without Mg-Stearate.

***Table 18**: Improved crushing methods for an industrial approach of the freeze-dried rutin nanosuspensions.*

short name	detailed description
Mortar grinder	Freeze-dried rutin NC without cryo-protectant, crushing with the addition of coarse mannitol using the RM 200 (Retsch) with mortar and pestle made of stainless steel, vertical pressure at level 4 for 20min.
Lactose, CryoMill	Freeze-dried rutin NC with mannitol as cryo-protectant, crushing with the addition of lactose using the CryoMill (Retsch) with a 50ml cup and 14 beads (Ø = 10 mm) of stainless steel, 5 min pre-cooling and 18 x 5 min cycles with 30 s cooling in between.

Both technical methods (**Table 18**) led to an MMAD of about 3.7 µm, whereas the FPF values differed by about five percentage points with the CryoMill being better (13 vs. 18%) (**Figure 75**). Although the MMDA was reduced noticeably, the proportion of inhalable microparticles has increased comparatively slightly. Automated mortar grinding can therefore be regarded as slightly better than the manual method. In contrast, the concept of making the particles more brittle seemed to succeed with cryo-milling. Nevertheless, the formulation itself played an essential role in improving the aerodynamic property of the lyophilizates. By adding Mg-Stearate up to a final concentration of 0.2%, the FPF was increased about two times. Finally, by adjusting the formulation, a powder was developed from which 34% could reach the deeper lung region (**Figure 75**). Due to this modification, the rutin nano-in microparticles could be successfully dispersed loosely, resulting in fewer agglomerates and a fine particle population that was visualized by microscopy (**Figure 76**).

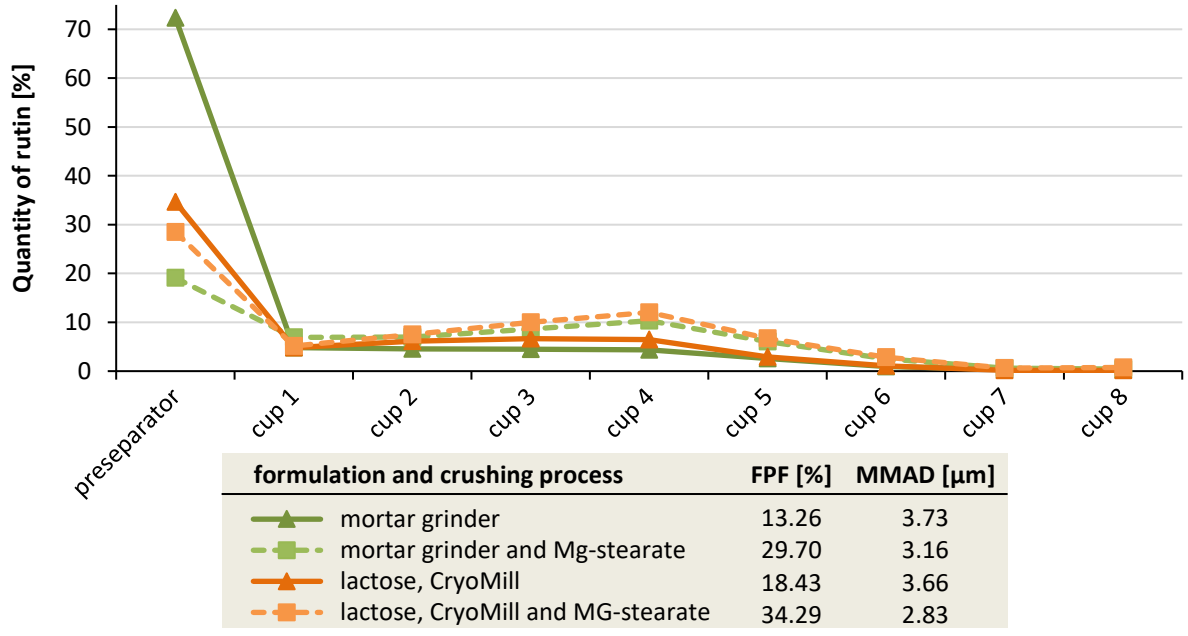

***Figure 75:** Aerodynamic characterization of particles produced by a mortar grinder (green) and a CryoMill (orange). Formulations were afterward enriched with magnesium stearate (dotted line).*

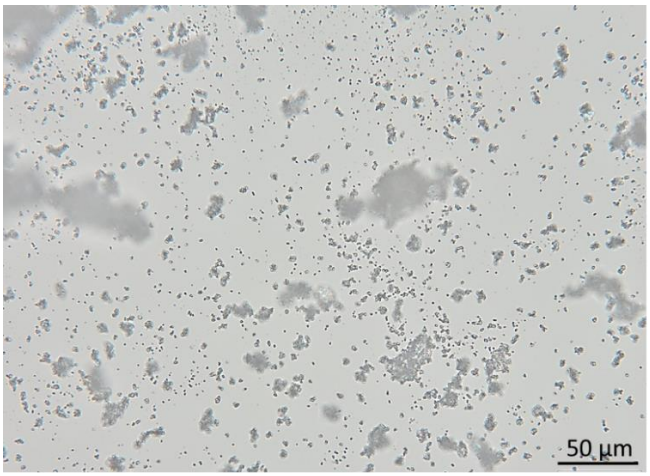

Figure 76: *Microscopic image of the cryo-milled lyophilizate blended with Mg-Stearate, 400-fold.*

Some larger fragments were observed by microscopy (**Figure 76**), which are essential for a good performance of a dry powder for inhalation. This can be explained as follows: Due to their high surface energy, micron-sized particles stick to each other (cohesion) or other surfaces (adhesion). Their adhesive and cohesive nature and the low application quantities hence require an effective formulation to ensure sufficient pulmonary drug delivery. For example, formulations were modified by forcing a controlled adhesion on a carrier, where lactose is mostly used. Such a drug-carrier adhesive force determines the performance dispersion of a dry powder during aerosolization [271]. In general, the adhesion of a microparticle to a solid surface is determined by physical forces. Main forces include especially the Van-der-Waals force as well as the interlocking force, the electrostatic forces and the capillary forces. The interlocking force is involved in case the microparticles fit into cavities upon intimate contact with the carrier while capillary forces gain importance when a liquid bridge between microparticle and carrier has developed. Therefore, the size, shape, and crystallinity of the carrier play a crucial role in how strongly microns will be attached on. However, it could be shown that a drug-carrier ratio of 1:67.5 performs best for successful dispersion during aerosolization, but this ratio impedes the formulation of high drug doses [273,274]. Additionally, for the success of those formulations, two oppositional requirements must be fulfilled. On the one hand, the adhesion between carrier and microparticle must be strong enough to allow handlings such as the filling. On the other hand, adhesion should be weak enough to release the drug during aerosolization. After detachment, the carrier particles remain in the inhaler device or deposit in the oropharynx due to their large size. Serval types of dispersion forces were found including drag and lift forces from the moving air as well as shear and impaction forces generated in the inhaler [275].

In this study, a combination of FlowLac® 100 characterized by larger particles of about 100-200 µm and InhaLac® 500 with smaller particles of about 5-10 µm were used and revealed the best result with an FPF of 18.4% and an MMAD of 3.7 µm (**Figure 75**). To improve the flowability and dispersibility of the

powder, a common approach is blending it with large lactose carrier particles, which usually have a size of about 30-90 µm. It was also demonstrated that an additional amount of fine lactose carrier particles (fines) improves the performance of a powder for inhalation purposes [276]. This can be explained by two circumstances. First, the fines could bind on the strongest site of the carrier preventing the drug microparticles from. Second, they are able to build agglomerates with drug particles that are more easily dispersed and de-agglomerated during aerosolization [276,277]. Therefore, fines with similar geometric sizes compared to the drug microparticles should be used [278]. This is also in good agreement with the results in this study where after the cryo-milling the drug particles and lactose carriers showed similar size and shape (**Figure 76**).

Even though lactose is widely used today, its disadvantage as reducing sugar and the patient's intolerance possibility remains. In contrast, mannitol is also widely used in pharmaceutical production, possesses a well-investigated toxicity profile, and does not possesses such drawbacks. In contrast, a high dose of mannitol was found to increase mucus secretion and mucociliary clearance [279]. Due to this feature, there are two mannitol products on the market: Aridol® for pulmonary diagnostic and Bronchitol® for the treatment of cystic fibrosis and chronic bronchitis.
For these reasons, the addition of mannitol as an alternative bulking carrier was investigated in this study. However, the addition of coarse mannitol led to FPF of the dry rutin NC of about 12.5% (**Table 16**), 13.3% (**Figure 75**) and 16.2% (**Figure 74**) which is in good agreement with a similar study by S.K. Tee and co-workers [280]. Hence, the use of coarse mannitol seemed less suitable for the formulation of a dry powder for inhalation with high FPF. Also, a recent study demonstrated that a binary mixture of coarse mannitol and drug particles had twice as high FPF compared to coarse lactose [280]. The low FPF can be improved tremendously as known for lactose formulation by modifying the mannitol powder and adding fines [281]. It was expected that the crushing methods would also affect the size and shape of the coarse mannitol which in turn would change the dispersibility and thus the FPF. Whatever adjustments are carried out on the mannitol particles, the performance of the powder is unaffected by the size of the carrier particles when applying the Handihaler® [282]. This explains why different crushing methods led to similar results, considering that this work was also carried out with the Handihaler® (**Table 16**, **Figure 74** and **75**).

Other approaches to weaken the adhesion include smoothing the carrier surface by using ternary mixtures with hydrophobic components, e.g. Mg-stearate and amino acids. Those are also defined as force control agents as they enable a reduction of the inter-particle bonds between drug microparticle and carrier [283,284]. The reduction can be explained by the following mechanism: Mg-Stearate covered the carrier completely and unevenly, i.e. flaws and irregularities are filled leading to a relative smoothing of the particle surface and a surface polishing effect. Recent studies demonstrated the

reduction in surface area and roughness by using atomic force microscopy [285]. Consequently, reduced surface energy behavior as well as less interlocking force altered the electrostatic force and reduced the resulting capillary forces. It must be considered that the optimal amount of Mg-Stearate depends strongly on the adhesiveness of the drug themselves to the carrier and Mg-Stearate. Additionally, the mixing process influences greatly the optimal amount of Mg-Stearate required [286]. In this work, Mg-Stearate was added after the crushing processes and admixed gently by hand to allow Mg-Stearate to interact with and properly cover all the microparticles. This was indirectly shown by microscopy as the developed dry powder was fine and well dispersed, no aggregate formation occurred and rounder particles were observed (**Figure 76**).

The more pronounced result was that about one third of the powder would reach the deeper lung area. Further small optimizations could be achieved by strengthening the mixing process or by finding the most suitable Mg-Stearate concentration for the lyophilized rutin NC. Again, the addition of Mg-Stearate increased the FPF by 224 and 186%, respectively (**Figure 75**). The same improvement was found in the study of P. Begat and co-workers, where the addition of Mg-Stearate improved the FPF by up to 272% [287]. They also showed that this approach can significantly reduce the retention of drug particles in the device.

With an inhalable proportion of about 34%, the result is in good agreement with the existing powder inhalers on the market, whose FPF varies between 15 and 50% [187,269]. There are different inhalers, test parameters (airflow, time) and test devices such as the NGI or the Anderson cascade impactor which impedes comparability of commercial or newly developed powders for inhalation. Therefore, the same test conditions should be adopted to evaluate the powder developed in this work. By using the NGI under the same conditions M. Mohan et al. demonstrated an FPF of 33 and 29% for the Spiriva Handihaler® and Foradil Aerolizer®, respectively [187]. The Foradil Aerolizer® corresponds to the Breezhaler® in structure and function, and thus both are comparable. Although the centrifugal force generated by the spinning capsule will facilitating the powder ejection through the capsule holes, no further benefit was recognized regarding the FPF. Furthermore, a higher FPF was found by Relenza Diskhaler® at much lower humidity (48 vs. 31% at a humidity of 18 and 57%). Therefore, this work successfully developed a dry powder for a capsule-based inhaler with an inhalable fraction comparable to inhalers on the market. Nowadays, single-unit and multiple-unit dose inhalers are investigated which omit the capsules and thus the disadvantageous preceding release through their perforation. Since there were no issues with retention of the powder in this study, it could be assumed that the developed and optimized powder would also be suitable for those kinds of inhalers. Further studies in the future would be necessary to confirm this.

4.3.2.4 Hollow particles by spray-freeze-drying

As mentioned before, the aerodynamic diameter (d_{aero}) of particles in an airflow depends on their size, shape and density and can therefore be approximately calculated as follows:

$$d_{aero} = d_{geo} \cdot \sqrt{\frac{\rho}{\chi \cdot \rho_0}}$$

where d_{geo} is the geometric diameter, ρ_0 is the unit density (1 mg/mL) and ρ is the density of the particle investigated. The dynamic shape factor χ is defined as the ratio of the drag force on a particle to the drag force on the equivalent sphere at the same velocity, i.e. 1.0 for perfect spheres and > 1 for shaped particles [186]. Theoretically, a smaller d_{aero} can also be achieved with non-spherical particles like rods, fibers or platelets, which was the predominant shape in the previously discussed chapter.

Based on the equation, the aerodynamic particle size can also be reduced by a low density. For this purpose, a novel technique, the so-called spray-freeze-drying was performed. By doing so, the atomized liquid drops caused by the spraying step were frozen instantly and then dried under the triple point of water through sublimation [288]. As a result, the drops retain their shape and size and then become porous and consequently acquire a low density. The porous structure obtained in turn promotes its dissolution and thus increases the release of the embedded NC. Another advantage of spray-freeze-drying to spray-drying is the ability to use heat-sensitive API and excipients like biologicals and polymer or lipid nanoparticles with a low glass transmission temperature [289]. Similar to freeze-drying the presence of adjuvants might be required to act as a lyo- and cryoprotectant for preventing inter-nanoparticle contacts upon freezing and to form carrier bridges that facilitate stability of the resulting particles.

The first investigation in this field was carried out with mannitol and PVA in different concentrations without the addition of rutin NC to get the first insight into the size and inhalation performance. Likewise, methylene blue was dissolved in the solution prior to the spray-freeze-drying procedure. In this way, visualization by microscopy was facilitated, and additionally, a chromophore was included that allowed to calculate the content precisely by UV-Vis spectroscopy.

In this thesis, perfectly spherical particles having a geometric size of around 50 µm were obtained (**Figure 77**). Presuming that the shape remains stable during atomization, the form factor is about 1. Thus, a particle density of ≤ 0.01 mg/mL would be necessary to reach the deeper lung, i.e. to have an aerodynamic size ≤ 5 µm. Using mannitol as a carrier led to more porous particles visualized by light microscopy due to irregular staining. Furthermore, a few particles showed partially fractured as a result of their fragility caused by their high porosity. In contrast, using PVA as carrier generated spherical particles that appeared neither porous nor fragile in their structure. It has been observed that PVA accumulates at interfaces and in this way a thin film is generated in form of the droplets produced [290]. Additionally, PVA solutions form a glassy state during freezing at which the nucleation of larger

and heterogenous ice crystals is inhibited [291]. Thereafter, cavities and pores such as those in mannitol, that are caused by the removal of ice crystals during drying, could not be observed microscopically for PVA (**Figure 77**).

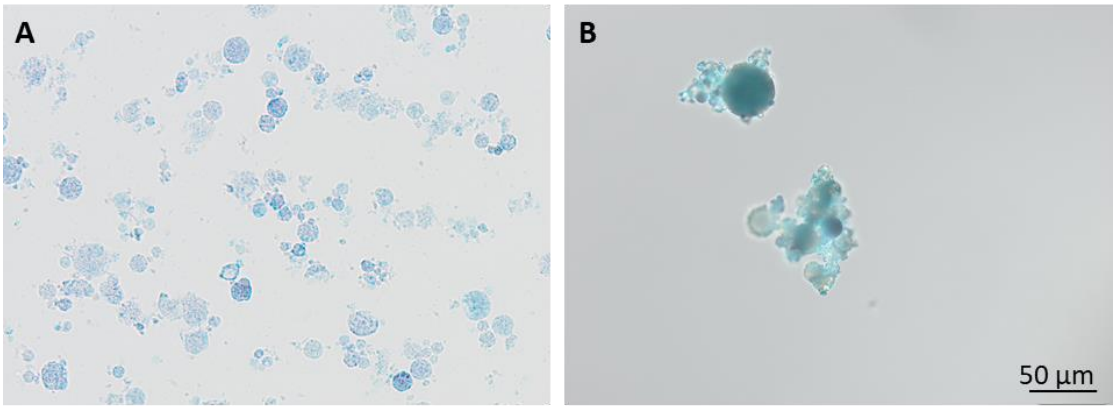

Figure 77: *Microscopy images of the spray-freeze-dried particles, using a 200- fold magnification (A) and 400-fold magnification (B).*

All spherical microparticles obtained by the spray freeze-drying were characterized by NGI. Results revealed poor inhalability performance as only an FPF of about 1% was determined. The small amount could only be increased by reducing the geometric particle size. However, this approach was not applicable due to technical conditions such as the airstream in the drying chamber. In contrast, the study from W.S. Cheow et al. produced smaller mannitol and PVA nano-in-microparticles using spray-freeze-drying [139]. Likewise, despite their calculated aerodynamic diameter of about 3-5 µm (by density and geometric diameter), their performances regarding FPF only reached 10-14% [289]. Therefore, the production of hollow particles is theoretically more promising but might need some improvements to develop an industrially manufacturable and ready-to-market product. In contrast, the study of M. Ehab Ali and A. Lamprecht succeed in developing inhalable dry powder by spray-freeze-drying with different kinds of nanoparticles by reaching an FPF of 46% with the Handihaler® [288]. They were also able to reveal the advantage over classical spray-drying when formulating heat-sensitive lipid nanoparticles. Hence, the issues of spray-drying related to the NC formulation, e.g. with Tween 80 as a stabilizer (c.f. section 4.3.2.1), could thus be overcome.

4.3.3 *In-vitro* investigations

Up to this point of the study, stable tailor-made rutin NC formulatons were produced to treat COPD and asthma. It was demonstrated that the stability of the nanosuspension was extended when stored in a frozen state. Sublimation of the water, i.e. freeze-drying, was another approach to transform the NC into a transportable, long-term stable and dry form. In the final step, this lyophilizate was successfully converted into a powder for inhalation, which could now be applied pulmonary for the treatment of oxidative stress-induced lung diseases. The poorly water-soluble rutin acts as an antioxidant. Hence, the first and the second sub-aim of this section were achieved and a powder for inhalation was developed.

Thus, after all the process steps, the final sub-goal was to investigate whether the formulation and pre-formulation steps fulfilled their main property of increasing the antioxidant activity of rutin. To assess this, the kinetic solubility, release and dissolution velocity was investigated in dissolution studies, the antioxidant capacity was determined in a radical scavenging in-vitro assay, and finally, the antioxidant effect was studied in the complex environment of a cell culture model.

4.3.3.1 Dissolution studies

The dissolution is one of the crucial prerequisites for the effective absorption of an API into the body and plays thus a key role in the treatment and therapy. A size-depending increase in the solubility and dissolution rate of hesperetin nanosuspensions in a saturated test medium was demonstrated in section 4.2.2.2. In this section now, dissolution studies were performed to investigate the dissolution rate of the differently dried rutin NC formulations. The idea behind this was that different carriers/ cryoprotectants, in which the NC were embedded, could delay the release of the NC and thus slow down the dissolution rate. At first, to ensure that the sink condition will have been respected during the dissolution studies, a saturation solubility of rutin was determined in water and phosphate buffer. As a result, a solubility of 0.2 mg/mL was determined in both dissolution media. On this basis, the amount of formulations required was calculated as not exceeding 10% of the solubility of rutin, i.e. the formulations were added to the dissolution media to a final concentration of 0.02 mg/mL rutin.

At first, the dissolution profiles of the spray-dried NC were investigating and compared to the bulk material and the nanosuspension. The nano-formulations, including the suspension as well as the spray-dried powder, exhibited an excellent dissolution behavior with a fast dissolution velocity (**Figure 78**). After addition in water, the nanosuspension dissolved within 10 min and the spray-dried formulations within 15min. For comparison, after dissolution times of 15 min and 120 min, the bulk material was dissolved to only 55% and 62%, respectively.

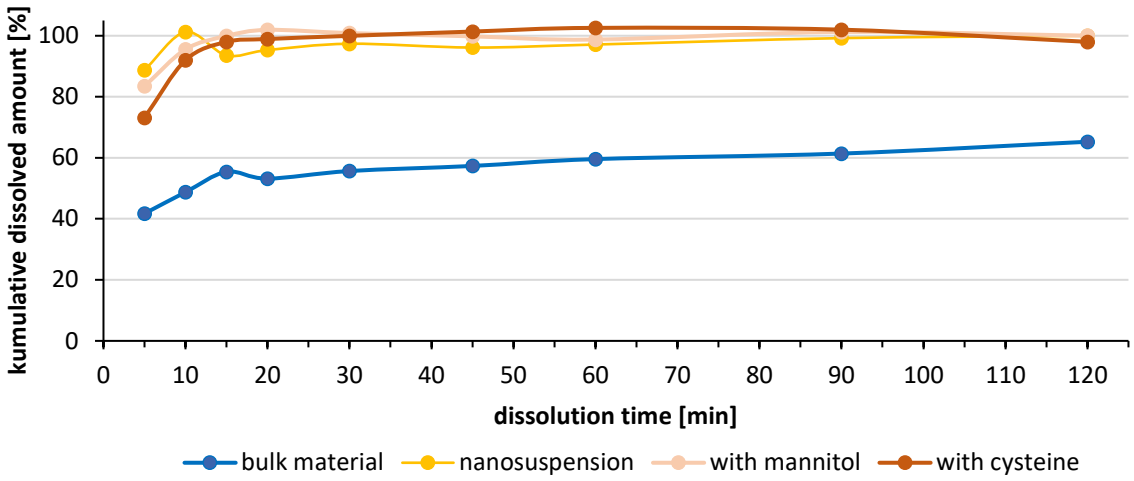

Figure 78: *Dissolution profile of rutin bulk material, nanosuspension and its dried forms from spray-drying with mannitol or cysteine, over 2 h of dissolution time in water.*

However, the nanosuspension showed only a slight recrystallization effect after 15 min of dissolution time, similar to that of the Hesperetin NC observed and discussed in section 4.2.2.2. on the other hand, the decrease in concentration after 15 min dissolution time could also be due to a measurement or dilution error because re-crystallization effects would not be expected under sink conditions. The same could be used to explain the concentration peak of the bulk release curve after 15 minutes.

Compared to the nanosuspension, the spray-dried rutin NC dissolved fast but slightly slower, whereas the formulation with mannitol was faster than that with cysteine (**Figure 78**). In general, the NC are embedded in the matrix of mannitol and cysteine, from which they need to be released before dissolving. In consequence, complete dissolution occurs more slowly than as suspension, where the NC were immediately in contact with the dissolution medium when added to it. As previously described (c.f. section 4.3.2.2), cysteine is characterized by a substantially slower dissolution rate that explains its delay in releasing the NC compared to mannitol. Furthermore, it has been recently observed that mannitol acted as a dissolution enhancer and thus increased the dissolution rate in the spray-dried nano-formulation [188]. Hence, this is another reason why the formulation spray-dried with mannitol dissolved faster than the one with cysteine. However, the superiority of the NC over bulk in terms of dissolution velocity was impressively demonstrated.

The coarse bulk material did not dissolve completely, but only 62% within 2 hours (**Figure 78**). Its dissolution rate seemed to be linear from the 20th minute (t_{20}), when considering the drug release kinetics in a mathematic model. With a regression of R^2=0.9732 (t_{20} to t_{120}), it can be attributed to a high linearity which in turn corresponds to a zero-order kinetic release model. In other words, the same amount of rutin dissolves constantly per unit time and independent of concentration. In general, suspensions with poorly aqueous soluble and large API crystals can act as galenic retard release as the preceding diffusion diminishes the dissolution of the solid active ingredient. This can be also explained

by Fick's first law at which the mass diffusion depends on the concentration gradient and the individual diffusion coefficient which remains constant if the number of particles and their radius are stagnant. By applying the kinetic release model according to Higuchi's square root law, a diffusion-controlled drug release can be described. In this model, the square root of the dissolution time is plotted against the cumulative released drug amount and the linearity is determined. Applying this model to the bulk material dissolution profile yielded a regression of R^2=0.9856, indicating high linearity (**Figure 79**).

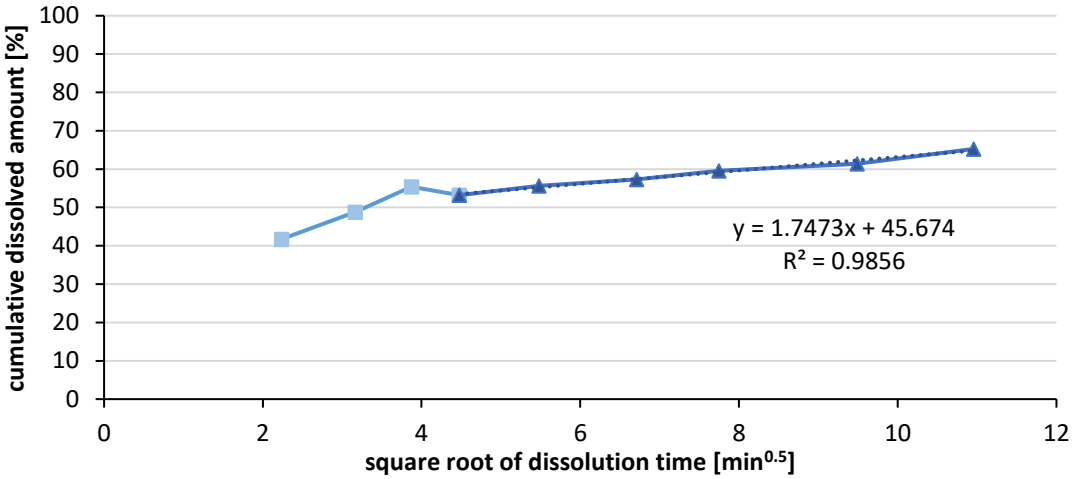

Figure 79: *Dissolution profile of the rutin bulk material after Higuchi's square root law. Only the darker highlighted part between 20 and 120 min of dissolution time was used to evaluate a linear relationship.*

In the following, the freeze-dried rutin NC formulations were investigated regarding dissolution velocity in phosphate buffer (pH 6.8). Similar to the spray-dried formulation, the lyophilizates of the NC dissolved differently fast depending on the carrier in with the NC are embedded (**Figure 80**). As expected, the nanosuspension was the fastest with a dissolution time of 5min. The lyophilizate with mannitol as carrier approximated the release curve of the suspension most closely. Based on the percentage of the API dissolved after two minutes of dissolution time, the matrix carrier used can be ranked in a decreasing order as follows: mannitol > lactose > isomaltose > cysteine > soy saccharide > without additional adjuvants (pure). A statistical evaluation of the dissolution curves over the entire period and among each other is discussed afterward.

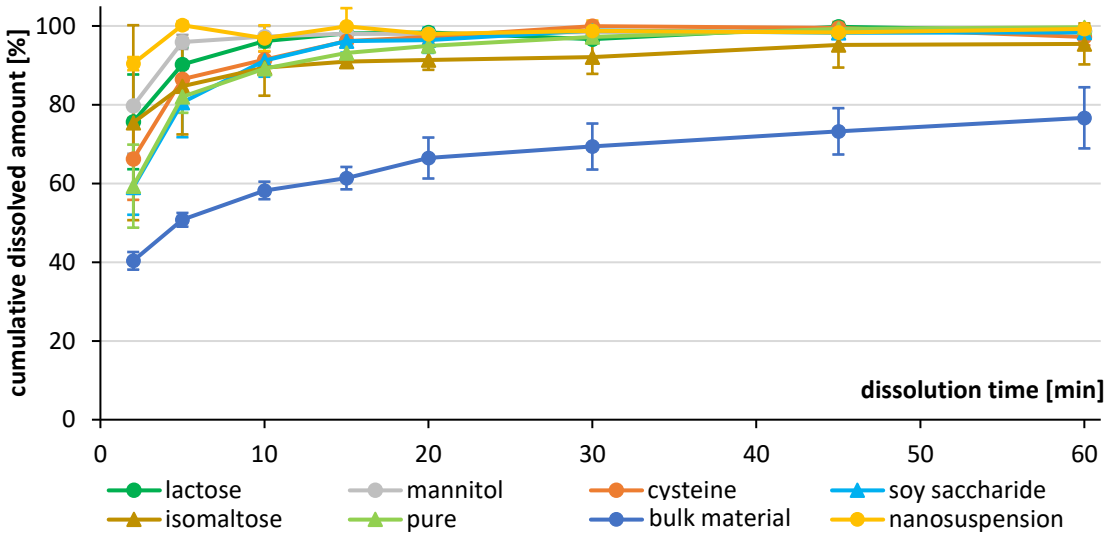

Figure 80: *Dissolution profile of the rutin nanosuspension freeze-dried with lactose, mannitol, cysteine, soy saccharide, isomaltose or without additives (pure), compared to the liquid nanosuspension and solid bulk material.*

Interestingly, dried nanosuspensions without a real matrix former, meaning pure and soy saccharide, initially showed the lowest solubility and their dissolution profiles were approximately identical (**Figure 80**). It was expected that these lyophilizates would dissolve the fastest because: On the one hand, by replacing the cavities (formed during the freeze-drying process) with water, the native nanosuspension should be immediately recovered and on the other hand, there was no matrix from which the NC would need to be released first. However, the results could be explained as follows: After initial ice formation and the subsequent concentrating matrix carrier solution, the viscosity of this residual solution continues to increase until a viscoelastic "rubber" was formed. On further cooling, this "rubber-elastic" system solidifies as solid, amorphous glass at a point being known as the glass transition temperature (Tg'). The formation of those amorphous glasses provides benefits, as proteins and nanoparticles can be stabilized in such solidified liquids [290,292,293]. In a comparative freeze-drying study of resveratrol and quercetin NC, the better stability efficacy of mannitol compared to sucrose and lactose as cryoprotectants was already demonstrated, which was also reflected in an improved release [294]. Finally, the NC embedded in an amorphous liquid-like matrix could enhance the release as well as the dissolution velocity. In contrast, the pure, as well as soy saccharide-stabilized formulation did not form such an amorphous matrix, because the formulations did not contain any substances that could create such a rubber matrix. Instead, loose aggregates could have formed in both formulations which needed to be re-dispersed. Consequently, as larger units – even if only through loose cohesions – are associated with a slower dissolution velocity, those of both formulations were also slower compared to the other NC formulations (**Figure 80**). Additionally, hydrophilic compounds, which are absent in pure or soya saccharide containing lyophilizates, can serve as

dissolution enhancers, which has been shown for mannitol where the solubility and dissolution rate are increased with higher concentrations [188]. Moreover, trehalose succeeded such as mannitol and it is widely known to cryo-protect excellently and universally due to its high Tg'. Indeed, in this study, mannitol dissolved fastest when compared to all freeze-dried formulations (**Figure 80**).

The dissolution curves of the bulk material in water and that in phosphate buffer seemed to differ (**Figure 78** and **80**). Mathematical models for kinetic release were applied to describe the dissolution profiles of the bulk material by an empirical equation. The most common models include zero order, first order Hixon-Crowell and Higuchi among others. As a result, the dissolution profile of the rutin bulk material can be described best with the square root model according to Higuchi and an exponential function according to Ritger, Korsmeyer and Peppas, where the correlation R^2 is 0.9260 and 0.9838, respectively (**Table 19**). Although the latter kinetic release model seemed to be the best, it must not be used in this case for two reasons: This model was designed to estimate the Fickian diffusion of drug particles from a (non-)swelling matrix system [295,296]. The exponent of the resulting exponential function is then used for estimation, which ranges between 0.43 and 1.00 depending on selling degree, matrix form and way of transportation, e.g. diffusion. In this study, the exponent factor is 0.185 and thus too low to characterize what type of diffusion and transport of molecules is involved (**Table 19**). However, this low value and the fact that the best kinetic model was thus the Higuchi equation, might suggest diffusion-controlled drug release, where the solubility is limited due to higher drug concentrations surrounding.

Interestingly, the zero order release kinetic model seemed to suit the least when rutin bulk material was dissolved in phosphate buffer. Again, the zero order kinetic model suited the best when applied in water as dissolution medium. The reasons for this cannot be explained at this point, but seem to be related to pH and phosphate ions, respectively.

Table 19: *Kinetic models to characterize the dissolution profile of the coarse rutin material. A modification of the values for the x- and y-axis (time and concentration) should aim to linearize the curve. The model is most accurate when the correlation coefficient reaches the value of 1.000.* C_0 *is the cumulative drug concentration,* C_{NR} *is the drug concentration that is non-released, and* C_i *is the total initial drug amount.*

Drug release model	x-axis	y-axis	resulting function, $C_{t\%}$ =	R^2
Zero order kinetics	time	C_0	$0.53 \cdot t + 49.68$	0.7946
First order kinetics	time	$\ln(C_{NR})$	$100 - e^{-0.0145 \cdot t + 3.93}$	0.8944
Higuchi model	$\sqrt{\mathrm{time}}$	C_0	$5.36 \cdot \sqrt{t} + 38.57$	0.9260
Hixson-Crowell model	time	$\sqrt[3]{C_i} - \sqrt[3]{C_{NR}}$	$100 - (-0.016 \cdot t + 3.7)^3$	0.8638
Ritger– and Korsmeyer–Peppas model	$\log(\mathrm{time})$	$\log(C_0)$	$36.7 \cdot t^{0.1847}$	0.9838

In contrast, applying those kinetic release models on the nano-formulations would not be meaningful because the maximum release was reached after 15 minutes of dissolution time. Hence, too few data points are available to create an appropriate correlation. Also, it should be evaluated which formulations do not differ statistically in the dissolution profile from the nanosuspension and can therefore be considered equivalent. For this reason, a statistical non-model test was chosen to compare the difference between the percentage of drug dissolved per unit time.

When comparing full dissolution profiles, the multivariate analysis of the difference factor f_1 and the similarity factor f_2 were applied to prove the closeness of the dried NC to the nanosuspension [297]. Both factors were calculated as follows:

$$f_1 = \left(\frac{\sum_{t=1}^{n} |R_t - T_t|}{\sum_{t=1}^{n} R_t} \right) \cdot 100$$

$$f_2 = 50 \cdot log\left(\left[1 + \frac{1}{n} \sum_{t=1}^{n} (R_t - T_t)^2 \right]^{-0.5} \cdot 100 \right)$$

where n is the number of dissolution number samplings, R_t and T_t are the dissolved amount (%) of the reference and the test dissolution at each time point t. Those model-independent approaches can be used to compare a pair of drug dissolution profiles over a defined time interval [297].

If the difference between the two profiles to be examined is very small, the difference also approaches a very small value or even zero if they are identical, which means that f_1 also becomes zero. The reciprocal relationship in equation f_2 in turn, results in a maximum value of 100 if both dissolution profiles were identical. Therefore, to fulfill the requirements of this test the values must be between 0-15 and 100-50, respectively.

When plotting the dried NC formulations against the nanosuspension it is apparent that the dissolution profiles of pure and soya saccharide formulated dry powders not only had the highest values, but they also did not fulfill the requirements of the difference factor within the first 15 min of dissolution time f_1(15 min), (**Table 20**). That means both formulations differ statistically in the dissolution profile to suspension in the first 15 min. However, after a dissolution time of 30 min or longer, their profiles became no longer different from the nanosuspension, i.e. the f_1-values were < 15. The tendency that the values approached zero as the test time increased, was noted in all samples. This is logical since all samples are completely dissolved and thus fewer differences are included in the calculation. Mannitol and lactose were found to be the best matrix carriers in terms of a fast release. By applying the analysis of the similarity factor f_2, only mannitol and lactose were able to satisfy the requirements (> 50) and could be thus considered as similar to the nanosuspension in terms of dissolution rate within 15 min

or longer (**Table 20**). The other freeze-dried formulations proved to be statistically not similar to the nanosuspension except for isomaltose after 1 h of dissolution time.

Table 20: *The difference factor (f_1) and the similarity factor (f_2) at different time points of the dissolution study of the freeze-dried rutin NC in relation to the nanosuspension.*

Last point for dissolution [min]	f_1- values related to the matrix carrier					
	lactose	mannitol	cysteine	isomaltose	soy saccharide	pure
15	7.0	4.5	12.2	12.1	15.6	16.5
20	5.7	3.6	9.8	11.0	12.8	13.8
30	5.1	3.0	8.4	10.3	10.6	11.7
45	4.6	2.6	7.3	9.3	9.1	10.2
60	4.1	2.4	6.7	8.6	8.1	8.9

Last point for dissolution [min]	f_2- values related to the matrix carrier					
	lactose	mannitol	cysteine	isomaltose	soy saccharide	pure
15	52.24	61.34	42.19	45.48	36.19	36.33
20	54.62	63.69	44.59	47.14	38.59	38.67
30	56.42	65.58	46.54	48.40	40.56	40.62
45	57.99	67.16	48.19	49.90	42.23	42.28
60	59.40	68.53	49.57	51.12	43.66	43.72

4.3.3.2 Determination of antioxidante capacity

By solidifying the nanosuspension, it was aimed to avoid physical and chemical instabilities. While the one-year physical stability has been confirmed in section 4.3.2.2, this section focused on the chemical stability by determining the AOC. If chemical alterations such as oxidation or hydrolysis have occurred during the whole process from nanosizing to crushing of the lyophilizates, the AOC of coarse rutin would decline.

Furthermore, the reaction kinetics were investigated, i.e. after which time unit and at which concentration the maximal AOC is reached. It was recently demonstrated that hesperetin possessed a time-depending reaction kinetic (c.f. section 4.2.3.1). Thus, the question arose if the same would apply to rutin and whether the reaction rate could be influenced by additional excipients. Formulations freeze-dried with mannitol and cysteine were used for this study, because mannitol showed the best dissolution performance and cysteine may have additional antioxidant effects, respectively. The AOCs were compared to the formulation without any carrier (the pure formulation), rutin bulk material, and ascorbic acid (vitamin C) as the strongest water-soluble antioxidant.

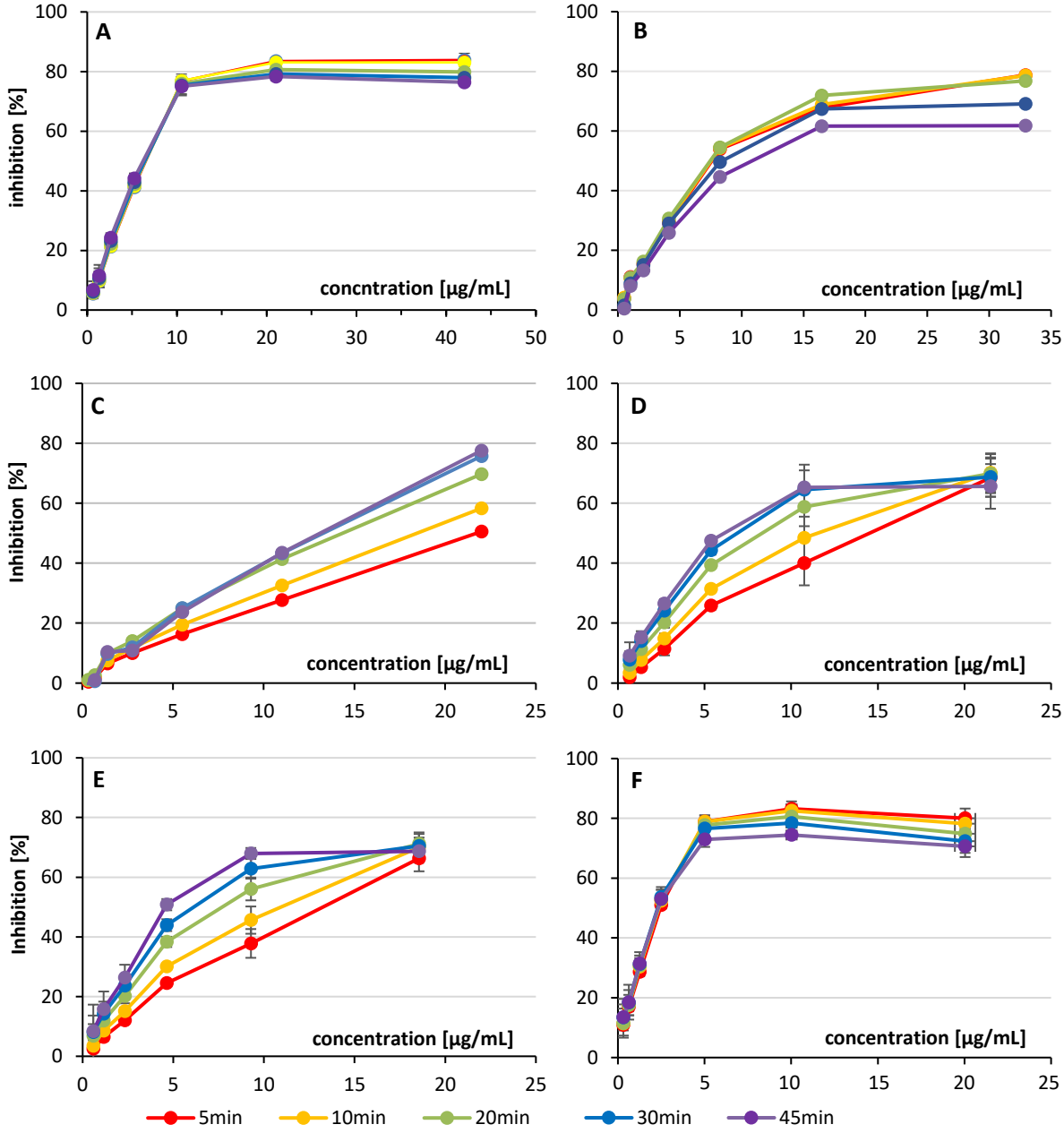

Figure 81: *AOC of different compounds and formulations expressed as depletion (inhibition) of the DPPH radical in relation to the initial amount over the concentration and various incubation times, where A is ascorbic acid, B cysteine only, C coarse rutin, D the rutin nanosuspension freeze-dried without additive (pure), E freeze-dried with mannitol, and F is the freeze-dried with cysteine.*

Results showed pronounced differences between the different formulations (**Figure 81**). Ascorbic acid reacted very immediately (**Figure 81 A**) and pure cysteine reacted almost instantly (**Figure 81 B**), while the rutin formulations revealed pronounced delayed reaction kinetics (**Figure 81 C-E**), with exception of the cysteine-stabilized rutin formulation that showed a fast reaction kinetic (**Figure 81 F**). Also, the antioxidant activity (inhibition [%]) decreased when using ascorbic acid and cysteine at higher concentrations and longer reaction times, which could be a hint of pro-oxidative effects. Likewise, the rutin nano-formulations possessed a higher antioxidant potential as its bulk material at the same concentrations (**Figure 81 D**, **E** vs. **C**). Interestingly, the curve of the concentration-dependent

antioxidant activity of the bulk material followed a straight line (linear function like) (**Figure 81 C**) while the nano-formulations approached a limited growth function (**Figure 81 D-F**). Finally, the combination of cysteine and rutin resulted in a synergistic effect, i.e. concentration needed to scavenge the radicals was reduced compared to the compounds alone, the reaction velocity (kinetic profile) was increased and the effectiveness was decreased at higher concentrations and incubation times as observed for cysteine alone (**Figure 81 F**).

From the AOC curves, the IC_{50} values were determined according to the standard protocol after an incubation time of 30 min and at 50% inhibition, obtaining a mass concentration (mg/L). However, for comparing the different antioxidants used, this mass concentration was converted to the molar concentration (µmol/L) (**Table 21**). The IC_{50} values obtained from the combined formulations, rutin with mannitol or cysteine, were calculated only to the content of rutin in the formulations, i.e. the carriers were omitted from the calculation. Due to the proven additional antioxidant effects of cysteine (**Figure 81 B**), an adjusted calculation was performed for the rutin-cysteine formulation which included the mass and molarity of rutin and cysteine combined (**Table 21**).

Table 21: *The IC_{50} values of all formulations determined from the DPPH assay with an incubation time of 30 min. Combined formulations were calculated by the amount of rutin alone [a)] or on all antioxidants in this formulation [b)].*

formulation	[µg/mL]	[µM]
ascorbic acid	6.67	37.9
pure cysteine	10.71	88.4
rutin bulk material	13.20	21.6
NC freeze-dried without carrier	7.57	12.4
NC freeze-dried with mannitol	6.70 [a)]	11.0 [a)]
NC freeze-dried with cysteine	2.78 [a)] 7.23 [b)]	4.6 [a)] 41.3 [b)]

Based on the mass concentration, ascorbic acid was most effective, because only 6.67 µg/mL had to be used to scavenge 50% of the free radical DPPH, whereas 10.71 and 13.80 µg/mL were required for cysteine and rutin, respectively. This result was completely reversed when considering the number of molecules required for the effect, where rutin was revealed to be the most potent antioxidant. Thus, the molar IC_{50} value for coarse rutin was 21.6 µM and, however, for ascorbic acid 37.9 µM (**Table 21**). As already mentioned, the AOC can be increased by a nano-formulation due to the increased dissolution velocity and saturation solubility. In this study, the AOC of rutin bulk material was almost doubled through the production of NC. After including cysteine of the combined formulation in the

calculation of the IC_{50} values, it is apparent that the antioxidant effect is not purely additive but represents a mean of both compounds.

Interestingly, although mannitol showed no effect in the DPPH assay, its formulations nevertheless seemed to have a slight advantage compared to the formulation without any other excipients (**Table 21**). This phenomenon is analogous to the behavior already observed in the dissolution studies (c.f. section 4.3.3.1). Therefore, the increased dissolution velocity and solubility of the mannitol-stabilized formulation might enhance the AOC which corresponds to a lower IC_{50}. However, the DPPH assay was performed in methanol and thus the results obtained by the dissolution studies cannot simply be extrapolated because the solubility and dissolution rate in methanol is considerably faster. Furthermore, all active ingredients were already completely dissolved by previous dilution steps before the DPPH has been added to the solution. For this reason, the explanation of dissolution enhancing properties cannot be applied in this case and thus further chemical in-depth investigations would be necessary to explain the beneficial effect of mannitol. Again, mannitol itself possessed no antioxidant effects when applied to the DPPH assay (results not shown). Likewise, the delayed antioxidant effect of rutin cannot be explained by the slow dissolution rate either.

The obtained data can also be expressed differently by plotting all IC_{50} values of a specific incubation time as a function of time. This plot clearly displays the reversal course of cysteine, i.e. the longer the incubation time, the higher the IC_{50} and hence negatively directed the AOC (**Figure 82**).

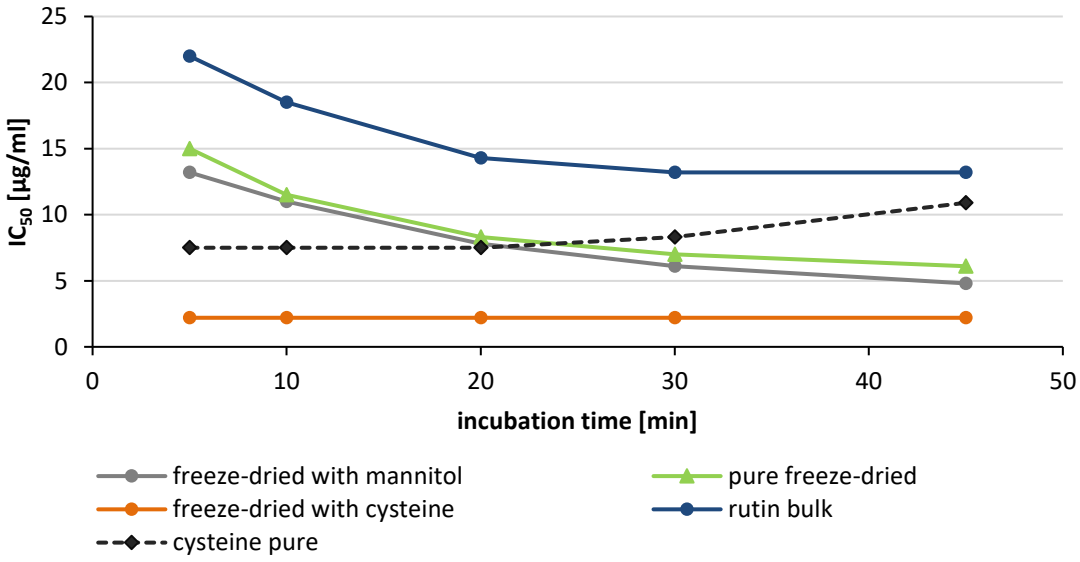

Figure 82: *The reaction velocity with the DPPH radical, expressed as IC_{50} values of the antioxidants over the incubation time. A slope of 0 means that the reaction is completed, while positive and negative slopes give the direction of reaction in radical scavenging and inducing, respectively.*

It shows that the determination of the AOC of rutin depends strongly on the incubation time and that the complete reaction and thus the steady-state seemed to be not reached after 45 min (**Figure 82**). Therefore, a standardized reaction time of 30 min is not always useful for the comparison of different substances or substance mixtures such as extracts. Combinations might have an additive and synergistic effect on their AOC. For example, the prolonged IC_{50} reduction using rutin was compensated by cysteine and at the same time the increase in IC_{50} observed when pure cysteine was used, could be prevented by adding rutin. As result, a fully stable equilibrium over the entire incubation time was obtained. However, when freeze-dried with mannitol, the reaction time did not change compared to the pure lyophilizate (**Figure 82**).

The fact that the steady-state was not reached even after 45 min for rutin-containing formulations without cysteine was independent of its concentration. This means that at a concentration below or above the IC_{50}, the reaction is also not completed after 45 min (**Figure 83**). Also, after the incubation time of 45 min, it has been observed that the maximum inhibition ranges from 60 to 80% (**Figure 81** and **83**). Consequently, an equilibrium is achieved between the free radical and the antioxidant. This means in reverse that the radical can be also recovered from the oxidized antioxidant. This was found for ascorbic acid and cysteine, where a higher dose each had a higher scavenging potential within 5min but decreased within 45min (**Figure 83 A** and **B**). Especially, ascorbic acid showed a stable equilibrium over time with an inhibition of about 77% at a concentration of 59 µM. Using a higher concentration led to an approximation to this inhibition equilibrium of 77%. In other words, a higher concentration of fast-acting antioxidants will not increase its scavenging efficacy in a radical-limited environment.

Interestingly, pure cysteine followed a different pattern, where a sudden decrease in antioxidant activity (inhibition) was observed after holding the equilibrium for 20 min (**Figure 83 B**). In terms of the rutin NC formulations, an approximation of the radical inhibition to about 68% was observed (**Figure 83 D, E** and **F**). Also in this case, the use of a high concentration or high levels of antioxidants decreased the AOC to this equilibrium value. The difference, however, is that a smaller concentration approaches this equilibrium over time. Again, the radical scavenging reaction was not completed after 45 min. However, the equilibrium was reached within 5 minutes when using a rutin concentration of 30 and 35 µM for the pure and mannitol freeze-dried formulations, respectively (**Figure 83 D** and **E**). Halving the concentration (15 and 18 µM) required 45 minutes to reach the same inhibition of about 69 and 65%, which in turn means that a delayed activity can be achieved with rutin. Interestingly, the inhibitory equilibrium seemed to play a crucial role in the long-term radical scavenging effect. So, the synergistic effect obtained with the cysteine-rutin combination was also reduced from initially more than 80% in inhibition to almost 70% within 45 min (**Figure 83 F**). It can be concluded that the equilibrium value could be the defining parameter for both the highest beneficial concentration and the incubation time at a given concentration when dealing with free radicals. Thus,

for the treatment of oxidative stress triggered by ROS in a cellular environment, rutin could scavenge radicals for a long time and thus protect cells in the long term.

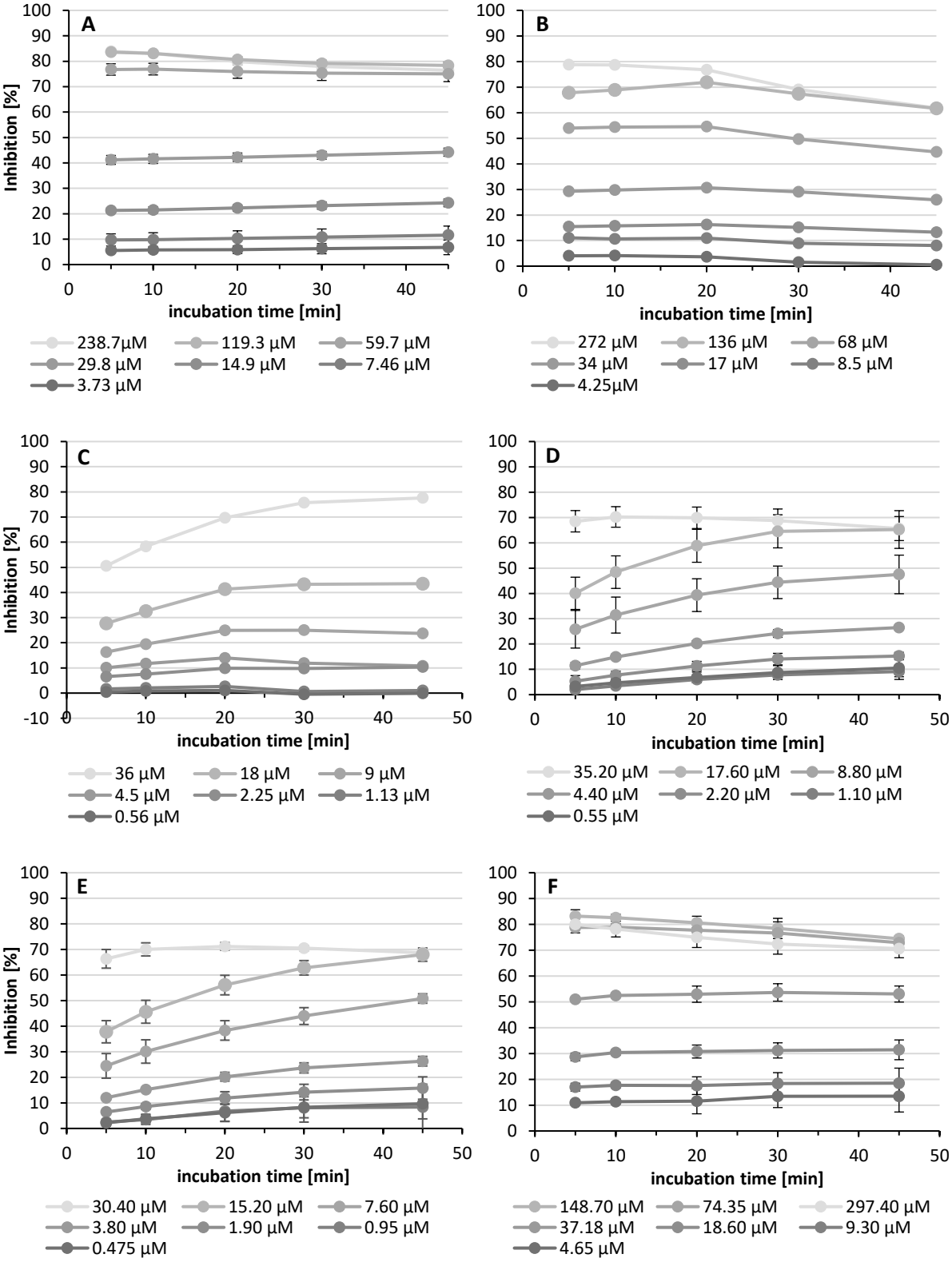

Figure 83: *Rection velocity of different compounds and their concentrations. The steady-state and thus the equilibrium is reached at a slop of 0, i.e. a parallel line to the time axis. A is ascorbic acid, B cysteine only, C coarse rutin, D the rutin nanosuspension freeze-dried without additive (pure), E freeze-dried with mannitol, and F is the freeze-dried with cysteine.*

In summary, the antioxidants show different behavior in terms of reaction rate and long-term adjustment of the equilibrium. This is in good agreement with previous studies that classified antioxidants regarding reaction time for scavenging DPPH until reaching the steady-state, in the categories fast (<30 min), medium (30-60 min), and slow (>60min) [298,299]. However, the use of pure cysteine deviates from the observation in this work, as a decrease in AOC is observed after 20 min reaction time at all concentrations (**Figure 83 B**). In addition to the theory that there is an equilibrium between the free radical and the reduced form, the elevated DPPH levels could also give a hint of a pro-oxidant effect.

To explain these findings, a deeper understanding is required of how the reactions proceed in general and what products the antioxidants are oxidized to. This assay is based on the reversible reduction from DPPH· radical to $DPPH_2$ upon uptake of a hydrogen atom from the scavenging molecule, i.e. the antioxidant. The resulting and less reactive antioxidant radical in turn can react with another antioxidant radical as well as the DPPH· radical. As an interesting side note, the assay was first designed by Blois in 1958 by proving the H-atom scavenger cysteine.

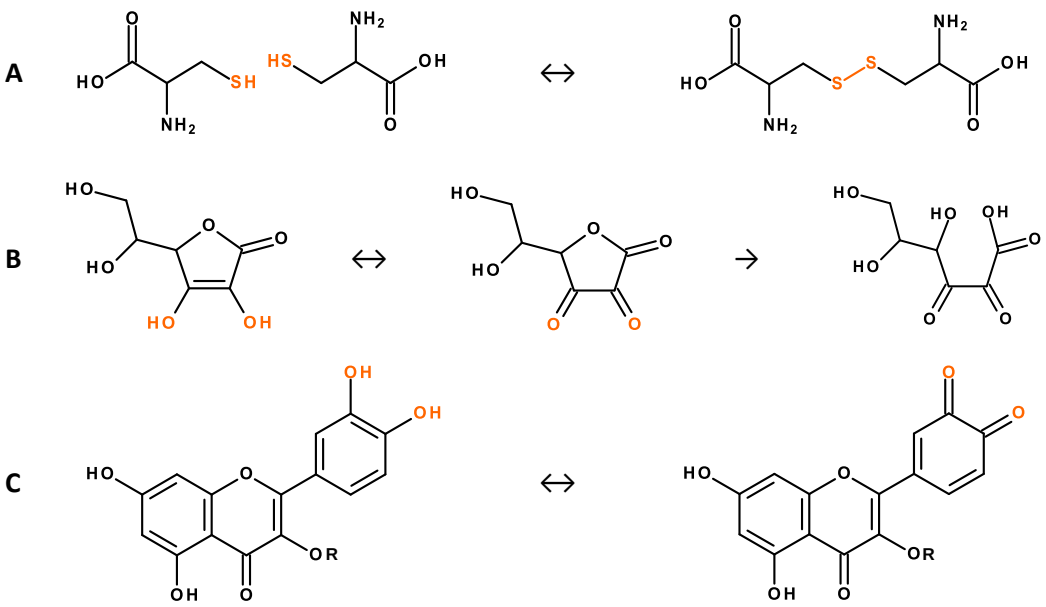

Figure 84: *Oxidation reaction of* cysteine to cystine (A), ascorbic acid to dehydroascorbic acid and 2,3-diketgulonic acid (B), and rutin to dehydrorutin. Orange colored highlights are the loci of reaction. -R = the disaccharide rutinose.

To balance the radicalization, all antioxidants used in this study deliver two H-atoms each. For this reaction, cysteine requires two molecules that bind to each other to generate cystine by forming a disulfide bridge (**Figure 84 A**). Considering the stoichiometry of the reaction, two moles of cysteine are required to reduce DPPH by two moles, while each one mole of ascorbic acid and rutin are equivalent to the same effect. This can be used to explain why the IC_{50} of cysteine is more than twice as high as

for ascorbic acid (**Table 21**). However, the oxidized form of ascorbic acid, dehydroascorbic acid, can be irreversibly converted to 2,3-diketogulonic acid by an addition reaction with water (**Figure 84 B**). The equilibrium can be thus shifted more on the antioxidant side, which would explain the equilibrium of the observed 77% of inhibition (**Figure 81 A**). In addition to the vicinal hydroxy groups (*O*-hydroquinone) of rutin, which are susceptible to oxidation (*O*-quinone), rutin has the disaccharide rutinose (**Figure 84 C**). When bound to the aglycone quercetin, it is not a reducing sugar. Only if theoretically a small portion of the sugar is hydrolytically separated from the aglycone, this would result in the release of the more antioxidative quercetin on top [300]. In contrast, in two independent studies, only the product dehydrorutin was found when using the DPPH assay [301,302]. Likewise, the antioxidative potential increases with an increasing number of hydroxyl groups. Both the size and the fact that the rutin-radical intermediate is stabilized in the electrode system could hinder the rapid release of both H-atoms and thus are explanations for the slow reaction velocity.

Mathematically, the order of reaction kinetic of DPPH and antioxidant is strongly dependent on the ratio of reactants. If the concentration of antioxidants is higher than the DPPH, the kinetic follows a pseudo first order kinetics. Hence, the reaction time depends on the antioxidant and its concentration used [299]. Moreover, it has been shown that the reaction time was also affected by the DPPH concentration, even if the DPPH to antioxidant ratio remained constant [303]. Furthermore, the IC_{50} also depends on the medium used. It has been demonstrated that the addition of water shifted the IC_{50} value and the antioxidant activity might be consequently misinterpreted when comparing different APIs against each other. For example, when comparing the IC_{50} values obtained in a methanolic to a half methanolic aqueous medium, the IC_{50} was halved for gallic acid, while it was more than doubled for α-tocopherol or curcumin and remained the same for ascorbic acid or sesamol [299]. The influence of the medium on the deprotonation of the phenolic group plays a crucial role. For example, methanol was found to decrease the reaction rate constant for catechols [304]. Since rutin, possessing a catechol partial structure, was reacted with DPPH in methanol, the observed high reaction time becomes reasonable.

In addition to the problem of the deprotonation mechanism, other studies have also demonstrated the reversibility of $DPPH_2$ to DPPH, indicating that many antioxidant phenolic structures were under-estimated in their antioxidant activity. For this reason, it is necessary to find a valid and convincing *in-vivo* correlation and thus the antioxidant capacity within a cell culture model was investigated next.

4.3.3.3 Cell culture studies

4.3.3.3.1 A549 human lung adenocarcinoma cell line

The rutin nanosuspension and the dried NC demonstrated their increased solubility and antioxidative efficiency when compared to the larger bulk material. To obtain more information about the possible application for the treatment of oxidative stress-related lung diseases like COPD, cell culture studies were conducted. The A549 human lung adenocarcinoma cell line was used as a model of type II pneumocytes. Established in 1972, A549 epithelial cells typically grow in confluent monolayers, produce lung surfactant consisting mainly of phospholipids, and are commonly used as a suitable model for investigating drug metabolism processes [305].

To demonstrate the antioxidant activity of rutin against COPD, cells must first be stressed in a suitable manner that induces the production of ROS. Such substances are *tert*-butyl hydroperoxide (TBH), an organic peroxide widely used in various oxidation processes and as a radical polymerization initiator, as well as lipopolysaccharide (LPS), which is known as endotoxin from gram-negative bacteria. *In-vivo*, after binding to receptors especially of cells of the immune system, pro-inflammatory cytokines, nitric oxide and eicosanoids are released [111]. As a result, a cellular stress response is induced by the release of ROS that finally introduces the cell death pathway. Depending on the concentration and incubation time applied, the number of active cells is reduced which is expressed as cell viability. Hence, both stress generators TBH and LPS were applied to the A549 cells for 4 – 12 h to identify the appropriate concentration and incubation time. The cell viability was determined using an MTT assay, with untreated cells (control) serving as a 100% viability reference, and cells treated with Triton-X 100 serving as a negative control and a measure of maximum cell death.

Increasing the concentration and incubation time of TBH led to a decrease in cell viability (**Figure 85**). By treating cells with 200 µM TBH for 6 h or more its effectiveness was comparable to the negative control, which was considered to damage the cells completely, and thus there was no further "negative increase" possible. An intermediate chance of cell survival was achieved at 100 µM after 8 h and 200 µM after 4 h incubation time. The latter combination was chosen for the study with rutin in order not to affect the incubation time and thus the cell count too much. Since a long incubation time increases the number of living cells, the difference in viability between treated and untreated cells is influenced by time alone and the result could be statistically biased. Interestingly, when treated with LPS, the cell viability increased with incubation time and was generally not significantly affected (**Figure 85**). This result was not expected and is in contradiction to previous studies and can therefore not be explained at this point.

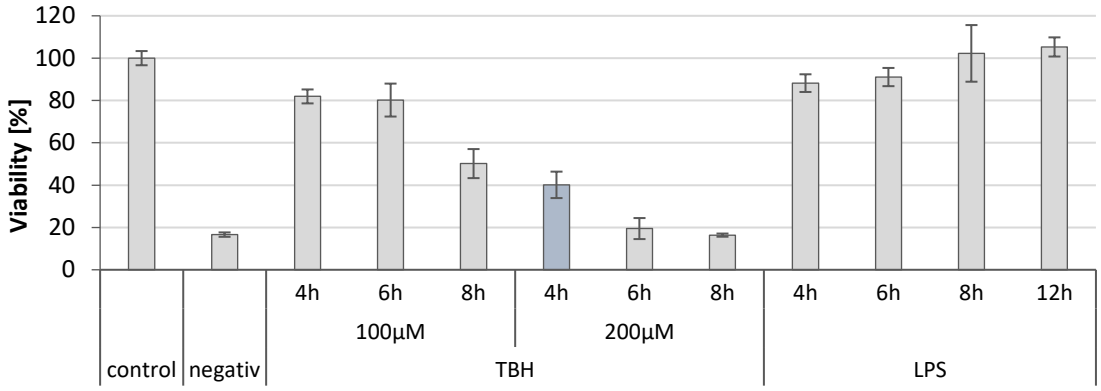

Figure 85: *The cell viability after treating A549 with TBH and LPS for 4, 6, 8, and 12 h. Negative control cells were treated with Triton-X 100 to create maximum cell death. Data are normalized to control cells and represented as mean ± SD; n=8.*

Both stress generators were given along with different concentrations of freeze-dried rutin NC on the A549 cells and their viability was determined (**Figure 86**). First, the cell viability was evaluated without adding any stress generators but with rutin and the controls, i.e. mannitol and cysteine as adjuvants in the freeze-dried rutin powder as well as ascorbic acid as a classical antioxidant serving as a positive control. The cell viability decreased slightly with increasing concentrations of rutin (**Figure 86**). Additionally, mannitol and especially cysteine possessed a significant effect on the cell viability when compared to the untreated cells. From this, it can be assumed that the decreasing cell viability at higher rutin concentrations was a consequence of the likewise elevated amount of the adjuvant cysteine and mannitol, respectively. Ascorbic acid, on the other hand, exhibited a slightly positive effect on cell survival, since the number of cells increased compared to the control of untreated cells (**Figure 86**).

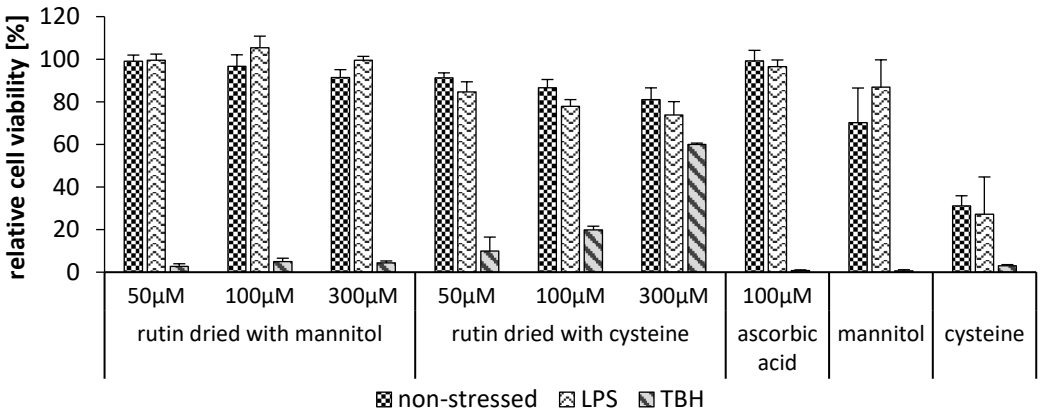

Figure 86: *The relative viability of A549 cells after additon of freeze-dried rutin NC formulations and non, TBH or LPS exposure. Ascorbic acid served as positive control and mannitol and cysteine as vehicle control. Data are normalized to non-treated control (100%) and Triton-X 100 treated negative cells (0%) and represented as mean ± SD; n=4.*

When THB was added, rutin seemed to possess a minimal antioxidant effect compared to non-protected cells (**Figure 86**). In contrast, cysteine alone, mannitol and even the intra- and extra-cellular effecting ascorbic acid, had no protective effect resulting in cell death of almost 100%. However, rutin in combination with cysteine revealed a significant increase in cell viability.

One explanation is that cysteine is involved in the natural cellular antioxidant system, e.g. as part of glutathione, whereas rutin is known to be a very good scavenger for hydroxyl radicals and possibly only protects the extracellular space. It was already shown that TBH triggered equally both necrotic and non-necrotic cell death pathways [306]. Consequently, TBH could simultaneously induce different types of cell death pathways. In the same study, it was demonstrated that N-acetyl-cysteine was able to inhibit partially cell death when stressed with the exogenous ROS H_2O_2 and BTH but unable to protect them when treating with TNF-α, the inducer of the endogenous mitochondrial-depending apoptotic pathway. Since different pathways are involved when using TBH, the protective effect of cysteine, the precursor of glutathione, and rutin can only occur after its uptake and conversion into glutathione. Due to its kinetically slow action, rutin could be hampered by reducing the high number of radicals in time. To gain an understanding of how quickly the cells react within the cells with ROS, experiments were carried out afterward under different incubation times of the antioxidants before treating them with TBH.

The use of LPS alone did not seem to interfere with the life cycle of the cells. Thus, the results regarding the cell viability were very similar to those obtained without further stress generators (**Figure 86**). Interestingly, adding cysteine showed again a negative effect, where the resulting cell viability was significantly lower than that of the other antioxidants. LPS did not cause significant cell death but it, nevertheless, might have slightly increased the level of intracellular stress mediators (ROS) that the more robust tumor cells managed to deal with.

To assess the possible increase in intracellular oxidative stress in terms of the ROS amount, an assay with 2',7'-dichlorofluorescin-diacetate (DCFDA) was performed [189]. In this cell culture assay, the fluorescin-derivative penetrates the cells and is deacetylated enzymatically. This leads to an enhanced hydrophilic substance that is unable to leave the cells. The resulting DCFH molecule reacts specifically with ROS and is oxidized to the fluorescent molecule DCF. Hence, the more ROS is generated intracellularly the higher is the fluorescence detected. In following experiments, the change in fluorescence of the non-stressed and non-treated cells (control) was set to 100% and related to the signal obtained by the cells treated with TBH and LPS. Calculating the ratio is important because constantly ongoing redox reactions occur with energy production and metabolism [189]. In consequence, fluorescence signals will be obtained by each intakt cell independent of external ROS induction.

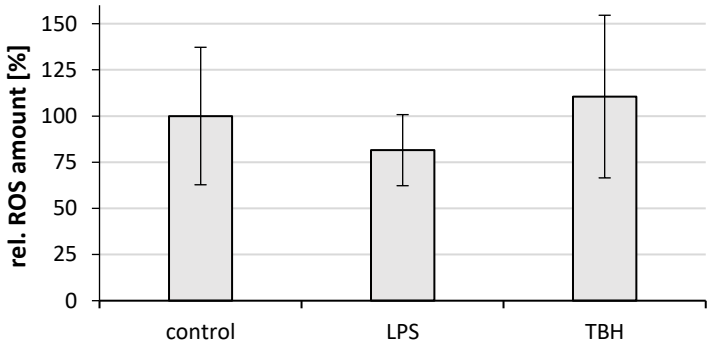

Figure 87: *Intracellular ROS amount of A549 cells stressed by LPS and TBH, normalized to control (non-stressed cells), data represented as mean ± SD; n=4, no statistical significance (p ≤ 0.05, ANOVA).*

The results of the DCFDA assay pointed to a higher intracellular ROS production when the cells were treated with TBH and a lower one with LPS compared to control each (**Figure 87**). This tendency is not significant and would give only a slight hint for the contradictory observation for the cell growth (**Figure 85**).

Therefore, further cell culture studies focus on treating the THB exposure by rutin, as this could identify the radical scavenging effect from elevated ROS amount to ideally normal or lower levels within the cells. For this purpose, rutin NC freeze-dried with mannitol and cysteine, its coarse bulk material and controls were applied to A549 cells either simultaneously to TBH or cells were pre-incubated for 24 h and then stressed by TBH for 30 min.

If the antioxidants and controls are applied to the cells alone and followed directly by the stress generator TBH, the first tendencies can be noticed: The radical scavenging efficacy of rutin increased with its concentration, whereas the trend is only very low for the coarse material (**Figure 88** upper). Rutin NC freeze-dried with mannitol was most successful with a relative ROS amount of about 40%, followed by cysteine-formulated ones of about 70% (**Figure 88** upper). However, no radical scavenging effects in the cell model were observed when treating with ascorbic acid. This was unexpaected as ascorbic acid demonstrated fast radical scavenging activity in the DPPH assay (**Figure 81 A)**. The lyo-/ cryoprotectant mannitol and cysteine served as vehicle control and revealed also no effect on the intracellular ROS amount. The addition of TBH in this trial could not increase the stress level within the cells of the non-treated control. Despite this, positive and negative effects of rutin formulations still showed a trend, even though TBH did not seem to have induced ROS elevation in this case.

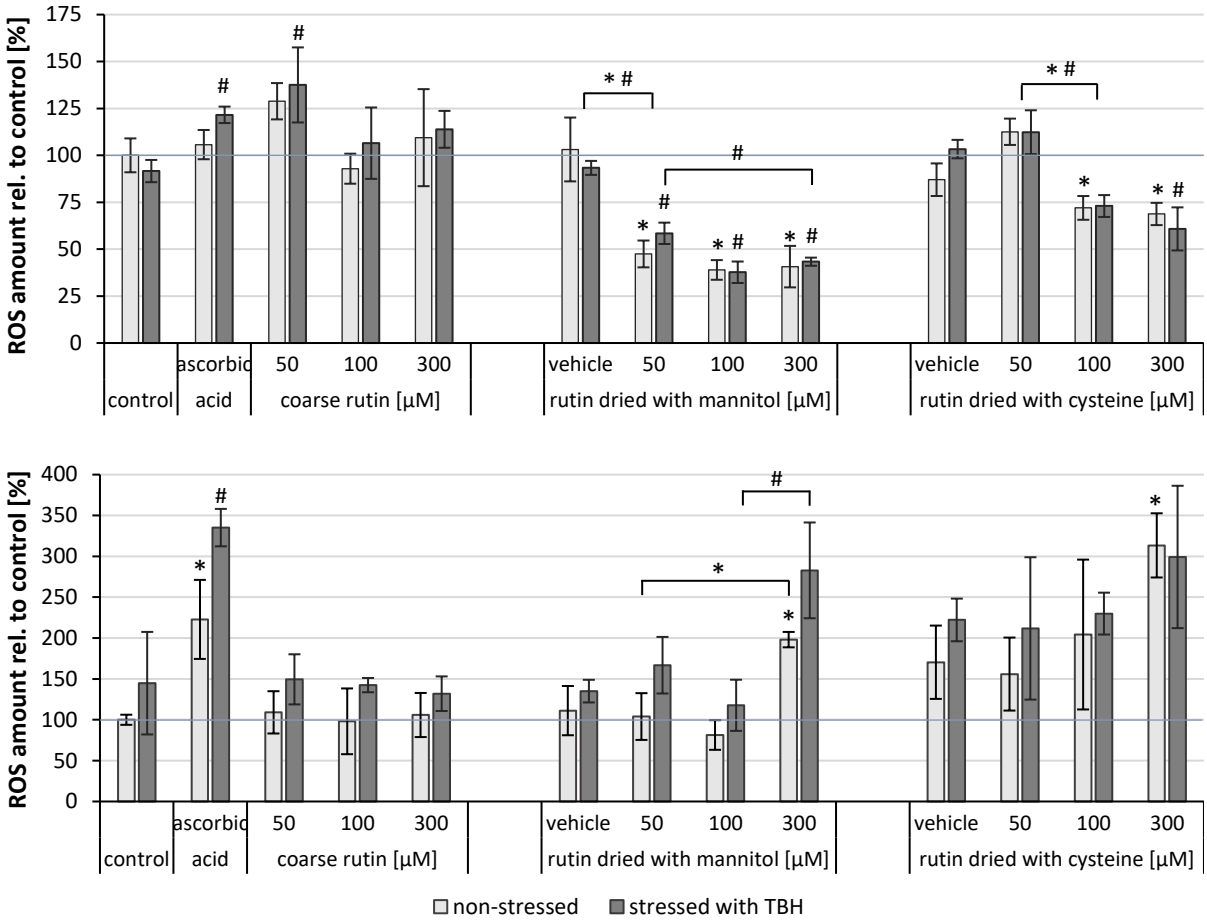

Figure 88: *Detected intracellular ROS amount of A549 cells treated with the formulations only (light grey) or additionally stressed with TBH (dark grey). Cells were treated with different rutin formulations and controls simultaneously (upper) or pre-incubated for 24 h and washed before adding TBH (lower). Data are normalized to control and represented as mean ± SD, n=4; * indicates statistical significance of non-stressed formulations to non-stressed control, # indicates statistical significance between stressed formulations to stressed control (p ≤ 0.05, ANOVA).*

After the pre-incubation time of 24 h with rutin, almost all rutin formulations showed an intracellular ROS amount being at the same level or even significantly higher compared to the non-treated non-stressed control (**Figure 88** lower). For example, rutin NC freeze-dried with cysteine (300 µM) resulted in 3.5 times higher ROS amounts. The additives also slightly increased the intracellular ROS amount compared to the control, and ascorbic acid even significantly increased it to about twofold (**Figure 88** lower). Despite the unfavorable high initial ROS amount after pre-incubation with different rutin formulations, the externally induced ROS production by TBH was not significantly higher compared to the non-treated TBH-stressed control (**Figure 88** lower). The highest ROS amount in cells stressed with TBH was detected when ascorbic acid was used. Ascorbic acid has been demonstrated to scavenge the DPPH radical immediately (**Figure 81**), so it can be assumed that it was completely metabolized during the 24 h cellular incubation time. In consequence, no additional antioxidant was inside the cells to neutralize the radical TBH and its ROS induction pathway, but a possibly downregulated oxidant-antioxidant-balance. In contrast, the slow reaction kinetic of rutin characterized in the DPPH assay

(**Figure 81**) seemed to be advantageous in protecting and treating oxidative stress-induced cellular pathways for acute treatment and preventive purposes. So, rutin could be taken up into cells but not entirely oxidized by cellular respiratory processes during the 24 h incubation time (**Figure 88** lower).

A longer radical scavenging capacity of rutin was also confirmed when enlarging the TBH incubation time (**Supplementary Figures 14** and **15**). So, the formulations prevented intracellular ROS formation in both non-stressed and stressed cells, although TBH affected the cells for 60, 90, and 120 min.

However, a significantly higher concentration of intracellular ROS was detected when the cells were treated with rutin NC freeze-dried with cysteine when compared to the control (**Figure 88**). This observation stands in contradiction to the study of cell viability, where the cysteine-formulated NC was significantly superior to all others (**Figure 86**). To explain this, it must be considered that the fluorescence assay used can only perform successfully if DCFDA was deacetylated by intact cells prior to the oxidation processes. Therefore, the results are underestimated if the vital cell number is less or the esterases are inactive. Conversely, this means that a high proliferation rate due to the protective properties of the cysteine formulation must concurrently indicate a high ROS reactivity, as more metabolism in general and to DCFH had occurred. In other words, more living cells have more metabolism in total, resulting in a higher rate of DCFDA uptake and thus a higher rate of oxidation to the fluorescent metabolite. This thesis could also be applied for the cysteine and ascorbic acid controls, where the cellular stress level was increased, too (**Figure 88** lower).

Based on the assumption that an increased concentration of the antioxidants contributed to inducing cell growth and/or increased metabolism, the pre-incubation times were varied. Indeed, time and concentration-dependency in improving performance could be observed after 4 h or more of pre-incubation time with rutin NC (**Figure 89**). When treating cells 2 h with antioxidants no significant alteration in the ROS amount was observed compared to the control (**Figure 89 A**). Also, the rutin NC formulations were statistically more effective in reducing the ROS amount within an incubation time. Likewise, when stressing the cells with TBH after an incubation time of 2 h with the antioxidants even a reduction in cellular ROS amount was observed. In terms of the incubation time of 4 h with the formulations, concentrations-depending higher cellular ROS amounts were detected than in the control (**Figure 89 B**). At this high level, it is rather unlikely that cell proliferation to this extent has occurred. Hence, it is also conceivable that the high concentration of rutin additionally stressed the cells resulting in a higher amount of ROS detected. These could then be compensated by the cellular antioxidant system after some hours. This would explain why the ROS amounts between the formulations and the control, both stressed and non-stressed, were aligned after an incubation time of 8 h (**Figure 89 C**). Therefore, further studies are necessary to investigate the uptake of rutin and the resulting expression of apoptosis markers in detail.

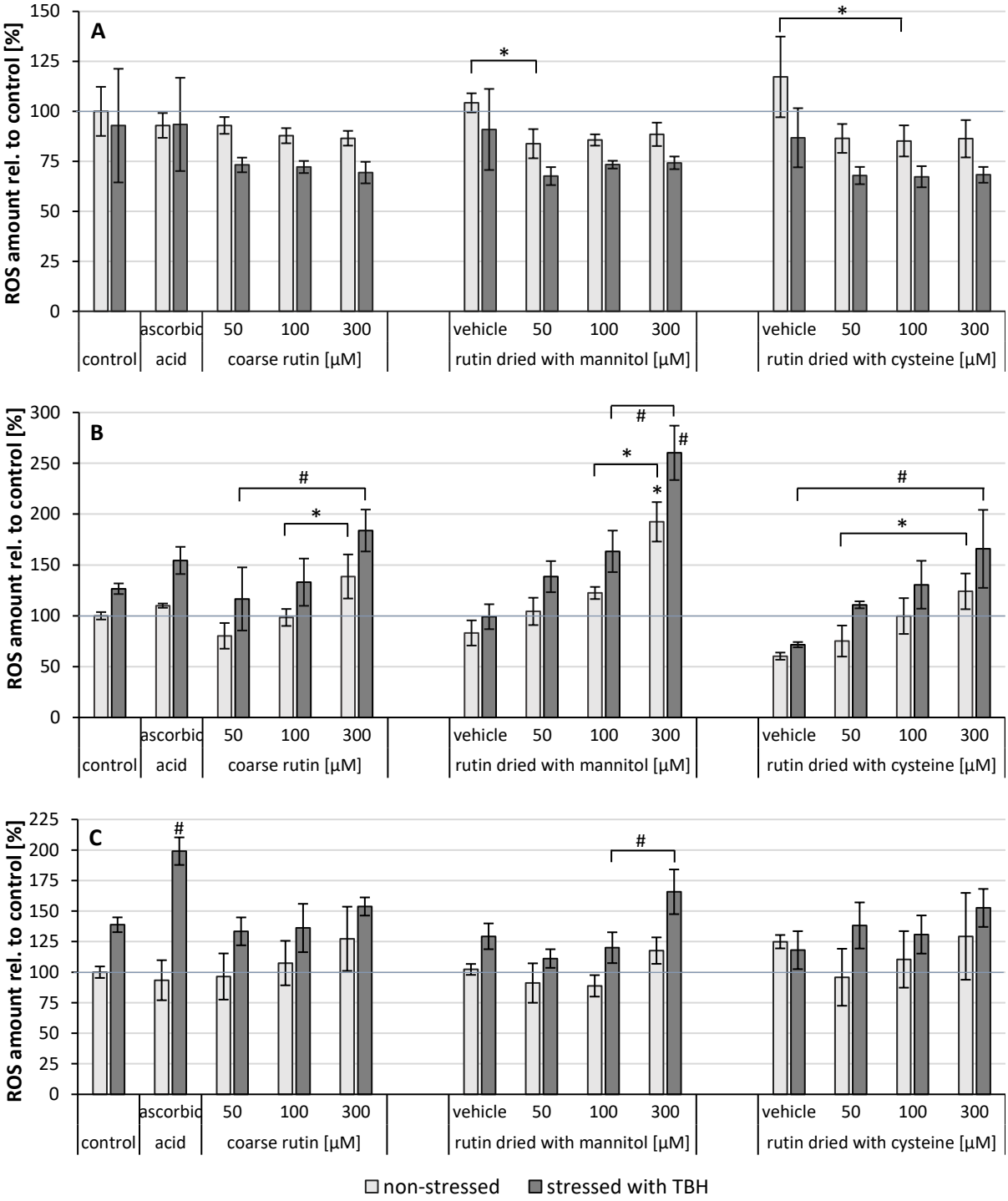

Figure 89: *Detected intracellular ROS amount of A549 cells treated with the formulations only (light grey) or additionally stressed with TBH (dark grey). Cells were treated with different rutin formulations and controls for an incubation time of 2 h (A), 4 h (B) and 8 h (C). Then, the cells were washed and stressed by TBH for 30 min Data are normalized to control and represented as mean ± SD, n=4; * indicates statistical significance of non-stressed formulations to non-stressed control, # indicates statistical significance between stressed formulations to stressed control (p ≤ 0.05, ANOVA).*

When plotting the different concentrations of the rutin NC formulations against time, the alternation of antioxidant effect and a possible rebound regulatory process becomes visible as a function of concentration (**Figure 90**). Using the mannitol-containing formulation, it was observed that a short

incubation time led to a reduction of the ROS amount to below 50% compared to the untreated control. However, when the time is extended to 4h, the ROS amount of the 300 µM rutin formulation increases to almost double the ROS amount as compared to the control (**Figure 90** left). A lower concentration of rutin (≤ 100 µM) did not increase the ROS amount even after long incubation times of 24h, but also did not reduce it. The use of mannitol as a control (vehicle) showed no effect on the ROS amount. So, it can be assumed that the high concentration of rutin could cause oxidative stress within the A549 cells, and thus, adequate dosing needs to be ensured.

In the formulation containing cysteine, an increase in the ROS amounts was also observed as the rutin concentration and incubation time increased (**Figure 90** right). Up to an incubation time of 8 h, the rutin-cysteine formulation at a concentration of ≤ 100µM did not significantly increase the intracellular oxidative stress. Even the highest rutin concentration used (300 µM) led to a slight increase in the ROS amount. It could be assumed that the use of cysteine in the formulation compensated the stress-triggering property of highly concentrated rutin because cysteine has demonstrated antioxidant effects in the DPPH radical scavenging assay (c.f. section 4.3.3.2). Interestingly, the use of cysteine alone (vehicle) caused an increase in the measured ROS after an incubation time of 24 h (**Figure 90** right). This observation can be used to explain the increasing ROS amount in all rutin formulations after the 24 h incubation. There are two feasible reasons for this. First, cell proliferation is induced by cysteine as a component of protein synthesis and as an antioxidant that might create a stress-reduced environment for the cells. Then, if more cells were present more metabolisms would result, and hence, more DCFDA was oxidized which would falsely imply relatively high oxidative stress. Secondly, the intracellular amount of ROS could be increased by pharmacological side effects, e.g. hindering a cysteine-dependent transport channel, suppressing other important amino acids in the cell process, or coupling disulfide bonds at the wrong sites. Further, studies would be necessary to elucidate this.

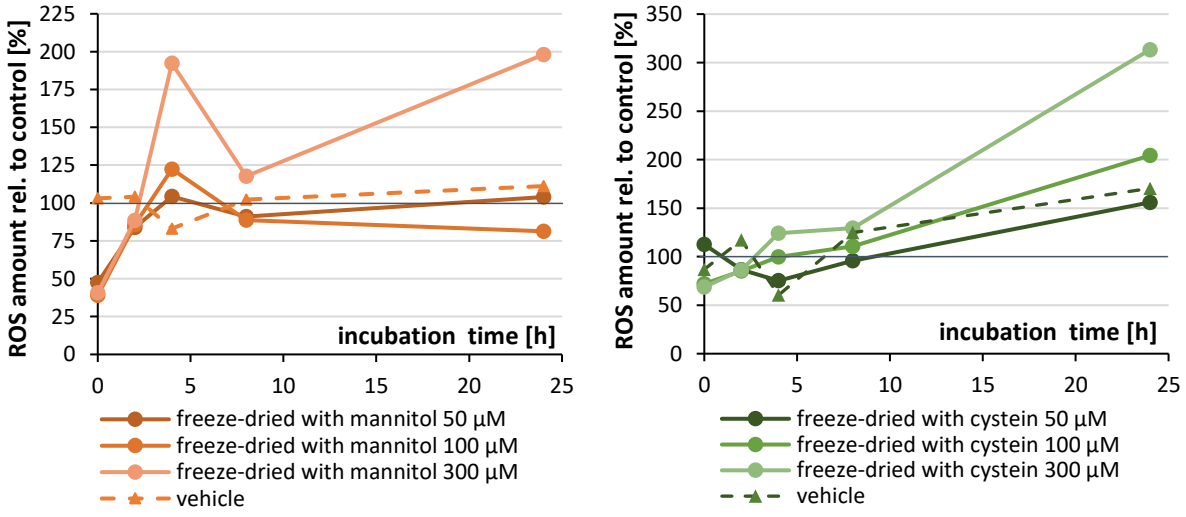

Figure 90: *Intracellular ROS amount of A549 cells after different incubation times with the rutin NC formulations freeze-dried with mannitol (left) and cysteine (right), as well as their rutin-free vehicle.*

4.3.3.3.2 H441 human lung adenocarcinoma cell line

In order to get more idea of how the formulations would affect when applying to the lung, a second cell line was used. The aim was to confirm or disprove the recent observation and related theories by the use of a physiologically different lung cell line. For this, the same trial was repeated with the difference of using the H441 cell line, which is known as lung surfactant-producing adenocarcinoma epithelial cell line [307]. The lung surfactant prevents the alveoli from collapsing due to rapid changes in air pressure and regulates the innate immunity, too. It consists of phospholipids and four proteins, of which SFTP-A and SFTP-D are involved in the removal of apoptotic cells, among other functions. Furthermore, SFTP-C binds bacterial lipopolysaccharide to inhibit inflammation processes and, together with SFTP-A, stimulates cells for resorption of phospholipids [307]. Hence, because of the reduced response to LPS regarding intra-cellular ROS production, and better comparability to the A549 cell culture studies, the trial on H441 cells was also carried out with the stress generator TBH. Due to the different physiology of the H441 cells compared to A549 it was expected that the cellular stress-induction by TBH and rutin could be influenced. Therefore, the suitable concentration and incubation time of TBH on H441 cells were first identified.

As a result and similar to the viability study performed using the A549 cell line, the viability of the H441 cell line was about 40% when TBH was added to the cells in a concentration of 200 µM for 4 h (**Figure 91**). These parameters were used for subsequent investigations. By doing so, it provides the best comparability to the results from the A549 cell culture studies and it also offers a good compromise between the incubation time and cell viability. As already explained, a longer incubation period could bias the results as the untreated and non-stressed cells increase in number. However, lowering the concentration led to slightly higher cell viability, while altering the incubation time by 2 h resulted in significantly higher and lower viabilities, respectively (**Figure 91**).

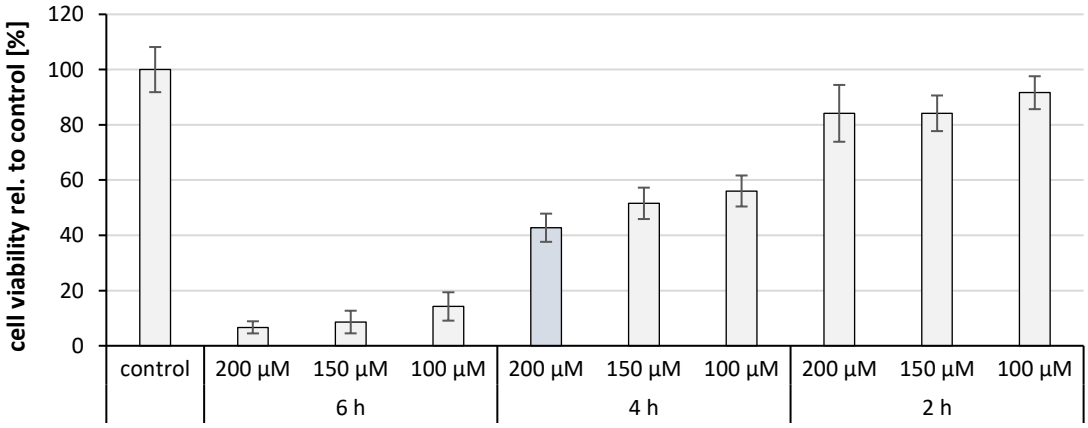

Figure 91: *The cell viability after treating H441 cells with TBH at concentrations of 100 - 200 µM for 2 - 6 h. Data are normalized to control (100%) and negative (Triton-X 100, 0%) and represented as mean ± SD; n=8.*

Next, the H441 cells were incubated with antioxidants including freeze-dried rutin NC formulations, ascorbic acid, and vehicles (carrier and PLX) itself but also stressed with TBH after the incubation. Incubation times of 0, 2, 4, 8 and 24 h were chosen as performed for the A549 cell line described above. For the A549 cell line, the most interesting incubation times were 4 and 24 h, as the highest intracellular ROS amount was detected in a concentration and formulation-based manner (**Figure 88** and **89**). When compared to the H441 cell line with an incubation time of 4 and 24 h a different effect was observed. The intracellular ROS amounts were equal or slightly higher compared to the control, but not statically significant (**Figure 92**). However, when the stressor TBH was added, the ROS amount of the treated cells remained unchanged, whereas the untreated control showed an increase. Thus, the higher concentrations of the rutin formulations on H441 were neither toxic nor did they induce the cell proliferation.

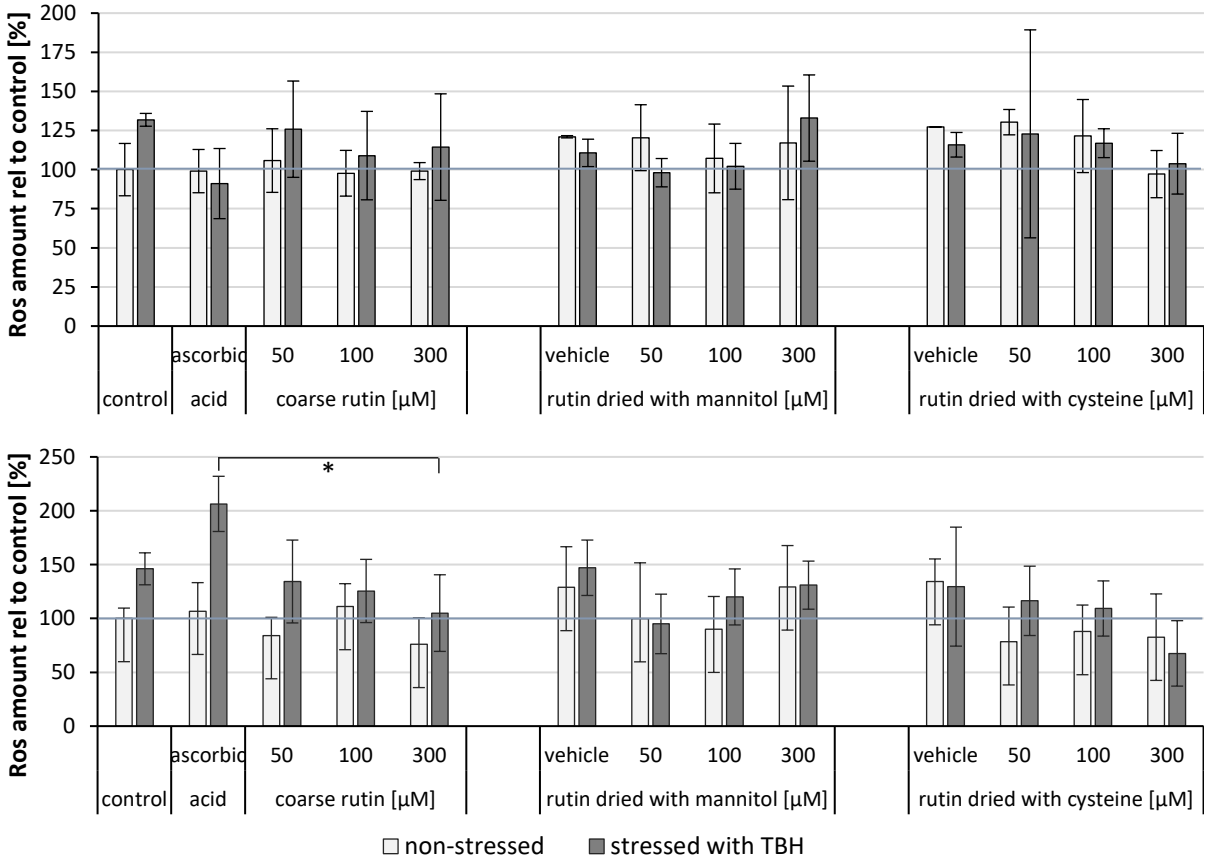

Figure 92: *Detected intracellular ROS amount of H441 cells treated with the formulations only (light grey) or additionally stressed with TBH (dark grey). Cells were treated with different rutin formulations and controls for 4 h (upper) and 24 h (lower) before exposure with TBH. Data are normalized to control and represented as mean ± SD, n=4; * indicates statistical significance (p ≤ 0.05, ANOVA).*

An increase in the cellular ROS amount was also detected when the cells were treated with ascorbic acid for 24 h, and interestingly, the vehicles showed the highest ROS amounts within the formulation group at both incubation times. This was not expected, because mannitol should possess no effects on

the ROS amount and cysteine would rather reduce it due to its antioxidant activity demonstrated above (c.f. section 4.3.3.2). Assuming that the vehicle used to stabilize the formulation affects negatively the antioxidant balance, rutin can be regarded as having a positive effect that compensates for the imbalance. The effect of the vehicles on the H441 cell line became more apparent when examined over time, i.e. at multiple time points within 24 h. By doing so, the intracellular ROS amount was detected to be always higher than the non-treated control and more pronounced for the cysteine containing vehicle (**Figure 93**; and more details in the appendix, **Supplementary Figure S15** and **S16**).

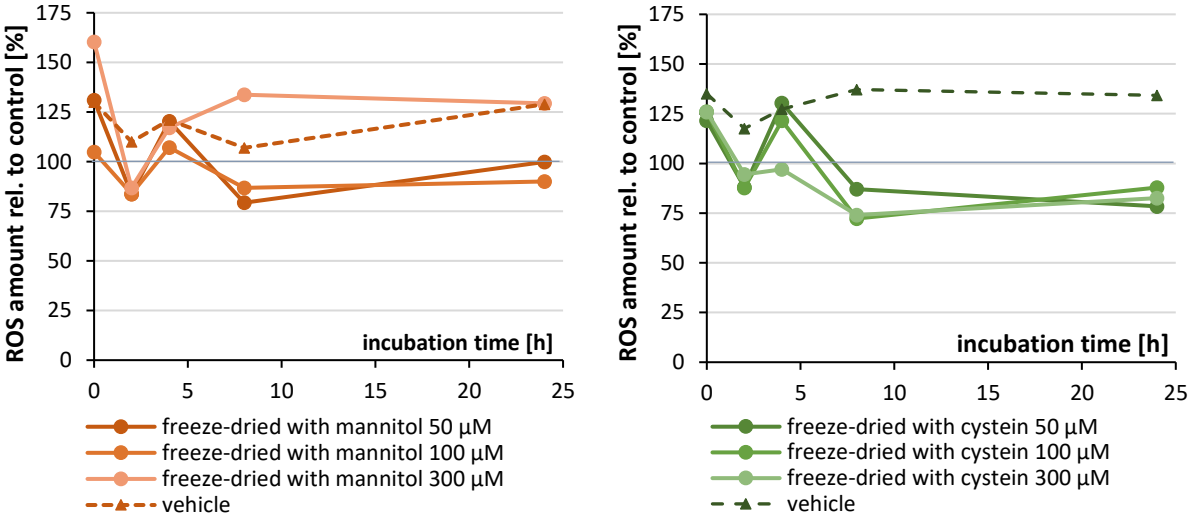

Figure 93: *Intracellular ROS amount of H441 cells after different incubation times with the rutin NC formulations freeze-dried with mannitol (left) and cysteine (right), as well as their rutin-free vehicle.*

Considering the NC formulations in terms of antioxidant activity as a function of concentration and time, the concentrations 50 and 100µM are found to be beneficial in this model (H441), i.e. the ROS amount could be reduced (**Figure 93**). Similar to the study with the A549 cell line, the ROS amount increased after 4 h and then decreased under the norm level (**Figure 90** and **93**). It can be assumed that the rutin formulations slightly stress the cells in a medium period, depending on the concentration used. This could be due, for example, to a negative response in the cell physiology or the depletion of antioxidants. Further studies would be needed to understand the mechanism to counteract. However, in contrast to the study with the A549 cell line, there was no increase in the intracellular ROS amount after prolonged incubation time when treating with the cysteine-containing NC formulation. It has been argued that the formulation stimulated the A549 cells to grow because the oxidants are scavenged and thus interfering less within the cell process. The H441 cells grow much more slowly so that such a possible increase in the cell number would not be expected compared to the untreated control. Consequently, the cysteine-containing formulation still possessed an antioxidant activity after 24 h (**Figure 93**).

It can be concluded that a beneficial effect might have been obtained through the combination of rutin and cysteine, but this enhancement. Only the nanosizing of rutin or rutin itself did not protect the cells from death nor from an increase in the intracellular ROS production. Concerning nanonization, it can be recorded that already in this work, for example, the BID inhibitor NC (c.f. chapter 4.1), clearly proved a benefit. Likewise, other studies are confirming the efficacy of NC [158,172,173]. Regarding rutin as a potential antioxidant, previous studies are developing a structure-activity relationship between flavonoids and their antioxidative potential in the treatment of lung diseases. Flavones, which include rutin, and flavan-3-ols have been characterized as the most effective. The antioxidative and radical scavenging properties are associated with three structural characteristics: an ortho-dihydroxyl group (catechol) at the B ring, a double bond on C2 and C3 combined with an oxo-group on C4, and hydroxyl groups at the C3 and C5 (**Figure 94**) [87].

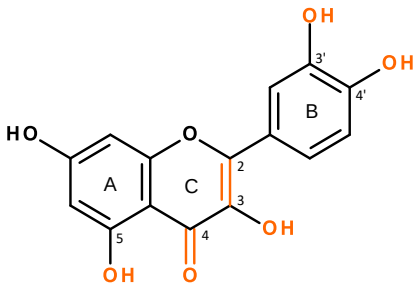

Figure 94: *Chemical structure of quercetin, the aglycone of rutin.*

However, due to the glycosylation of one of the essential hydroxyl groups, the flavonoid suffers a loss of the effective structure characteristic. This blocks in turn the capability of removing radicals and metal chelating properties [87]. Furthermore, due to the large glycoside group, the accessibility of the membrane could be declined. Consequently, the antioxidant activity of aglycons was reported to be higher than that of the corresponding glycosylated derivatives [91,100]. On the other hand, inhibition of cyclooxygenase and pro-inflammatory cytokines such as TNF-α and IL-1 by rutin was reported [97]. Also, the 3-O-glucuronopyranoside quercetin derivate significantly reduced the ROS amount in oesophageal epithelial cells, where the oxidative stress was induced by acid (pH 4), LPS, indomethacin and ethanol [308]. Moreover, the complexity of the lung cell composition with its manifold enzymes could provide for de-glycosylation, whereby rutin can be classified as a pro-drug. Its aglycone quercetin has already been identified in several *in-vitro* and *in-vivo* studies as one of the most effective flavonoids for the treatment of COPD [309].

4.3.3.3.3 Primary mouse macrophages

In both previous cell culture studies, adenocarcinoma cells were used to assess ROS inhibition. They offer a versatile model for lung epithelial cells, which in turn are the main cell type in the bronchi. Nevertheless, oxidative stress-related lung diseases such as COPD or asthma originates mainly in macrophages [55,57]. For this reason, a short study was carried out in cooperation with the Frauenhofer Institute (Germany) on primary alveolar macrophages as the forecasted target.

Rutin NC freeze-dried with cysteine was used in this study as it has been demonstrated the best antioxidant activity. Triton-X 100 as negative control was used to evaluate 100% cell death and $KBrO_3$ was used as an oxidative agent. In interaction with Glutathione, $KBrO_3$ forms the highly reactive 8-oxodesoxy-guanosine and thereby initiates a DNA double-strand break [310,311]. As a result, a toxic dose of rutin NC freeze-dried with cysteine was observed (**Figure 95**).

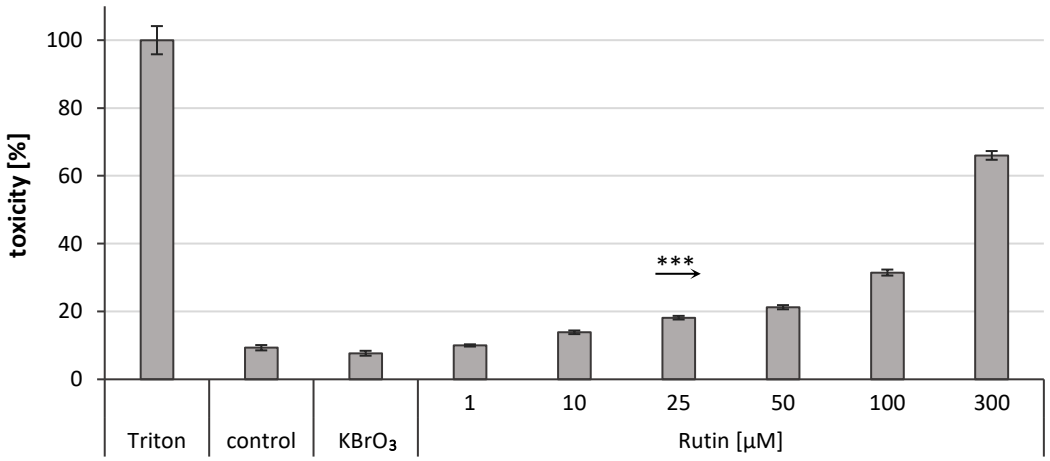

Figure 95: *Dose-dependent toxicity study of rutin freeze-dried with cysteine using an LDH-assay on primary alveolar macrophages. Triton-X 100 serves as a marker for 100% cell death, while the oxidant $KBrO_3$ and an untreated fraction act as controls; n = 8, mean ± SD; ∗ p < 0.05; ∗∗ p < 0.01, ∗∗∗ p < 0.001 (ANOVA).*

In contrast to previous trials, the rutin formulation seemed to be toxic to alveolar macrophages at concentrations of 25 µM or higher. Although there is a particle size-related uptake by macrophages with a clear maximum in diameter between 2 and 3 µm, the dependency of phagocytosis arises from the attachment step [312]. Particles with a size >10 µm or < 0.2 µm can elude phagocytosis. Thus, compared to the epithelial cell lines, the uptake by macrophages might be increased because they "consume" the NC as a whole particle. In this way, the macrophages can also take up the stabilizer PLX adhered to the particle surface. In a recent study, it was demonstrated that nanoparticles stabilized with PLX were absorbed most rapidly compared to non-stabilized and otherwise-stabilized particles [313]. Moreover, these PLX-stabilized particles showed a dose-dependent cytotoxicity as well as a significant release of IL-6 and enhanced release of IL-8 and TNF-α after exposure to macrophages. Hence, the dose-dependent toxicity of rutin-NC in macrophages could be triggered by the cell death

pathway due to higher concentrations of PLX (**Figure 95**). In the cell culture studies with A549 and H441, higher doses of the rutin formulations and the application of the vesicle indicated the induction of intracellular ROS. If the ROS amount reaches a critical concentration, i.e. the point of no return the cell death pathway is induced [33]. Since the macrophages have consumed a larger amount by endocytosis of the whole particles, the critical concentration suggested being lower.
Consequently, beneficial effects of the tailor-made rutin NC could be obtained *in-vivo* for the treatment of oxidative stress in macrophages if the appropriate dosage would be considered. For this, the first step for identifying which dosages are appropriate has been accomplished. Further investigations are now necessary to determine the antioxidant effects of rutin NC in a more specific environment and cell culture model for oxidative stress-related diseases.

To sum up, this chapter was divided into three parts to achieving the aim of producing a tailor-made rutin NC formulation that is suitable for the pulmonary application. In the first two parts, the production of the rutin nanosuspension was optimized and by freezing it, an ideal solution was found to store the suspension for a long time physically, chemically and microbially. By sublimation, the water was removed from the frozen state to obtain a powder that can be stored at room temperature. Then, the technological transformation into a powder for inhalation succeeded.
In the last part, the powder was investigated and compared to the bulk material regarding the dissolution velocity, the radical scavenging capacity and kinetics, as well as the antioxidative efficacy in a cell culture model. As a result, it has been demonstrated that the dry rutin NC formulations were superior. The addition of other excipients was used to control and improve the dissolution rate and the antioxidative effect of rutin. For example, the formulation with the addition of cysteine slightly reduced the dissolution rate of the NC compared to the nanosuspension, but it showed an increase in the AOC and was highly effective in the cell culture model. The cell culture model suggested differences in antioxidant efficacy depending on incubation time and uptake mechanism. Taking into account the concentration, a fast and even long-term effect of rutin could be obtained and thus, the aim of the development of tailor-made NC for the treatment of COPD and asthma was reached.

5 Conclusion

The overall aim of this thesis was to develop tailor-made NC for the treatment of oxidative stress-related diseases. For this purpose, three different active ingredients, namely BI-6C9, hesperetin and rutin, were differently prepared to be successfully applied by different application routes such as i.v., oral and pulmonary, respectively. Despite the diversity of APIs and the restrictive requirements to meet the application needs, such as particle size limitations and GRAS status, tailor-made NC were successfully obtained. As a result, the diversity of active ingredients, production techniques and stabilizers created the ideal basis for drawing conclusions.
Therefore, this chapter intends to discuss the similarities and differences in the production of tailor-made nanocrystals.

The first question about the successful production of drug NC is, which stabilizer is best suited for this purpose. That means, which stabilizer can be used to achieve the smallest particle size after the nanonization and/ or to physically stabilize them the longest. It was demonstrated in the study of rutin NC that the use of different stabilizers can impact the resulting particle size. It was also found that the particle size on the day of the production did not correlate with its long-term stability. To estimate the appropriate stabilizer or stabilizer mixture for long-term stability, it was observed that certain chemical structures of the surfactant preferentially interact with the particle surface, depending on the hydrophilic/lipophilic surface characteristic. So, the aliphatic partial structure of SDS was more like to adsorb on the surface of BI-6C9. In addition to the CH_2-chain that is also present, Tween 80 has a comparatively high proportion of hydrophilic polyethylene chains which complicates adsorption. Although hesperetin and rutin differ in their hydrophilicity due to the glycoside group, PLX was suitable in physically stabilizing both flavonoids. The use of a very hydrophobic stabilizer can adhere well to a particle with a very hydrophobic surface, but is poorly accepted in the aqueous medium. Therefore, the combination with an additional rather hydrophilic stabilizer proved to be synergistic.
The hesperetin NC stabilized with PLC revealed less stability in cell culture medium and long-term stability when produced by BM. It was assumed that the surface was more hydrophobic compared to those produced by HPH, which could thus make the surface less attractive for the hydrophilic stabilizer. Hence, the surface property and particle size were also affected in varying process conditions for HPH. Similar to this, when applying a higher number of pre-milling cycles, i.e. homogenization cycles at low or medium pressure, larger particles were obtained since imperfections are filled and more stable crystals are created. The same effect was observed for the scale-up process, where the longer cooling time led also to more perfect and stable crystals. In other words, the production conditions directly affect the resulting particle size and indirectly the physical stability when the surface hydrophobicity is changed.

Such changes in surface hydrophobicity caused by different production methods (BM vs HPH and lab scale vs. scale-up) were detected by lower ZP values. Thus, ZP measurements could not only be used to predict the long-term stability of the nanosuspension regarding the API-stabilizer-combination but also to identify the best-suited production technique and processing condition.

In the DPPH-assays both flavonoids showed a time-dependent efficacy in scavenging the free radicals. This could be an advantage, as flavonoids exert their effects over a long time and thus a renewed administration after longer periods is sufficient. At the same time, it would not disturb the natural cellular respiration processes and cause a possible rebound. The cell tests confirmed that the antioxidant effect was sustained after a longer incubation period. For rutin NC, the antioxidative efficacy was found 24 h after the treatment. At the same time, cell growth or the formation of cellular defense enzymes against RONS were induced. However, such investigations also nicely demonstrated that NC (BI-6C9 and hesperetin) were as effective as the corresponding solution.

Owing to various approaches for the development of tailor-made drug NC, improvements in size, stability, and effectiveness have been investigated that can be applied to other NC formulations while respecting the physico-chemical properties of the API and especially their resulting surface properties.

6 Summary

In the present work, the NC of three poorly water-soluble antioxidants, BI-6C9, hesperetin and rutin, were prepared, characterized, and tested in suitable cell culture models. In addition, the production was optimized to obtain tailor-made NC for the treatment of oxidative stress-related diseases. These should be formulated to increase the solubility and thus bioavailability of the antioxidants used, while meeting the requirements of different administration routes regarding particle size, physical stability, and the final formulation.

The synthesized compound, BI-6C9, was aimed to be converted into a formulation suitable for i.v. application in a resource-saving manner. This was successfully realized by using a small scale BM process in a batch size of 2 mL. A time and resource-saving pre-screening of four stabilizers (SDS, PLC, Tween 80, Span 20) was performed by microscopy, where SDS was identified to be the most suitable stabilizer. Then, BI-6C9 was successfully converted to NC with an average particle size of about 600 nm applying a milling time of 24 h. However, only the stabilizer Tween 80 is approved as save for intracortical or intracerebral application. By optimizing the milling time to 90 h, a Tween 80-stabilized nanosuspension was successfully produced and comparable to the SDS formulation regarding particle size and stability over seven days of storage. Also, in a cell culture model of oxidative stress-induced neuronal cell death, both nanosuspensions showed the same protective dose-response curve as a BI-6C9 solution in DMSO. This means that both NC formulations have reached their highest pharmacological efficacy because a formulation cannot become more effective than its solution. In addition, as an advantage, no harmful solvents were used for the cell culture studies and, especially, for a possible *in-vivo* application. By optimizing the preparation and stabilization with Tween 80 and SDS, tailor-made i.v. or orally applicable NC formulations were successfully developed for the treatment of neuronal oxidative stress.

Concerning the use of hesperetin, the aim was to produce NC with different sizes by using different methods, to get more knowledge about the size-dependent efficacy of NC. For this purpose, hesperetin was stabilized with PLC and tailor-made NC in the range of 170 to 800 nm were prepared by modifying the HPH or using a BM process. It was shown that the BM process resulted in the smallest NC with the narrowest size distribution and in particles with a more hydrophobic surface. The NC formulations differing in size were then tested in solubility studies and methods to determine the AOC. The dissolution velocity, solubility in water, and AOC increased with decreasing particle size, and was thus most pronounced for NC < 200 nm. Moreover, contrary to expectations, the NC exhibited a higher AOC than their solution. A similar effect was also observed in an Alzheimer's cell model, where the NC at low concentration showed the same efficacy as a hesperetin solution but with increasing concentration, even a higher efficacy compared to a hesperetin solution was observed. When using

higher concentrations of the hesperetin solution the efficacy started to decrease. In terms of the NC particle size dependency, the antioxidant effect of hesperetin NC in the cell model increased with concentration and with decreasing particle size. It has been shown that the AOC and the antioxidant effect in cell culture model of a hesperetin solution decreased because partial precipitations have occurred. The formation of these only microscopically visible hesperetin crystals lowered the drug concentration in solution and thus the possibility of uptake by the cells. To avoid misinterpretation of a declining dose-response curve in the future, it is important to investigate the dilution used in advance. The full potential of NC was shown the smaller they are, i.e. no solvent impairments along with an increased dissolution rate, kinetic solubility, and biological activity. Therefore, if possible, NC with an average particle size < 200 nm should preferably be prepared.

Finally, rutin should be formulated for a pulmonary application with additionally improved solubility. For this purpose, in the first step, rutin NC were successfully prepared from 13 different stabilizers and stabilizer mixtures by using HPH in an extensive study and the stability was determined over a period of one year. The rutin nanosuspensions exhibited an average particle size of 300 to 400 nm which was depending on the stabilizer used. For further process steps, the most stable nanosuspension was used. The idea behind this was, that the most stable formulation would lead to the least issues, such as agglomeration or particle growth, in subsequent processing steps. Interestingly, the formulation with the smallest NC was not the most stable and the one with the largest NC was not the most unstable over a storage period of one year. For long-term physical stabilization, it was shown that a combination of two chemically and structurally different stabilizers can complement each other synergistically. In this case, small lipophilic surfactants rapidly adhere onto the hydrophobic particle surface and are complemented by large slightly more hydrophilic surfactants. Thus, the larger NC surfactant structure becomes more hydrophilic on the outside and thus well-accepted in the aqueous medium and also sterically shielded other particles.

The nanosuspensions were stable for at least three months depending on the stabilizer, but the nanosuspensions decreased in physical and/or microbiological stability after one year of storage. This was prevented when the nanosuspensions were stored in a frozen state, i.e. the nanosuspension can be easily thawed at any time without a loss of biological, chemical and physical stability. However, it had also been shown that the addition of other additives, such as a preservative, can be disturbing for the freeze-thaw process and in turn jeopardize the physical stability of the nanosuspension. Hence, freeze-thawing has been demonstrated to be a complementary method to assess the degree of stability of the nano-formulation. If interfering excipients were added, the nanosuspension broke after thawing, which would otherwise only have been noted after some days of storage during the stability study. Proceeding from the frozen rutin nanosuspension, the water can be easily removed by sublimation during lyophilization, resulting in a dried NC formulation that is stable over the long-term.

Again, the aim was to develop a NC formulation for the pulmonary application. The idea was, therefore, to formulate a dry powder for inhalation from the dried nanosuspension. This was realized after using a cryomill and optimizing the formulation. The greatest effect was achieved by adding magnesium stearate, which doubled the inhalable fraction to about 34%. For comparison, an inhalable formulation should be developed using spray-drying. Despite extensive adjustments in the process parameters and the formulation, no powder for pulmonary application could be obtained.

The next step was to characterize the freeze-dried powder for inhalation and test it *in-vitro* for kinetic solubility, dissolution velocity, and antioxidant activity. Even though the NC could be successfully freeze-dried without further additives, the use of mannitol and cysteine provided advantages. So, the use of mannitol not only proved to be a good cryo-/lyoprotectant but also was effective as a solubility enhancer and hence the release of the NC with the almost immediate dissolution of rutin was comparable to the nanosuspension. With the use of cysteine as cryo-/lyoprotectant, the release was slightly delayed, but the antioxidant activity was improved when compared to the nanosuspension. Both flavonoids rutin and hesperetin also showed a time-dependent AOC, of which the reaction kinetic was additionally influenced by the solvent. In the cell culture study of oxidative stress using lung epithelial cells, it was shown that the combination of freeze-dried rutin NC with cysteine protected the cells best from oxidative stress. A simultaneous application of rutin NC and a peroxide in the presence of the cells also protected them from damaging effects. The reason for this was the radical scavenging properties of flavonoids.

To conclude, tailor-made NCs for different targets and application routes were successfully prepared in this dissertation. These not only showed sufficient stability, excellent solubility and increased dissolution velocity compared to the coarse material but were at least as good as a corresponding solution of the drug in cell culture studies.

7 Zusammenfassung der Arbeit

In der vorliegenden Arbeit wurden Nanokristalle (NC) von drei schwer wasserlöslichen Antioxidantien, BI-6C9, Hesperetin und Rutin, hergestellt, charakterisiert und in geeigneten Zellkultur-modellen getestet. Darüber hinaus wurde die Herstellung so optimiert, dass für die Behandlung von aus oxidativem Stress bedingten Erkrankungen maßgeschneiderte NC gewonnen wurden. Diese sollten so formuliert werden, dass die Löslichkeit und die damit verbundene Bioverfügbarkeit der verwendeten Antioxidantien erhöht und sie gleichzeitig den Anforderungen verschiedener Applikationswege gerecht wurden in Hinblick auf Partikelgröße, physikalische Stabilität und Endformulierung.

Die synthetisierte Verbindung, BI-6C9, sollte ressourcensparend in eine Formulierung überführt werden, die sich zur i.v.-Anwendung eignet. Dies wurde erfolgreich mittels Perlenmahlens (BM) in einem kleinen Maßstab von 2 mL zu NC realisiert. Mit Hilfe eines mikroskopischen Vor-screenings mit vier Stabilisatoren (SDS, Tween 80, PLC, Span 20) konnte zeit- und ressourcen-sparend SDS als geeignetster Stabilisator ermittelt werden. So wurde bereits nach einer Mahldauer von 24 h BI-6C9 erfolgreich zu NC mit einer mittleren Partikelgröße von etwa 600 nm überführt. Für die intrakortikale oder intrazerebrale Anwendung ist jedoch nur Tween 80 als Stabilisator zugelassen. Durch Optimierung der Mahldauer auf 90 h konnte eine Tween 80-stabilisierte Nanosuspension produziert werden, die hinsichtlich der Partikelgröße und der Stabilität über einem Zeitraum von sieben Tagen der SDS-Formulierung vergleichbar war. Auch zeigten beide Nanosuspensionen in einem Zellkultur-model für durch oxidativen Stress ausgelösten neuronalen Zelltod die gleiche protektive Dosis-Wirkungs-Kurve wie eine BI-6C9-Lösung in DMSO. Das heißt, dass die beiden NC Formulierungen ihre maximale pharmakologische Wirksamkeit erreicht haben, denn besser wirksam als ihre Lösung kann eine Formulierung nicht werden. Hinzu kommt der Vorteil, dass sowohl für die Zellkulturstudien und vor allem bei einer möglichen *in-vivo* Anwendung keinerlei schädliche Lösungsmittel zum Einsatz kommen. Mittels optimierter Herstellung und Stabilisierung durch Tween 80 oder SDS wurde eine maßgeschneiderte i.v. bzw. oral applizierbare NC-Formulierung zur Behandlung von neuronalem oxidativem Stress erfolgreich entwickelt.

Bei der Verwendung von Hesperetin war es das Ziel, durch verschiedene Verfahren NC mit unterschiedlicher Größe zu erzeugen, mit deren Hilfe eine Aussage über die größenabhängige Wirkung getroffen werden kann. Dafür wurde Hesperetin mit PLC stabilisiert und mit Hilfe einer modifizierten HPH oder eines BM Verfahrens maßgeschneiderte NC im Bereich von 170 bis 800 nm hergestellt. Es wurde gezeigt, dass das BM-Verfahren zu den kleinsten NC mit der geringsten Größenverteilung sowie zu Partikeln mit einer hydrophoberen Oberfläche führte. Die sich in Größe unterscheidenden NC Formulierungen wurden anschließend in Löslichkeitsstudien und Methoden für eine antioxidative Wirkung getestet. Die Auflösungsgeschwindigkeit, die Löslichkeit in Wasser und die antioxidative

Kapazität nahmen mit abnehmender Partikelgröße zu, besonders bei NC < 200 nm. Zudem wiesen die NC entgegen den Erwartungen, auch eine höhere Kapazität als ihre Lösung auf. Ein ähnlicher Effekt wurde auch an einem Alzheimer Zellmodel festgestellt, bei dem die NC in niedriger Konzentration gleiche aber mit steigender Konzentration sogar eine höhere Wirksamkeit als eine Hesperetin-Lösung zeigte, weil die Wirksamkeit der Hesperetin-Lösung im Gegensatz zu den NC mit steigender Konzentration wieder abnahm. Bezogen auf die Größenanhängigkeit, stieg die Wirksamkeit der Hesperetin-NC im Zellmodell mit der Konzentration und mit sinkender Partikelgröße. Es konnte gezeigt werden, dass die antioxidative Kapazität und zelluläre antioxidative Wirkung der Hesperetin-Lösung abnahm, weil es zu einer partialen Ausfällung kam. Die Bildung dieser mikroskopisch sichtbaren Hesperetin-Kristalle senkten die Wirkstoff-Konzentration in Lösung und damit auch die Möglichkeit der Zellaufnahme. Um in Zukunft Fehlinterpretationen einer abfallenden Dosis-Wirkungs-Kurve zu vermeiden, ist es wichtig, im Vorfeld die verwendete Verdünnung zu untersuchen. Das volle Potenzial von NC, d.h. keine Beeinträchtigung durch Lösungsmittel neben einer erhöhter Auflösungsrate, kinetischer Löslichkeit und biologischer Aktivität, zeigte sich, je kleiner sie waren. Daher sollten, wenn möglich, vorzugsweise NC mit einer mittleren Partikelgröße < 200 nm hergestellt werden.

Zu guter Letzt sollte Rutin für eine inhalative Anwendung mit verbesserter Löslichkeit formuliert werden. Hierfür wurden im ersten Schritt in einer umfangreichen Studie aus 13 verschiedenen Stabilisatoren(-gemischen) Rutin-NC erfolgreich mittels HPH hergestellt und die Stabilität über einem Zeitraum von einem Jahr bestimmt. Die hergestellten Rutin-Nanosuspensionen wiesen eine mittlere Partikelgröße von 300 bis 400 nm abhängig vom Stabilisator auf. Für weitere Prozessschritte wurde die stabilste Nanosuspension verwendet, vor dem Hintergrund, dass für diese die wenigsten Probleme, wie Agglomeration oder Partikelwachstum, in weiteren Prozessschritten erwartet werden. Interessanterweise war die Formulierung mit den kleinsten NC nicht die stabilste und die mit den größten NC nicht die instabilste über ein Lagerungszeitraum von einem Jahr. Für eine physikalische Langzeitstabilisierung konnte gezeigt werden, dass eine Kombination aus zwei chemisch-strukturell unterschiedlichen Stabilisatoren synergistisch eine optimale Ergänzung ergeben können. Hierbei lagern sich kleine lipophile Tenside schnell an der hydrophoben Partikeloberfläche an und werden von großen hydrophileren Tensiden ergänzt. Damit wird die größere NC-Tensid-Struktur nach außen hydrophiler und im wässrigen Medium akzeptiert und von anderen Partikeln sterisch abgeschirmt.
Die Nanosuspensionen waren abhängig vom Stabilisator für mindestens drei Monate stabil, jedoch zeigten die Nanosuspensionen Einbußen in der physikalischen und/ oder mikrobiologischen Stabilität nach der Lagerung für ein Jahr. Diese konnte erheblich gesteigert werden, wenn die Nanosuspensionen im gefrorenen Zustand gelagert wurden, d.h. die Nanosuspension konnte jeder Zeit ohne Verluste der biologischen, chemischen und physikalischen Stabilität leicht aufgetaut werden. Es hat sich jedoch auch gezeigt, dass der Zusatz weiterer Zusatzstoffe, wie Konservierungsmittel, den Gefrierprozess

stören kann und damit die physikalische Stabilität gefährdet. Das Einfrieren und Auftauen bewies sich auch als ergänzende Methode, um abzuschätzen, inwieweit die Nanoformulierung stabil ist. Wurden störende Hilfsstoffe hinzugegeben, ist die Nanosuspension nach dem Auftauen gebrochen, was sonst erst nach Tagen einer aufwendigen Stabilitätsstudie aufgefallen wäre. Ausgehend von der gefrorenen Rutin Nanosuspension, kann das Wasser durch Sublimation während der Lyophilisation leicht entfernt werden, wodurch eine getrocknete langzeitstabile NC-Formulierung entsteht.
Ziel war es eine NC-Formulierung für die pulmonale Anwendung zu entwickeln. Die Idee war daher, aus der getrockneten Nanosuspension ein Trockenpulver zur Inhalation zu formulieren. Das wurde nach Einsatz einer Kryomühle und der Optimierung der Formulierung realisiert. Der größte Effekt wurde durch Zusatz von Magnesiumstearat erreicht, womit der Anteil der inhalierbaren Fraktion auf 34% verdoppelt wurde. Zum Vergleich sollte eine inhalierbare Formulierung mittels Sprühtrocknung entwickelt werden. Trotz umfangreichen Anpassungen in den Prozessparametern und der Formulierung konnte kein Pulver zur pulmonalen Anwendung gewonnen werden.
Das gefriergetrocknete Pulver zur Inhalation sollte im nächsten Schritt charakterisiert und *in-vitro* auf Löslichkeit, Lösungsgeschwindigkeit und antioxidative Aktivität getestet werden. Auch wenn sich die NC ohne weitere Zusatzstoffe erfolgreich gefriertrocknen ließen, konnten durch Mannitol und Cystein Vorteile gewonnen werden. So erwies sich der Einsatz von Mannitol nicht nur als guter Kryo-/ Lyoprotektor, sondern überzeugte auch als Lösungsvermittler, d.h. die Freisetzung der NC und damit nahezu sofortige Auflösung des Rutins war der Nanosuspension vergleichbar. Mit dem Einsatz von Cystein als Kryo-/ Lyoprotektor wurde die Freisetzung leicht verzögert, aber die antioxidative Aktivität verbessert. Die beiden Flavonoide Rutin und Hesperetin zeigten außerdem eine zeitabhängige antioxidative Kapazität, deren Geschwindigkeit zusätzlich vom Lösungsmittel beeinflusst wurde. Im Zellversuch zum oxidativen Stress an Lungen-Epithelzellen konnte gezeigt werden, dass die kombinierte Gefriertrocknung aus Cystein mit Rutin NC die Zellen am besten vor oxidativen Stress schützte. Eine gleichzeitige Anwendung von Rutin NC und einem Peroxid in Gegenwart der Zellen schütze diese ebenfalls vor schädlichen Folgen. Grund dafür sind die radikalfangenden Eigenschaften von Flavonoiden.

Abschließend lässt sich zusammenfassen, dass maßgeschneiderte NC für verschiedene Targets und Applikationsformen erfolgreich im Rahmen dieser Dissertation hergestellt wurden. Diese zeigten nicht nur eine ausreichende Stabilität, hervorragende Löslichkeit und erhöhte Lösungsgeschwindigkeit verglichen mit dem Rohmaterial, sondern waren mindestens genauso gut wie eine entsprechende Lösung des Wirkstoffes in *in-vitro* Zellstudien.

8 Appendix

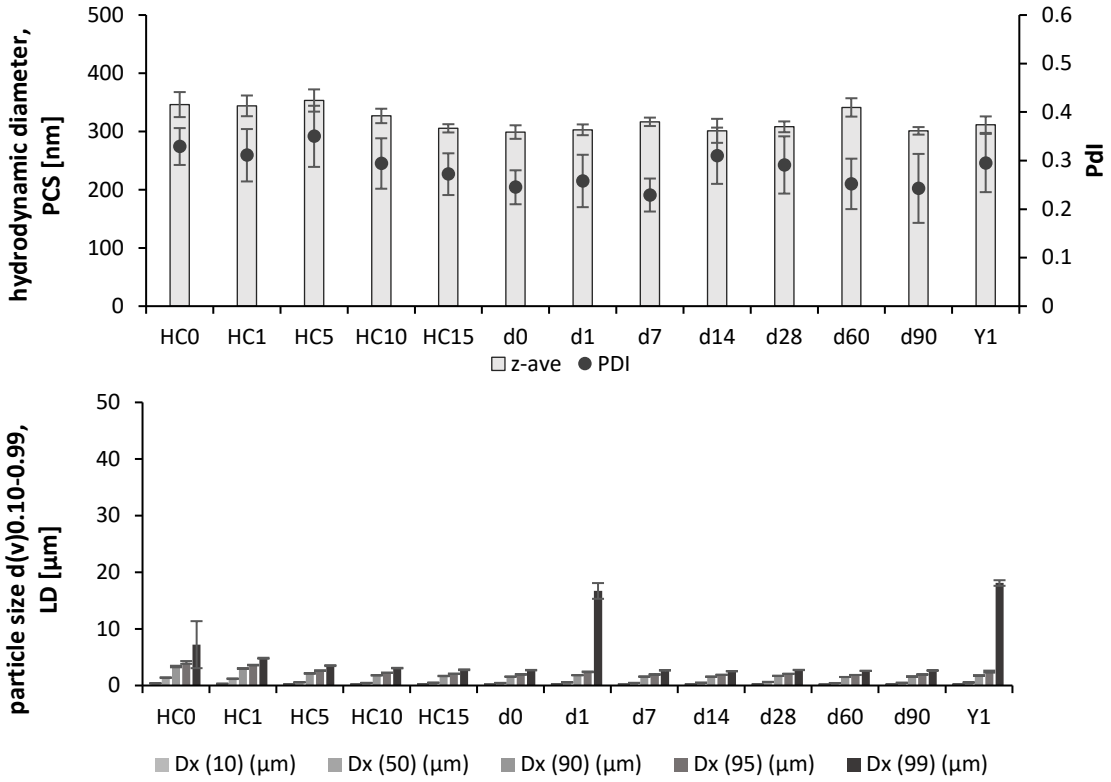

Supplementary Figure S1: Rutin NC stabilized with BSA. *Particles were characterized by PCS regarding hydrodynamic diameter and polydispersity (PdI) (upper), and by LD (lower), during the process after determined numbers of homogenization cycles (HC) and days of storage (d0-90) up to one year (Y1).*

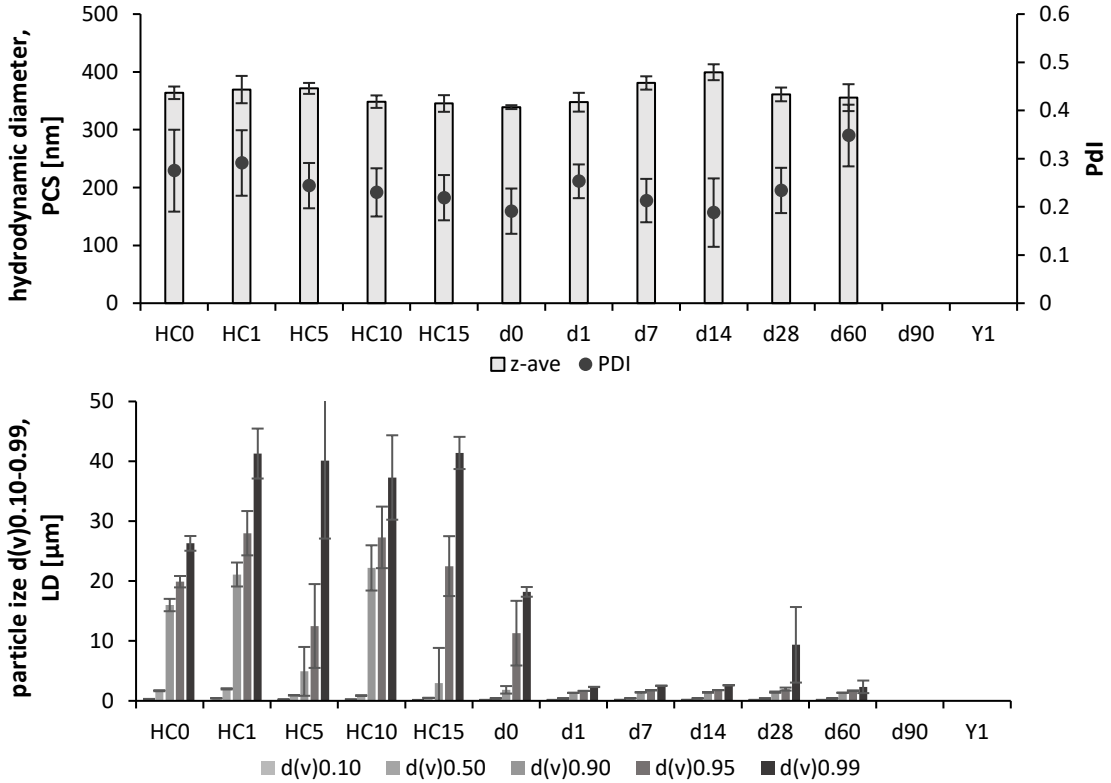

Supplementary Figure S2: Rutin NC stabilized with Tween 80.

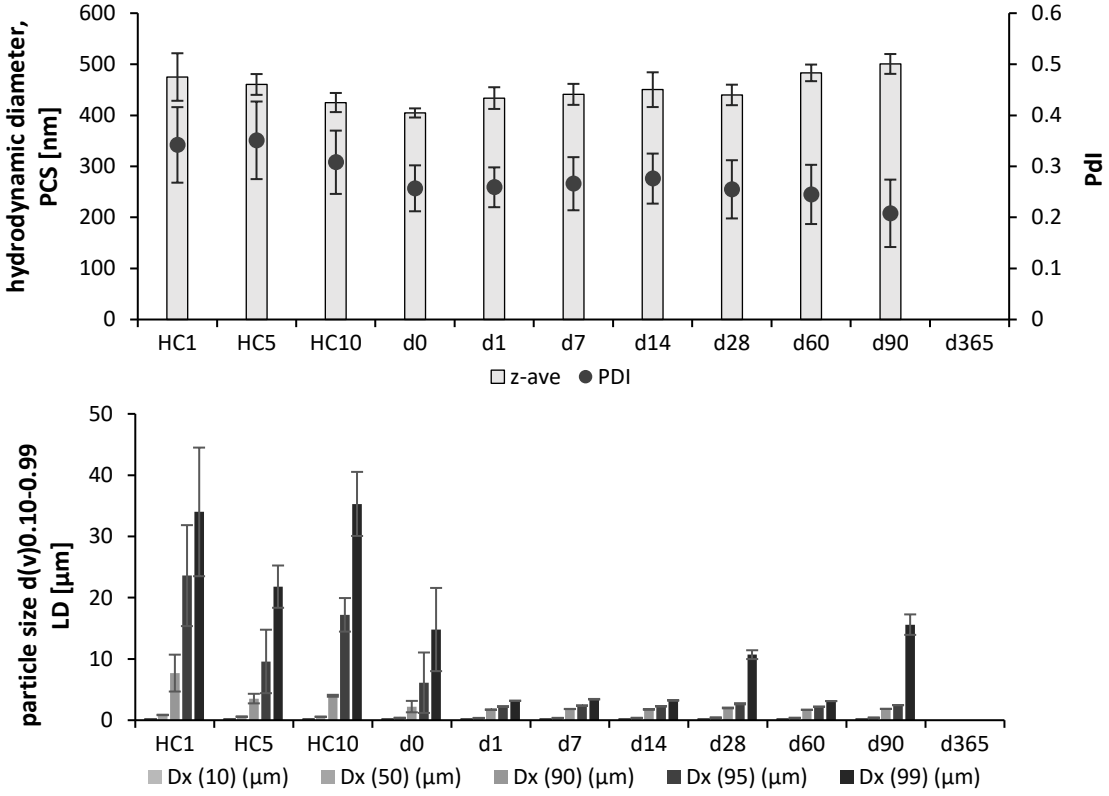

Supplementary Figure S3: Rutin NC stabilized with Lecithin S75.

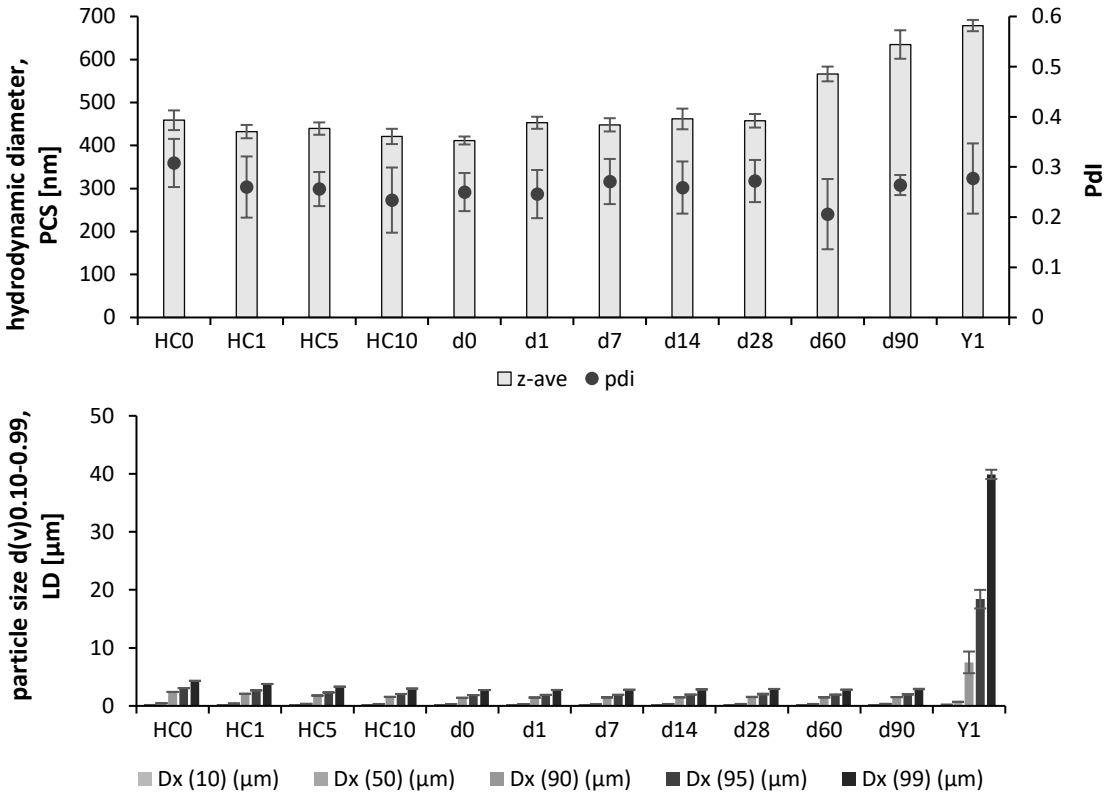

Supplementary Figure S4: Rutin NC stabilized with Lecithin E80.

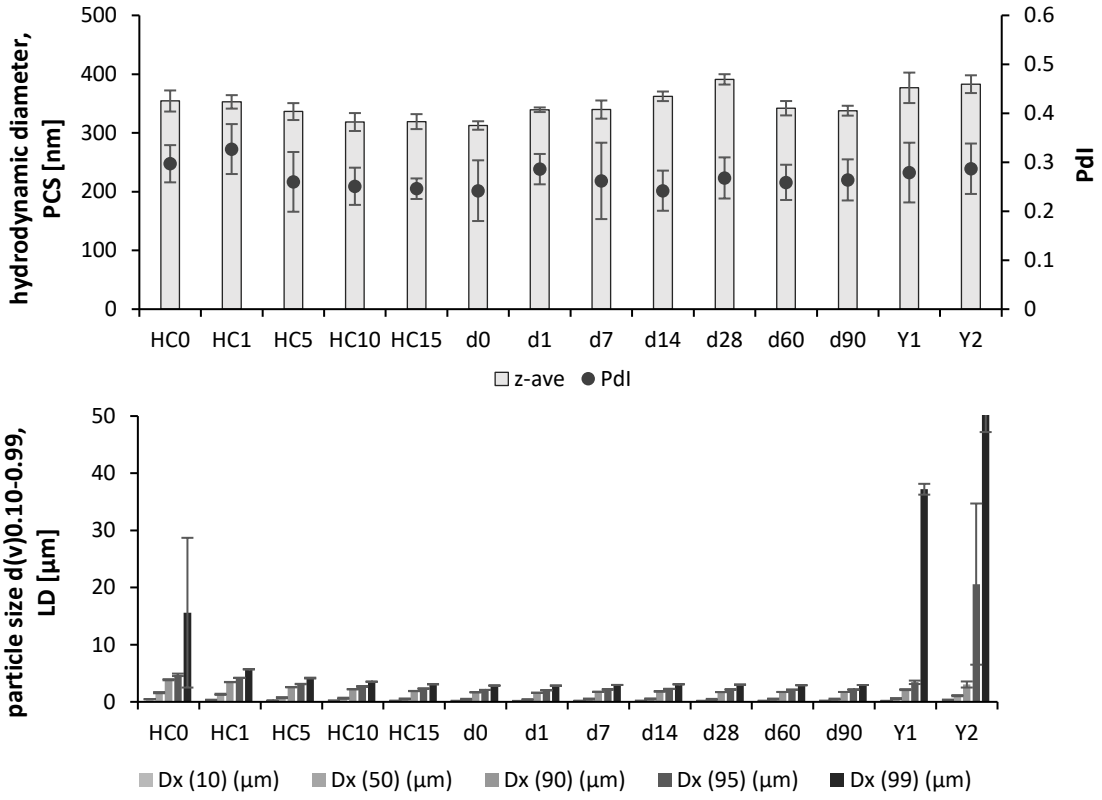

Supplementary Figure S5: Rutin NC stabilized with Poloxamer 188.

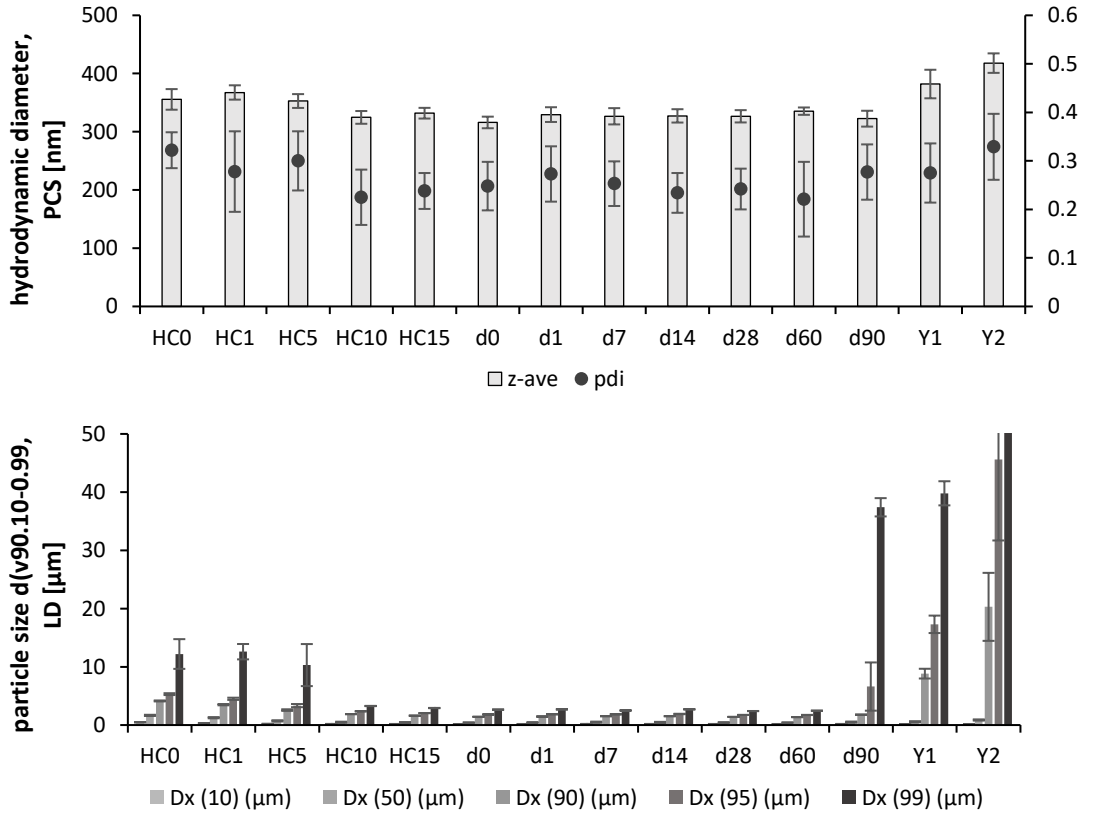

Supplementary Figure S6: Rutin NC stabilized with a mixture of BSA and Tween 80.

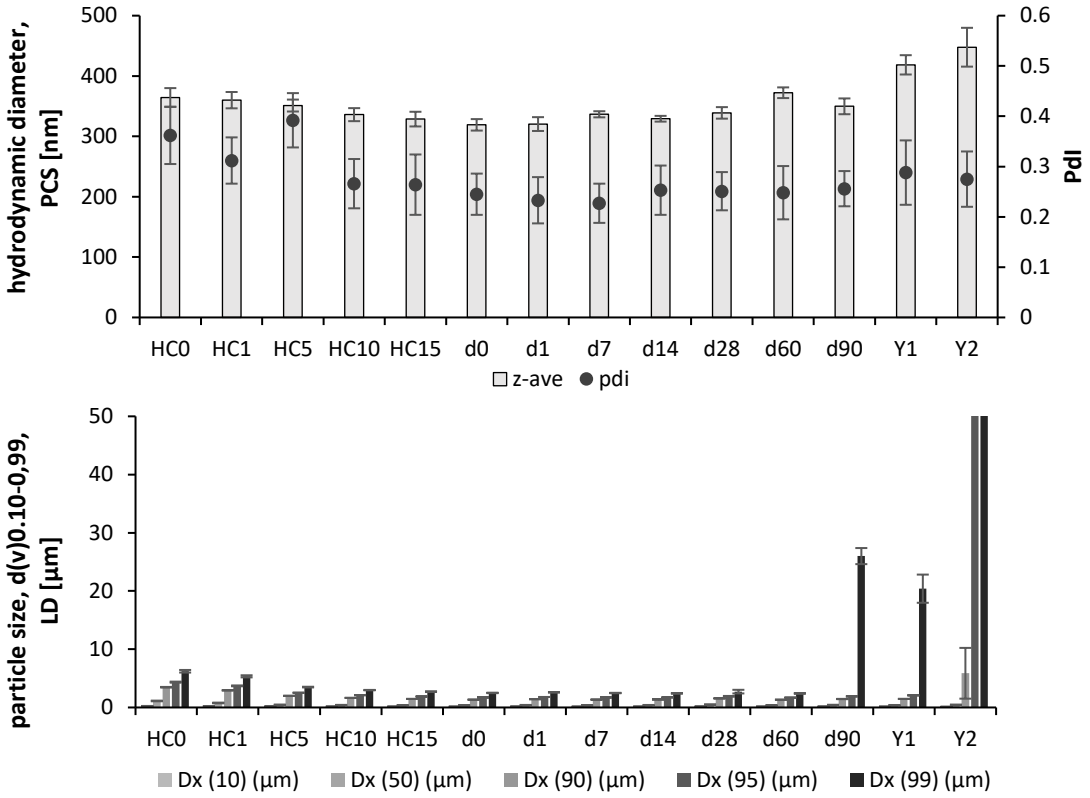

Supplementary Figure S7: Rutin NC stabilized with a mixture of BSA and Lecithin S75.

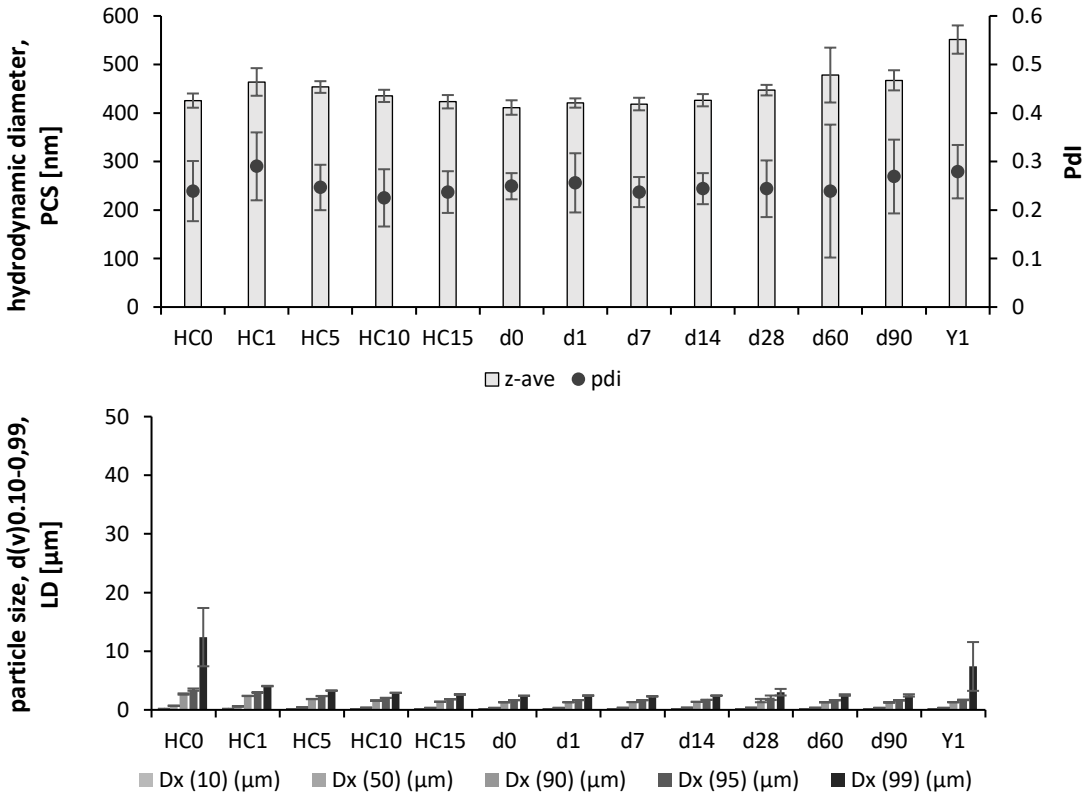

Supplementary Figure S8: Rutin NC stabilized with a mixture of BSA and Lecithin E80.

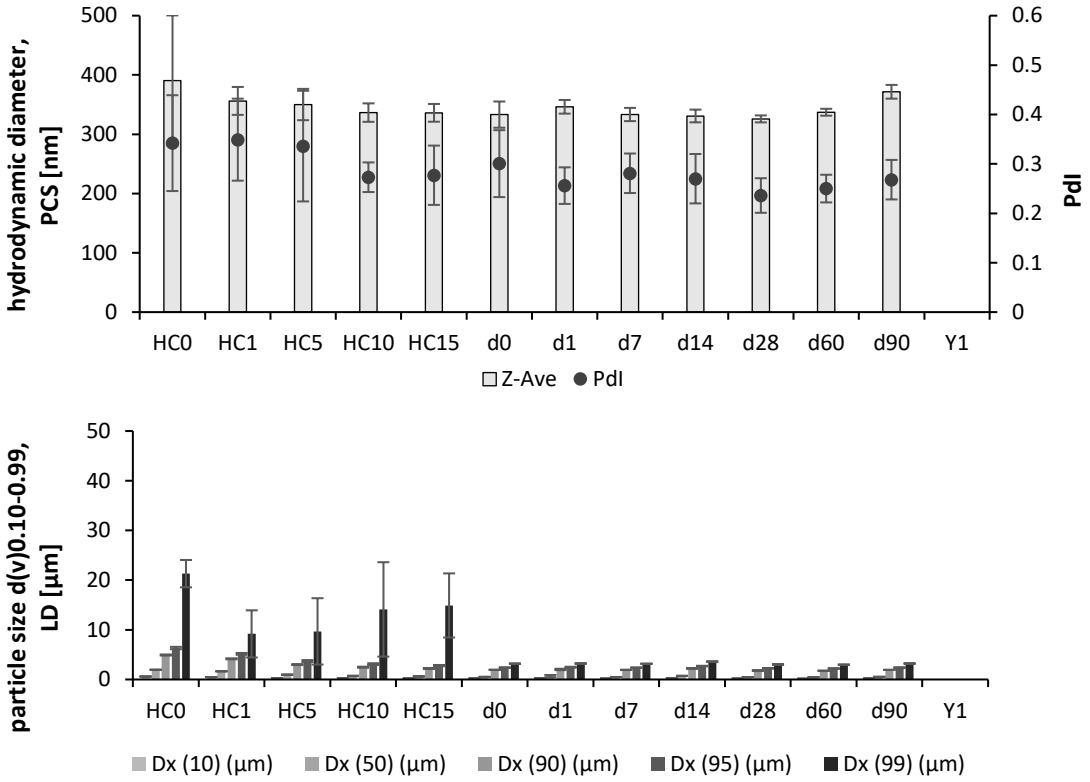

Supplementary Figure S9: Rutin NC stabilized with a mixture of BSA and Poloxamer 188.

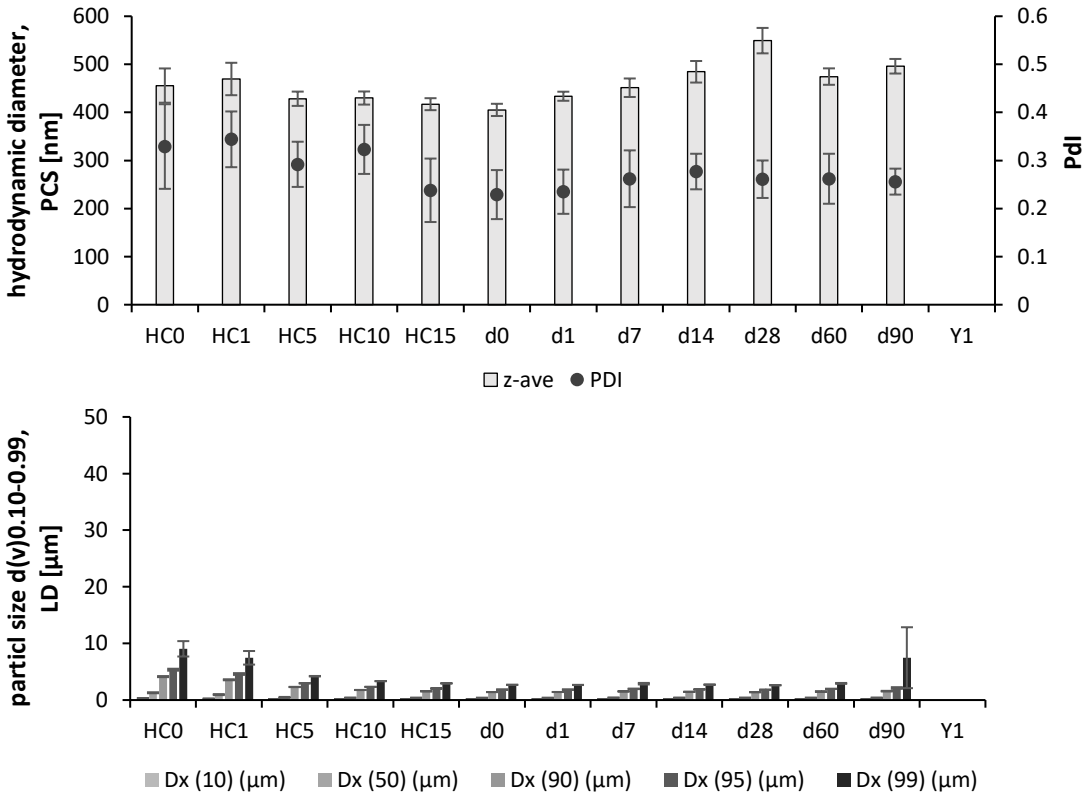

Supplementary Figure S10: Rutin NC stabilized with a mixture of Lecithin S75 and Poloxamer 188.

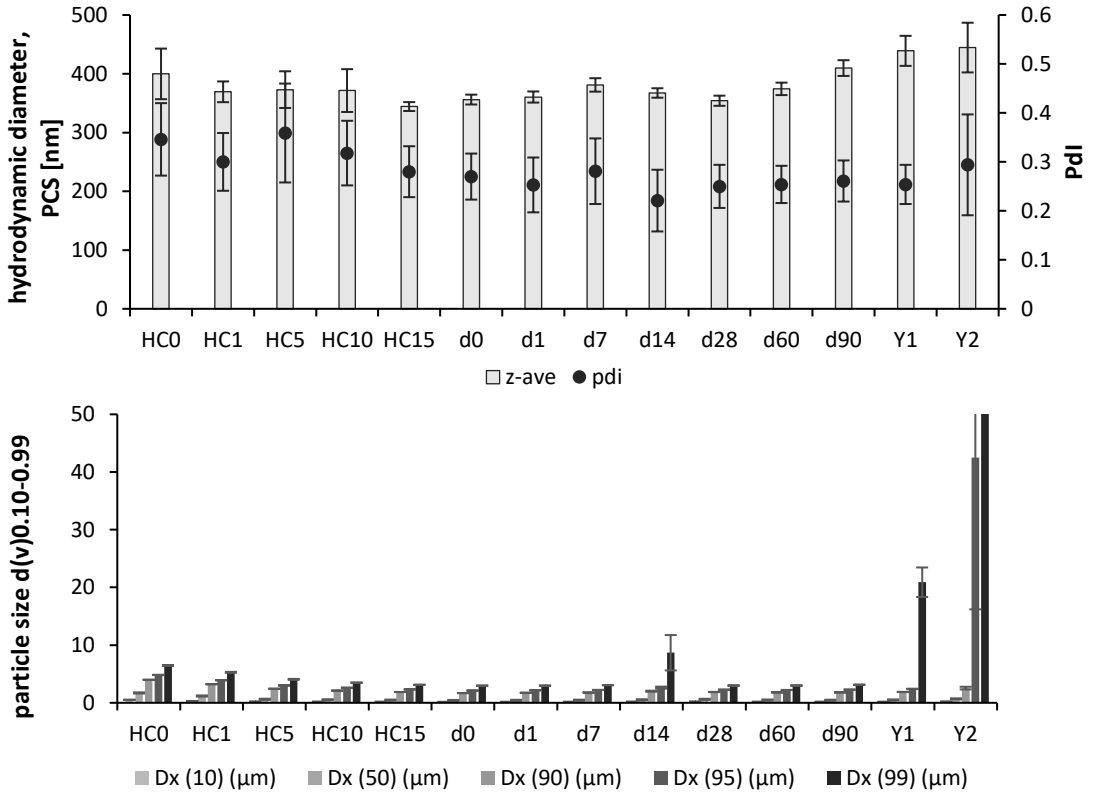

Supplementary Figure S11: Rutin NC stabilized with a mixture of Lecithin S75 and Tween 80.

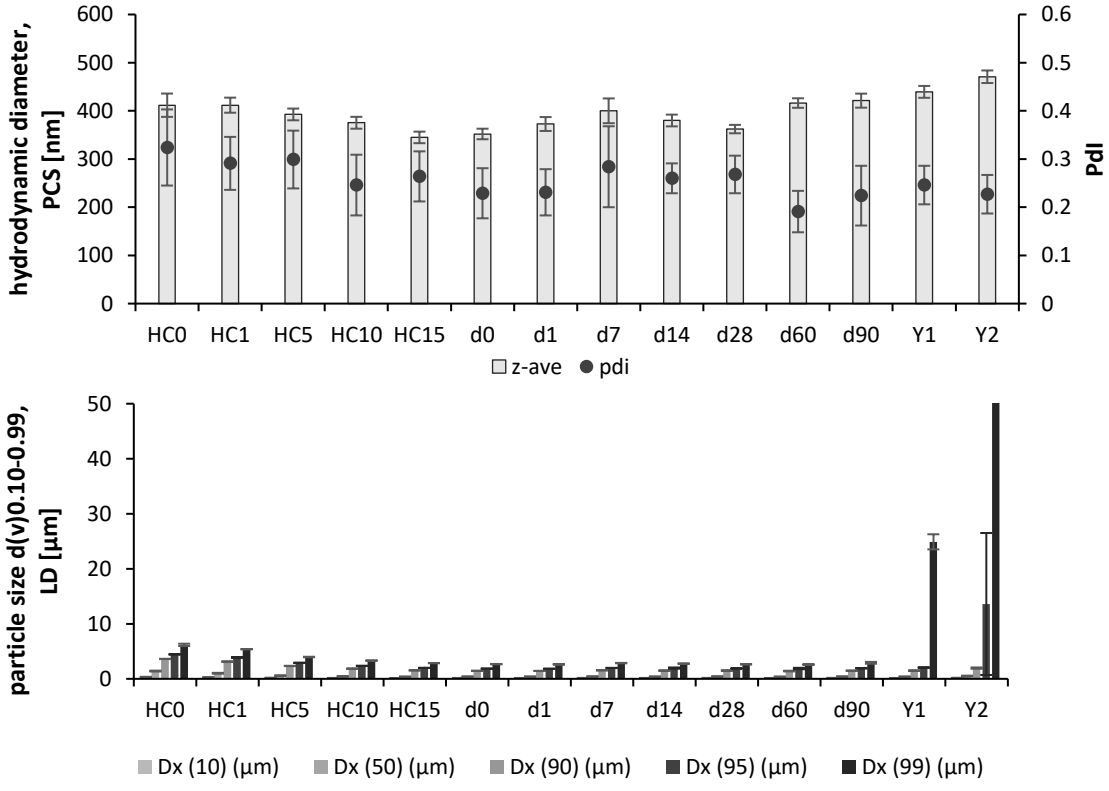

Supplementary Figure S12: Rutin NC stabilized with a mixture of Lecithin E80 and Tween 80.

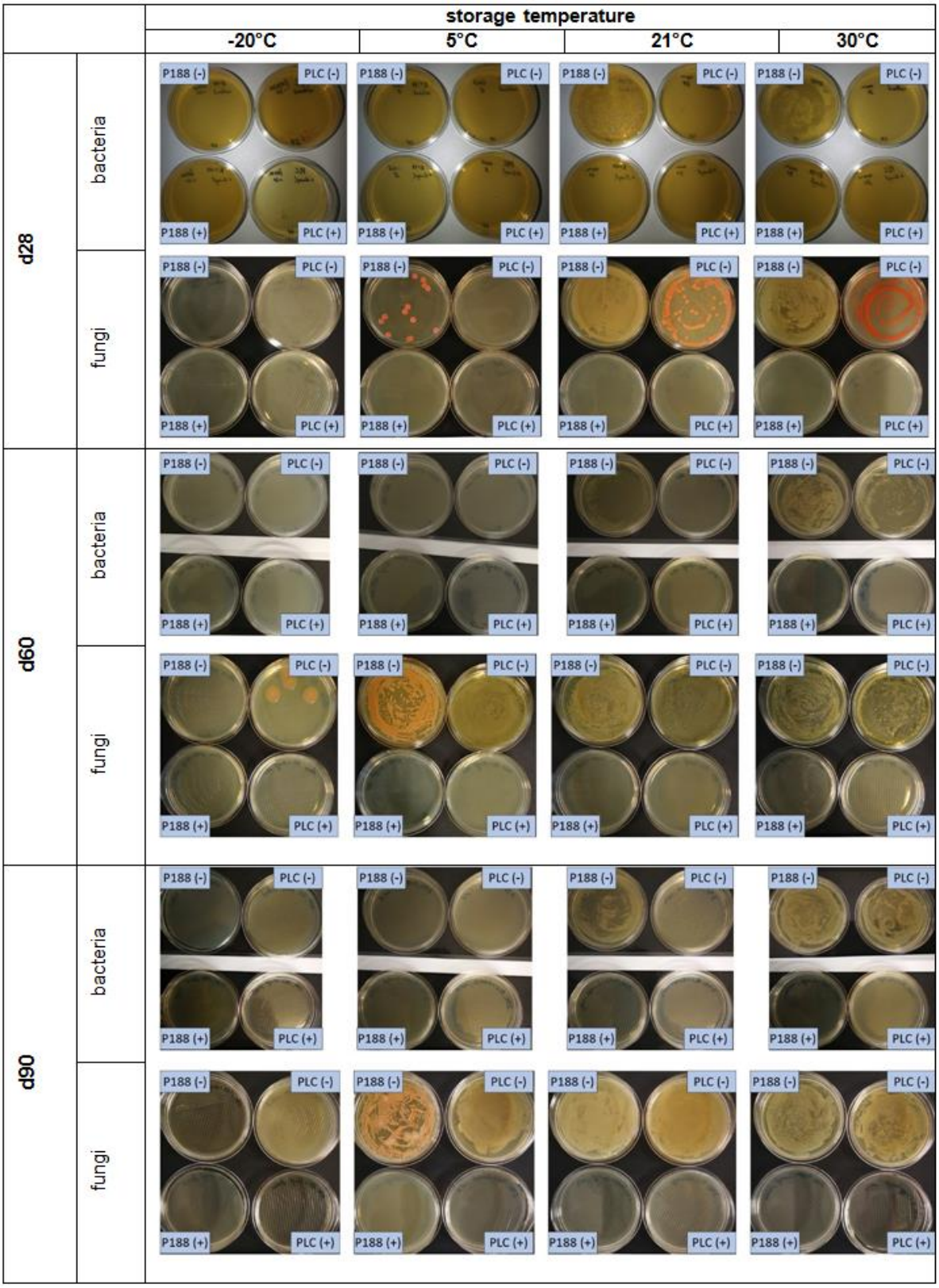

Supplementary Figure S13: *Images of the incubated petri dishes for the determination of microbial stability over three months of storage. rutin nanosuspension stabilized with Poloxamer 188 (P188), stabilized with Plantacare 2000 (PLC), (+) = preserved with Euxyl PE9010, (-) non-preserved.*

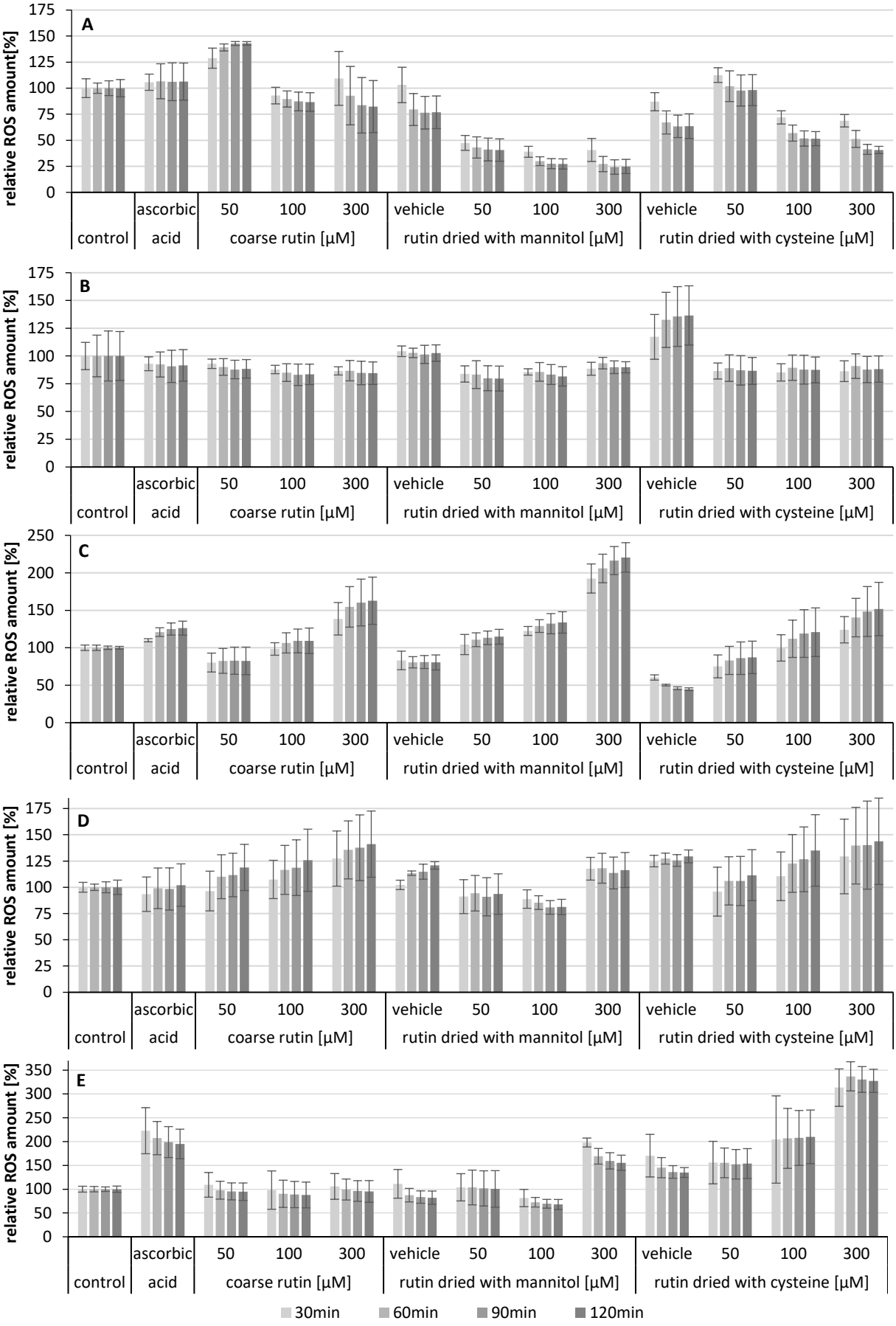

Supplementary Figure S14: *A549 cells were treated with antioxidants simultaneously (A), or pre-incubated for 2h (B), 4h (C), 8h (D) and 24h (E), ROS amount was measured after 30, 60, 90 and 120 min incubation time using the DCFDA-assay.*

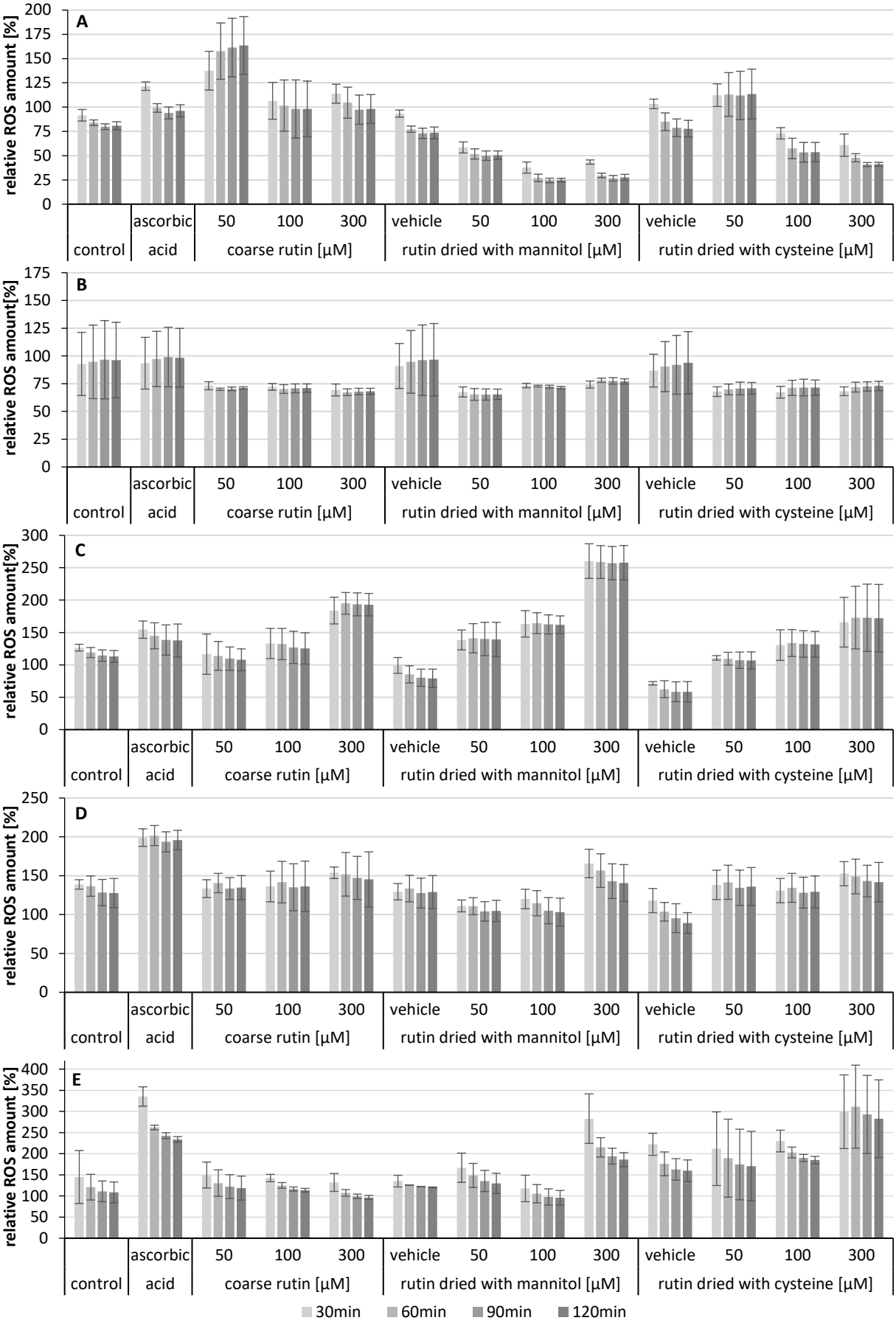

Supplementary Figure S15: *A549 cells were first incubated with antioxidants simultaneously (A), or pre-incubated for 2h (B), 4h (C), 8h (D) and 24h (E), and then stressed with TBH for 30, 60, 90 and 120 min. ROS amount was determined using the DCFDA-assay.*

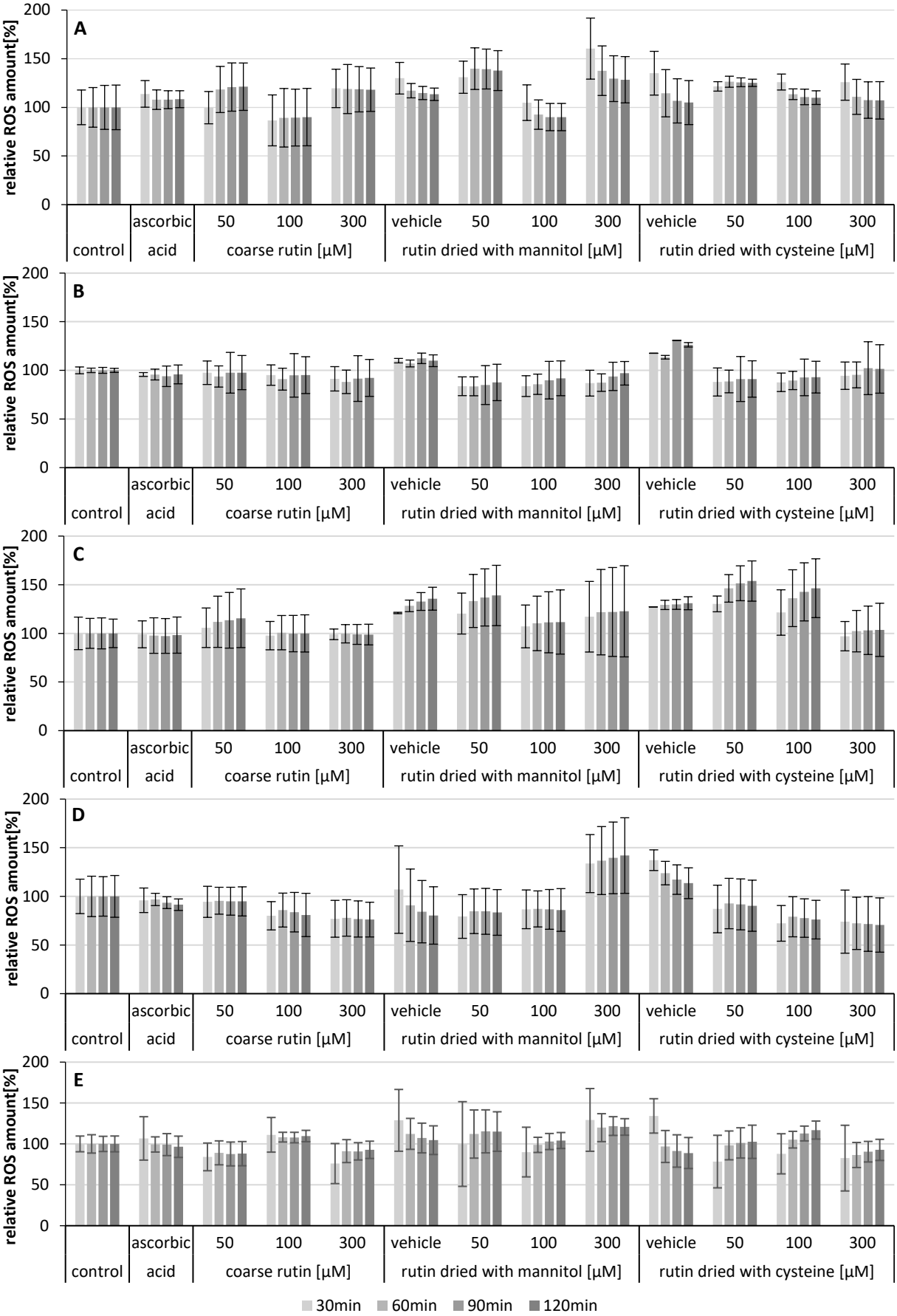

Supplementary Figure S16: *H441 cells only treated with antioxidants simultaneously (A), or after a pre-incubation time of 2h (B), 4h (C), 8h (D) and 24h (E). ROS amount was measured after 30, 60, 90 and 120 min incubation time using the DCFDA-assay.*

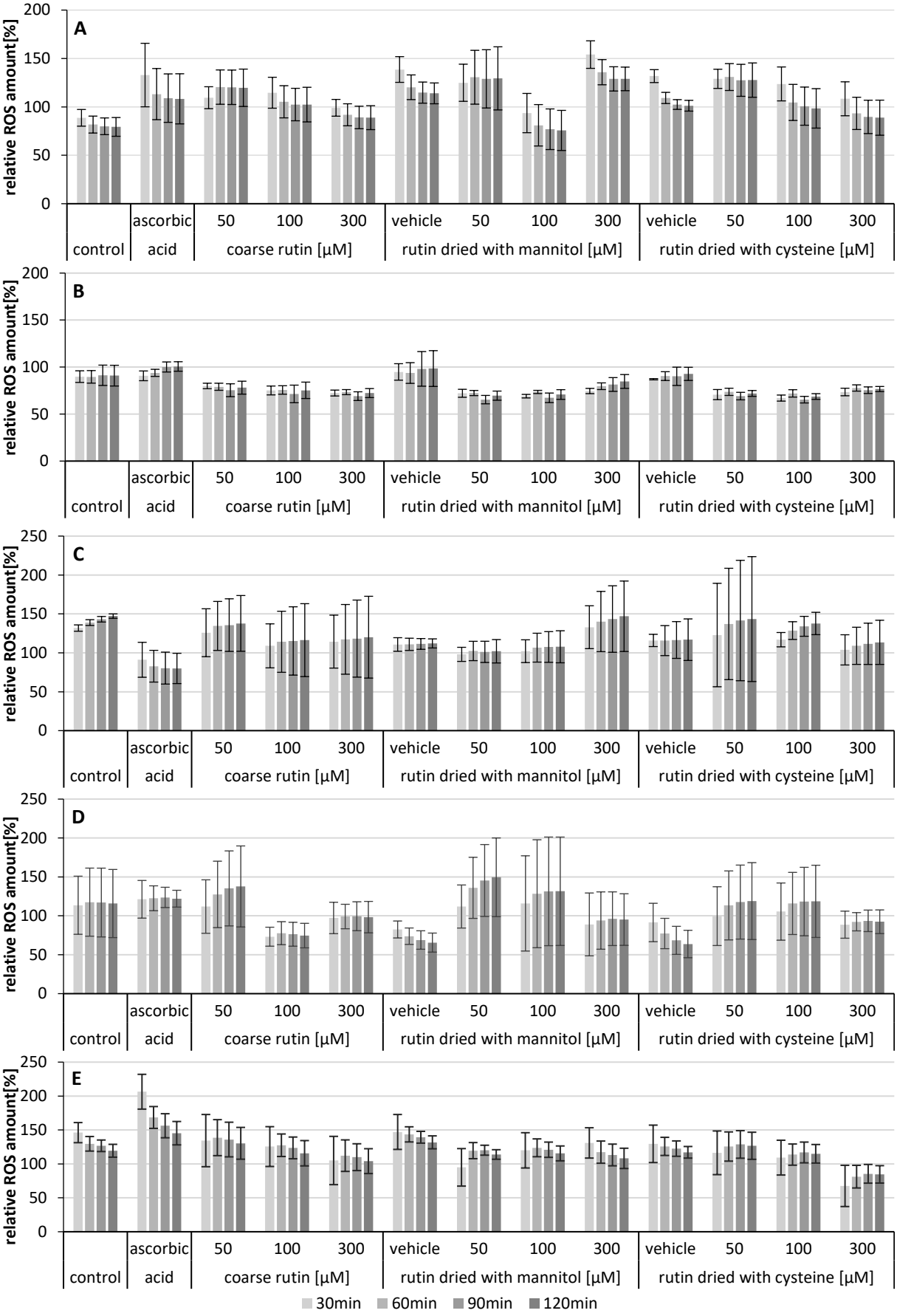

Supplementary Figure S17: *H441 cells were first treated with antioxidants simultaneously (A), or after a pre-incubation time of 2h (B), 4h (C), 8h (D) and 24h (E), and then stressed with TBH for 30, 60, 90 and 120 min. ROS amount was measured using the DCFDA-assay.*

9 Abbreviations

Aβ	amyloid beta peptide
AD	Alzheimer's disease
AOC	antioxidant capacity
API	active pharmaceutical ingredient
ATP	adenosine triphosphate
BCS	biopharmaceutics classification system
BID	BH3 interacting-domain death agonist
BM	Bead milling
BSA	bovine serum albumin
CD	cyclodextrin
CFU	colony forming unit
COPD	chronic obstructive pulmonary disease
COX	cyclooxygenase
DCF	2',7'-dichlorofluorescein
DCFDA	2',7'-dichlorofluorescein diacetate
$d_{hydrodynamic}$	hydrodynamic diameter
DLS	dynamic light scattering
DMEM	Dulbecco's Modified Eagle's Medium
DMSO	dimethyl sulfoxide
DNA	deoxyribonucleic acid
DPPH	2,2-diphenyl-1-picrylhydrazyl
DSC	differential scanning calorimetry
d(v)	volume-based particle diameter
e.g.	"exempli gratia" – for example
FBS	fetal bovine serum
FCS	fetal calf serum
FDA	US Food & Drug Administration
FT-ATR-IR	Fourier-transform attenuated total reflection infrared spectroscopy
GSH	glutathione
HC	high pressure homogenization cycle(s)
HLB	Hydrophilic Lipophilic Balance
HPH	high pressure homogenization
HPLC	high performance liquid chromatography
IC_{50}	half maximal inhibitory concentration
i.e.	"id est" – that means
IUPAC	International Union of Pure and Applied Chemistry
i.v.	intra venous

LPS	lipopolysaccharide
LDH	lactate dehydrogenase
MPO	myeloperoxidase
MTT	3-(4,5-dimethylthiazol-2-yl)-2,5-diphenyltetrazolium bromide
NADPH	nicotinamide adenine dinucleotide phosphate
NC	nanocrystal(s)
NGI	next generation pharmaceutical impactor
N/V	not available
PBS	phosphate buffered saline
PCS	photon correlation spectroscopy
PdI	polydispersity index
PEO	polyethylene oxide
PLC	Plantacare® 2000 UP
PLX	Poloxamer 188
PON	paraoxonase
PPO	polypropylene oxide
PVA	polyvinyl alcohol
PXRD	powder X-ray diffraction
ROS	reactive oxygen species
ROT	Rotenone
rpm	revolutions per minute
RPMI 1640	Gibco Roswell Park Memorial Institute, cell culture medium
SD	standard deviation
SDS	sodium dodecyl sulfate
SOD	superoxide dismutase
TBH	*tert*-butyl hydroperoxide
Tg	glass transition temperature
TNF	tumor necrose factor
Tw80	Tween® 80
UV-Vis	ultraviolet - visible light
w/w	weight/weight
ZP	zeta potential

10 References

1. Wiegman CH, Michaeloudes C, Haji G, Narang P, Clarke CJ, et al. Oxidative stress-induced mitochondrial dysfunction drives inflammation and airway smooth muscle remodeling in patients with chronic obstructive pulmonary disease. J Allergy Clin Immunol 136 (2015): 769-80.
2. Ansari MA, Scheff SW. Oxidative stress in the progression of Alzheimer disease in the frontal cortex. J Neuropathol Exp Neurol 69 (2010): 155-67.
3. Ozcan A, Ogun M. Biochemistry of Reactive Oxygen and Nitrogen Species. In: Gowder SJT, editor. Basic Principles and Clinical Significance of Oxidative Stress. InTech; 2015.
4. Giustarini D, Dalle-Donne I, Tsikas D, Rossi R. Oxidative stress and human diseases: Origin, link, measurement, mechanisms, and biomarkers. Crit Rev Clin Lab Sci 46 (2009): 241-81.
5. Salisbury D, Bronas U. Reactive oxygen and nitrogen species: impact on endothelial dysfunction. Nurs Res 64 (2015): 53-66.
6. Valavanidis A, Vlachogianni T, Fiotakis K, Loridas S. Pulmonary oxidative stress, inflammation and cancer: respirable particulate matter, fibrous dusts and ozone as major causes of lung carcinogenesis through reactive oxygen species mechanisms. Int J Environ Res Public Health 10 (2013): 3886-907.
7. Khosravi M, Poursaleh A, Ghasempour G, Farhad S, Najafi M. The effects of oxidative stress on the development of atherosclerosis. Biol Chem 400 (2019): 711-32.
8. Sakamoto T, Imai H. Hydrogen peroxide produced by superoxide dismutase SOD-2 activates sperm in Caenorhabditis elegans. J Biol Chem 292 (2017): 14804-13.
9. Harrison JE, Schultz J. Studies on the chlorinating activity of myeloperoxidase. J Biol Chem 251 (1976): 1371-4.
10. Adams L, Franco MC, Estevez AG. Reactive nitrogen species in cellular signaling. Exp Biol Med (Maywood) 240 (2015): 711-7.
11. Wei SJ, Botero A, Hirota K, Bradbury CM, Markovina S, et al. Thioredoxin nuclear translocation and interaction with redox factor-1 activates the activator protein-1 transcription factor in response to ionizing radiation. Cancer Res 60 (2000): 6688-95.
12. Winter AN, Ross EK, Daliparthi V, Sumner WA, Kirchhof DM, et al. A Cystine-Rich Whey Supplement (Immunocal®) Provides Neuroprotection from Diverse Oxidative Stress-Inducing Agents In Vitro by Preserving Cellular Glutathione. Oxid Med Cell Longev 2017 (2017): 3103272.
13. Shekhanawar M, Shekhanawar SM, Krisnaswamy D, Indumati V, Satishkumar D, et al. The role of 'paraoxonase-1 activity' as an antioxidant in coronary artery diseases. J Clin Diagn Res 7 (2013): 1284-7.
14. Huang Y, Wu Z, Riwanto M, Gao S, Levison BS, et al. Myeloperoxidase, paraoxonase-1, and HDL form a functional ternary complex. J Clin Invest 123 (2013): 3815-28.
15. Devarajan A, Bourquard N, Hama S, Navab M, Grijalva VR, et al. Paraoxonase 2 deficiency alters mitochondrial function and exacerbates the development of atherosclerosis. Antioxid Redox Signal 14 (2011): 341-51.
16. Schweikert E-M, Devarajan A, Witte I, Wilgenbus P, Amort J, et al. PON3 is upregulated in cancer tissues and protects against mitochondrial superoxide-mediated cell death. Cell Death Differ 19 (2012): 1549-60.
17. Drifte G, Dunn-Siegrist I, Tissières P, Pugin J. Innate immune functions of immature neutrophils in patients with sepsis and severe systemic inflammatory response syndrome. Crit Care Med 41 (2013): 820-32.
18. Nakae H, Endo S, Inada K, Takakuwa T, Kasai T, et al. Relationship between cytokines and leukotriene B4 in sepsis. Res Commun Chem Pathol Pharmacol 83 (1994): 151-6.
19. Osborn L. Leukocyte adhesion to endothelium in inflammation. Cell 62 (1990): 3-6.
20. Wynn TA, Vannella KM. Macrophages in Tissue Repair, Regeneration, and Fibrosis. Immunity 44 (2016): 450-62.
21. Vasavda C, Kothari R, Malla AP, Tokhunts R, Lin A, et al. Bilirubin Links Heme Metabolism to Neuroprotection by Scavenging Superoxide. Cell Chem Biol 26 (2019): 1450-1460.e7.

22. Reddy R. Reduced plasma antioxidants in first-episode patients with schizophrenia. Schizophr Res 62 (2003): 205-12.

23. Yao JK, Reddy R, McElhinny LG, van Kammen DP. Reduced status of plasma total antioxidant capacity in schizophrenia. Schizophr Res 32 (1998): 1-8.

24. Pisoschi AM, Pop A. The role of antioxidants in the chemistry of oxidative stress: A review. Eur J Med Chem 97 (2015): 55-74.

25. Sheehan JP, Swerdlow RH, Miller SW, Davis RE, Parks JK, et al. Calcium Homeostasis and Reactive Oxygen Species Production in Cells Transformed by Mitochondria from Individuals with Sporadic Alzheimer's Disease. J. Neurosci. 17 (1997): 4612-22.

26. Surmeier DJ, Guzman JN, Sanchez-Padilla J, Schumacker PT. The role of calcium and mitochondrial oxidant stress in the loss of substantia nigra pars compacta dopaminergic neurons in Parkinson's disease. Neuroscience 198 (2011): 221-31.

27. Tompkins MM, Basgall EJ, Zamrini E, Hill WD. Apoptotic-like changes in Lewy-body-associated disorders and normal aging in substantia nigral neurons. Am J Pathol 150 (1997): 119-31.

28. Starkov AA, Chinopoulos C, Fiskum G. Mitochondrial calcium and oxidative stress as mediators of ischemic brain injury. Cell Calcium 36 (2004): 257-64.

29. Qu J, Chen W, Hu R, Feng H. The Injury and Therapy of Reactive Oxygen Species in Intracerebral Hemorrhage Looking at Mitochondria. Oxid Med Cell Longev 2016 (2016): 2592935.

30. Rink A, Fung KM, Trojanowski JQ, Lee VM, Neugebauer E, et al. Evidence of apoptotic cell death after experimental traumatic brain injury in the rat. Am J Pathol 147 (1995): 1575-83.

31. Savitskaya MA, Onishchenko GE. Mechanisms of Apoptosis. Biochemistry (Mosc) 80 (2015): 1393-405.

32. Vanden Berghe T, Linkermann A, Jouan-Lanhouet S, Walczak H, Vandenabeele P. Regulated necrosis: the expanding network of non-apoptotic cell death pathways. Nat Rev Mol Cell Biol 15 (2014): 135-47.

33. Jelinek A, Heyder L, Daude M, Plessner M, Krippner S, et al. Mitochondrial rescue prevents glutathione peroxidase-dependent ferroptosis. Free Radic Biol Med 117 (2018): 45-57.

34. Landshamer S, Hoehn M, Barth N, Duvezin-Caubet S, Schwake G, et al. Bid-induced release of AIF from mitochondria causes immediate neuronal cell death. Cell Death Differ 15 (2008): 1553-63.

35. Neitemeier S, Jelinek A, Laino V, Hoffmann L, Eisenbach I, et al. BID links ferroptosis to mitochondrial cell death pathways. Redox biology 12 (2017): 558-70.

36. Li H, Zhu H, Xu C, Yuan J. Cleavage of BID by Caspase 8 Mediates the Mitochondrial Damage in the Fas Pathway of Apoptosis. Cell 94 (1998): 491-501.

37. Gross A, Yin XM, Wang K, Wei MC, Jockel J, et al. Caspase cleaved BID targets mitochondria and is required for cytochrome c release, while BCL-XL prevents this release but not tumor necrosis factor-R1/Fas death. J Biol Chem 274 (1999): 1156-63.

38. Jang YC, Lustgarten MS, Liu Y, Muller FL, Bhattacharya A, et al. Increased superoxide in vivo accelerates age-associated muscle atrophy through mitochondrial dysfunction and neuromuscular junction degeneration. FASEB J 24 (2010): 1376-90.

39. Beal MF. Oxidative damage as an early marker of Alzheimer's disease and mild cognitive impairment. Neurobiol Aging 26 (2005): 585-6.

40. Lovell MA, Markesbery WR. Oxidative damage in mild cognitive impairment and early Alzheimer's disease. J Neurosci Res 85 (2007): 3036-40.

41. Ron Brookmeyer, Elizabeth Johnson, Kathryn Ziegler-Graham, and H. Michael Arrighi. FORECASTING THE GLOBAL BURDEN OF ALZHEIMER'S DISEASE. Johns Hopkins Bloomberg School of Public Health (2007).

42. Alonso A, Zaidi T, Novak M, Grundke-Iqbal I, Iqbal K. Hyperphosphorylation induces self-assembly of tau into tangles of paired helical filaments/straight filaments. Proc Natl Acad Sci USA 98 (2001): 6923-8.

43. Hou Y, Song H, Croteau DL, Akbari M, Bohr VA. Genome instability in Alzheimer disease. Mech Ageing Dev 161 (2017): 83-94.

44. Lovell M, Robertson J, Teesdale W, Campbell J, Markesbery W. Copper, iron and zinc in Alzheimer's disease senile plaques. J Neurol Sci 158 (1998): 47-52.

45. Bondy SC, Guo-Ross SX, Truong AT. Promotion of transition metal-induced reactive oxygen species formation by β-amyloid. Brain Res 799 (1998): 91-6.

46. Huang X, Atwood CS, Hartshorn MA, Multhaup G, Goldstein LE, et al. The A beta peptide of Alzheimer's disease directly produces hydrogen peroxide through metal ion reduction. Biochemistry 38 (1999): 7609-16.

47. Prasad MR, Lovell MA, Yatin M, Dhillon H, Markesbery WR. Regional membrane phospholipid alterations in Alzheimer's disease. Neurochem Res 23 (1998): 81-8.

48. Church DF, Pryor WA. Free-radical chemistry of cigarette smoke and its toxicological implications. Environ Health Perspect 64 (1985): 111-26.

49. Pryor WA, Stone K. Oxidants in cigarette smoke. Radicals, hydrogen peroxide, peroxynitrate, and peroxynitrite. Ann N Y Acad Sci 686 (1993): 12-27; discussion 27-8.

50. Zang L-Y, Stone K, Pryor WA. Detection of free radicals in aqueous extracts of cigarette tar by electron spin resonance. Free Radic Biol Med 19 (1995): 161-7.

51. Donaldson K, Brown DM, Mitchell C, Dineva M, Beswick PH, et al. Free radical activity of PM10: iron-mediated generation of hydroxyl radicals. Environ Health Perspect 105 Suppl 5 (1997): 1285-9.

52. Ichinose M. Differences of inflammatory mechanisms in asthma and COPD. Allergol Int 58 (2009): 307-13.

53. Kanazawa H, Kurihara N, Hirata K, Takeda T. The role of free radicals in airway obstruction in asthmatic patients. Chest 100 (1991): 1319-22.

54. Sedgwick JB, Geiger KM, Busse WW. Superoxide generation by hypodense eosinophils from patients with asthma. Am Rev Respir Dis 142 (1990): 120-5.

55. Bourdonnay E, Zasłona Z, Penke LRK, Speth JM, Schneider DJ, et al. Transcellular delivery of vesicular SOCS proteins from macrophages to epithelial cells blunts inflammatory signaling. J Exp Med 212 (2015): 729-42.

56. Berenson CS, Garlipp MA, Grove LJ, Maloney J, Sethi S. Impaired phagocytosis of nontypeable Haemophilus influenzae by human alveolar macrophages in chronic obstructive pulmonary disease. J Infect Dis 194 (2006): 1375-84.

57. Fitzpatrick AM, Holguin F, Teague WG, Brown LAS. Alveolar macrophage phagocytosis is impaired in children with poorly controlled asthma. J Allergy Clin Immunol 121 (2008): 1372-1378.e3.

58. Taylor AE, Finney-Hayward TK, Quint JK, Thomas CMR, Tudhope SJ, et al. Defective macrophage phagocytosis of bacteria in COPD. Eur Respir J 35 (2010): 1039-47.

59. Tran HB, Ahern J, Hodge G, Holt P, Dean MM, et al. Oxidative stress decreases functional airway mannose binding lectin in COPD. PLoS ONE 9 (2014): e98571.

60. Schauer U, Leinhaas C, Jäger R, Rieger CH. Enhanced superoxide generation by eosinophils from asthmatic children. Int Arch Allergy Appl Immunol 96 (1991): 317-21.

61. Teramoto S, Shu CY, Ouchi Y, Fukuchi Y. Increased spontaneous production and generation of superoxide anion by blood neutrophils in patients with asthma. J Asthma 33 (1996): 149-55.

62. Nakashima H, Ando M, Sugimoto M, Suga M, Soda K, et al. Receptor-mediated O2- release by alveolar macrophages and peripheral blood monocytes from smokers and nonsmokers. Priming and triggering effects of monomeric IgG, concanavalin A, N-formyl-methionyl-leucyl-phenylalanine, phorbol myristate acetate, and cytochalasin D. Am Rev Respir Dis 136 (1987): 310-5.

63. Lapenna D, Gioia S de, Mezzetti A, Ciofani G, Consoli A, et al. Cigarette smoke, ferritin, and lipid peroxidation. Am J Respir Crit Care Med 151 (1995): 431-5.

64. Thompson AB, Bohling T, Heires A, Linder J, Rennard SI. Lower respiratory tract iron burden is increased in association with cigarette smoking. J Lab Clin Med 117 (1991): 493-9.

65. Pignatelli B, Li CQ, Boffetta P, Chen Q, Ahrens W, et al. Nitrated and oxidized plasma proteins in smokers and lung cancer patients. Cancer Res 61 (2001): 778-84.

66. Ito K, Herbert C, Siegle JS, Vuppusetty C, Hansbro N, et al. Steroid-Resistant Neutrophilic Inflammation in a Mouse Model of an Acute Exacerbation of Asthma. Am J Respir Cell Mol Biol 39 (2008): 543-50.

67. Hercberg S, Czernichow S, Galan P. Tell me what your blood beta-carotene level is, I will tell you what your health risk is! The viewpoint of the SUVIMAX researchers. Ann Nutr Metab 54 (2009): 310-2.

68. Hercberg S, Galan P, Preziosi P, Bertrais S, Mennen L, et al. The SU.VI.MAX Study: a randomized, placebo-controlled trial of the health effects of antioxidant vitamins and minerals. Arch Intern Med 164 (2004): 2335-42.

69. Klein EA, Thompson IM, Tangen CM, Crowley JJ, Lucia MS, et al. Vitamin E and the risk of prostate cancer: the Selenium and Vitamin E Cancer Prevention Trial (SELECT). JAMA 306 (2011): 1549-56.

70. Chen AY, Lü J-M, Yao Q, Chen C. Entacapone is an Antioxidant More Potent than Vitamin C and Vitamin E for Scavenging of Hypochlorous Acid and Peroxynitrite, and the Inhibition of Oxidative Stress-Induced Cell Death. Med Sci Monit 22 (2016): 687-96.

71. Chen Q, Espey MG, Sun AY, Pooput C, Kirk KL, et al. Pharmacologic doses of ascorbate act as a prooxidant and decrease growth of aggressive tumor xenografts in mice. Proc Natl Acad Sci USA 105 (2008): 11105-9.

72. Clément MV, Ramalingam J, Long LH, Halliwell B. The in vitro cytotoxicity of ascorbate depends on the culture medium used to perform the assay and involves hydrogen peroxide. Antioxid Redox Signal 3 (2001): 157-63.

73. Pearson P, Lewis SA, Britton J, Young IS, Fogarty A. The pro-oxidant activity of high-dose vitamin E supplements in vivo. BioDrugs 20 (2006): 271-3.

74. Ou-Yang S-S, Lu J-Y, Kong X-Q, Liang Z-J, Luo C, et al. Computational drug discovery. Acta Pharmacol Sin 33 (2012): 1131-40.

75. Waldmeier PC. Prospects for antiapoptotic drug therapy of neurodegenerative diseases. Prog Neuropsychopharmacol Biol Psychiatry 27 (2003): 303-21.

76. Yin XM, Wang K, Gross A, Zhao Y, Zinkel S, et al. Bid-deficient mice are resistant to Fas-induced hepatocellular apoptosis. Nature 400 (1999): 886-91.

77. McDonnell JM, Fushman D, Milliman CL, Korsmeyer SJ, Cowburn D. Solution Structure of the Proapoptotic Molecule BID. Cell 96 (1999): 625-34.

78. Becattini B, Culmsee C, Leone M, Zhai D, Zhang X, et al. Structure-activity relationships by interligand NOE-based design and synthesis of antiapoptotic compounds targeting Bid. Proc Natl Acad Sci USA 103 (2006): 12602-6.

79. Becattini B, Sareth S, Zhai D, Crowell KJ, Leone M, et al. Targeting apoptosis via chemical design: inhibition of bid-induced cell death by small organic molecules. Chem Biol 11 (2004): 1107-17.

80. Carlsen MH, Halvorsen BL, Holte K, Bøhn SK, Dragland S, et al. The total antioxidant content of more than 3100 foods, beverages, spices, herbs and supplements used worldwide. Nutr J 9 (2010): 3.

81. Galasso C, Orefice I, Pellone P, Cirino P, Miele R, et al. On the Neuroprotective Role of Astaxanthin: New Perspectives? Mar Drugs 16 (2018).

82. Noorafshan A, Ashkani-Esfahani S. A review of therapeutic effects of curcumin. Curr Pharm Des 19 (2013): 2032-46.

83. Yeh S-L, Wang W-Y, Huang C-S, Hu M-L. Flavonoids suppresses the enhancing effect of beta-carotene on DNA damage induced by 4-(methylnitrosamino)-1-(3-pyridyl)-1-butanone (NNK) in A549 cells. Chem Biol Interact 160 (2006): 175-82.

84. Ganeshpurkar A, Saluja AK. The Pharmacological Potential of Rutin. Saudi Pharm J 25 (2017): 149-64.

85. Lee K-H, Yoo C-G. Simultaneous inactivation of GSK-3β suppresses quercetin-induced apoptosis by inhibiting the JNK pathway. Am J Physiol Lung Cell Mol Physiol 304 (2013): L782-9.

86. Juan D, PÉrez-Vizcaíno F, JimÉnez J, Tamargo J, Zarzuelo A. Flavonoids and cardiovascular diseases. In: Bioactive Natural Products (Part F). Elsevier; 2001. p. 565–605.

87. Wolfe KL, Liu RH. Structure-activity relationships of flavonoids in the cellular antioxidant activity assay. J Agric Food Chem 56 (2008): 8404-11.

88. Chanput W, Krueyos N, Ritthiruangdej P. Anti-oxidative assays as markers for anti-inflammatory activity of flavonoids. Int Immunopharmacol 40 (2016): 170-5.

89. Pietta PG. Flavonoids as antioxidants. J Nat Prod 63 (2000): 1035-42.

90. Hollman PC, Bijsman MN, van Gameren Y, Cnossen EP, Vries JH de, et al. The sugar moiety is a major determinant of the absorption of dietary flavonoid glycosides in man. Free Radic Res 31 (1999): 569-73.

91. Morand C, Manach C, Crespy V, Remesy C. Respective bioavailability of quercetin aglycone and its glycosides in a rat model. Biofactors 12 (2000): 169-74.

92. Cos P, Ying L, Calomme M, Hu JP, Cimanga K, et al. Structure-activity relationship and classification of flavonoids as inhibitors of xanthine oxidase and superoxide scavengers. J Nat Prod 61 (1998): 71-6.

93. Fiander H. Dietary ortho phenols that induce glutathione S-transferase and increase the resistance of cells to hydrogen peroxide are potential cancer chemopreventives that act by two mechanisms: the alleviation of oxidative stress and the detoxification of mutagenic xenobiotics. Cancer Lett 156 (2000): 117-24.

94. Laughton MJ, Evans PJ, Moroney MA, Hoult J, Halliwell B. Inhibition of mammalian 5-lipoxygenase and cyclo-oxygenase by flavonoids and phenolic dietary additives. Biochem Pharmacol 42 (1991): 1673-81.

95. Amrutha K, Nanjan P, Shaji SK, Sunilkumar D, Subhalakshmi K, et al. Discovery of lesser known flavones as inhibitors of NF-κB signaling in MDA-MB-231 breast cancer cells--A SAR study. Bioorg Med Chem Lett 24 (2014): 4735-42.

96. Velagapudi R, El-Bakoush A, Olajide OA. Activation of Nrf2 Pathway Contributes to Neuroprotection by the Dietary Flavonoid Tiliroside. Mol Neurobiol 55 (2018): 8103-23.

97. Liu L-L, Zhang Y, Zhang X-F, Li F-H. Influence of rutin on the effects of neonatal cigarette smoke exposure-induced exacerbated MMP-9 expression, Th17 cytokines and NF-κB/iNOS-mediated inflammatory responses in asthmatic mice model. Korean J Physiol Pharmacol 22 (2018): 481-91.

98. Jung CH, Lee JY, Cho CH, Kim CJ. Anti-asthmatic action of quercetin and rutin in conscious guinea-pigs challenged with aerosolized ovalbumin. Arch Pharm Res 30 (2007): 1599-607.

99. Shahid A, Ali R, Ali N, Hasan SK, Rashid S, et al. Attenuation of genotoxicity, oxidative stress, apoptosis and inflammation by rutin in benzo(a)pyrene exposed lungs of mice: plausible role of NF-κB, TNF-α and Bcl-2. J Complement Integr Med 13 (2016): 17-29.

100. Ioku K, Tsushida T, Takei Y, Nakatani N, Terao J. Antioxidative activity of quercetin and quercetin monoglucosides in solution and phospholipid bilayers. Biochim Biophys Acta 1234 (1995): 99-104.

101. Lee N-K, Choi S-H, Park S-H, Park E-K, Kim D-H. Antiallergic activity of hesperidin is activated by intestinal microflora. Pharmacology 71 (2004): 174-80.

102. Benavente-García O, Castillo J. Update on uses and properties of citrus flavonoids: new findings in anticancer, cardiovascular, and anti-inflammatory activity. J Agric Food Chem 56 (2008): 6185-205.

103. Bonina F. Flavonoids as potential protective agents against photo-oxidative skin damage. Int J Pharm 145 (1996): 87-94.

104. Al Shaal L, Müller RH, Keck CM. Preserving hesperetin nanosuspensions for dermal application. Pharmazie 65 (2010): 86-92.

105. Mishra PR, Al Shaal L, Müller RH, Keck CM. Production and characterization of Hesperetin nanosuspensions for dermal delivery. Int J Pharm 371 (2009): 182-9.

106. Proteggente AR, Basu-Modak S, Kuhnle G, Gordon MJ, Youdim K, et al. Hesperetin glucuronide, a photoprotective agent arising from flavonoid metabolism in human skin fibroblasts. Photochem Photobiol 78 (2003): 256-61.

107. Cha JY, Cho YS, Kim I, Anno T, Rahman SM, et al. Effect of hesperetin, a citrus flavonoid, on the liver triacylglycerol content and phosphatidate phosphohydrolase activity in orotic acid-fed rats. Plant Foods Hum Nutr 56 (2001): 349-58.

108. Youdim KA, Dobbie MS, Kuhnle G, Proteggente AR, Abbott NJ, et al. Interaction between flavonoids and the blood-brain barrier: in vitro studies. J Neurochem 85 (2003): 180-92.

109. Hwang S-L, Yen G-C. Neuroprotective effects of the citrus flavanones against H2O2-induced cytotoxicity in PC12 cells. J Agric Food Chem 56 (2008): 859-64.

110. Vauzour D, Vafeiadou K, Rice-Evans C, Williams RJ, Spencer JPE. Activation of pro-survival Akt and ERK1/2 signalling pathways underlie the anti-apoptotic effects of flavanones in cortical neurons. J Neurochem 103 (2007): 1355-67.

111. Muhammad T, Ikram M, Ullah R, Rehman SU, Kim MO. Hesperetin, a Citrus Flavonoid, Attenuates LPS-Induced Neuroinflammation, Apoptosis and Memory Impairments by Modulating TLR4/NF-κB Signaling. Nutrients 11 (2019).

112. Ikram M, Muhammad T, Rehman SU, Khan A, Jo MG, et al. Hesperetin Confers Neuroprotection by Regulating Nrf2/TLR4/NF-κB Signaling in an Aβ Mouse Model. Mol Neurobiol 56 (2019): 6293-309.

113. Lipinski CA, Lombardo F, Dominy BW, Feeney PJ. Experimental and computational approaches to estimate solubility and permeability in drug discovery and development settings 1PII of original article: S0169-409X(96)00423-1. The article was originally published in Advanced Drug Delivery Reviews 23 (1997) 3–25. 1. Adv Drug Deliv Rev 46 (2001): 3-26.

114. Stegemann S, Leveiller F, Franchi D, Jong H de, Lindén H. When poor solubility becomes an issue: from early stage to proof of concept. Eur J Pharm Sci 31 (2007): 249-61.

115. Amidon GL, Lennernäs H, Shah VP, Crison JR. A theoretical basis for a biopharmaceutic drug classification: the correlation of in vitro drug product dissolution and in vivo bioavailability. Pharm Res 12 (1995): 413-20.

116. Butler JM, Dressman JB. The developability classification system: application of biopharmaceutics concepts to formulation development. J Pharm Sci 99 (2010): 4940-54.

117. Harry G. Brittain. Strategy for the Prediction and Selection of Drug Substance Salt Forms. Pharm Tech 31 (2007): 78-88.

118. O'Connor KM, Corrigan OI. Preparation and characterisation of a range of diclofenac salts. Int J Pharm 226 (2001): 163-79.

119. Agatemor C, Ibsen KN, Tanner EEL, Mitragotri S. Ionic liquids for addressing unmet needs in healthcare. Bioeng Transl Med 3 (2018): 7-25.

120. FDA. Regulatory Classification of Pharmaceutical Co-Crystals Guidance for Industry. U.S. Department of Health and Human Services: Food and Drug Administration - Center for Drug Evaluation and Research (CDER) (2018).

121. Harrison WTA, Yathirajan HS, Bindya S, Anilkumar HG, Devaraju. Escitalopram oxalate: co-existence of oxalate dianions and oxalic acid molecules in the same crystal. Acta Crystallogr C 63 (2007): o129-31.

122. Iacobazzi RM, Cutrignelli A, Stefanachi A, Porcelli L, Lopedota AA, et al. Hydroxy-Propil-β-Cyclodextrin Inclusion Complexes of two Biphenylnicotinamide Derivatives: Formulation and Anti-Proliferative Activity Evaluation in Pancreatic Cancer Cell Models. Int J Mol Sci 21 (2020).

123. Cuiné JF, Charman WN, Pouton CW, Edwards GA, Porter CJH. Increasing the proportional content of surfactant (Cremophor EL) relative to lipid in self-emulsifying lipid-based formulations of danazol reduces oral bioavailability in beagle dogs. Pharm Res 24 (2007): 748-57.

124. Griffin BT, Kuentz M, Vertzoni M, Kostewicz ES, Fei Y, et al. Comparison of in vitro tests at various levels of complexity for the prediction of in vivo performance of lipid-based formulations: case studies with fenofibrate. Eur J Pharm Biopharm 86 (2014): 427-37.

125. Park S-H, Choi H-K. The effects of surfactants on the dissolution profiles of poorly water-soluble acidic drugs. Int J Pharm 321 (2006): 35-41.

126. Vinarov Z, Gancheva G, Katev V, Tcholakova SS. Albendazole solution formulation via vesicle-to-micelle transition of phospholipid-surfactant aggregates. Drug Dev Ind Pharm 44 (2018): 1130-8.

127. Vinarov Z, Katev V, Burdzhiev N, Tcholakova S, Denkov N. Effect of Surfactant-Bile Interactions on the Solubility of Hydrophobic Drugs in Biorelevant Dissolution Media. Mol Pharm 15 (2018): 5741-53.

128. Brewster ME, Vandecruys R, Peeters J, Neeskens P, Verreck G, et al. Comparative interaction of 2-hydroxypropyl-beta-cyclodextrin and sulfobutylether-beta-cyclodextrin with itraconazole: phase-solubility behavior and stabilization of supersaturated drug solutions. Eur J Pharm Sci 34 (2008): 94-103.

129. Chen J, Ormes JD, Higgins JD, Taylor LS. Impact of surfactants on the crystallization of aqueous suspensions of celecoxib amorphous solid dispersion spray dried particles. Mol Pharm 12 (2015): 533-41.

130. Rengarajan GT, Enke D, Steinhart M, Beiner M. Stabilization of the amorphous state of pharmaceuticals in nanopores. J. Mater. Chem. 18 (2008): 2537.

131. Loo, Register, Ryan. Polymer crystallization in 25-nm spheres. Phys Rev Lett 84 (2000): 4120-3.

132. Massa MV, Carvalho JL, Dalnoki-Veress K. Direct visualisation of homogeneous and heterogeneous crystallisation in an ensemble of confined domains of poly(ethylene oxide). Eur Phys J E Soft Matter 12 (2003): 111-7.

133. Hespeler D, Kaltenbach J, Pyo SM. Glabridin smartPearls - Silica selection, production, amorphous stability and enhanced solubility. Int J Pharm 561 (2019): 228-35.

134. Zhang J, Karmakar S, Yu M, Mitter N, Zou J, et al. Synthesis of silica vesicles with controlled entrance size for high loading, sustained release, and cellular delivery of therapeutical proteins. Small 10 (2014): 5068-76.

135. Lei C, Liu P, Chen B, Mao Y, Engelmann H, et al. Local release of highly loaded antibodies from functionalized nanoporous support for cancer immunotherapy. J Am Chem Soc 132 (2010): 6906-7.

136. Le T-T, Elzhry Elyafi AK, Mohammed AR, Al-Khattawi A. Delivery of Poorly Soluble Drugs via Mesoporous Silica: Impact of Drug Overloading on Release and Thermal Profiles. Pharmaceutics 11 (2019).

137. Dening TJ, Taylor LS. Supersaturation Potential of Ordered Mesoporous Silica Delivery Systems. Part 1: Dissolution Performance and Drug Membrane Transport Rates. Mol Pharm 15 (2018): 3489-501.

138. Mellaerts R, Mols R, Jammaer JAG, Aerts CA, Annaert P, et al. Increasing the oral bioavailability of the poorly water soluble drug itraconazole with ordered mesoporous silica. Eur J Pharm Biopharm 69 (2008): 223-30.

139. Abdelwahed W, Degobert G, Fessi H. A pilot study of freeze drying of poly(epsilon-caprolactone) nanocapsules stabilized by poly(vinyl alcohol): formulation and process optimization. Int J Pharm 309 (2006): 178-88.

140. Rabinow BE. Nanosuspensions in drug delivery. Nat Rev Drug Discov 3 (2004): 785-96.

141. Ostwald W. Über die vermeintliche Isomerie des roten und gelben Quecksilberoxyds und die Oberflächenspannung fester Körper. Zeitschrift für Physikalische Chemie 34U (1900).

142. Noyes AA, Whitney WR. THE RATE OF SOLUTION OF SOLID SUBSTANCES IN THEIR OWN SOLUTIONS. J Am Chem Soc 19 (1897): 930-4.

143. Senior JH. Nanoparticulate Drug Delivery Systems. Drug Dev Ind Pharm 34 (2008): 116.

144. van Eerdenbrugh B, Vermant J, Martens JA, Froyen L, van Humbeeck J, et al. Solubility increases associated with crystalline drug nanoparticles: methodologies and significance. Mol Pharm 7 (2010): 1858-70.

145. Tarr BD, Yalkowsky SH. Enhanced intestinal absorption of cyclosporine in rats through the reduction of emulsion droplet size. Pharm Res 6 (1989): 40-3.

146. VERWEY EJW. Theory of the stability of lyophobic colloids. J Phys Colloid Chem 51 (1947): 631-6.

147. Adair JH, Suvaci E, Sindel J. Surface and Colloid Chemistry. In: Encyclopedia of Materials: Science and Technology. Elsevier; 2001. p. 1–10.

148. Kesisoglou F, Panmai S, Wu Y. Nanosizing--oral formulation development and biopharmaceutical evaluation. Adv Drug Deliv Rev 59 (2007): 631-44.

149. Wu L, Zhang J, Watanabe W. Physical and chemical stability of drug nanoparticles. Adv Drug Deliv Rev 63 (2011): 456-69.

150. Einarson MB, Berg JC. Electrosteric Stabilization of Colloidal Latex Dispersions. J Colloid Interface Sci 155 (1993): 165-72.

151. Fritz G, Schädler V, Willenbacher N, Wagner NJ. Electrosteric Stabilization of Colloidal Dispersions. Langmuir 18 (2002): 6381-90.

152. Auweter H, André V, Horn D, Lüddecke E. THE FUNCTION OF GELATIN IN CONTROLLED PRECIPITATION PROCESSES OF NANOSIZE PARTICLES. J Dispers Sci Technol 19 (1998): 163-84.

153. Sinha B, Müller RH, Möschwitzer JP. Bottom-up approaches for preparing drug nanocrystals: formulations and factors affecting particle size. Int J Pharm 453 (2013): 126-41.

154. Müller RH, Mäder K, Krause K. Verfahren zur schonendenHerstellung von hochfeinen Mikropartikeln und Nanopartikeln: German Patent Application 199 32 157.4; (2000): PCT/EP00/06535.

155. Keck CM, Müller RH. Drug nanocrystals of poorly soluble drugs produced by high pressure homogenisation. Eur J Pharm Biopharm 62 (2006): 3-16.

156. Fichera MA, Wissing SA, Müller RH. Effect of 4000 bar Homogenization Pressure on Particle Diminution in Drug Suspensions. APV, Nürnberg 2004.

157. Kobierski S, Ofori-Kwakye K, Müller RH, Keck CM. Resveratrol nanosuspensions: interaction of preservatives with nanocrystal production. Pharmazie 66 (2011): 942-7.

158. Malamatari M, Taylor KMG, Malamataris S, Douroumis D, Kachrimanis K. Pharmaceutical nanocrystals: production by wet milling and applications. Drug Discov Today 23 (2018): 534-47.

159. George M, Ghosh I. Identifying the correlation between drug/stabilizer properties and critical quality attributes (CQAs) of nanosuspension formulation prepared by wet media milling technology. Eur J Pharm Sci 48 (2013): 142-52.

160. Xu K, Xiong X, Zhai Y, Wang L, Li S, et al. Effect of milling conditions on solid-state amorphization of glipizide, and characterization and stability of solid forms. J Pharm Biomed Anal 129 (2016): 367-77.

161. Juhnke M, Märtin D, John E. Generation of wear during the production of drug nanosuspensions by wet media milling. Eur J Pharm Biopharm 81 (2012): 214-22.

162. Kipp JE, Wong JCT, Doty MJ, Rebbeck, C. L. Microprecipitation method for preparing submicron suspension; (2006) US007037528B2.

163. Möschwitzer JP. Method for producing ultrafine submicronic suspensions; (2006) WO/2006/094808.

164. Müller RH, Möschwitzer JP. Method and apparatus for the production of ultrafine particles and coating of such particles.; (2005) US9168498B2.

165. Möschwitzer JP, Lemke A. Method for carefully producing ultrafine particle suspensions and ultrafine particles and use thereof; (2006) WO/2006/108637.

166. Sheokand S, Sharma J, Bansal AK. Effect of surfactants on the molecular mobility and crystallization kinetics of hesperetin. CrystEngComm 21 (2019): 3788-97.

167. Scholz P, Keck CM. Flavonoid nanocrystals produced by ARTcrystal®-technology. Int J Pharm 482 (2015): 27-37.

168. Na GC, Stevens HJ, Yuan BO, Rajagopalan N. Physical stability of ethyl diatrizoate nanocrystalline suspension in steam sterilization. Pharm Res 16 (1999): 569-74.

169. Gao L, Zhang D, Chen M, Duan C, Dai W, et al. Studies on pharmacokinetics and tissue distribution of oridonin nanosuspensions. Int J Pharm 355 (2008): 321-7.

170. Ben Zirar S, Astier A, Muchow M, Gibaud S. Comparison of nanosuspensions and hydroxypropyl-beta-cyclodextrin complex of melarsoprol: pharmacokinetics and tissue distribution in mice. Eur J Pharm Biopharm 70 (2008): 649-56.

171. Shegokar R, Singh KK. Surface modified nevirapine nanosuspensions for viral reservoir targeting: In vitro and in vivo evaluation. Int J Pharm 421 (2011): 341-52.

172. Lai F, Pireddu R, Corrias F, Fadda AM, Valenti D, et al. Nanosuspension improves tretinoin photostability and delivery to the skin. Int J Pharm 458 (2013): 104-9.

173. Britland S, Finter W, Chrystyn H, Eagland D, Abdelrahim ME. Droplet aerodynamics, cellular uptake, and efficacy of a nebulizable corticosteroid nanosuspension are superior to a micronized dosage form. Biotechnol Prog 28 (2012): 1152-9.

174. Romero GB, Keck CM, Müller RH. Simple low-cost miniaturization approach for pharmaceutical nanocrystals production. Int J Pharm 501 (2016): 236-44.

175. Pelikh O, Stahr P-L, Huang J, Gerst M, Scholz P, et al. Nanocrystals for improved dermal drug delivery. Eur J Pharm Biopharm 128 (2018): 170-8.

176. Filella M, Zhang J, Newman ME, Buffle J. Analytical applications of photon correlation spectroscopy for size distribution measurements of natural colloidal suspensions: capabilities and limitations. Colloids Surf, A Physicochem Eng Asp 120 (1997): 27-46.

177. Kakran M, Shegokar R, Sahoo NG, Shaal LA, Li L, et al. Fabrication of quercetin nanocrystals: comparison of different methods. Eur J Pharm Biopharm 80 (2012): 113-21.

178. Knoth D, Keck CM. Characterization of Nanosized Drug Carriers by Analytical Centrifugation. Phys. Status Solidi A 215 (2018): 1700962.

179. Keck CM, Müller RH. Size analysis of submicron particles by laser diffractometry--90% of the published measurements are false. Int J Pharm 355 (2008): 150-63.

180. Müller RH, Nitzsche R, Paulke B-R. Zetapotential und Partikelladung in der Laborpraxis: Einführung in die Theorie, praktische Meßdurchführung, Dateninterpretation ; Colloidal Drug Carriers - cdc - 1st Expert Meeting Berlin 15. - 17. 6 1995 ; mit 24 Tabellen. Stuttgart: Wiss. Verl.-Ges; 1996.

181. Sharma OP, Bhat TK. DPPH antioxidant assay revisited. Food Chem 113 (2009): 1202-5.

182. Kumar S, Xu X, Gokhale R, Burgess DJ. Formulation parameters of crystalline nanosuspensions on spray drying processing: a DoE approach. Int J Pharm 464 (2014): 34-45.

183. Leigh M, Kloefer B, Schaich M. Comparison of the Solubility and Dissolution of Drugs in FastedState Biorelevant Media (FaSSIF and FaSSIF-V2). Dissolution Technol. 20 (2013): 44-50.

184. Khan J, Bashir S, Khan MA, Mohammad MA, Isreb M. Fabrication and characterization of dexibuprofen nanocrystals using microchannel fluidic rector. Drug Des Devel Ther 12 (2018): 2617-26.

185. Shohin IE, Grebenkin DY, Malashenko EA, Stanishevskii YM, Ramenskaya GV. A Brief Review of the FDA Dissolution Methods Database. Dissolution Technol. 23 (2016): 6-10.

186. Hassan MS, Lau RWM. Effect of particle shape on dry particle inhalation: study of flowability, aerosolization, and deposition properties. AAPS PharmSciTech 10 (2009): 1252-62.

187. Mohan M, Lee S, Guo C, Peri SP, Doub WH. Evaluation of Abbreviated Impactor Measurements (AIM) and Efficient Data Analysis (EDA) for Dry Powder Inhalers (DPIs) Against the Full-Resolution Next Generation Impactor (NGI). AAPS PharmSciTech 18 (2017): 1585-94.

188. Yamasaki K, Kwok PCL, Fukushige K, Prud'homme RK, Chan H-K. Enhanced dissolution of inhalable cyclosporine nano-matrix particles with mannitol as matrix former. Int J Pharm 420 (2011): 34-42.

189. Wang H, Joseph JA. Quantifying cellular oxidative stress by dichlorofluorescein assay using microplate reader11Mention of a trade name, proprietary product, or specific equipment does not constitute a guarantee by the United States Department of Agriculture and does not imply its approval to the exclusion of other products that may be suitable. Free Radic Biol Med 27 (1999): 612-6.

190. Cerdeira AM, Mazzotti M, Gander B. Miconazole nanosuspensions: Influence of formulation variables on particle size reduction and physical stability. Int J Pharm 396 (2010): 210-8.

191. Stenger F, Mende S, Schwedes J, Peukert W. Nanomilling in stirred media mills. Chem Eng Sci 60 (2005): 4557-65.

192. Vo A, Feng X, Patel D, Mohammad A, Kozak D, et al. Factors affecting the particle size distribution and rheology of brinzolamide ophthalmic suspensions. Int J Pharm 586 (2020): 119495.

193. Verma S, Kumar S, Gokhale R, Burgess DJ. Physical stability of nanosuspensions: investigation of the role of stabilizers on Ostwald ripening. Int J Pharm 406 (2011): 145-52.

194. Seiler A, Schneider M, Förster H, Roth S, Wirth EK, et al. Glutathione peroxidase 4 senses and translates oxidative stress into 12/15-lipoxygenase dependent- and AIF-mediated cell death. Cell Metab 8 (2008): 237-48.

195. Rayane S.C.M.Q. Antonino, Michael Ruggiero, Zihui Song, Thais Leite Nascimento, Eliana Martins Lima, et al. Impact of drug loading in mesoporous silica-amorphous formulations on the physical stability of drugs with high recrystallization tendency. Int J Pharm X 1 (2019): 100026.

196. Ahern RJ, Hanrahan JP, Tobin JM, Ryan KB, Crean AM. Comparison of fenofibrate-mesoporous silica drug-loading processes for enhanced drug delivery. Eur J Pharm Sci 50 (2013): 400-9.

197. Hempel N-J, Brede K, Olesen NE, Genina N, Knopp MM, et al. A fast and reliable DSC-based method to determine the monomolecular loading capacity of drugs with good glass-forming ability in mesoporous silica. Int J Pharm 544 (2018): 153-7.

198. Mellaerts R, Fayad EJ, van den Mooter G, Augustijns P, Rivallan M, et al. In situ FT-IR investigation of etravirine speciation in pores of SBA-15 ordered mesoporous silica material upon contact with water. Mol Pharm 10 (2013): 567-73.

199. Balzer D, Lüders H, editors. Nonionic surfactants: Alkyl polyglucosides. New York, NY: Dekker; 2000.

200. Kovacevic A, Savic S, Vuleta G, Müller RH, Keck CM. Polyhydroxy surfactants for the formulation of lipid nanoparticles (SLN and NLC): effects on size, physical stability and particle matrix structure. Int J Pharm 406 (2011): 163-72.

201. Priemel PA, Grohganz H, Gordon KC, Rades T, Strachan CJ. The impact of surface- and nano-crystallisation on the detected amorphous content and the dissolution behaviour of amorphous indomethacin. Eur J Pharm Biopharm 82 (2012): 187-93.

202. Sarsfield BA, Davidovich M, Desikan S, Fakes M, Futernik S, et al. Powder x-ray diffraction detection of crystalline phases in amorphous pharmaceuticals. CJPDS-International Centre for Diffraction Data (2006): 322-7.

203. PubChem. Hesperetin. 72281. https ://pubch em.ncbi.nlm.nih.

204. Al Shaal L. smartCrystals® - investigations on preparation, preservation and long-term stability; PhD Thesis, 2011.

205. Sun J, Wang F, Sui Y, She Z, Zhai W, et al. Effect of particle size on solubility, dissolution rate, and oral bioavailability: evaluation using coenzyme Q_{10} as naked nanocrystals. Int J Nanomedicine 7 (2012): 5733-44.

206. Esmaeili AH, Hajizadeh Moghaddam A, Chaichi MJ. Identification, determination, and study of antioxidative activities of hesperetin and gallic acid in hydro-alcoholic extract from flowers of Eriobotrya japonica (Lindl.). Avicenna J Phytomed 4 (2014): 260-6.

207. Stockburger C, Gold VAM, Pallas T, Kolesova N, Miano D, et al. A cell model for the initial phase of sporadic Alzheimer's disease. J Alzheimers Dis 42 (2014): 395-411.

208. Joh Y, Choi W-S. Mitochondrial Complex I Inhibition Accelerates Amyloid Toxicity. Dev Reprod 21 (2017): 417-24.

209. Bast A, Haenen GR, Doelman CJ. Oxidants and antioxidants: State of the art. Am J Med 91 (1991): 2-13.

210. Halliwell B. Are polyphenols antioxidants or pro-oxidants? What do we learn from cell culture and in vivo studies? Arch Biochem Biophys 476 (2008): 107-12.

211. Calabrese V, Giordano J, Ruggieri M, Berritta D, Trovato A, et al. Hormesis, cellular stress response, and redox homeostasis in autism spectrum disorders. J Neurosci Res 94 (2016): 1488-98.

212. Radak Z, Ishihara K, Tekus E, Varga C, Posa A, et al. Exercise, oxidants, and antioxidants change the shape of the bell-shaped hormesis curve. Redox biology 12 (2017): 285-90.

213. Yen G-C, Duh P-D, Tsai H-L, Huang S-L. Pro-oxidative properties of flavonoids in human lymphocytes. Biosci Biotechnol Biochem 67 (2003): 1215-22.

214. Zhang J, Song J, Wu D, Wang J, Dong W. Hesperetin induces the apoptosis of hepatocellular carcinoma cells via mitochondrial pathway mediated by the increased intracellular reactive oxygen species, ATP and calcium. Medical oncology (Northwood, London, England) 32 (2015): 101.

215. Canada AT, Giannella E, Nguyen TD, Mason RP. The production of reactive oxygen species by dietary flavonols. Free Radic Biol Med 9 (1990): 441-9.

216. Elliott AJ, Scheiber SA, Thomas C, Pardini RS. Inhibition of glutathione reductase by flavonoids. Biochem Pharmacol 44 (1992): 1603-8.

217. Zerulla-Wernitz M, Maier M. Analysis of Sub-Visible Particles. Pharm Tech Partnering for Bio/Pharma Success Supplement (2019): 28-31.

218. Keck CM. Particle size analysis of nanocrystals: improved analysis method. Int J Pharm 390 (2010): 3-12.

219. Lim HJ, Jin H-G, Woo E-R, Lee SK, Kim HP. The root barks of Morus alba and the flavonoid constituents inhibit airway inflammation. J Ethnopharmacol 149 (2013): 169-75.

220. van Eerdenbrugh B, Vermant J, Martens JA, Froyen L, van Humbeeck J, et al. A screening study of surface stabilization during the production of drug nanocrystals. J Pharm Sci 98 (2009): 2091-103.

221. Mauludin R, Müller RH, Keck CM. Development of an oral rutin nanocrystal formulation. Int J Pharm 370 (2009): 202-9.

222. Martena V, Shegokar R, Di Martino P, Müller RH. Effect of four different size reduction methods on the particle size, solubility enhancement and physical stability of nicergoline nanocrystals. Drug Dev Ind Pharm 40 (2014): 1199-205.

223. Pyo S, Meinke M, Keck C, Müller R. Rutin—Increased Antioxidant Activity and Skin Penetration by Nanocrystal Technology (smartCrystals). Cosmetics 3 (2016): 9.

224. Gao L, Liu G, Wang X, Liu F, Xu Y, et al. Preparation of a chemically stable quercetin formulation using nanosuspension technology. Int J Pharm 404 (2011): 231-7.

225. Budai L, Kaszás N, Gróf P, Lenti K, Maghami K, et al. Liposomes for topical use: a physico-chemical comparison of vesicles prepared from egg or soy lecithin. Sci Pharm 81 (2013): 1151-66.

226. Merisko-Liversidge E, Liversidge GG, Cooper ER. Nanosizing: a formulation approach for poorly-water-soluble compounds. Eur J Pharm Sci 18 (2003): 113-20.

227. Chou DK, Krishnamurthy R, Randolph TW, Carpenter JF, Manning MC. Effects of Tween 20 and Tween 80 on the stability of Albutropin during agitation. J Pharm Sci 94 (2005): 1368-81.

228. Alexandridis P, Alan Hatton T. Poly(ethylene oxide)・poly(propylene oxide)・poly(ethylene oxide) block copolymer surfactants in aqueous solutions and at interfaces: thermodynamics, structure, dynamics, and modeling. Colloids Surf, A Physicochem Eng Asp 96 (1995): 1-46.

229. Kabanov AV, Nazarova IR, Astafieva IV, Batrakova EV, Alakhov VY, et al. Micelle Formation and Solubilization of Fluorescent Probes in Poly(oxyethylene-b-oxypropylene-b-oxyethylene) Solutions. Macromolecules 28 (1995): 2303-14.

230. Tsoneva I, Iordanov I, Berger AJ, Tomov T, Nikolova B, et al. Electrodelivery of drugs into cancer cells in the presence of poloxamer 188. J Biomed Biotechnol 2010 (2010).

231. Bhat PA, Dar AA, Rather GM. Solubilization Capabilities of Some Cationic, Anionic, and Nonionic Surfactants toward the Poorly Water-Soluble Antibiotic Drug Erythromycin. J. Chem. Eng. Data 53 (2008): 1271-7.

232. Rangel-Yagui CO, Pessoa A, Tavares LC. Micellar solubilization of drugs. J Pharm Pharm Sci 8 (2005): 147-65.

233. Luk AS, Kaler EW, Lee SP. Phospholipase C-induced aggregation and fusion of cholesterol-lecithin small unilamellar vesicles. Biochemistry 32 (1993): 6965-73.

234. Kirtil E, Dag D, Guner S, Unal K, Oztop MH. Dynamics of unloaded and green tea extract loaded lecithin based liposomal dispersions investigated by nuclear magnetic resonance T2 relaxation. Food Res Int 99 (2017): 807-14.

235. Guner S, Oztop MH. Food grade liposome systems: Effect of solvent, homogenization types and storage conditions on oxidative and physical stability. Colloids Surf, A Physicochem Eng Asp 513 (2017): 468-78.

236. Chebil L, Humeau C, Anthoni J, Dehez F, Engasser J-M, et al. Solubility of Flavonoids in Organic Solvents. J. Chem. Eng. Data 52 (2007): 1552-6.

237. Lee J, Lee S-J, Choi J-Y, Yoo JY, Ahn C-H. Amphiphilic amino acid copolymers as stabilizers for the preparation of nanocrystal dispersion. Eur J Pharm Sci 24 (2005): 441-9.

238. Cho D, Narsimhan G, Franses EI. Interactions of Spread Lecithin Monolayers with Bovine Serum Albumin in Aqueous Solution. Langmuir 13 (1997): 4710-5.

239. Sun W, Tian W, Zhang Y, He J, Mao S, et al. Effect of novel stabilizers--cationic polymers on the particle size and physical stability of poorly soluble drug nanocrystals. Nanomedicine 8 (2012): 460-7.

240. Jacobs C, Müller RH. Production and characterization of a budesonide nanosuspension for pulmonary administration. Pharm Res 19 (2002): 189-94.

241. Lai F, Pini E, Angioni G, Manca ML, Perricci J, et al. Nanocrystals as tool to improve piroxicam dissolution rate in novel orally disintegrating tablets. Eur J Pharm Biopharm 79 (2011): 552-8.

242. Lai F, Sinico C, Ennas G, Marongiu F, Marongiu G, et al. Diclofenac nanosuspensions: influence of preparation procedure and crystal form on drug dissolution behaviour. Int J Pharm 373 (2009): 124-32.

243. Liversidge GG, Conzentino P. Drug particle size reduction for decreasing gastric irritancy and enhancing absorption of naproxen in rats. Int J Pharm 125 (1995): 309-13.

244. Borzova VA, Markossian KA, Kleymenov SY, Kurganov BI. A change in the aggregation pathway of bovine serum albumin in the presence of arginine and its derivatives. Scientific reports 7 (2017): 3984.

245. Randolph TW, Jones LS. Surfactant-protein interactions. Pharm Biotechnol 13 (2002): 159-75.

246. Ruiz-Peña M, Oropesa-Nuñez R, Pons T, Louro SRW, Pérez-Gramatges A. Physico-chemical studies of molecular interactions between non-ionic surfactants and bovine serum albumin. Colloids Surf B Biointerfaces 75 (2010): 282-9.

247. Bhattacharyya J, Das KP. EFFECT OF SURFACTANTS ON THE PREVENTION OF PROTEIN AGGREGATION DURING UNFOLDING AND REFOLDING PROCESSES-COMPARISON WITH MOLECULAR CHAPERONE α - CRYSTALLIN. J Dispers Sci Technol 20 (1999): 1163-78.

248. Bernard L, Eljezi T, Clauson H, Lambert C, Bouattour Y, et al. Effects of flow rate on the migration of different plasticizers from PVC infusion medical devices. PLoS ONE 13 (2018): e0192369.

249. Deng J, Huang L, Liu F. Understanding the structure and stability of paclitaxel nanocrystals. Int J Pharm 390 (2010): 242-9.

250. Kakran M, Shegokar R, Sahoo NG, Gohla S, Li L, et al. Long-term stability of quercetin nanocrystals prepared by different methods. J Pharm Pharmacol 64 (2012): 1394-402.

251. Beirowski J, Inghelbrecht S, Arien A, Gieseler H. Freeze-drying of nanosuspensions, 1: freezing rate versus formulation design as critical factors to preserve the original particle size distribution. J Pharm Sci 100 (2011): 1958-68.

252. Obeidat WM, Schwabe K, Müller RH, Keck CM. Preservation of nanostructured lipid carriers (NLC). Eur J Pharm Biopharm 76 (2010): 56-67.

253. Diels AMJ, Michiels CW. High-pressure homogenization as a non-thermal technique for the inactivation of microorganisms. Crit Rev Microbiol 32 (2006): 201-16.

254. Jurado E, Fernández-Serrano M, Núñez Olea J, Lechuga M, Jiménez JL, et al. Acute toxicity of alkylpolyglucosides to Vibrio fischeri, Daphnia magna and microalgae: a comparative study. Bull Environ Contam Toxicol 88 (2012): 290-5.

255. Jurado E, Fernández-Serrano M, Núñez-Olea J, Luzón G, Lechuga M. Acute toxicity and relationship between metabolites and ecotoxicity during the biodegradation process of non-ionic surfactants: fatty-alcohol ethoxylates, nonylphenol polyethoxylate and alkylpolyglucosides. Water Sci Technol 59 (2009): 2351-8.

256. Cottrell SF. Yeast freeze-thaw survival rates as a function of different stages in the cell cycle. Cryobiology 18 (1981): 506-10.

257. Park JI, Grant CM, Attfield PV, Dawes IW. The freeze-thaw stress response of the yeast Saccharomyces cerevisiae is growth phase specific and is controlled by nutritional state via the RAS-cyclic AMP signal transduction pathway. Appl Environ Microbiol 63 (1997): 3818-24.

258. Dailey LA, Schmehl T, Gessler T, Wittmar M, Grimminger F, et al. Nebulization of biodegradable nanoparticles: impact of nebulizer technology and nanoparticle characteristics on aerosol features. J Control Release 86 (2003): 131-44.

259. Lai SK, Wang Y-Y, Hanes J. Mucus-penetrating nanoparticles for drug and gene delivery to mucosal tissues. Adv Drug Deliv Rev 61 (2009): 158-71.

260. Handscomb CS, Kraft M, Bayly AE. A new model for the drying of droplets containing suspended solids. Chem Eng Sci 64 (2009): 628-37.

261. Both EM, Boom RM, Schutyser M. Particle morphology and powder properties during spray drying of maltodextrin and whey protein mixtures. Powder Technol 363 (2020): 519-24.

262. Kumar S, Gokhale R, Burgess DJ. Sugars as bulking agents to prevent nano-crystal aggregation during spray or freeze-drying. Int J Pharm 471 (2014): 303-11.

263. Kumar S, Shen J, Zolnik B, Sadrieh N, Burgess DJ. Optimization and dissolution performance of spray-dried naproxen nano-crystals. Int J Pharm 486 (2015): 159-66.

264. Dolenc A, Kristl J, Baumgartner S, Planinsek O. Advantages of celecoxib nanosuspension formulation and transformation into tablets. Int J Pharm 376 (2009): 204-12.

265. Sharma A, Pasha JM, Deep S. Effect of the sugar and polyol additives on the aggregation kinetics of BSA in the presence of N-cetyl-N,N,N-trimethyl ammonium bromide. J Colloid Interface Sci 350 (2010): 240-8.

266. Li J, Krause ME, Chen X, Cheng Y, Dai W, et al. Interfacial Stress in the Development of Biologics: Fundamental Understanding, Current Practice, and Future Perspective. AAPS J 21 (2019): 44.

267. Kueltzo LA, Wang W, Randolph TW, Carpenter JF. Effects of solution conditions, processing parameters, and container materials on aggregation of a monoclonal antibody during freeze-thawing. J Pharm Sci 97 (2008): 1801-12.

268. Lee J, Cheng Y. Critical freezing rate in freeze drying nanocrystal dispersions. J Control Release 111 (2006): 185-92.

269. Chow AHL, Tong HHY, Chattopadhyay P, Shekunov BY. Particle engineering for pulmonary drug delivery. Pharm Res 24 (2007): 411-37.

270. Rebits LG, Bennett DJ, Bhagwat PA, Morin A, Sievers RE. Method for quantifying the sample collected by an Andersen Cascade Impactor using total organic carbon analysis. J Aerosol Sci 38 (2007): 1197-206.

271. Lavorini F, Pistolesi M, Usmani OS. Recent advances in capsule-based dry powder inhaler technology. Multidiscip Respir Med 12 (2017): 11.

272. Yoshida H, Kuwana A, Shibata H, Izutsu K-I, Goda Y. Comparison of Aerodynamic Particle Size Distribution Between a Next Generation Impactor and a Cascade Impactor at a Range of Flow Rates. AAPS PharmSciTech 18 (2017): 646-53.

273. Zeng XM, Martin GP, Marriott C, Pritchard J. The influence of carrier morphology on drug delivery by dry powder inhalers. Int J Pharm 200 (2000): 93-106.

274. Timsina MP, Martin GP, Marriott C, Ganderton D, Yianneskis M. Drug delivery to the respiratory tract using dry powder inhalers. Int J Pharm 101 (1994): 1-13.

275. Voss A, Finlay WH. Deagglomeration of dry powder pharmaceutical aerosols. Int J Pharm 248 (2002): 39-50.

276. Zeng XM, Martin GP, Tee S-K, Marriott C. The role of fine particle lactose on the dispersion and deaggregation of salbutamol sulphate in an air stream in vitro. Int J Pharm 176 (1998): 99-110.

277. Jones MD, Price R. The influence of fine excipient particles on the performance of carrier-based dry powder inhalation formulations. Pharm Res 23 (2006): 1665-74.

278. Beilmann B, Kubiak R, Grab P, Häusler H, Langguth P. Effect of interactive ternary mixtures on dispersion characteristics of ipratropium bromide in dry powder inhaler formulations. AAPS PharmSciTech 8 (2007): Article 31.

279. Daviskas E, Anderson SD, Eberl S, Chan HK, Bautovich G. Inhalation of dry powder mannitol improves clearance of mucus in patients with bronchiectasis. Am J Respir Crit Care Med 159 (1999): 1843-8.

280. Tee S, Marriott C, Zeng X, Martin G. The use of different sugars as fine and coarse carriers for aerosolised salbutamol sulphate. Int J Pharm 208 (2000): 111-23.

281. Steckel H, Bolzen N. Alternative sugars as potential carriers for dry powder inhalations. Int J Pharm 270 (2004): 297-306.

282. Donovan MJ, Kim SH, Raman V, Smyth HD. Dry powder inhaler device influence on carrier particle performance. J Pharm Sci 101 (2012): 1097-107.

283. Traini D, Scalia S, Adi H, Marangoni E, Young PM. Polymer coating of carrier excipients modify aerosol performance of adhered drugs used in dry powder inhalation therapy. Int J Pharm 438 (2012): 150-9.

284. Zhou QT, Qu L, Gengenbach T, Larson I, Stewart PJ, et al. Effect of surface coating with magnesium stearate via mechanical dry powder coating approach on the aerosol performance of micronized drug powders from dry powder inhalers. AAPS PharmSciTech 14 (2013): 38-44.

285. Ferrari F, Cocconi D, Bettini R, Giordano F, Santi P, et al. The surface roughness of lactose particles can be modulated by wet-smoothing using a high-shear mixer. AAPS PharmSciTech 5 (2004): e60.

286. Jetzer MW, Schneider M, Morrical BD, Imanidis G. Investigations on the Mechanism of Magnesium Stearate to Modify Aerosol Performance in Dry Powder Inhaled Formulations. J Pharm Sci 107 (2018): 984-98.

287. Begat P, Morton DAV, Shur J, Kippax P, Staniforth JN, et al. The role of force control agents in high-dose dry powder inhaler formulations. J Pharm Sci 98 (2009): 2770-83.

288. Ali ME, Lamprecht A. Spray freeze drying for dry powder inhalation of nanoparticles. Eur J Pharm Biopharm 87 (2014): 510-7.

289. Cheow WS, Ng MLL, Kho K, Hadinoto K. Spray-freeze-drying production of thermally sensitive polymeric nanoparticle aggregates for inhaled drug delivery: effect of freeze-drying adjuvants. Int J Pharm 404 (2011): 289-300.

290. Abdelwahed W, Degobert G, Fessi H. Investigation of nanocapsules stabilization by amorphous excipients during freeze-drying and storage. Eur J Pharm Biopharm 63 (2006): 87-94.

291. Wowk B, Leitl E, Rasch CM, Mesbah-Karimi N, Harris SB, et al. Vitrification enhancement by synthetic ice blocking agents. Cryobiology 40 (2000): 228-36.

292. Kadoya S, Fujii K, Izutsu K-I, Yonemochi E, Terada K, et al. Freeze-drying of proteins with glass-forming oligosaccharide-derived sugar alcohols. Int J Pharm 389 (2010): 107-13.

293. Depaz RA, Pansare S, Patel SM. Freeze-Drying Above the Glass Transition Temperature in Amorphous Protein Formulations While Maintaining Product Quality and Improving Process Efficiency. J Pharm Sci 105 (2016): 40-9.

294. Wang L, Ma Y, Gu Y, Liu Y, Zhao J, et al. Cryoprotectant choice and analyses of freeze-drying drug suspension of nanoparticles with functional stabilisers. J Microencapsul 35 (2018): 241-8.

295. Korsmeyer RW, Peppas NA. Solute and penetrant diffusion in swellable polymers. III. Drug release from glassy poly(HEMA-co-NVP) copolymers. J Control Release 1 (1984): 89-98.

296. Ritger PL, Peppas NA. A simple equation for description of solute release II. Fickian and anomalous release from swellable devices. J Control Release 5 (1987): 37-42.

297. Yuksel N. Comparison of in vitro dissolution profiles by ANOVA-based, model-dependent and -independent methods. Int J Pharm 209 (2000): 57-67.

298. Brand-Williams W, Cuvelier ME, Berset C. Use of a free radical method to evaluate antioxidant activity. LWT - Food Science and Technology 28 (1995): 25-30.

299. Mishra K, Ojha H, Chaudhury NK. Estimation of antiradical properties of antioxidants using DPPH assay: A critical review and results. Food Chem 130 (2012): 1036-43.

300. Aliaga C, Lissi EA. Comparison of the free radical scavenger activities of quercetin and rutin - An experimental and theoretical study. Can. J. Chem. 82 (2004): 1668-73.

301. Krishnamachari V, Levine LH, Paré PW. Flavonoid oxidation by the radical generator AIBN: a unified mechanism for quercetin radical scavenging. J Agric Food Chem 50 (2002): 4357-63.

302. Ohashi H, Kyogoku T, Ishikawa T, Kawase S, Kawai S. Antioxidative activity of tree phenolic constituents 1: Radical-capturing reaction of flavon-3-ols with radical initiator. J Wood Sci 45 (1999): 53-63.

303. Fadda A, Serra M, Molinu MG, Azara E, Barberis A, et al. Reaction time and DPPH concentration influence antioxidant activity and kinetic parameters of bioactive molecules and plant extracts in the reaction with the DPPH radical. J Food Compos Anal 35 (2014): 112-9.

304. Foti MC, Daquino C, Geraci C. Electron-transfer reaction of cinnamic acids and their methyl esters with the DPPH(*) radical in alcoholic solutions. J Org Chem 69 (2004): 2309-14.

305. Foster KA, Oster CG, Mayer MM, Avery ML, Audus KL. Characterization of the A549 cell line as a type II pulmonary epithelial cell model for drug metabolism. Exp Cell Res 243 (1998): 359-66.

306. Rincheval V, Bergeaud M, Mathieu L, Leroy J, Guillaume A, et al. Differential effects of Bcl-2 and caspases on mitochondrial permeabilization during endogenous or exogenous reactive oxygen species-induced cell death: a comparative study of H_2O_2, paraquat, t-BHP, etoposide and TNF-α-induced cell death. Cell Biol Toxicol 28 (2012): 239-53.

307. Rucka Z, Vanhara P, Koutna I, Tesarova L, Potesilova M, et al. Differential effects of insulin and dexamethasone on pulmonary surfactant-associated genes and proteins in A549 and H441 cells and lung tissue. Int J Mol Med 32 (2013): 211-8.

308. Lee MJ, Song HJ, Jeong JY, Park SY, Sohn UD. Anti-Oxidative and Anti-Inflammatory Effects of QGC in Cultured Feline Esophageal Epithelial Cells. Korean J Physiol Pharmacol 17 (2013): 81-7.

309. Lago JHG, Toledo-Arruda AC, Mernak M, Barrosa KH, Martins MA, et al. Structure-activity association of flavonoids in lung diseases. Molecules 19 (2014): 3570-95.

310. Ballmaier D, Epe B. DNA damage by bromate: mechanism and consequences. Toxicology 221 (2006): 166-71.

311. Parsons JL, Chipman JK. The role of glutathione in DNA damage by potassium bromate in vitro. Mutagenesis 15 (2000): 311-6.

312. Champion JA, Walker A, Mitragotri S. Role of particle size in phagocytosis of polymeric microspheres. Pharm Res 25 (2008): 1815-21.

313. Grabowski N, Hillaireau H, Vergnaud J, Tsapis N, Pallardy M, et al. Surface coating mediates the toxicity of polymeric nanoparticles towards human-like macrophages. Int J Pharm 482 (2015): 75-83.

11 Acknowledgements / Danksagung

Zunächst gilt mein Dank meiner Doktormutter, Frau Prof. Dr. Keck, die es mir ermöglicht hat, an diesen spannenden und interessanten Themen zu arbeiten. Sie gab mir die Freiheiten diese Arbeit nach meinen Vorstellungen anzufertigen. Ich bedanke mich für die wissenschaftliche Betreuung, die Motivation und die zielführenden Diskussionen während der gesamten Zeit.

Außerdem möchte ich mich bei Herrn Prof. Dr. Bakowsky für die Bereitstellung seiner Zellkulturlabore sowie für die Erstellung des Zweitgutachtens und die Prüfung der Dissertation bedanken.

Ich danke Frau Prof. Dr. Petersen für die Leitung der Prüfungskommission und die Prüfung der Dissertation als Nebenfachprüfer.
Auch vielen Dank an Herrn Prof. Dr. Hartmann für die Prüfung der Dissertation als Nebenfachprüfer.

Frau Dr. Jana Brüßler und Herrn Dr. Jens Schäfer danke ich für die fachlichen Gespräche, die fortwährenden Unterstützung, Hilfe und Ratschläge auf dem Weg zur fertigen Arbeit. Frau Eva Mohr und Herrn Dr. Pinnapireddy danke ich für die Einführung in die Zellkultur und die vielen hilfreichen Ratschläge.

Für das intensive Korrekturlesen meiner Arbeit, seinen organisatorischen Fähigkeiten und den vielen tiefgründigen Gesprächen danke ich Daniel Knoth. Für die langen Stunden zu Fragen, Anregungen und die kritische Betrachtung der statistischen Methoden bedanke ich mich sehr bei Minh Tam H. Nguyen. Ich danke Henriette Dietrich für ihr fröhliches, ausgeglichenes Wesen und die Arbeiten an der HPLC.

Mein besonderer Dank gilt ebenfalls Nathalie Goergen, Julia Schüer, Florian Stumpf und Ralph Eckert für die angenehmen, lustigen und ernsten Gespräche und Aktivitäten auch außerhalb der Pharmazie.

Herzlich bedanken möchte ich mich bei meinen Kollegen und Ehemaligen, Steffen Hartmann, Olga Pelikh, Jan Schulze, Sharoon Griffin, Verda Farida, Marc Schäfer, Yannik Soufi, Reem Alnemari, Abraham Abrahm, Noor Almohsen, Sabrina Wiemann, David Specht und Julia Michaelis, sowie Herrn Prof. Dr. Bakowsky und sein Team für das großartige Arbeitsklima, die schöne Zusammenarbeit, die Hilfe, die inspirierenden Anregungen und die gemeinsam erlebte Zeit.

Abschließend möchte ich mich insbesondere bei Sean Wewer, meinem Bruder Kevin und meinen Eltern für ihre emotionale Unterstützung und Geduld während der letzten Jahre bedanken.

12 Publications

12.1 Original papers

1. Pelikh O, **Stahr PL**, Huang J, Gerst M, Scholz P, et al. Nanocrystals for improved dermal drug delivery. Eur J Pharm Biopharm 128 (2018): 170-8.
2. **Stahr PL**, Keck CM. Preservation of rutin nanosuspensions without the use of preservatives. Beilstein J Nanotechnol 10 (2019): 1902-13.
3. Knoth D, Rincón-Fontán M, **Stahr PL**, Pelikh O, Eckert RW, et al. Evaluation of a biosurfactant extract obtained from corn for dermal application. Int J Pharm 564 (2019): 225-36.
4. **Stahr PL**, Grewal R, Eckert GP, Keck CM. Investigating hesperetin nanocrystals with tailor-made sizes for the prevention and treatment of Alzheimer's disease. Drug Deliv Transl Res 11 (2021): 659-674.
5. Babylon L, Grewal R, **Stahr PL**, Eckert RW, Keck CM, Eckert GP. Hesperetin nanocrystals improve mitochondrial function in a cell model of early Alzheimer's disease. Antioxidants (submitted)
6. Carrillo-Hormaza L, López-Parra S, **Stahr PL**, Keck CM, Osorio E. Development of a natural dispersion of biflavonoids from Garcinia madruno extracts: A green and sustainable processing to improve the solubility and dissolution rate. Colloids Surf B Biointerfaces (submitted)

12.2 Oral presentations

1. Transfer of rutin nanosuspensions into a solid dosage form, at the "Engineering of Functional Interfaces (ENFI)" conference in Marburg/ Germany on 29th August 2017.
2. Flavonoid nanocrystals for the treatment of oxidative stress in the lung, at the "International PhD Students/Postdoc Meeting of the German Pharmaceutical Society (DPhG)" conference in Bad Dürkheim/ Germany on 15th March 2018.
3. NANOMEDICINE - the smart therapy against aging at the "Menopause Andropause Anti-Aging" conference in Vienna/ Austria on 8th December 2018.

12.3 Poster presentations

1. Stahr PL, Keck CM. (2016) Tailor-made nanocrystals for optimised dermal drug delivery, 5th Galenus Workshop "The Advanced Use of Nanocarriers in Future Skin Drug Delivery", Berlin/ Germany, 16.-18. November.
2. Stahr PL, König A, Schneider M, Keck CM. (2017) Flavonoid nanocrystals for treatment of COPD, European Workshop on Particulate Systems (EWPS), Copenhagen/ Denmark, 19. – 20. January.
3. Stahr PL, Keck CM. (2017) Flavonoid nanosuspension for treatment of pulmonary disease, Controlled Release Society (CRS) Local Chapter Germany, Marburg/ Germany, 2. – 3. March.
4. Stahr PL, Keck CM. (2017) Rutin ArtCrystals for pulmonal application: Formulation Development and Scale-up, 9th Polish – German Symposium on Pharmaceutical Sciences, Krakow/ Poland, 26. – 27. May.
5. Stahr PL, Keck CM. (2017) Transfer of rutin nanosuspensions into a solid dosage form, Engineering of Functional Interfaces (ENFI) 2017, Marburg/ Germany, 28. – 29. August.

6. Stahr PL, Keck CM. (2017) Drying of flavonoid nanosuspensions – freeze drying versus spray drying, Annual Meeting of the German Pharmaceutical Society (DPhG), Saarbrücken/ Germany, 26. – 29. September.
7. Stahr PL, Keck CM. (2018) Flavonoid nanocrystals for the treatment of oxidative stress in the lung, 17th Fraunhofer seminar Translational Airway Research "Models of Lung Disease", Hannover/ Germany, 18.-19. January.
8. Stahr PL, Keck CM. (2018) Enabling rutin nanocrystals for dry powder inhalation, Controlled Release Society (CRS) Local Chapter Germany, Halle/ Germany, 1. – 2. March.
9. Stahr PL, Keck CM. (2018) Flavonoid nanocrystals for the treatment of oxidative stress in the lung, International PhD Students/Postdoc Meeting of the German Pharmaceutical Society (DPhG), Bad Dürkheim/ Germany, 14. – 16. March.
10. Stahr PL, Keck CM. (2018) Solid rutin nanocrystals in cysteine carrier for treatment of oxidative stress, 11th World Meeting on Pharmaceutics, Biopharmaceutics and Pharmaceutical Technology, Granada/ Spain, 19. – 22. March.
11. Stahr PL, Grewal R, Braun A, Schäfer KH, Eckert GP, Keck CM. (2018) NANOMEDICINE - THE “SMART” THERAPY AGAINST AGING, Menopause Andropause Anti-Aging, Vienna /Austria. 6. – 8. December.
12. Stahr PL, Keck CM. (2019) Treatment of pulmonary diseases through optimized anti-inflammatory formulation, 3rd European Conference on Pharmaceutics, Bologna/ Italy, 25. – 26. March.
13. Stahr PL, Müller RH, Pelikh O, Keck CM. (2019) Nanocrystals as universal formulation for treatment of oxidative stress related diseases, Controlled Release Society Annual Meeting, Valencia/ Spain, 20. – 24. July.